International School of Neutron Scattering
“Francesco Paolo Ricci”

September 25- October 6, 2006

Polarized Neutron Reflectometry

Gian Piero Felcher,
Argonne National Laboratory

Artwork prepared with the help of:

Chuck Majkrzak
Sunil Sinha
Suzanne te Velthuis
Frank Klose
Hartmut Zabel

Polarized Neutron Reflectometry
1. A primer of the 1D technique

The Spallation Neutron Source complex in Oak Ridge

The Neutron has Both Particle-Like and Wave-Like Properties

- Mass: $m_n = 1.675 \times 10^{-27}$ kg
- Charge = 0; Spin = ½
- Magnetic dipole moment: $\mu_n = -1.913\ \mu_N$
- Nuclear magneton: $\mu_N = eh/4\pi m_p = 5.051 \times 10^{-27}\ J\ T^{-1}$
- Velocity (v), kinetic energy (E), wavevector (k), wavelength (λ), temperature (T).
- $E = m_n v^2/2 = k_B T = (hk/2\pi)^2/2m_n;\ \ k = 2\ \pi/\lambda = m_n v/(h/2\pi)$

	Energy (meV)	Temp (K)	Wavelength (nm)
Cold	**0.1 – 10**	**1 – 120**	**0.4 – 3**
Thermal	**5 – 100**	**60 – 1000**	**0.1 – 0.4**
Hot	**100 – 500**	**1000 – 6000**	**0.04 – 0.1**

λ (nm) = 395.6 / v (m/s)

E (meV) = $0.02072\ k^2$ (k in nm^{-1})

Thermal Neutrons

Advantages

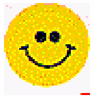

1) λ_n ~ Interatomic Spacing

2) Penetrates Bulk Matter (neutral particle)

3) Strong Contrasts Possible (e.g. H/D)

4) E_n ~ Elementary Excitations (phonons, magnons, etc.)

5) Scattered Strongly by Magnetic Moments

Disadvantages

1) Low Brilliance of Neutron Sources-Low Resolution or Intensities; Large Samples; Low Coherence; Surfaces Difficult

2) Some Elements Strongly Absorb (e.g. Cd, Gd, B)

3) Kinematic Restriction on Q for Large E Transfers

4) Restricted to Excitations ≤ 100 meV

The photon also has wave and particle properties

E=hν =hc/l= hck

Charge = 0 Magnetic Moment = 0

Spin = 1

E (keV)	λ (Å)
0.8	15.0
8.0	1.5
40.0	0.3
100.0	0.125

Brightness & Fluxes for Neutron & X-Ray Sources

	Brightness $(s^{-1}m^{-2}ster^{-1})$	dE/E (%)	Divergence $(mrad^2)$	Flux $(s^{-1}m^{-2})$
Neutrons	10^{15}	2	10×10	10^{11}
Rotating Anode	10^{20}	0.02	0.5×10	5×10^{14}
Bending Magnet	10^{27}	0.1	0.1×5	5×10^{20}
Undulator (APS)	10^{33}	10	0.01×0.1	10^{24}

Scattering amplitudes: Neutrons

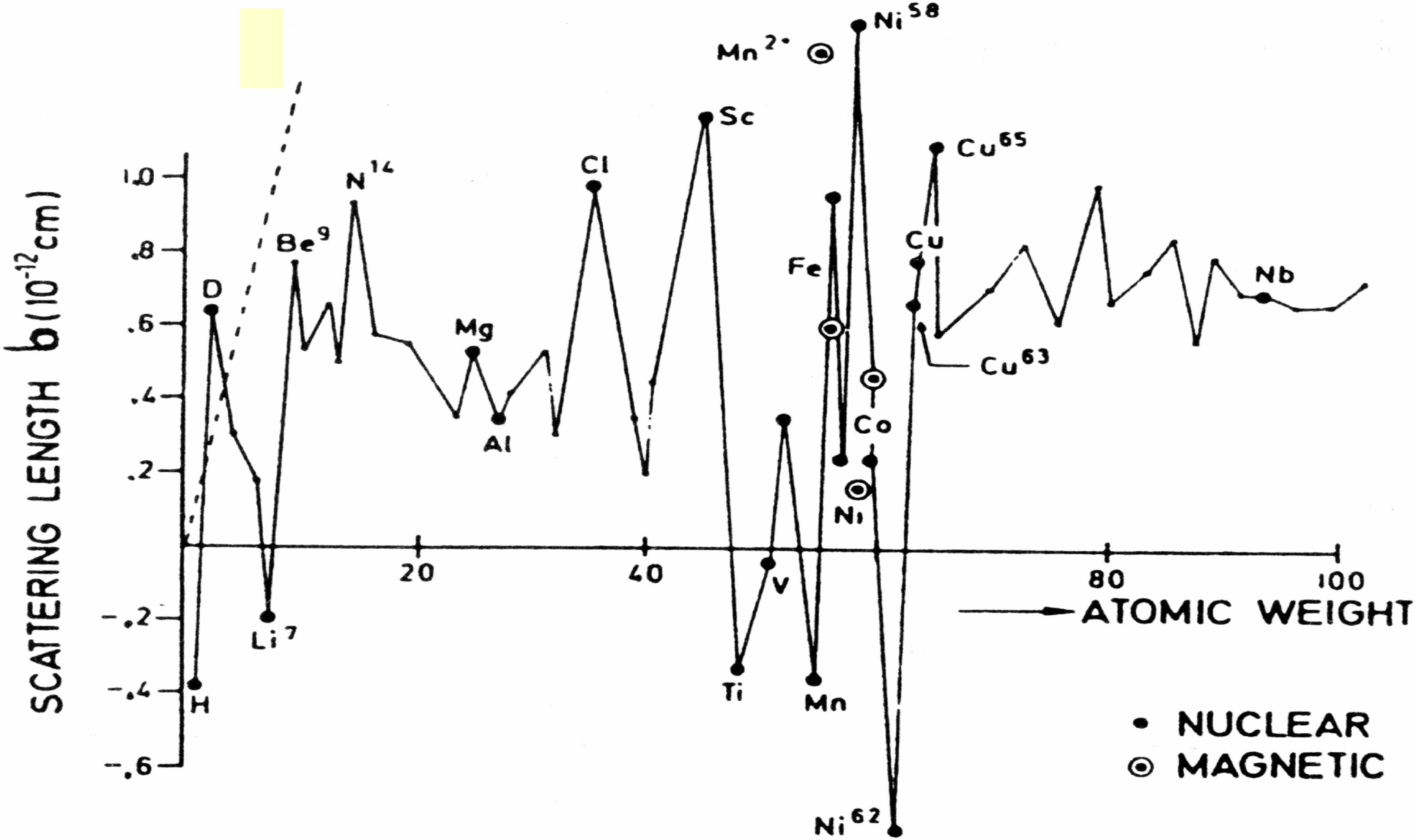

Reflection of Visible Light

Perfect & Imperfect „Mirrors“

Basic Equation: X-Rays

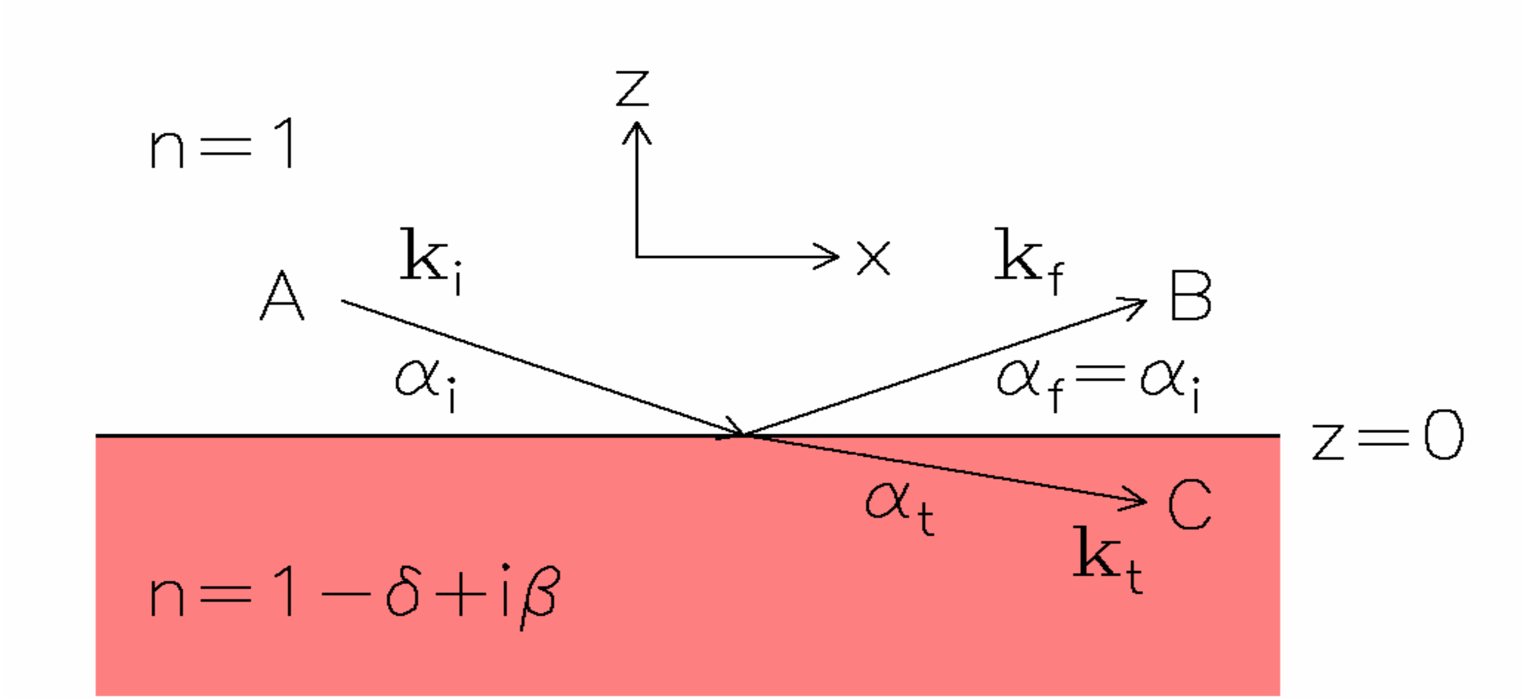

Helmholtz-Equation & Boundary Conditions

$$\Delta E(\vec{r}) + k^2\, n_{\mathrm{X}}^2(\vec{r})\, E(\vec{r}) = 0$$

Refractive Index: X-Rays

$$n(z) = 1 - \frac{\lambda^2}{2\,\pi}\, r_e\, \varrho(z) + \mathrm{i}\,\frac{\lambda}{4\,\pi}\,\mu(z)$$

$$\varrho(z) = \langle \varrho(x, y, z) \rangle_{x,y}$$

	$r_e\varrho\,(10^{10}\mathbf{cm}^{-2})$	$\delta(10^{-6})$	$\mu\,(\mathbf{cm}^{-1})$	$\alpha_c(°)$
Vacuum	0	0	0	0
PS $(C_8H_8)_n$	9.5	3.5	4	0.153
PMMA $(C_5H_8O_2)_n$	10.6	4.0	7	0.162
PVC $(C_2H_3Cl)_n$	12.1	4.6	86	0.174
PBrS $(C_8H_7Br)_n$	13.2	5.0	97	0.181
Quartz (SiO_2)	18.0–19.7	6.8–7.4	85	0.21–0.22
Silicon (Si)	20.0	7.6	141	0.223
Nickel (Ni)	72.6	27.4	407	0.424
Gold (Au)	131.5	49.6	4170	0.570

E = 8 keV λ = 1.54 Å

Electron Density *Profile* !

X-Ray Reflectivity: Principle

Visible Light Reflectivity: $n_2 > 1$

n_1

n_2

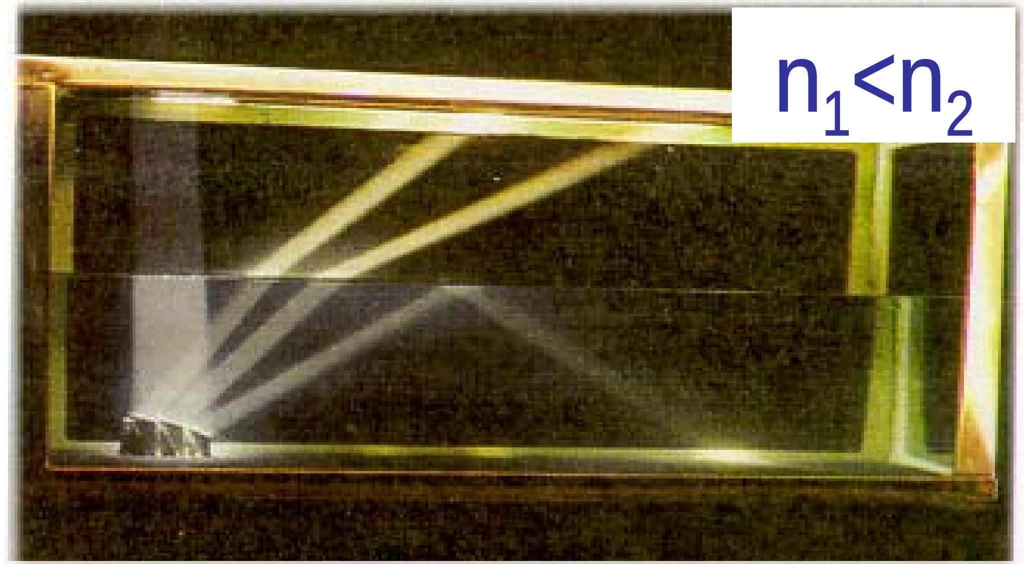

X-Ray Reflectivity: $n_2 < 1$

n_1

n_2

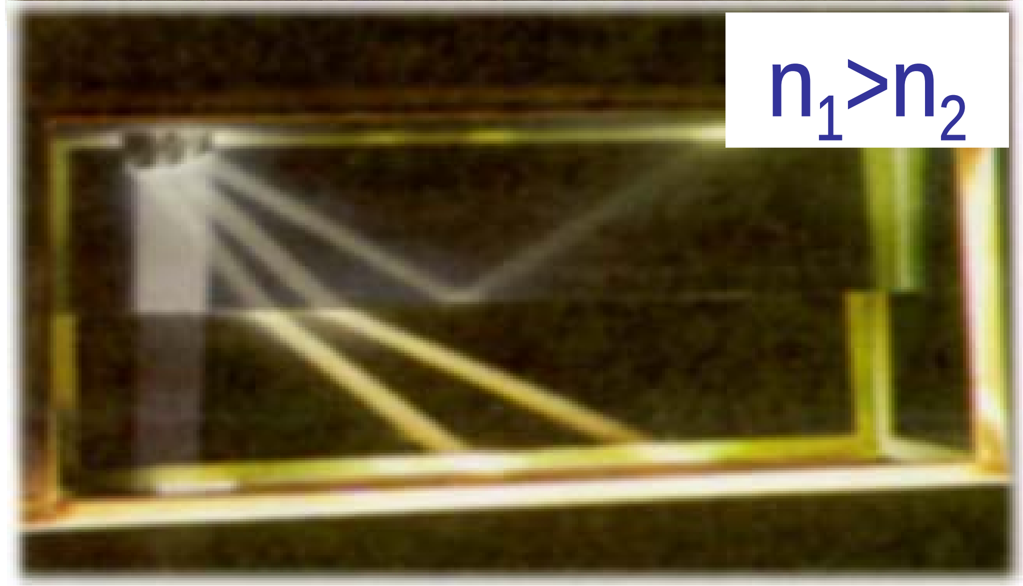

Total External Reflection

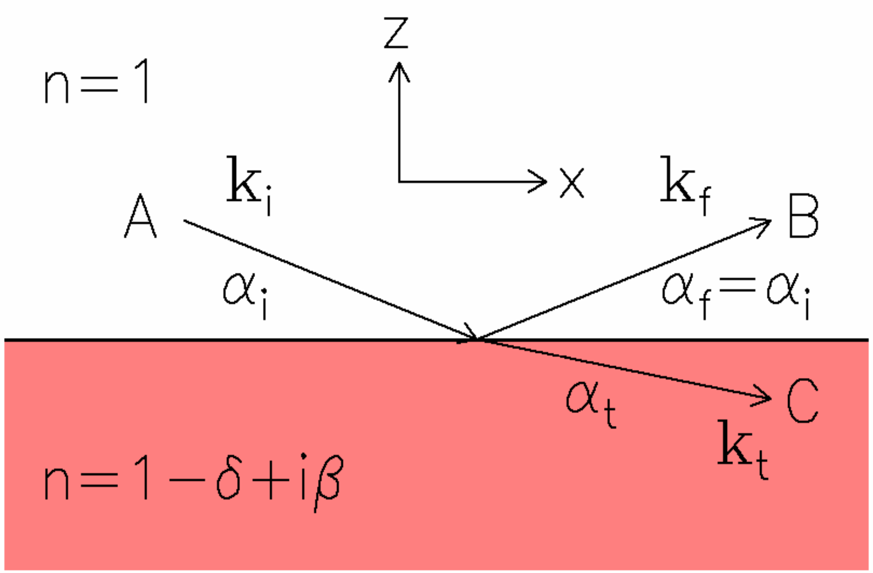

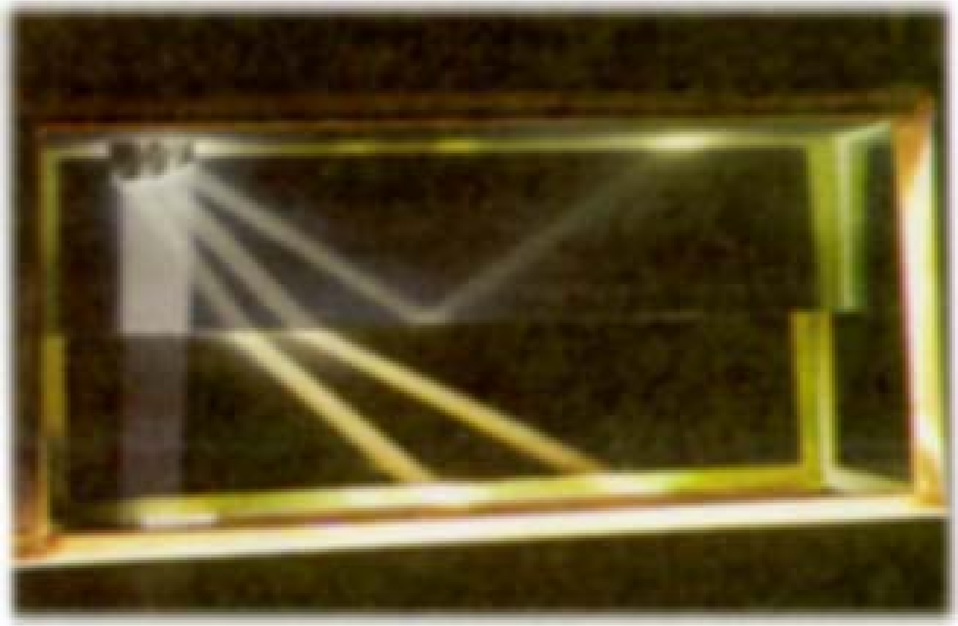

$$\cos\alpha_i = (1-\delta)\cos\alpha_t$$

$\alpha_t=0$ ⇒

Critical Angle:

$$\alpha_c \approx \sqrt{2\delta} \sim 0.3°$$

GRAZING ANGLES !!!

"SPECULAR" OR "MIRROR" REFLECTION OF A WAVE

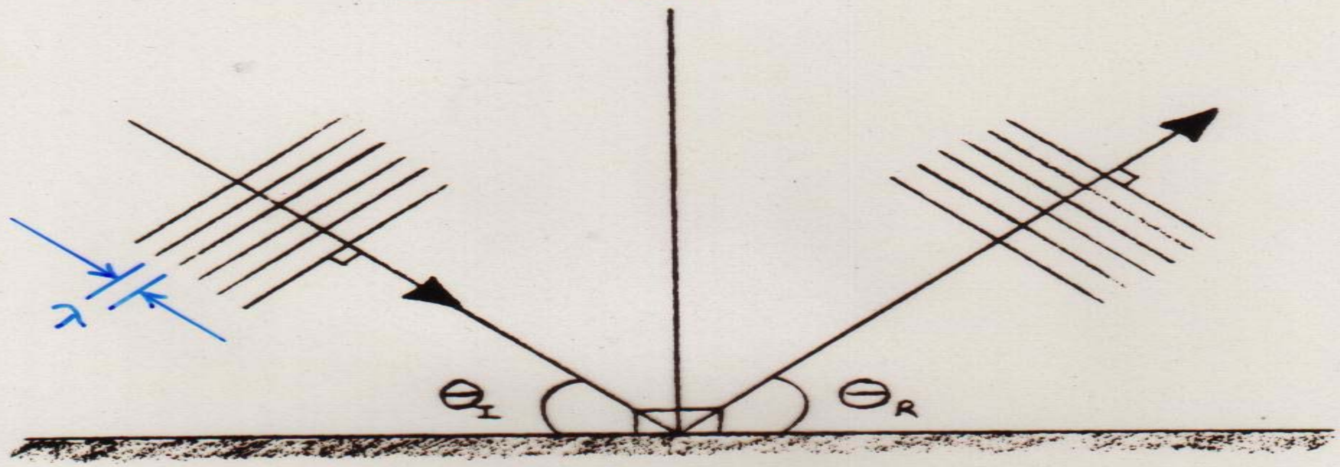

ANGLE OF INCIDENCE Θ_I
= ANGLE OF REFLECTION Θ_R

REFRACTION OF A LIGHT WAVE

$n_1 = 1$
(FOR VACUUM)

$n_1 \sin\theta_1 = n_2 \sin\theta_2$

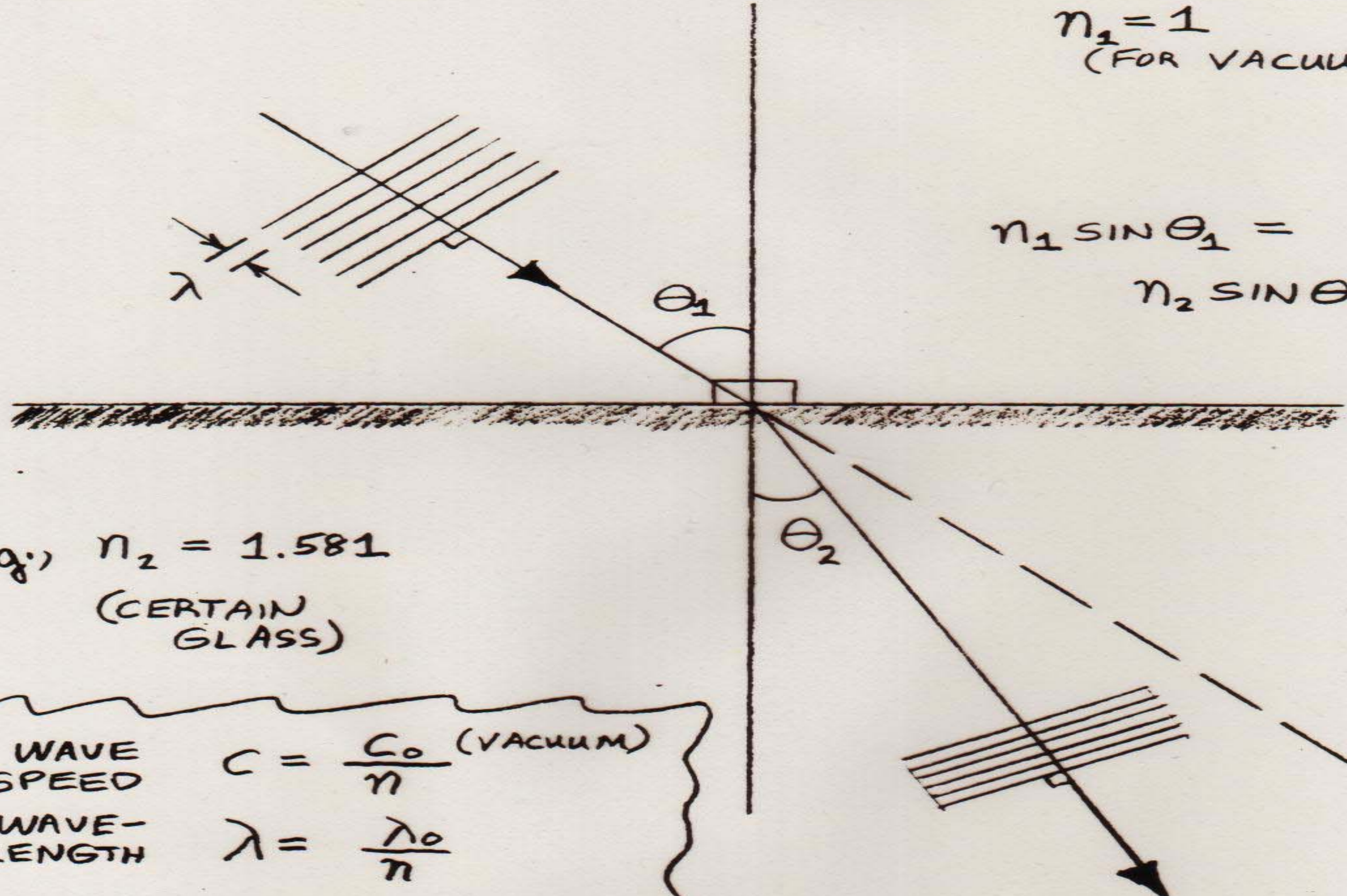

e.g.) $n_2 = 1.581$
(CERTAIN GLASS)

WAVE SPEED	$c = \frac{c_0}{n}$ (VACUUM)
WAVE-LENGTH	$\lambda = \frac{\lambda_0}{n}$
WAVE-VECTOR	$k = n k_0 = \frac{2\pi\nu}{c}$
FREQUENCY	ν = CONSTANT

REFRACTIVE INDEX n DEPENDS ON MATERIAL AND WAVELENGTH OF THE LIGHT

Single Interface: Vacuum/Matter

Fresnel-Formulae

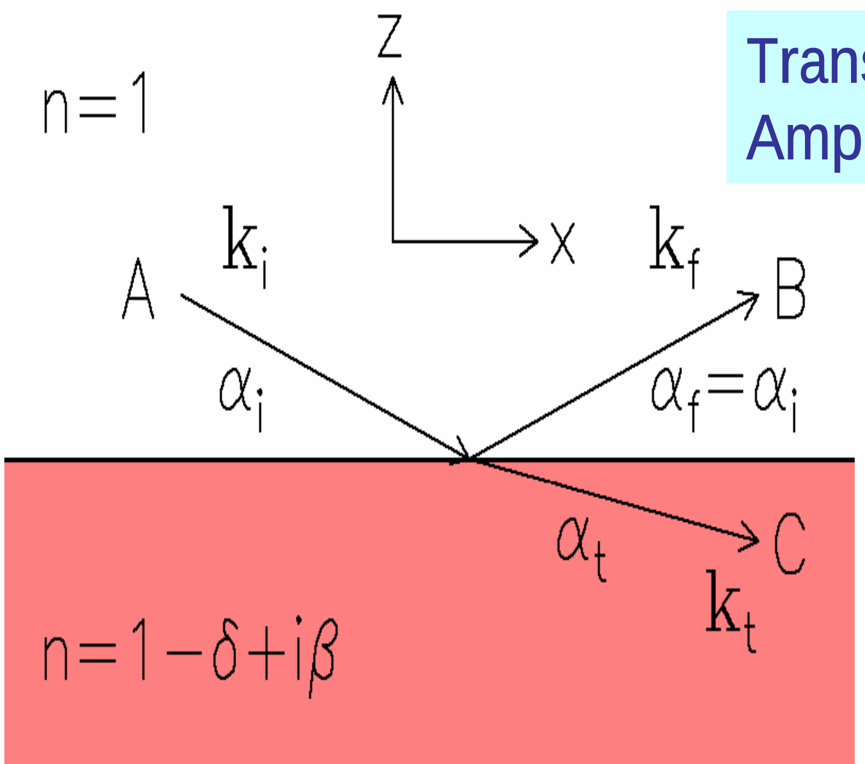

Reflected Amplitude

$$r = \frac{B}{A} = \frac{k_{\mathrm{i},z} - k_{\mathrm{t},z}}{k_{\mathrm{i},z} + k_{\mathrm{t},z}}$$

Transmitted Amplitude

$$t = \frac{C}{A} = \frac{2\,k_{\mathrm{i},z}}{k_{\mathrm{i},z} + k_{\mathrm{t},z}}$$

Wave-Vectors

$$k_{\mathrm{i},z} = k \sin \alpha_{\mathrm{i}}$$

$$k_{\mathrm{t},z} = k(n^2 - \cos^2 \alpha_{\mathrm{i}})^{1/2}$$

Fresnel Reflectivity: $R_F(\alpha_i)$

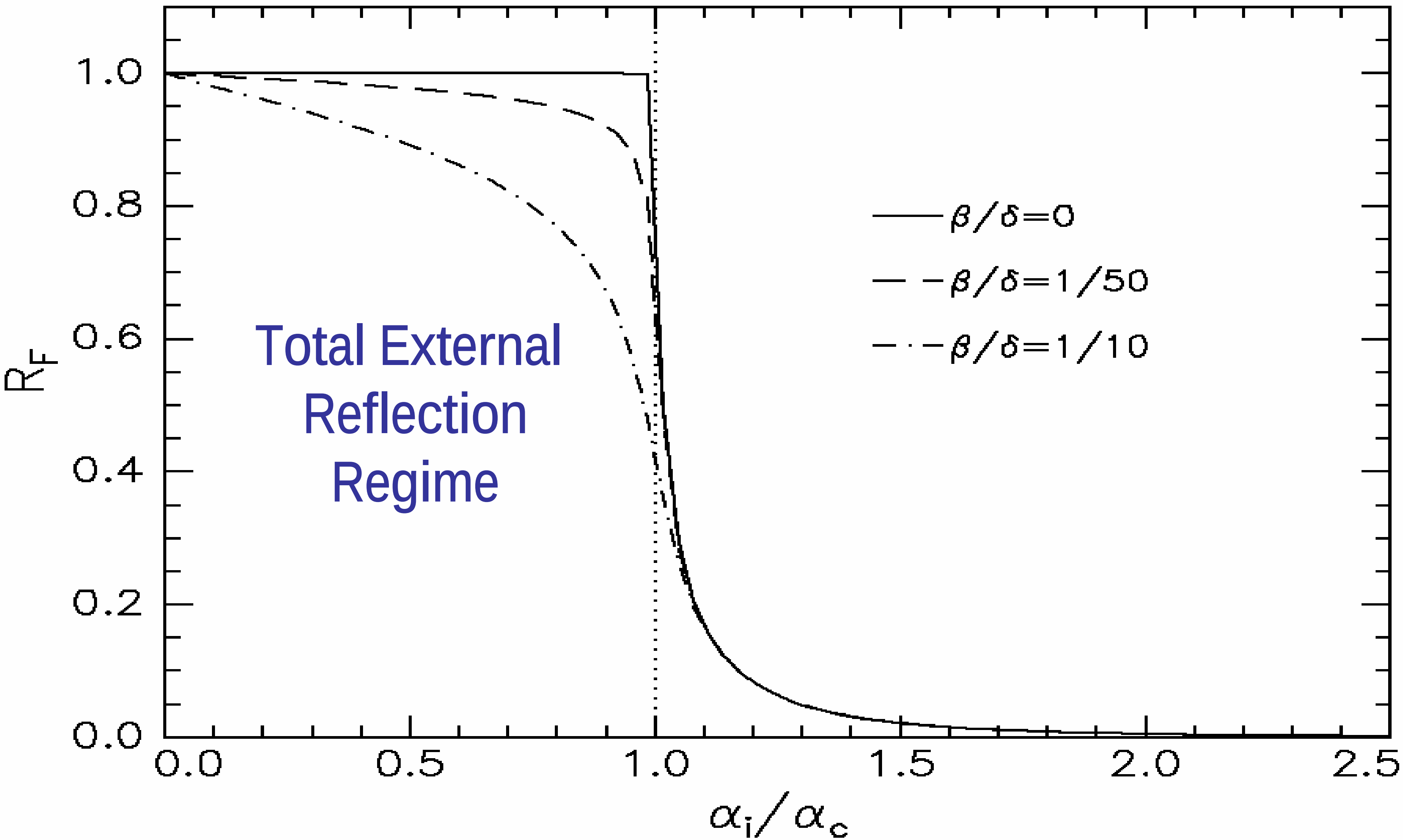

Roughness Damps Reflectivity

$\sigma_j = 10$ Å
$\lambda = 1.54$ Å

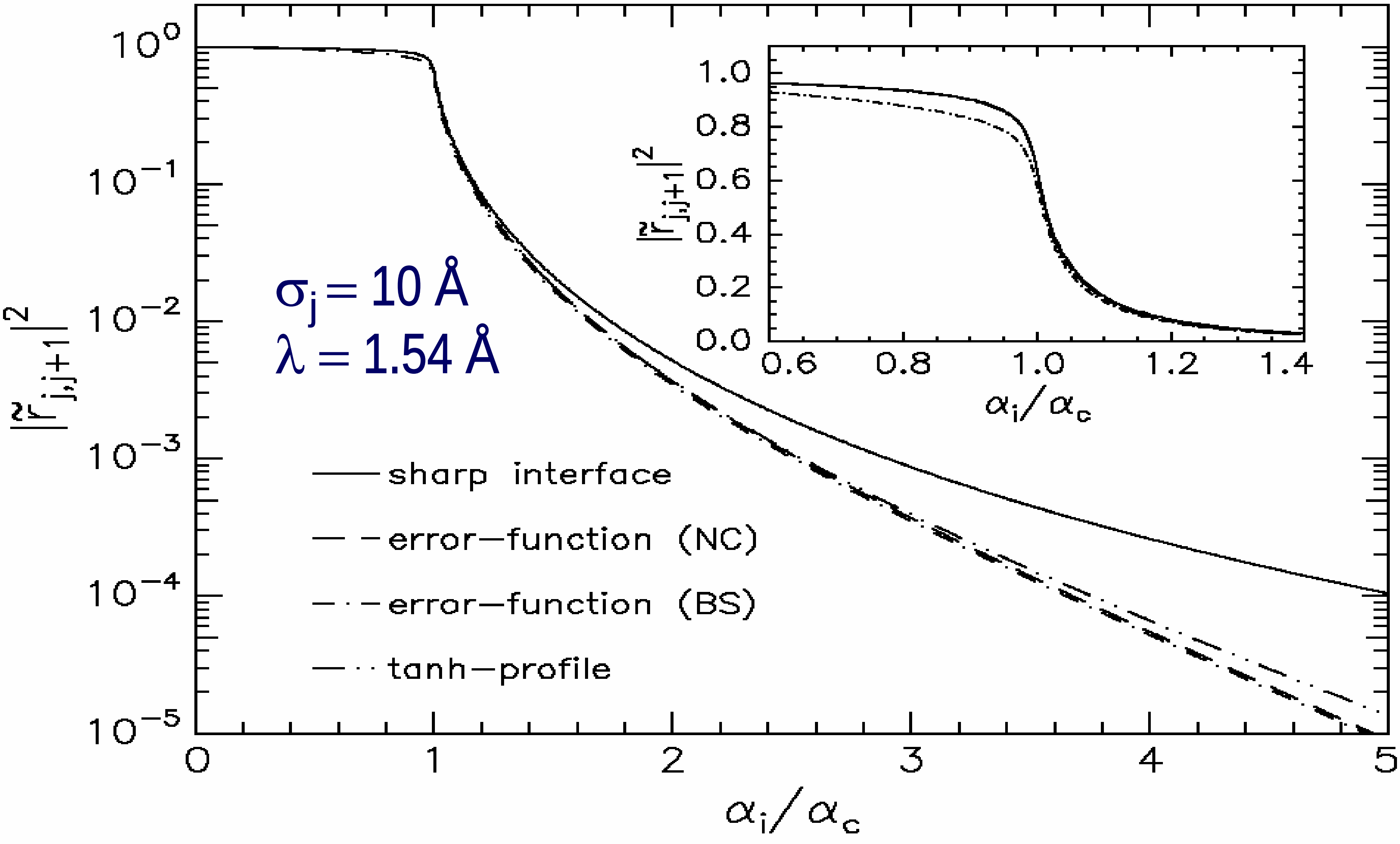

Total Reflection at Surfaces

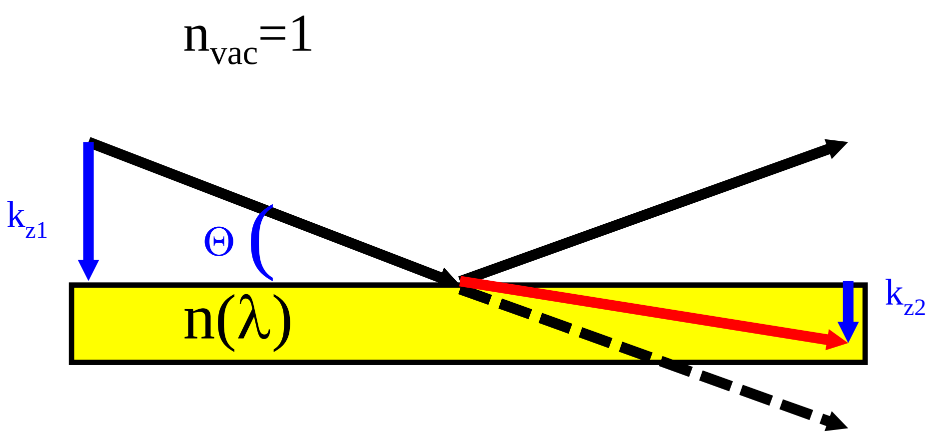

For neutrons (and X-rays) with wavelengths of a few Å, almost all materials have an optical index slightly smaller than 1.

=> Total reflection up to a critical angle $\Theta_{crit}(\lambda)$

Refraction index:

$n(\lambda) = k_{z2}$ (inside the media) / k_{z1}(outside)

Kinetic energy of a free particle:

$$E_1 = \hbar^2 k_{z1}^2/2m_N$$

Inside the media with potential V, k_{z2} is (in most cases) smaller (conservation of energy):

$$\hbar^2 k_{z2}^2/2m_N + V = E_1$$

$$\Rightarrow \quad k_{z2} = (k_{z1}^2 - 2m_N V/\hbar^2)^{1/2}$$

Connection to microscopic properties:

Fermi pseudo potential: $V = 2\pi \hbar^2 N b/m_N$

with N: number density [at/cm³]
b: coherent scattering length of the nuclei in the material [fm]

Critical angle for total reflection is reached, if $E_z=V$!

$$\Theta_{crit} = \sin^{-1}\lambda(N\cdot b/\pi)^{1/2} = \cos^{-1} n$$

or

$$Q_{crit} = 4\pi \sin\Theta/\lambda = 4(\pi N\cdot b)^{1/2}$$

Calculation of the reflectivity at a potential step

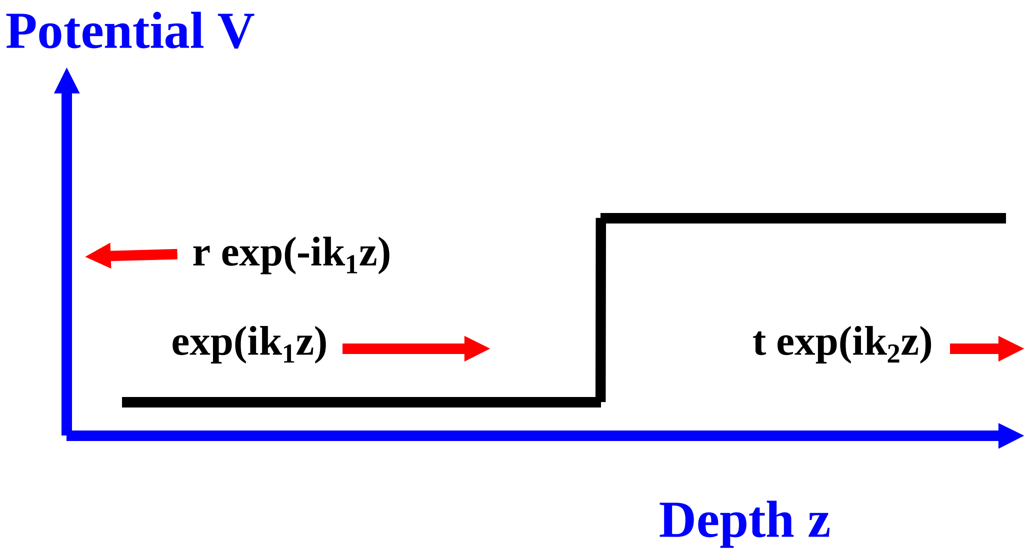

Solution of the quantum mechanic problem:

Fresnel equations

Reflectivity $R = |r|^2 = |(k_1 - k_2) / (k_1+k_2) \exp(i2k_1z)|^2$

Transmission $T = |t|^2 = |2k_1 / (k_1+k_2) \exp(i2(k_1 - k_2)z)|^2$

Example: Potential of a multilayer

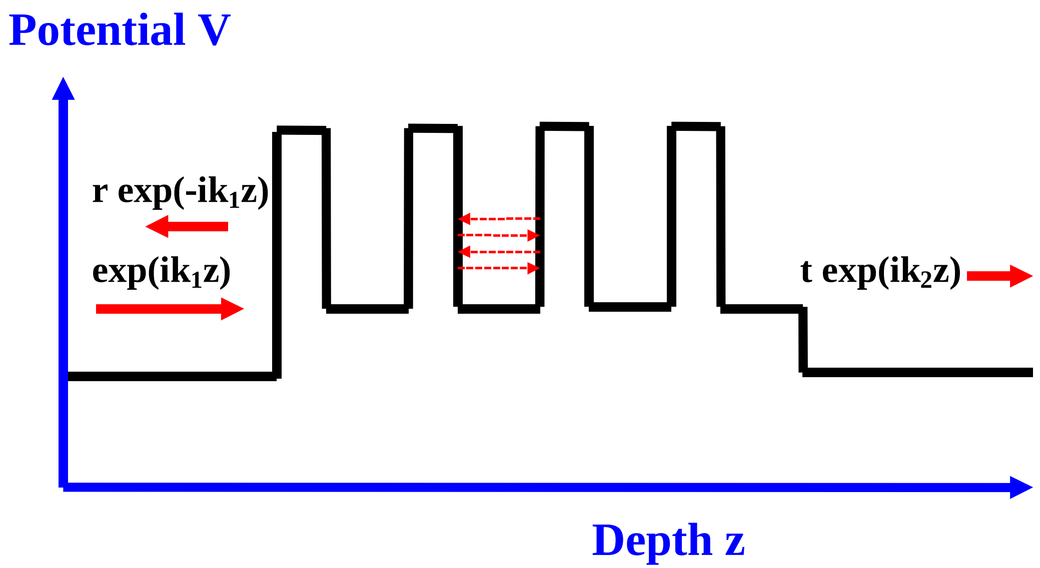

At each interface one has to take into account:

- **Refraction effects**
- **Multiple-scattering effects**

Reflectivity of Layered Structures

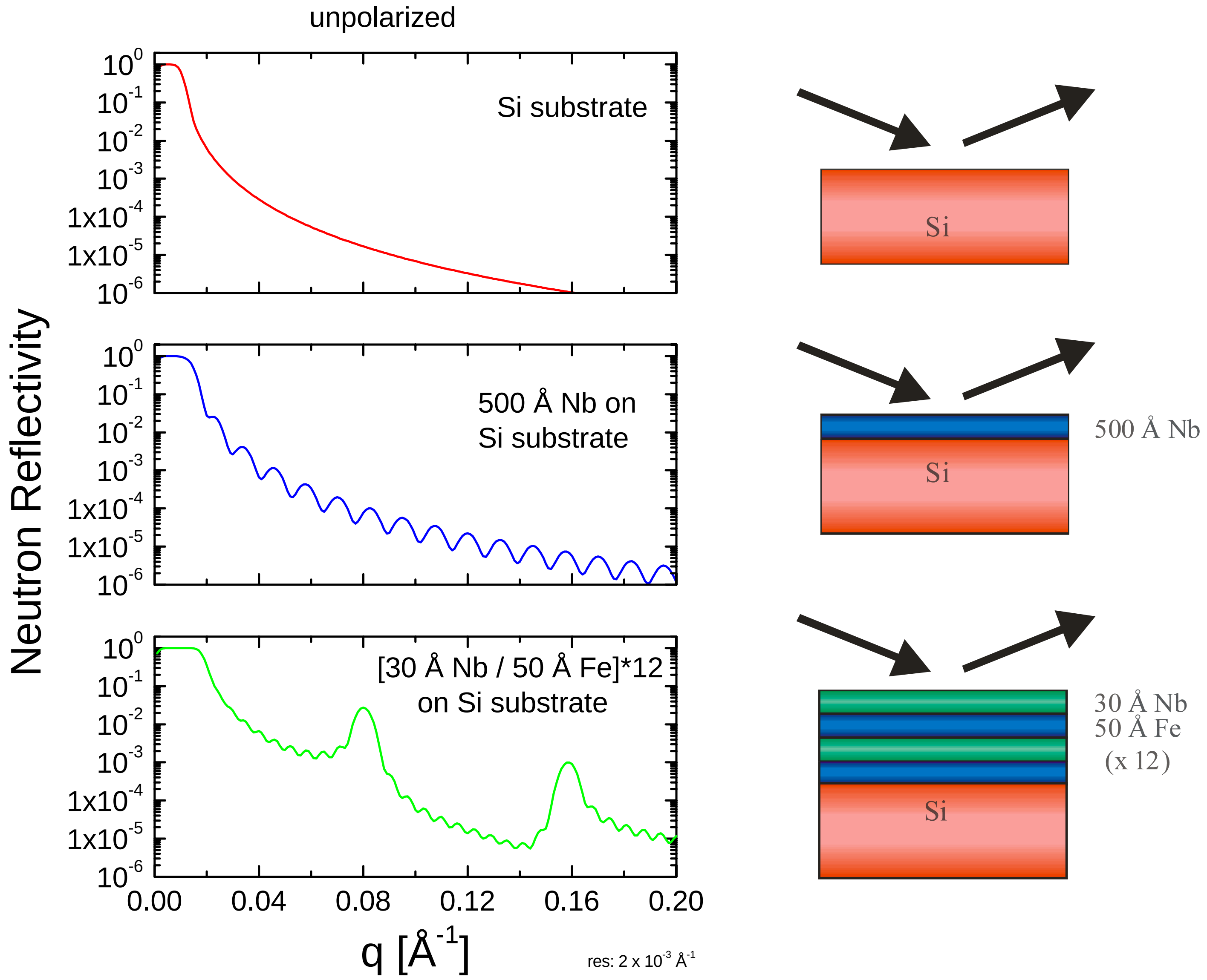

Neutron Reflectivity

$|\mathbf{k}| = 2\pi/\lambda$

Θ: angle of incidence
λ: wavelength

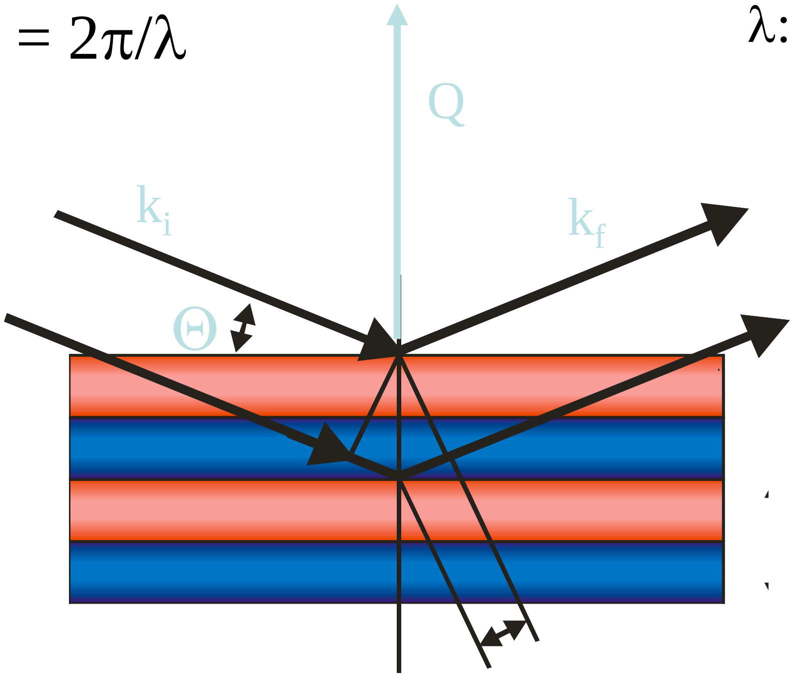

The reflectivity of the sample is measured as a function of the scattering vector Q

$$\mathbf{Q} = -\mathbf{k}_i + \mathbf{k}_f$$
$$|\mathbf{Q}| = 4\,\pi \sin\Theta / \lambda$$

=> two concepts for neutron reflectivity measurements:

a) fixed wavelength + variable angle

b) variable wavelength + fixed angle

The Filter/Collimation System of POSY I

Neutron spectrum of POSY I: 2.5 Å > λ > 14 Å

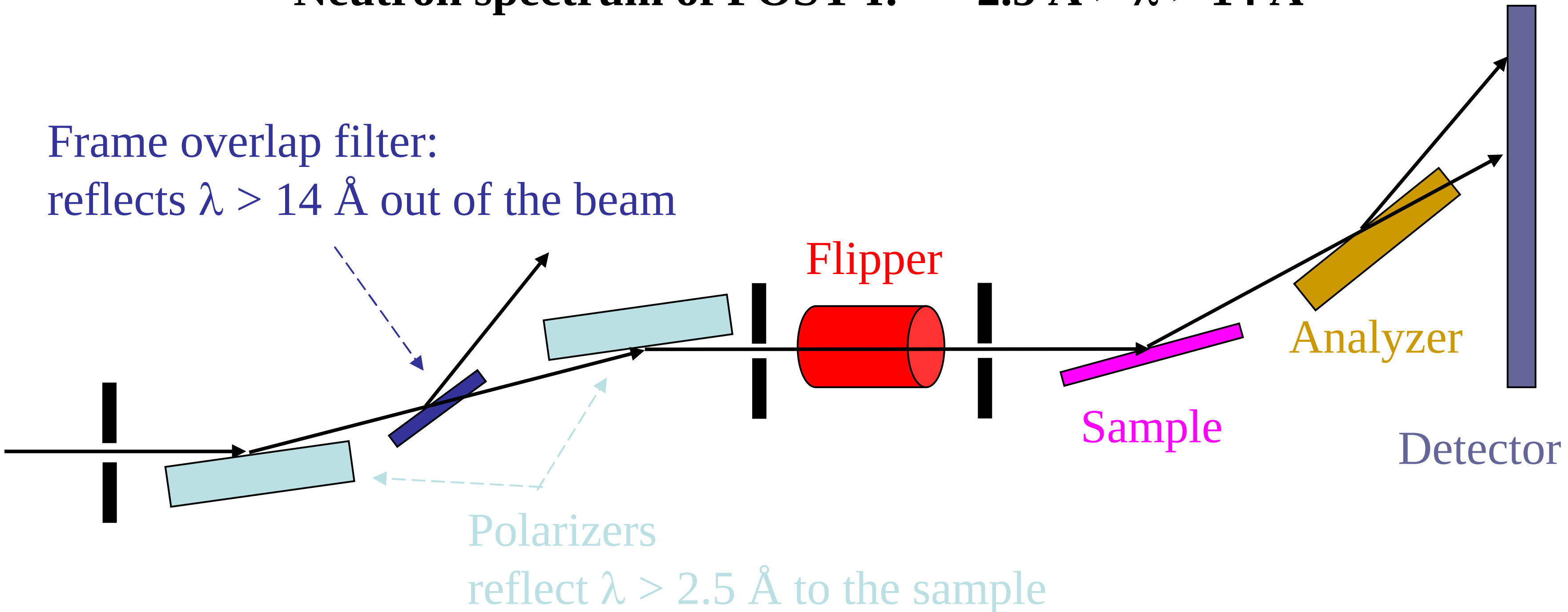

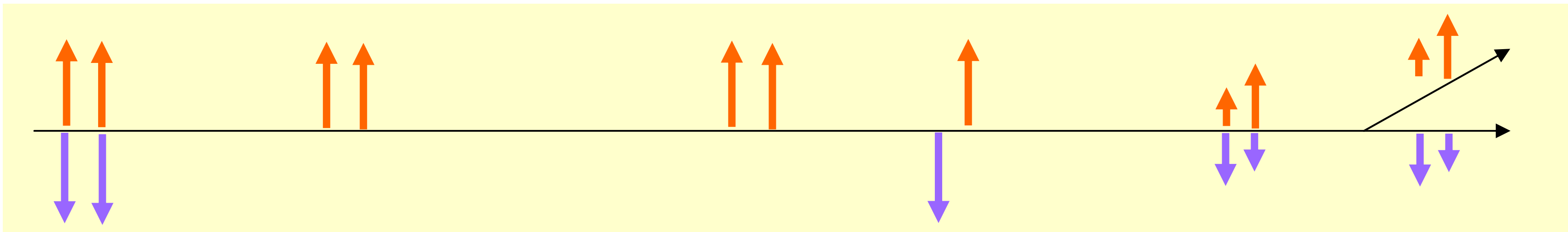

Reflectivity of Magnetic Layers

Fermi pseudo potential:

$$V = 2\pi\,\hbar^2\,N\,(b_n +/- b_{mag})/m_N$$

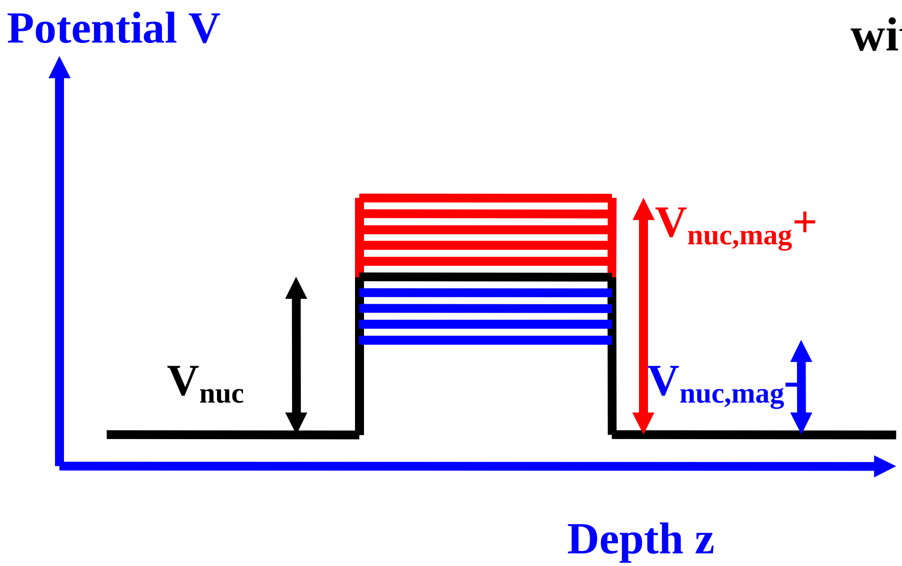

with b_{nuc}: nuclear scattering length [fm]

b_{mag}: magnetic scattering length [fm] ($1\ \mu_B$/Atom => 2.695 fm)

N: number density [at/cm^3]

m_N: neutron mass

Spin"up" neutrons see a high potential.
Spin"down" neutrons see a low potential.

Bragg's Law for Periodic Layered Structures

constructive interference if: $2d \sin\Theta = n \lambda$

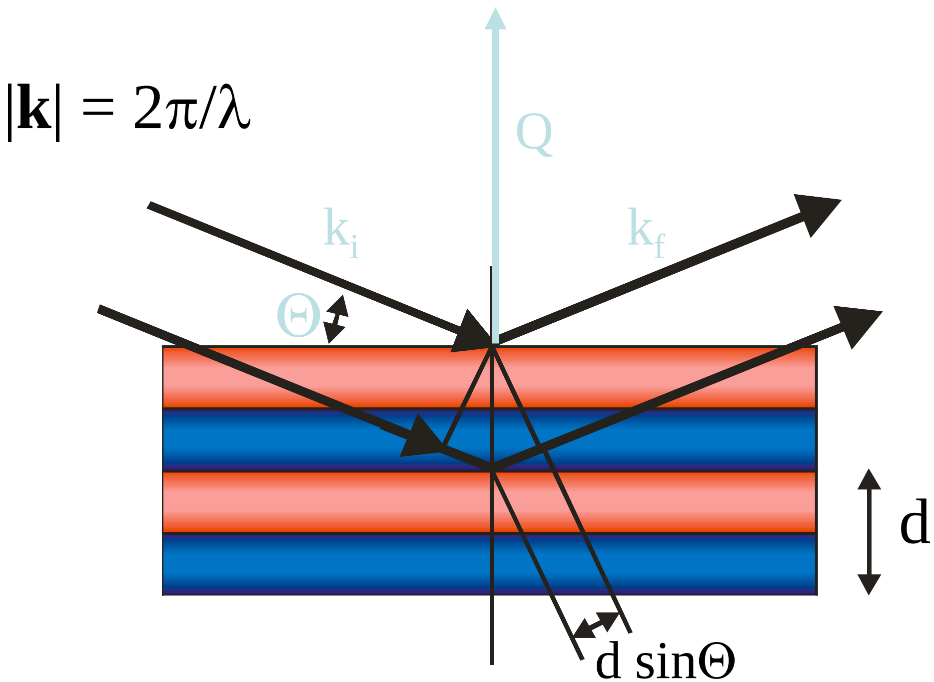

d: double layer thickness
Θ: angle of incidence
n: order number (0,1,2,...)
λ: wavelength

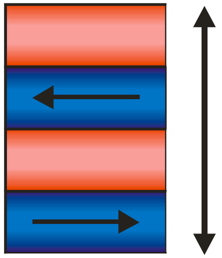

d_{mag}: magnetic periodicity

example:
antiferromagnetic coupling of magnetic layers

Polarized Neutron Reflectivity of Layered Magnetic Structures

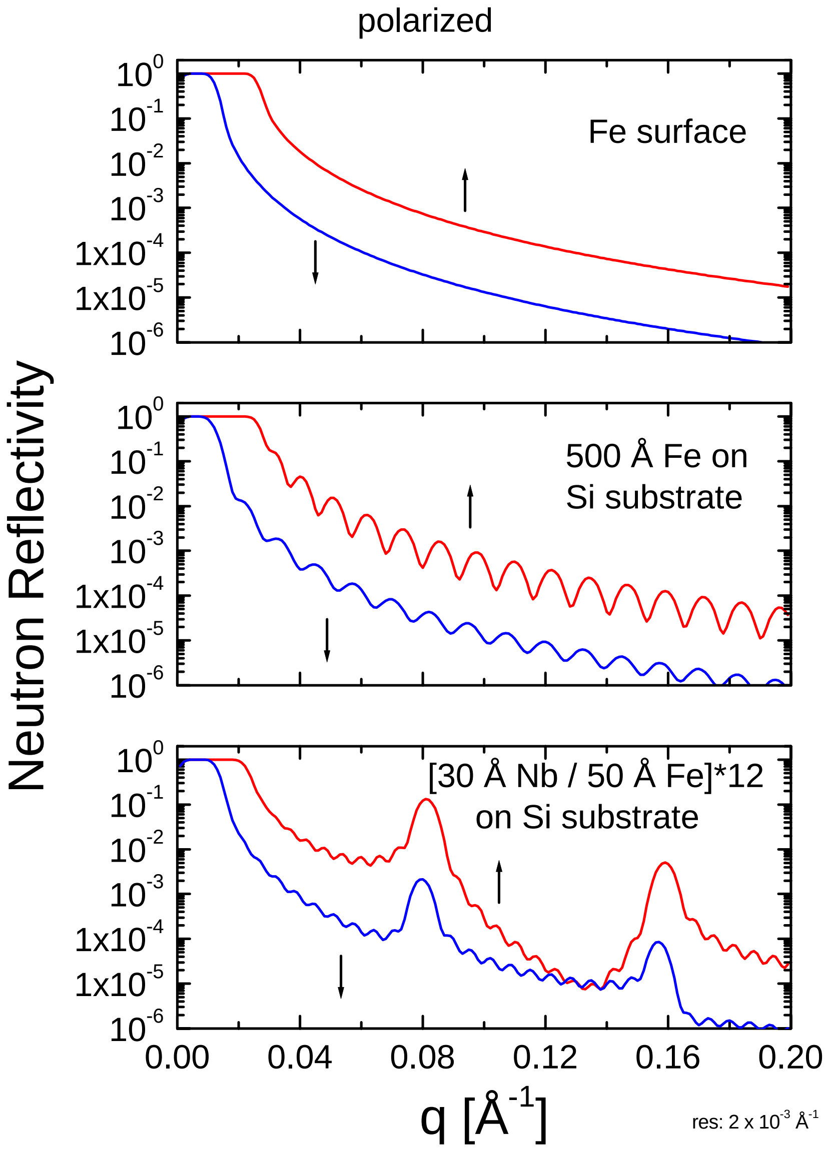

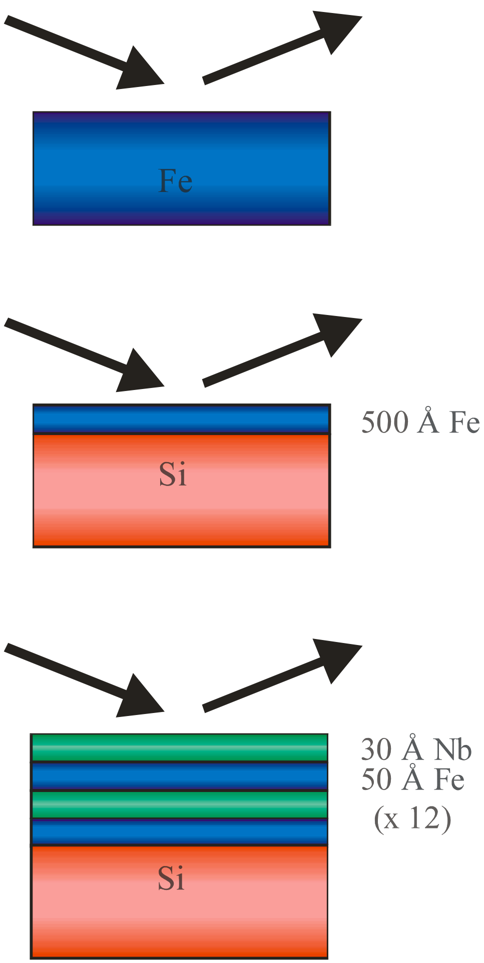

REFLECTION FROM AN IDEAL FILM OR SLAB OF MATERIAL

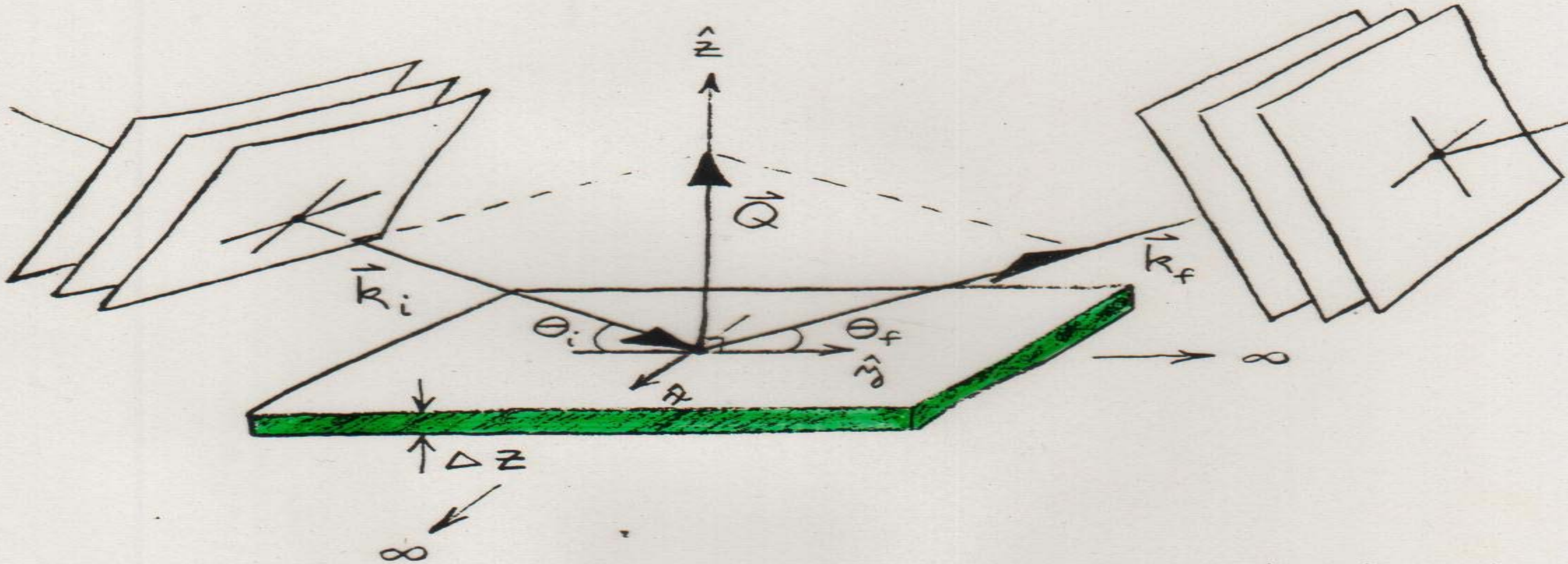

WAVEVECTOR TRANSFER $\vec{Q} = \vec{k}_f - \vec{k}_i$

$\rho = \rho(z)$ ONLY

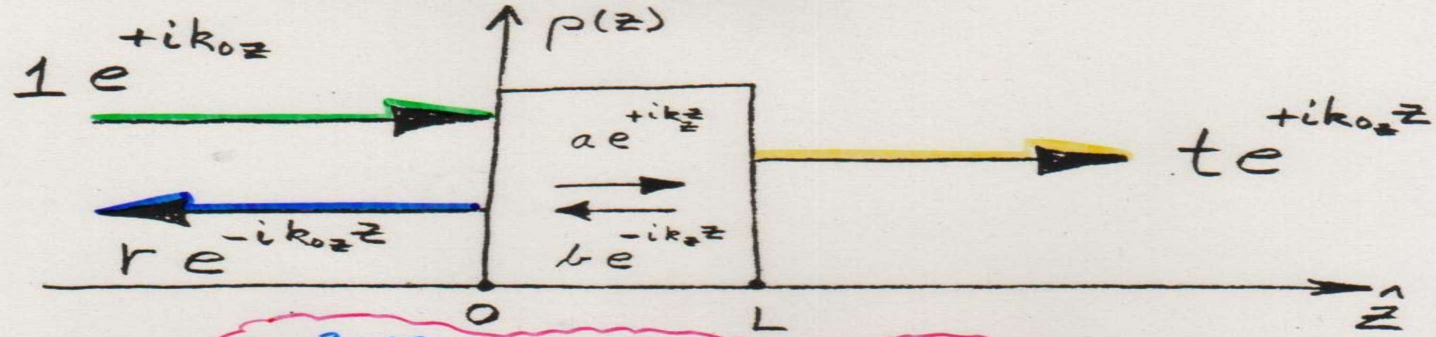

$$\frac{\partial^2 \psi(z)}{\partial z^2} + k_z^2 \psi(z) = 0$$

CONSERVATION OF MOMENTUM AND PARTICLE NUMBER REQUIRE THAT $\frac{\partial \psi}{\partial z}(z)$ AND $\psi(z)$

BE CONTINUOUS AT THE BOUNDARIES $z=0$ & $z=L$

$$\begin{pmatrix} t \\ it \end{pmatrix} e^{ik_{oz}L} = \begin{pmatrix} A & B \\ C & D \end{pmatrix} \begin{pmatrix} 1+r \\ i(1-r) \end{pmatrix}$$

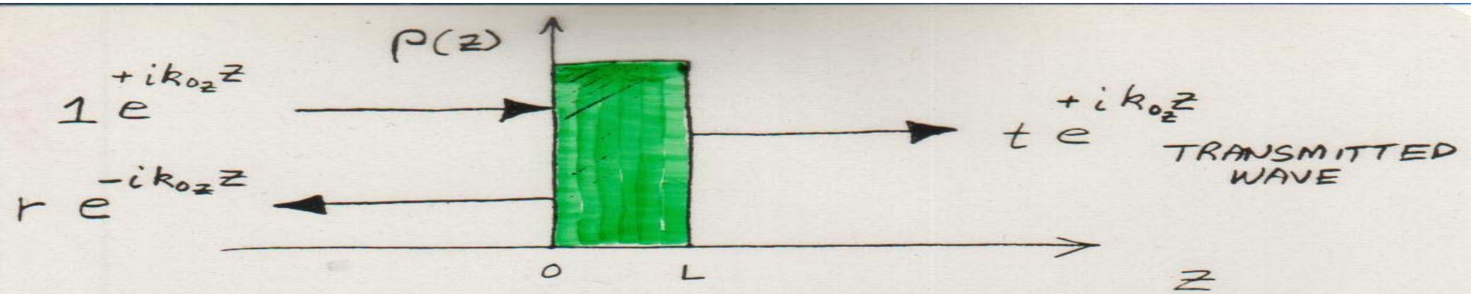

$$Q = 2k_{0z}$$

FROM THE WAVE EQUATION, IT IS POSSIBLE TO FIND A SOLUTION FOR THE REFLECTION AMPLITUDE IN INTEGRAL FORM (SEE ARTICLE PAGES) :

$$r(Q) = \frac{4\pi}{iQ} \int_{-\infty}^{+\infty} \Psi(z)\, \rho(z)\, e^{+ik_{0z}z}\, dz$$

WHAT IS LOCALIZED AT z IN THE SLD PROFILE $\rho(z)$ IN "REAL" SPACE, IS DISTRIBUTED OVER THE REFLECTION AMPLITUDE $r(Q)$ IN THE RELATED SCATTERING OR "RECIPROCAL" SPACE

Multilayer on Si

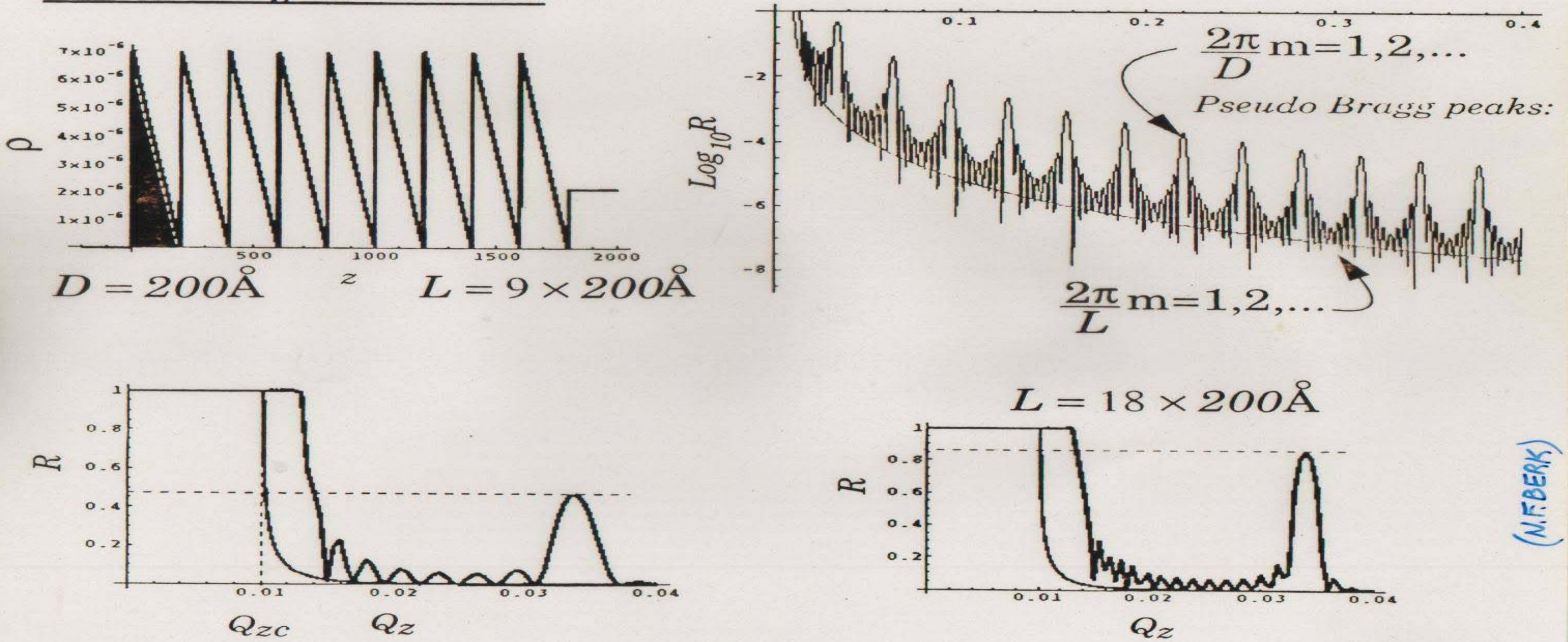

We would be better off if diffraction measured phase of scattering rather than amplitude! Unfortunately, nature did not oblige us.

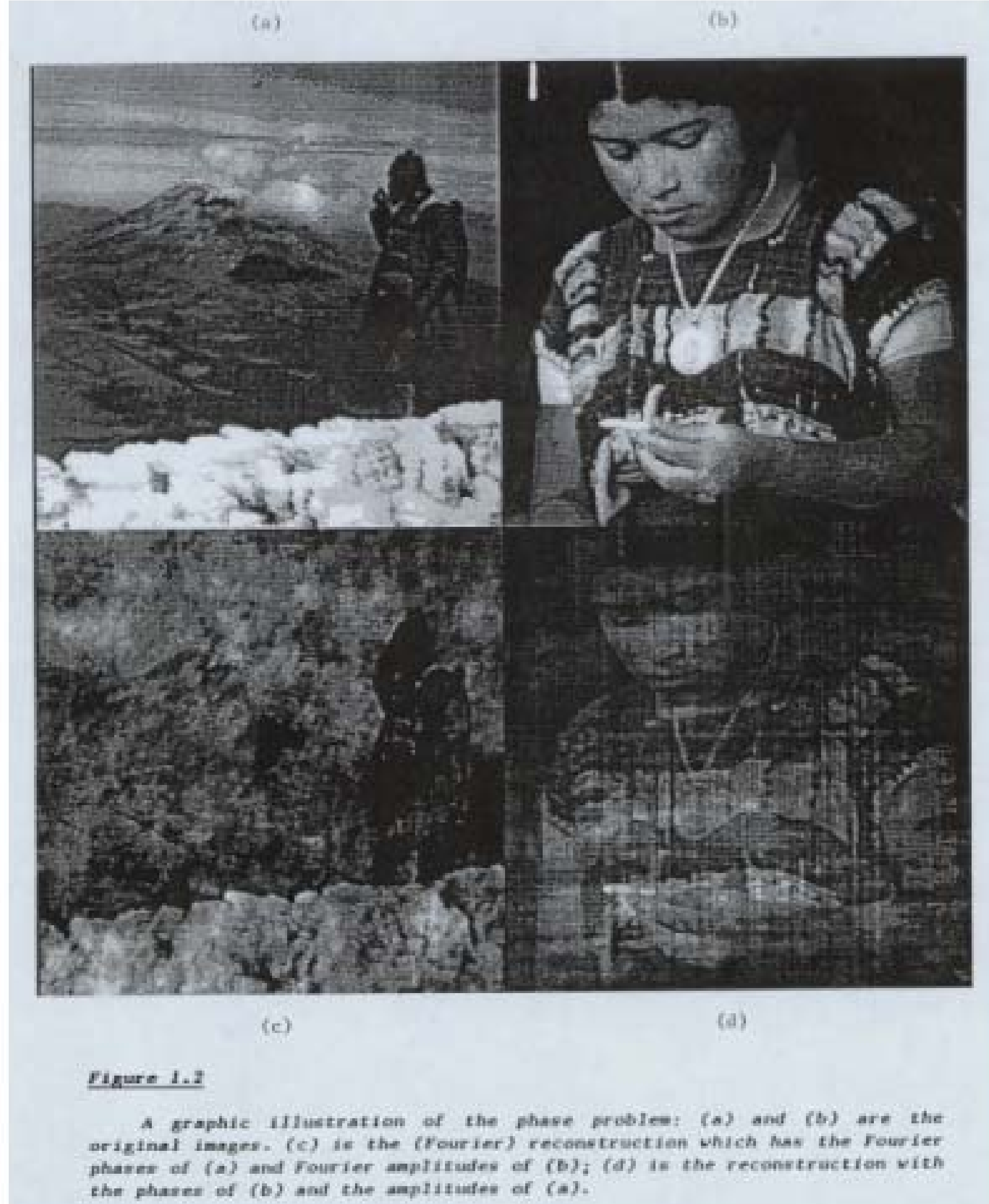

Picture by courtesy of D. Sivia

Calculation of Reflectivity

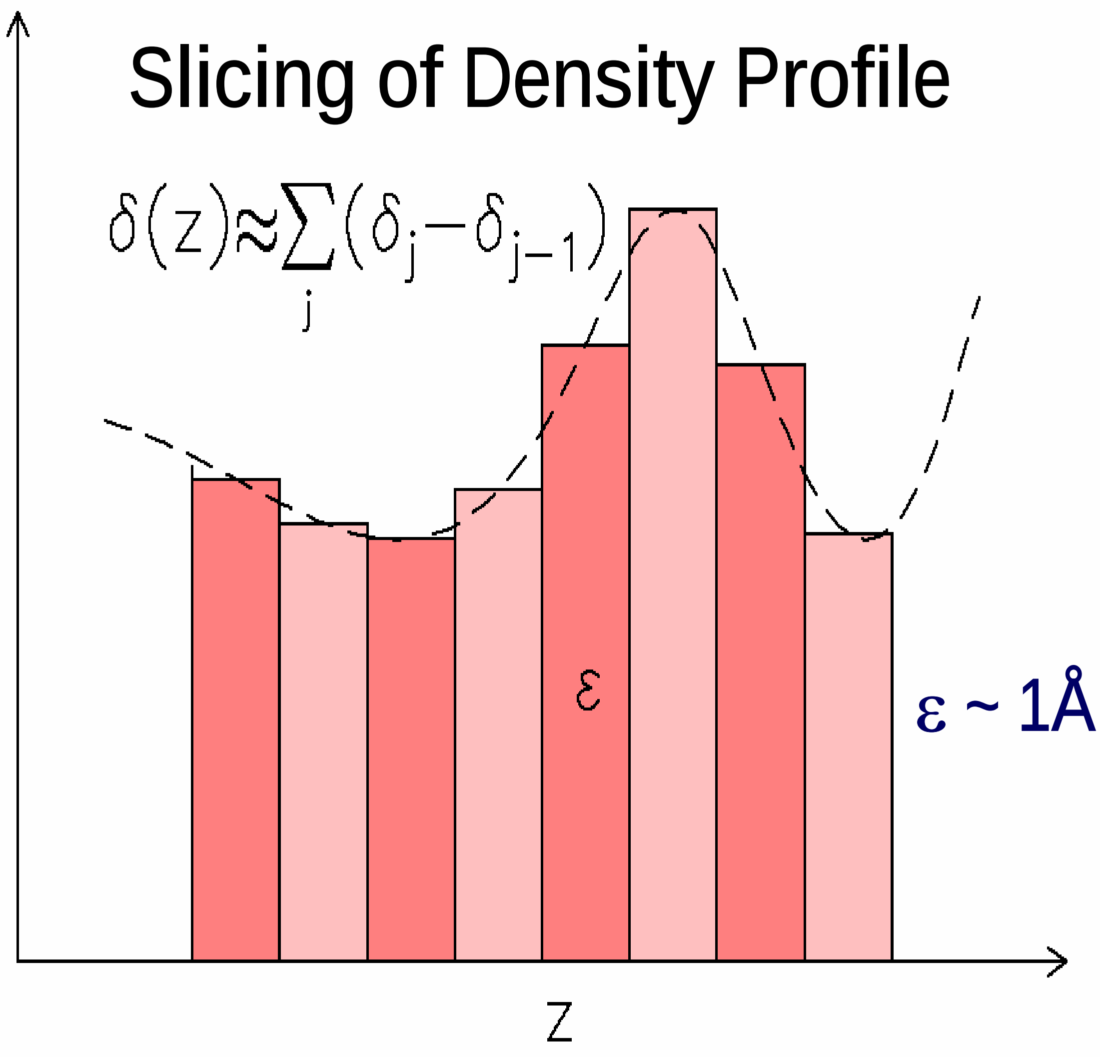

Slicing

&

Parratt-Iteration

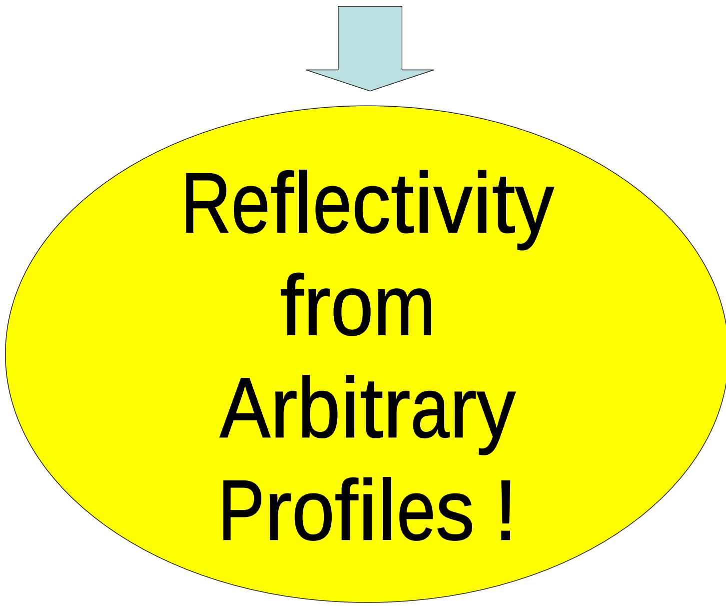

- Drawback:
  Numerical Effort !

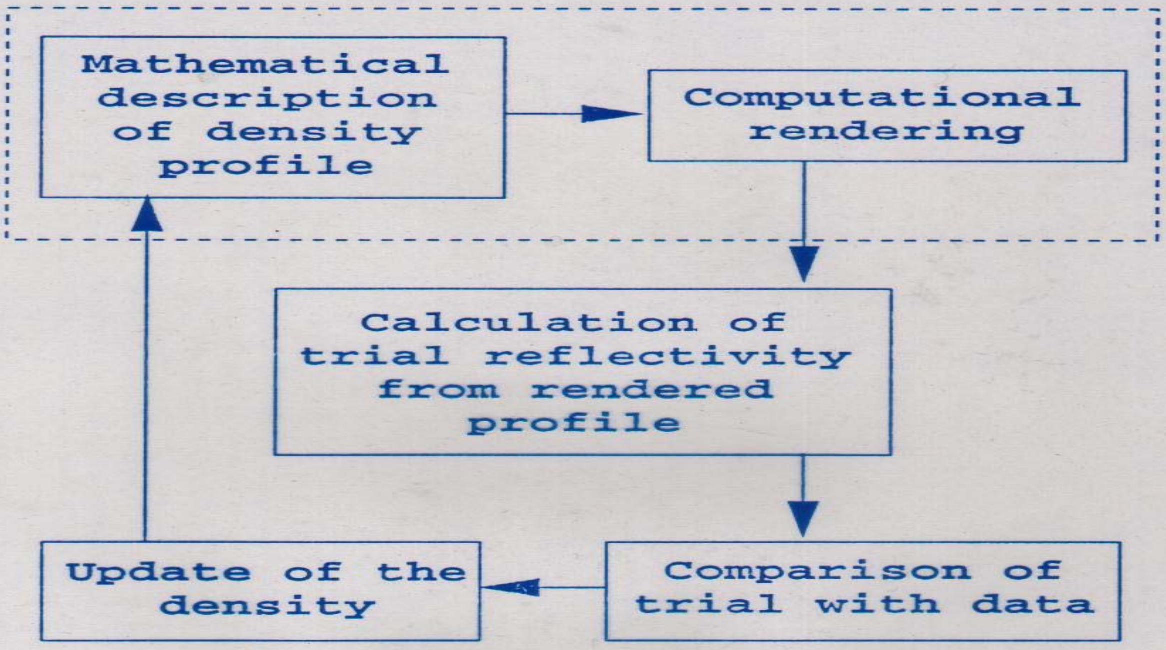

- BOTH MODEL-DEPENDENT & MODEL-INDEPENDENT FITTING METHODS CAN BE USED

(FIGURE AFTER BERK & MAJKRZAK)

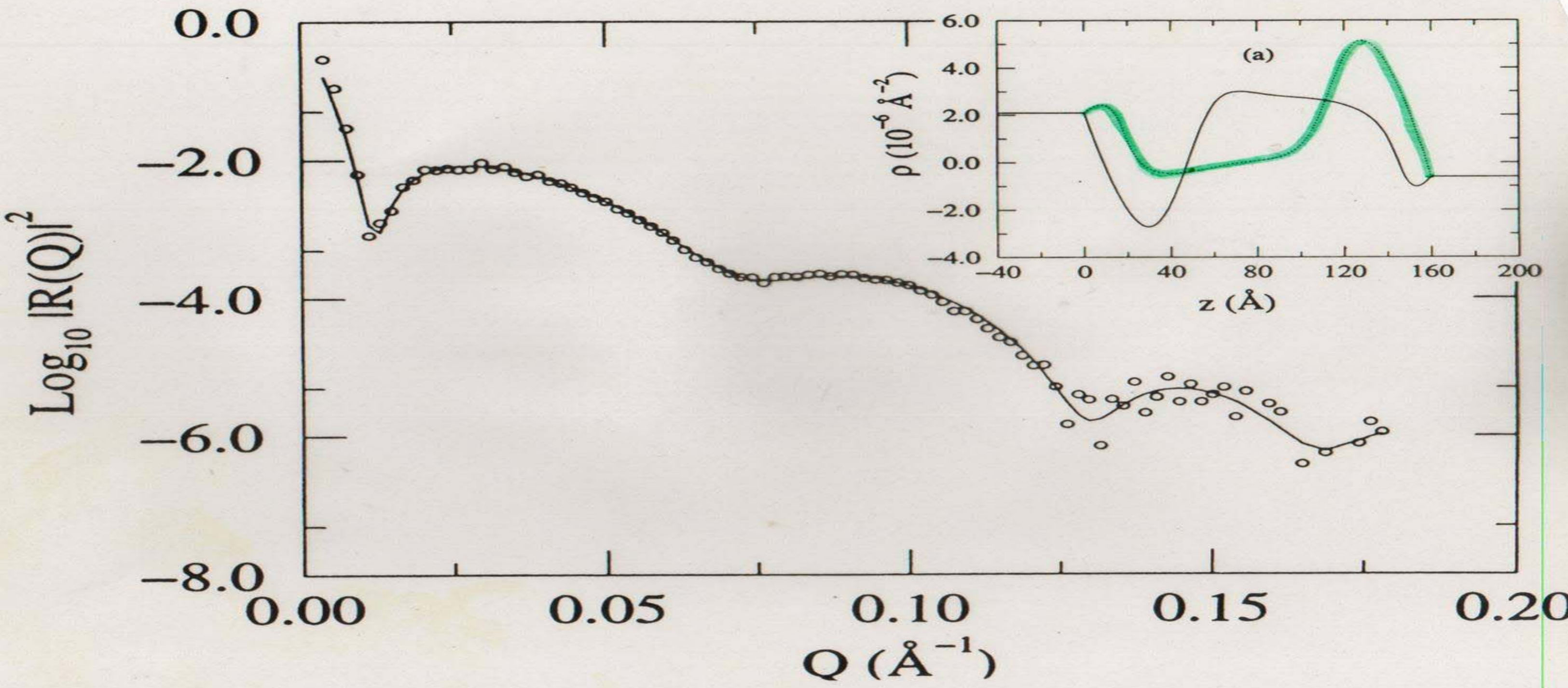

0.0
−2.0
−4.0
−6.0
−8.0
Log10 |R(Q)|2
0.00
0.05
0.10
0.15
0.20
Q (Å−1)
(a)
6.0
4.0
2.0
0.0
−2.0
−4.0
ρ (10−6 Å−2)
−40
0
40
80
120
160
200
z (Å)

International School of Neutron Scattering
"Francesco Paolo Ricci"

September 25- October 6, 2006

Polarized Neutron Reflectometry

Gian Piero Felcher,
Argonne National Laboratory

Artwork prepared with the help of:

Chuck Majkrzak
Sunil Sinha
Suzanne te Velthuis
Frank Klose
Hartmut Zabel

Polarized neutron reflectometry
2. Magnetic surfaces and multilayers

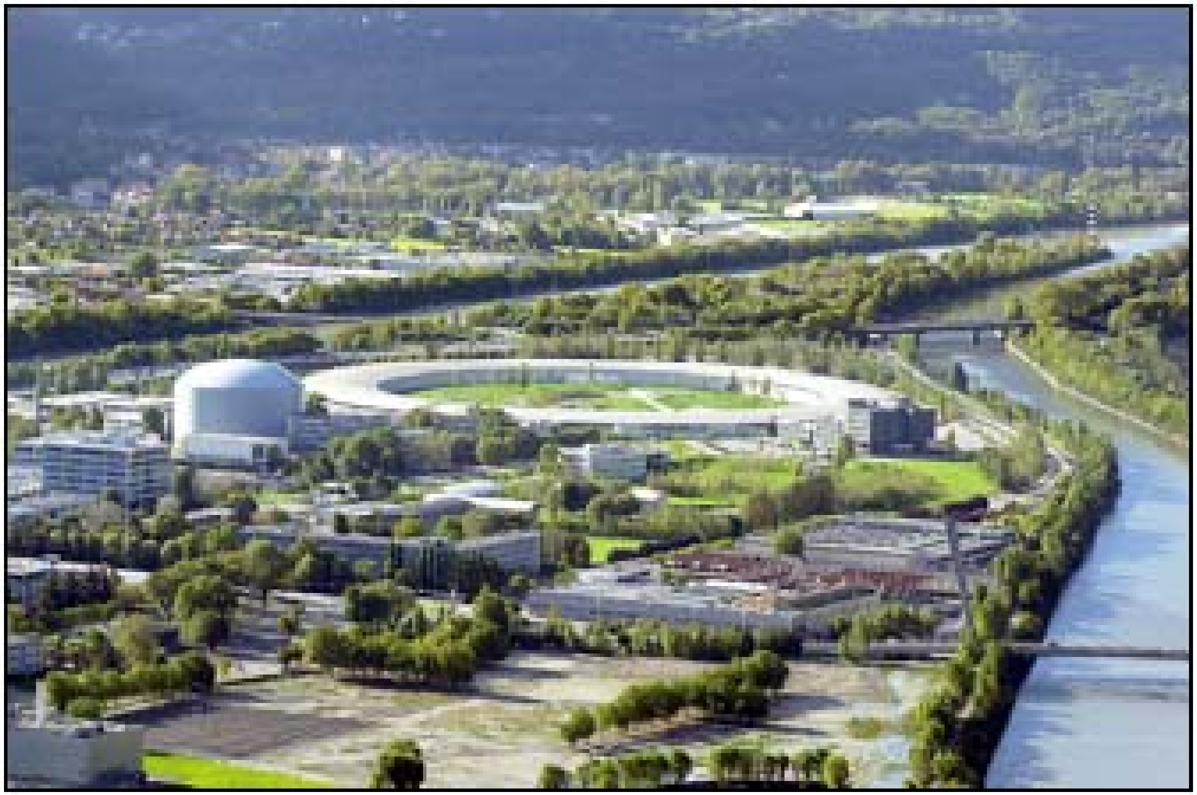

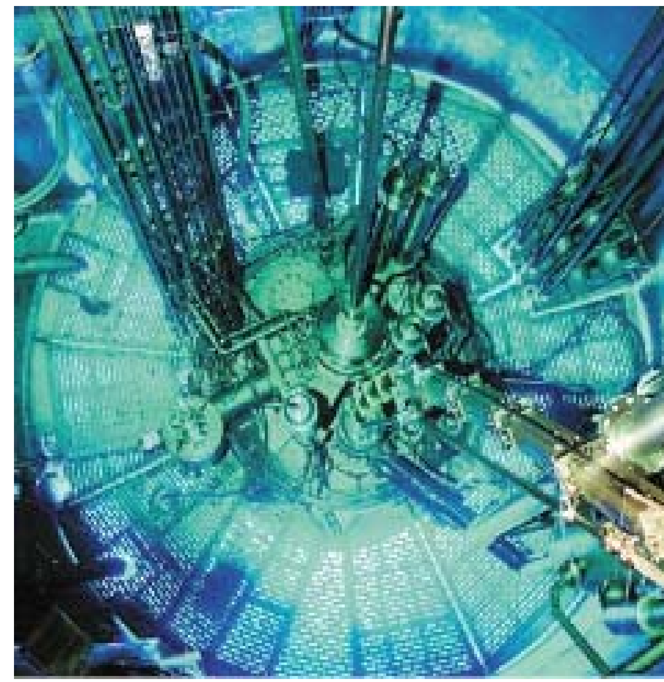

The ILL/ESRF complex in Grenoble. Reactor core

RKKY INTERACTION IN MULTILAYERS

Interlayer exchange coupling

• Period of oscillations is related to spanning vectors of the Fermi surface of the

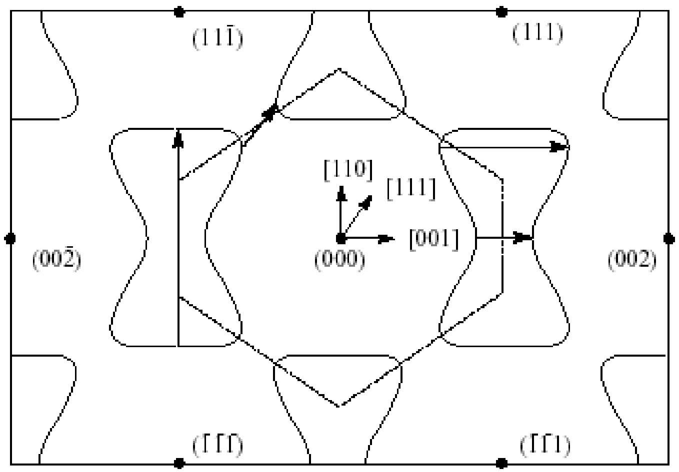

P. Bruno, J. Phys. Condens. Matter 11 (1999) 9403

• Long period (≈18Å, Fe/Cr)

• Short period (≈2Å, Fe/Cr)

  • Only observed for very smooth interfaces

Review: M.D. Stiles JMMM 200 (1999) 322

QuickTime™ and a
TIFF (LZW) decompressor
are needed to see this picture.

Coupling strength period

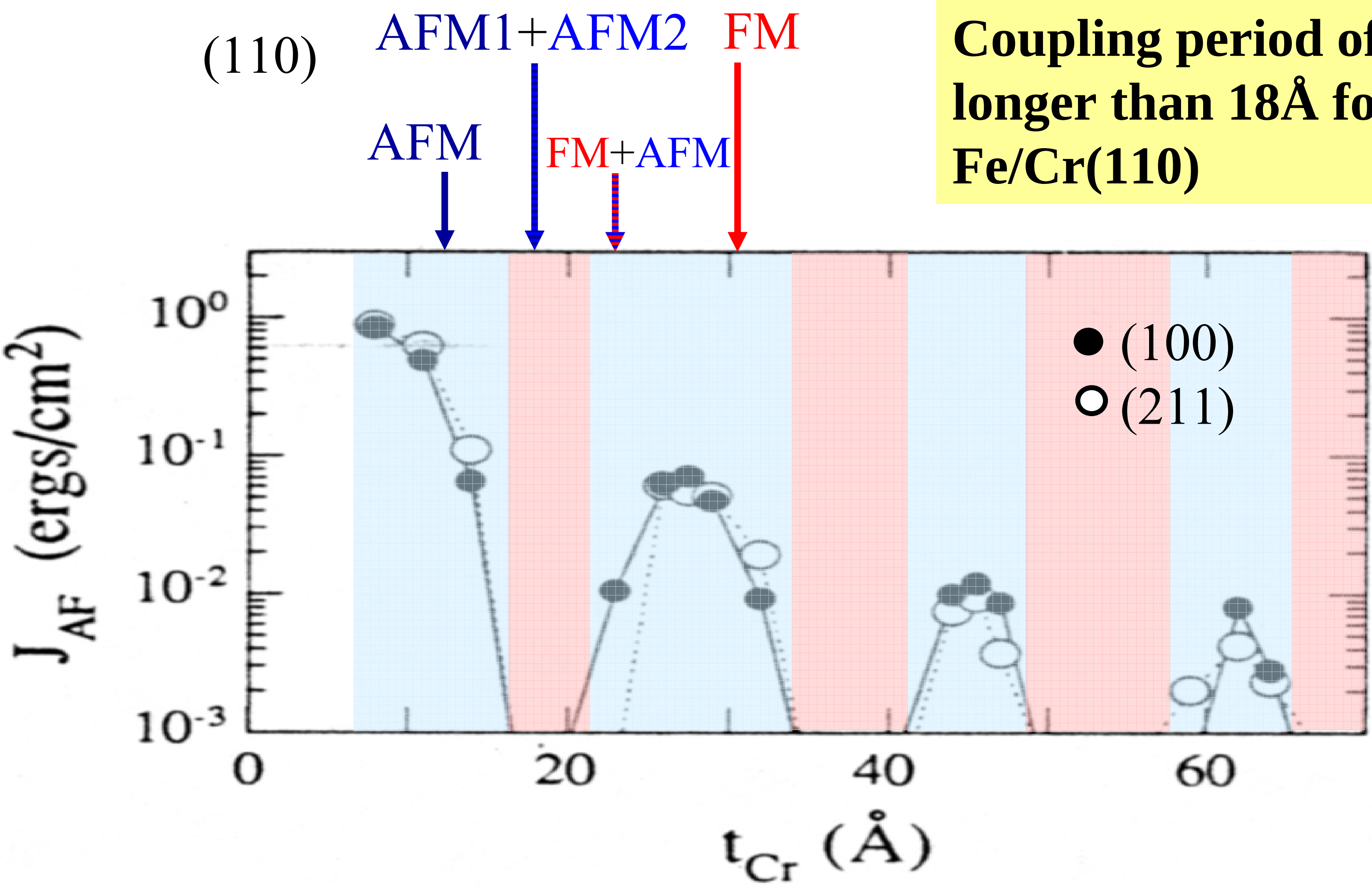

Coupling period of is longer than 18Å for Fe/Cr(110)

QuickTime™ and a
TIFF (LZW) decompressor
are needed to see this picture.

Interlayer exchange coupling

The exchange coupling *J* between ferromagnetic layers across a non-ferromagnetic spacer is oscillatory.

• Ferromagnetic coupling

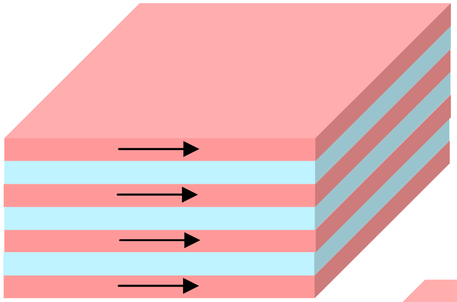

•Antiferromagnetic coupling

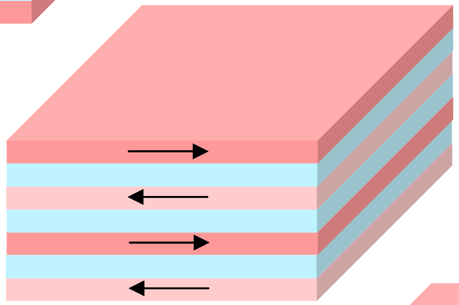

• Biquadratic coupling

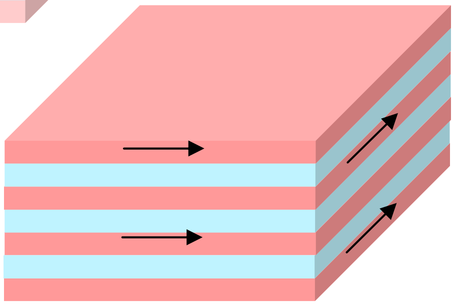

Reflectivity

$$k_z = \sqrt{k_{zo}^2 - 4\pi(b/V)}$$

$$q_z = 2k_{zo}$$

$$k_z^{\pm} = \sqrt{k_{zo}^2 - 4\pi[(b/V) \pm cB]}$$

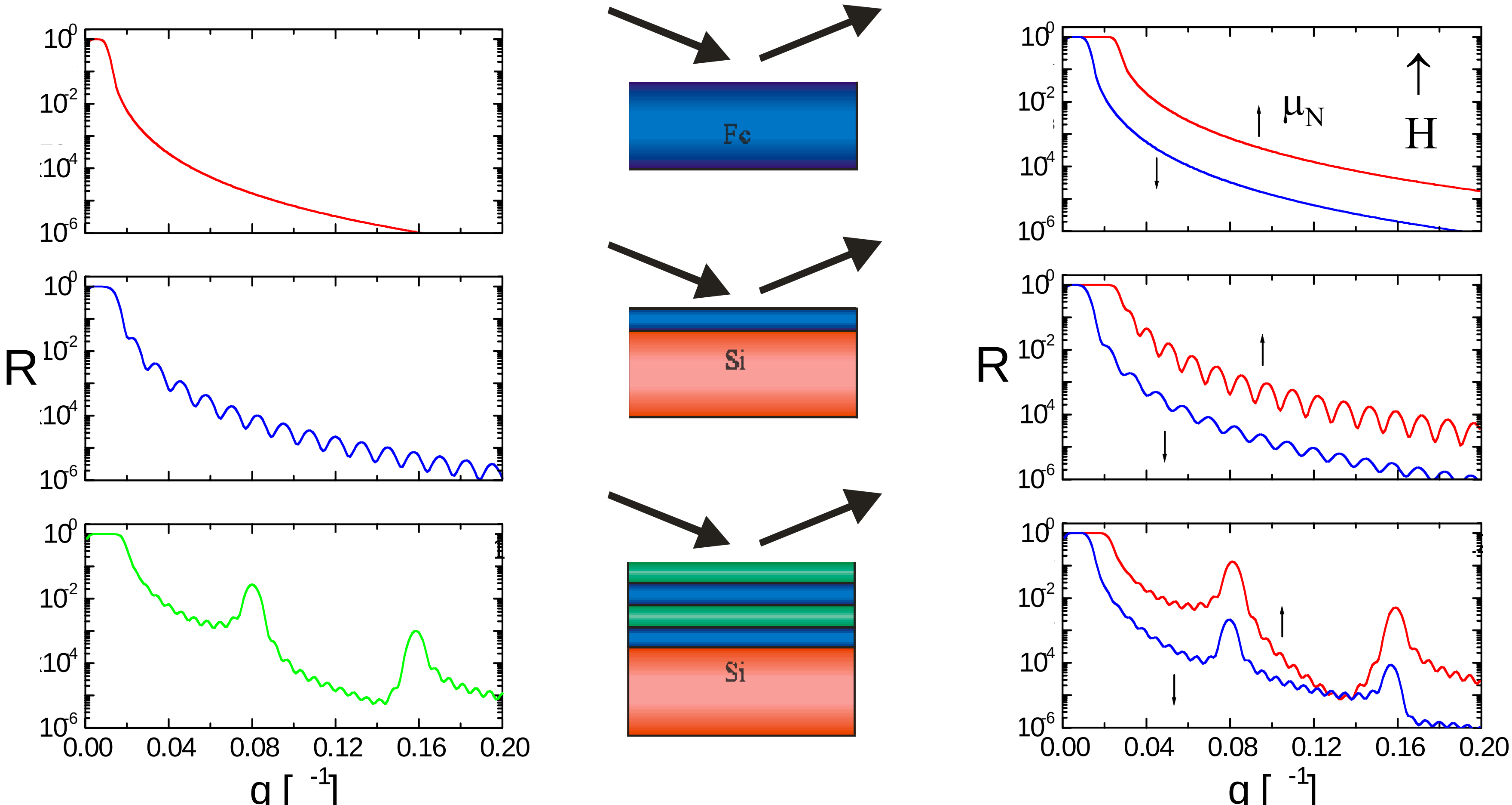

Courtesy of F. Klose

The Filter/Collimation System of POSY I

Neutron spectrum of POSY I: 2.5 Å > λ > 14 Å

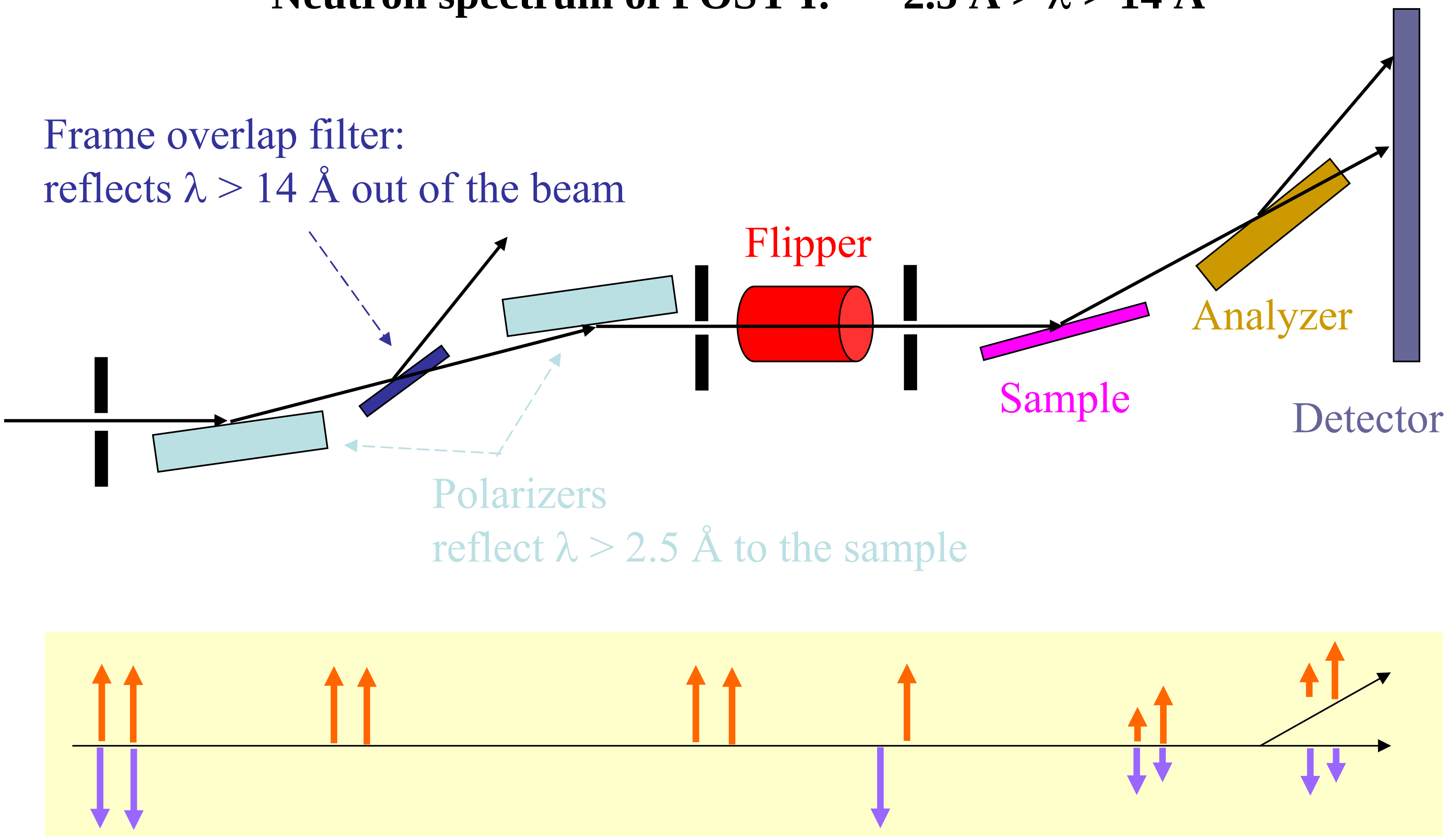

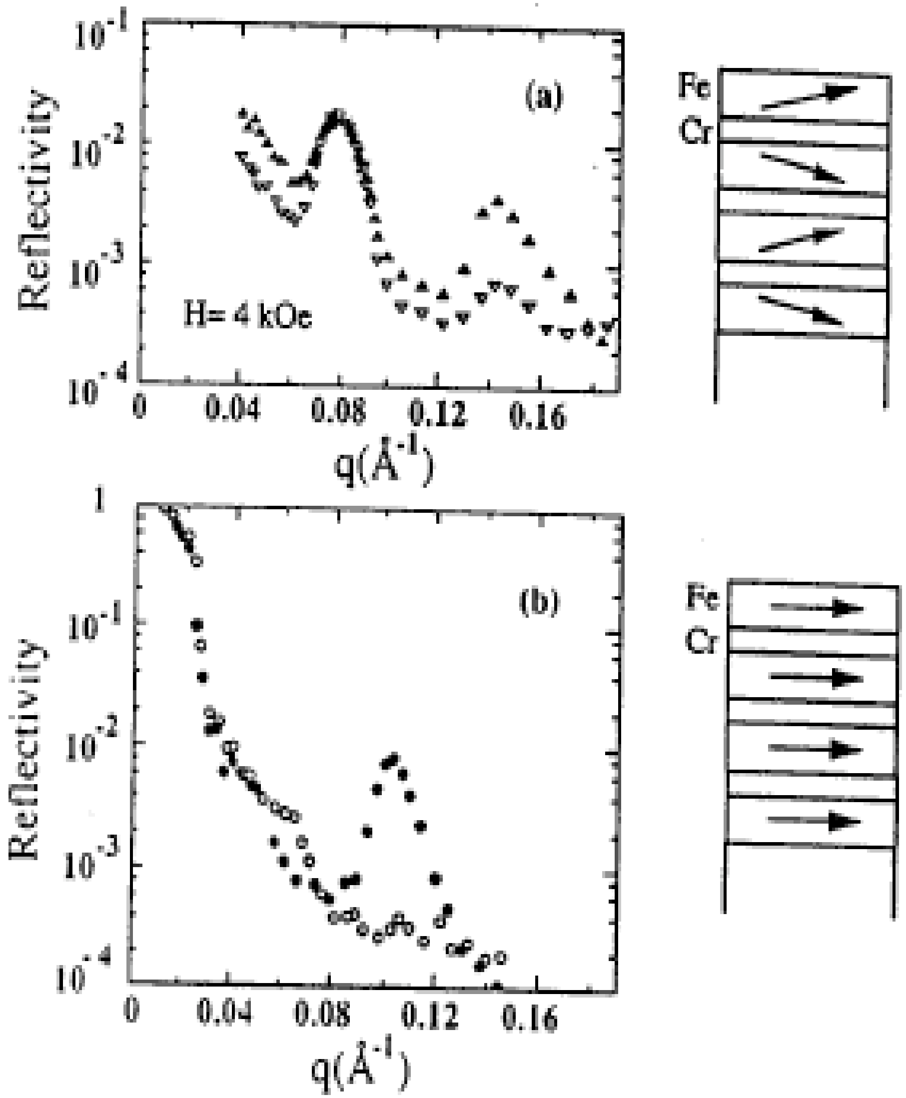

S.S.P. Parkin et al, APL 58, 1473 (1991)

Fig. 6. (a) PNR of $\{Fe(32\,Å)/Cr(10\,Å)\}_{20}$ in a magnetic field of 4 kOe. Solid triangles: spin +. Open triangles: spin −. The magnetic moments of the Fe layers are canted, and the AF component gives rise to the spin-independent peak at $q = 0.08\,Å^{-1}$, the F component to the peak at $q = 0.143\,Å^{-1}$. (b) Effect of the magnetic field on the AF peak of $\{Fe(20\,Å)/Cr(10\,Å)\}_{20}$. Solid dots: spin averaged reflectivity at $H = 4$ kOe. A field of 14 kOe saturates the sample, causing the disappearance of the AF peak at $q = 0.11\,Å^{-1}$ (open dots) (see ref. [43]).

Polarized Neutron Reflectivity

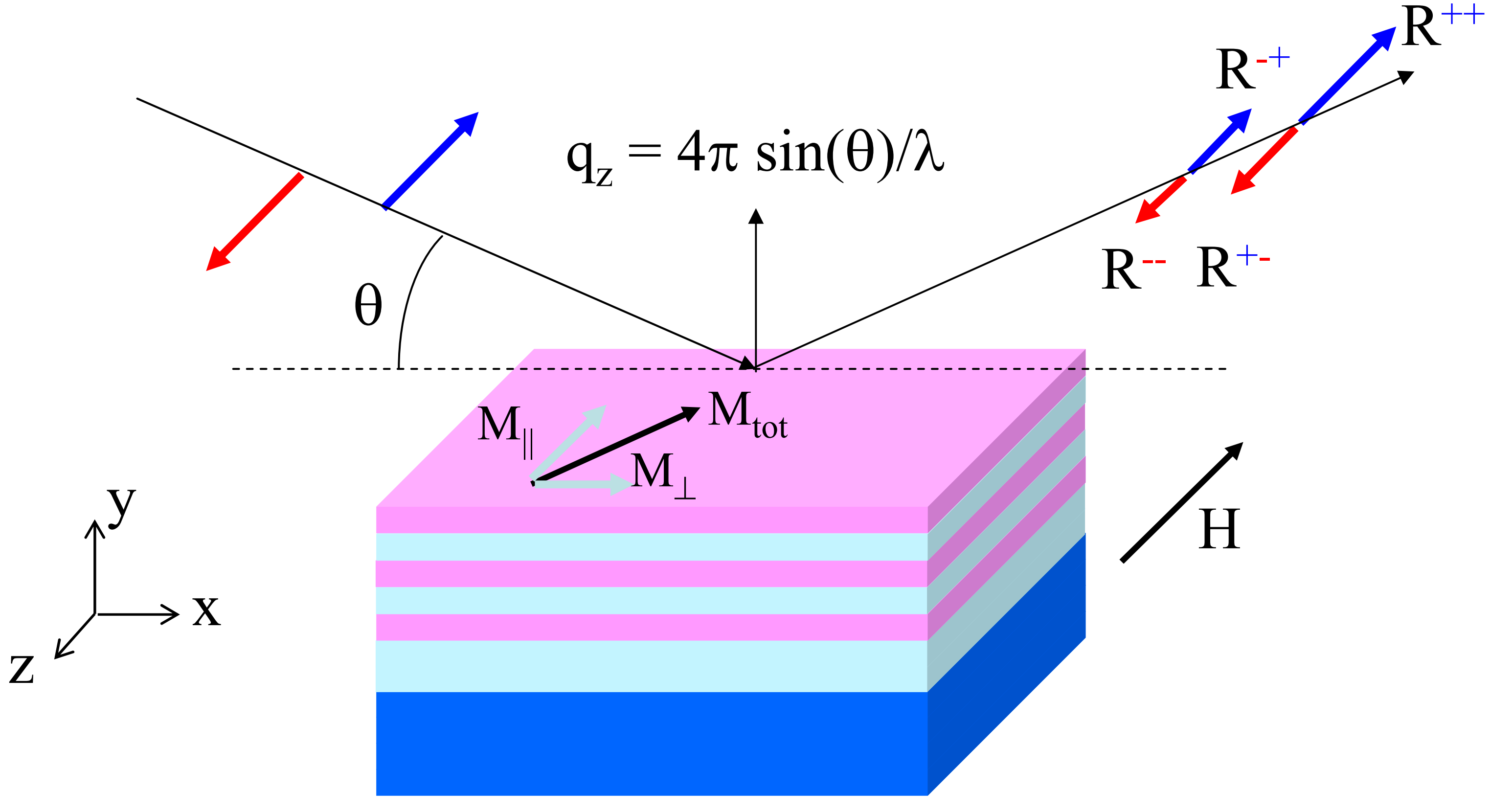

$(R^{++} - R^{--}) \propto M_{\|}$

$R^{-+} = R^{+-} \propto M_{\perp}^{2}$

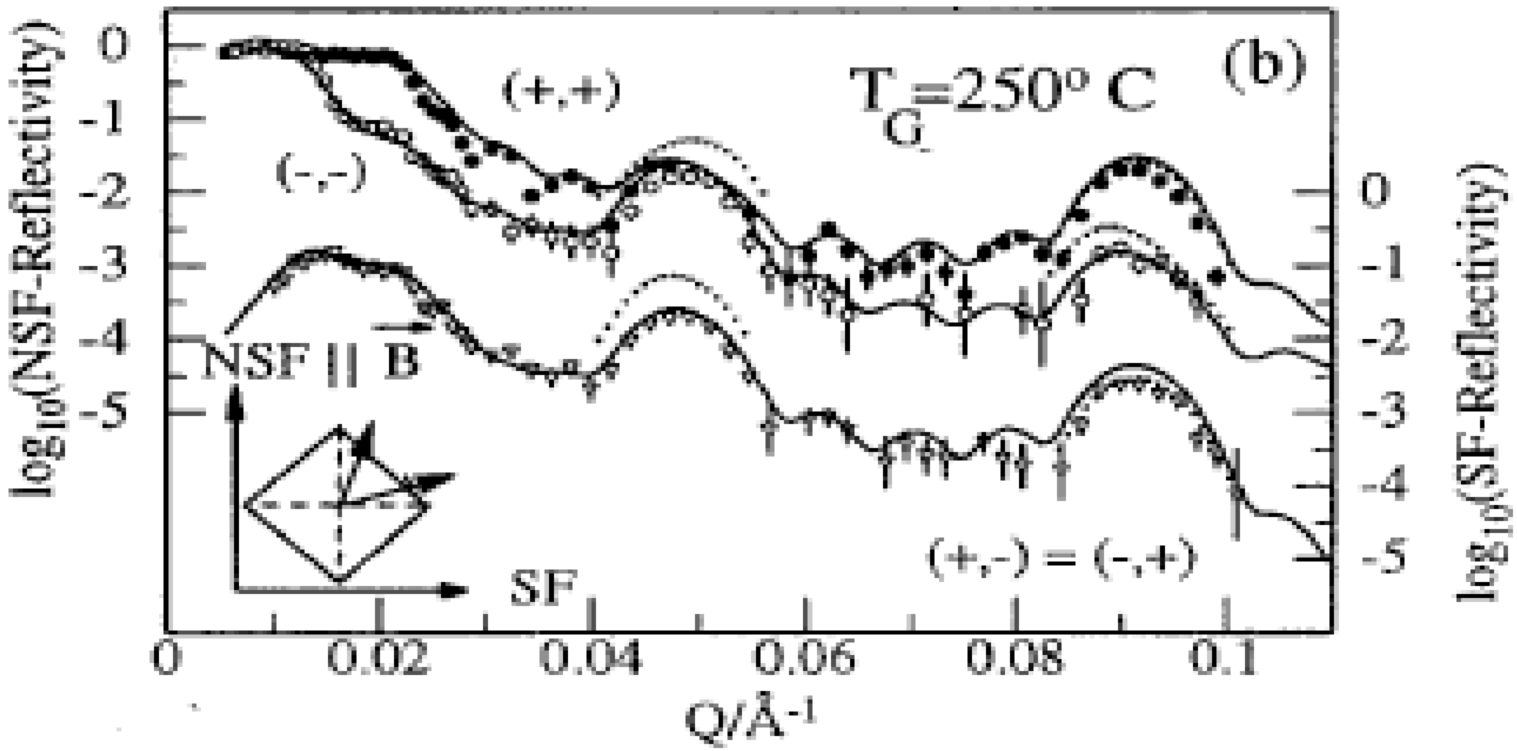

Fig. 3. Spin-polarized neutron reflectivity measured in remanence for a superlattice [Fe(52 Å)/Cr(17 Å)]. The sample exhibits strong spin–flip scattering which, when modeled with the non-spin–flip intensity, reveals that successive Fe layers align symmetrically with respect to the sample anisotropy axes forming an angle of 50°.

A. Schreyer et al, PRB 52, 16066 (1995)

Fe/Nb: reduction of the exchange by charging with hydrogen
F. Klose et al, PRL 78,1150 (1997)

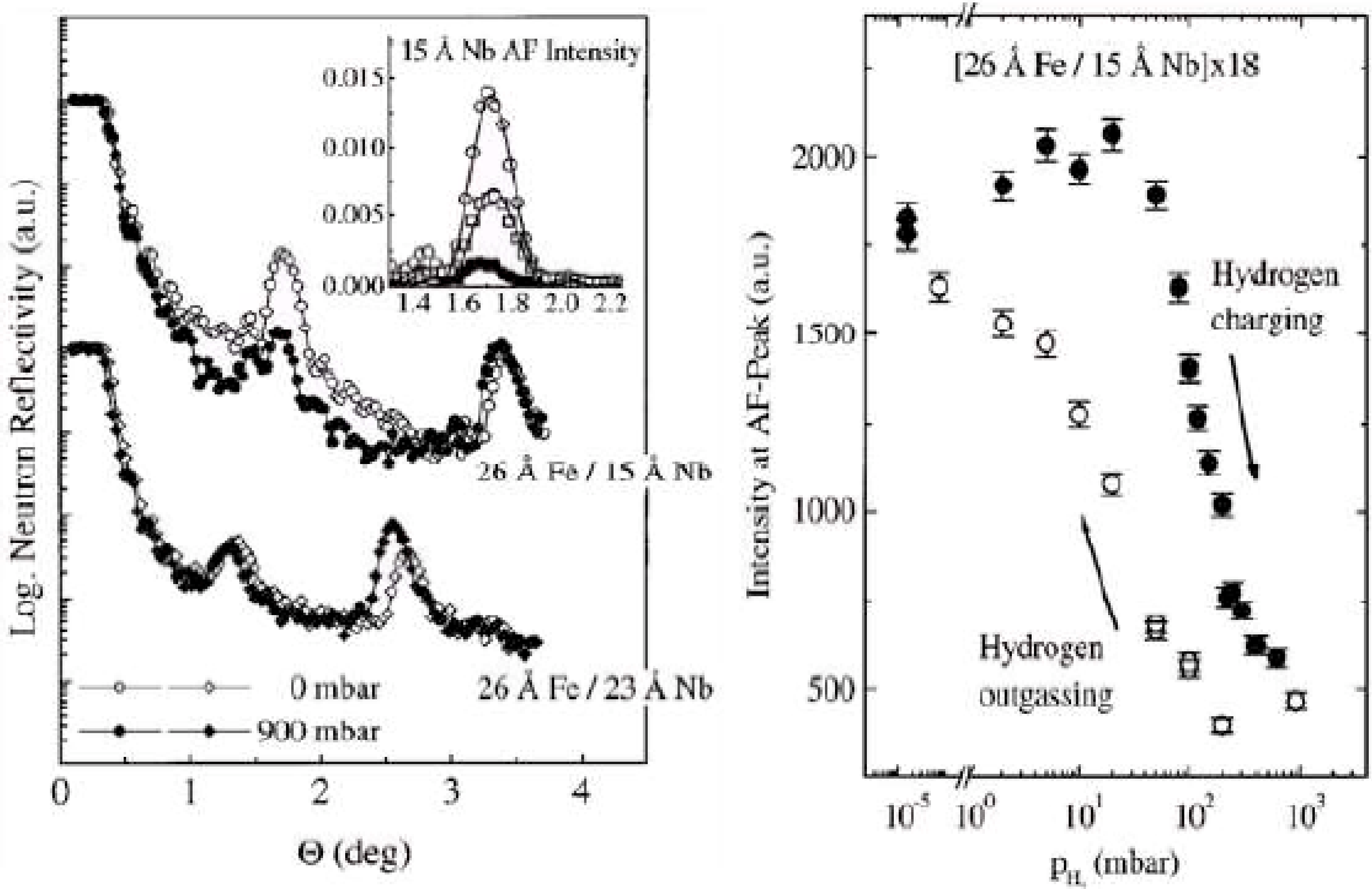

SPIN-FLOP TRANSITION IN MULTILAYERS

Spin-flop Transition in Bulk Antiferromagnets

- A bulk antiferromagnet undergoes a 1st order "spin-flop" transition if a sufficiently high field is applied along the easy-axis
  - First predicted by L. Néel
    Ann. Phys. (Paris) **5** (1936) 232
- Spin-flop:
  - Reorientation of AF component perpendicular to easy-axis
  - Finite magnetization along field

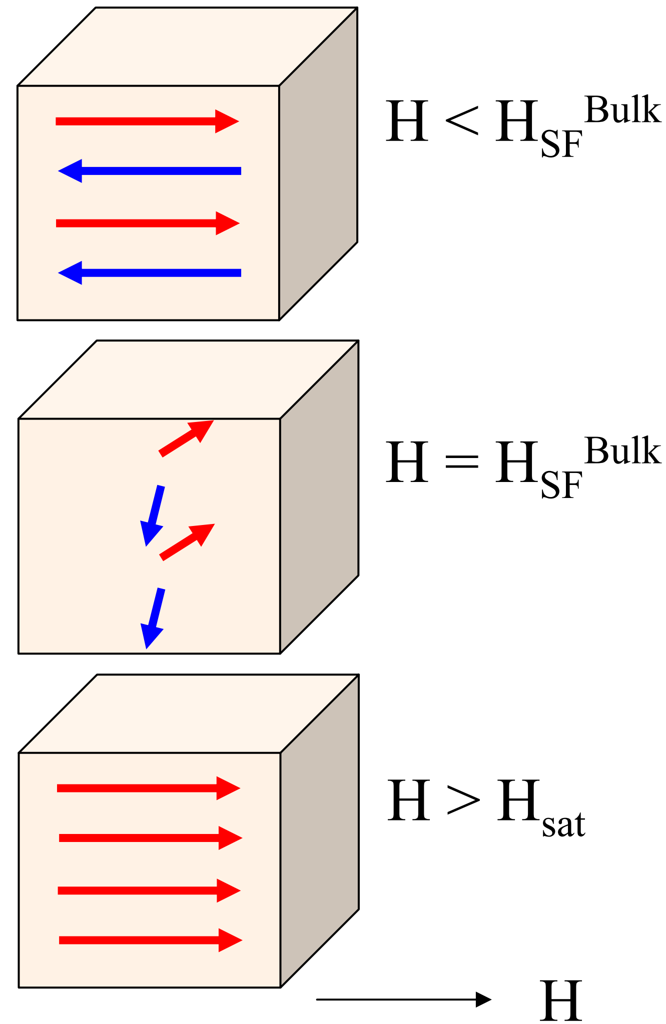

Spin-flop Transition in Finite Antiferromagnets

- In a finite AFM there is a surface spin-flop transition at a field below the bulk spin-flop transition.

  D.L. Mills and W.M. Saslow, Phys. Rev. **171** (1968) 488

- Spins near the surface rotate into a flopped state and creating an AF domain wall.
- The wall penetrates through the system until it reaches the center
- The spin-flopped region expands throughout.

  F. Keffer and H. Chow, PRL **31** (1973) 1061

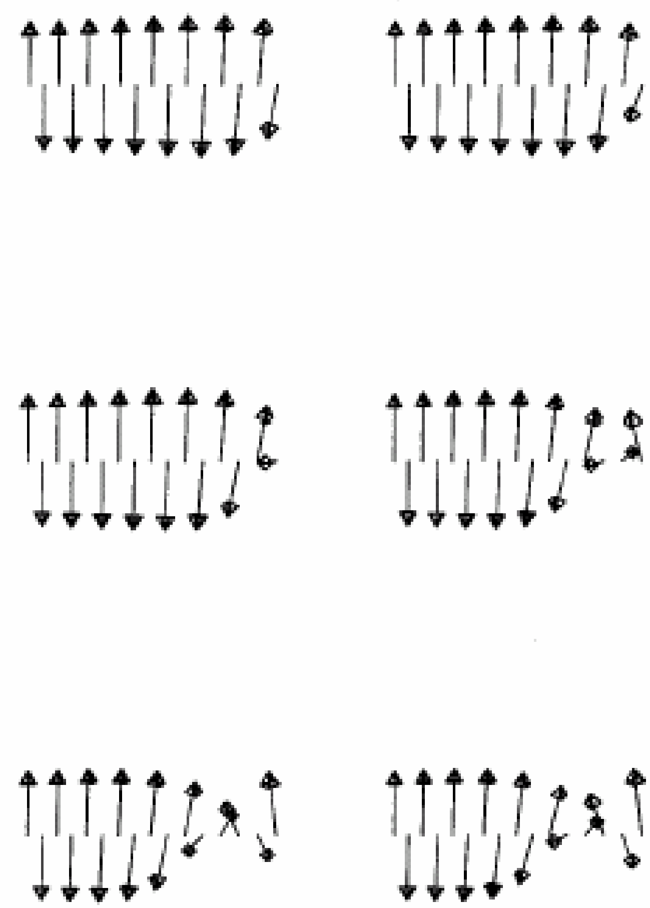

S.Rakhmanova, *et al.*, PRB **57** (1998) 476

Spin-flop Transition in Finite Antiferromagnets

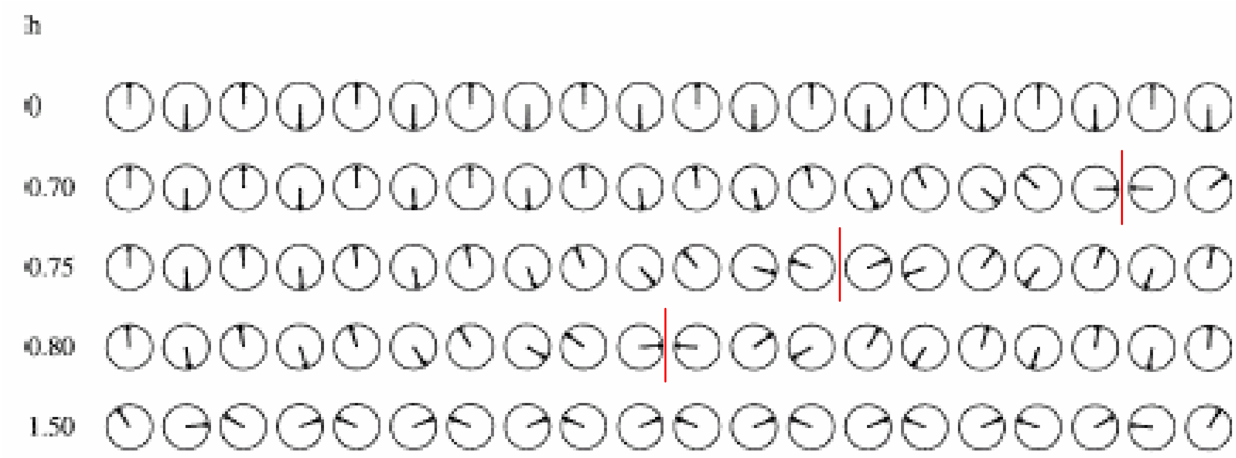

N. Papanicolaou,
J. Phys.: Condens. Matter **10**, L131 (1998)

- Wall divides system in two (anti-phase) domains separated by a "discommensuration"
  C. Micheletti *et al.* PRB **59** (1999) 6239

- Domain wall moves toward center by pairs of layers switching
  L. Trallori, PRB **57** (1998) 5923

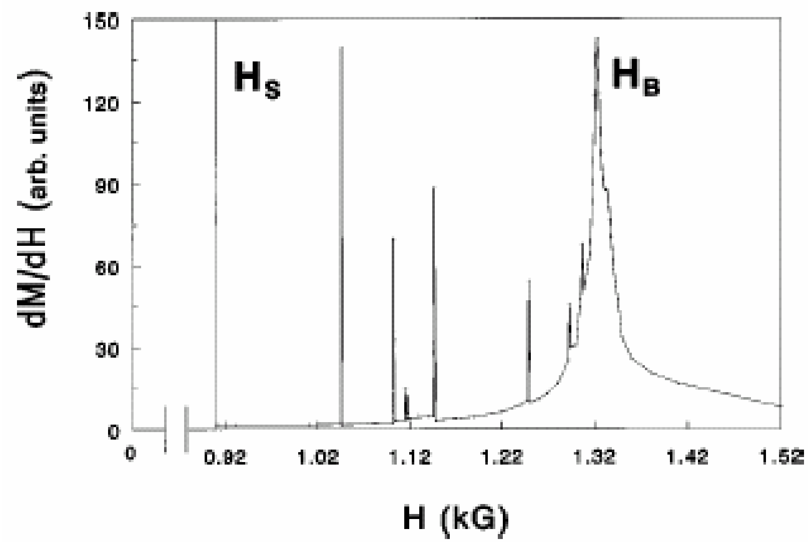

Experimental Evidence of Surface Spin-Flop Transition

• Fe/Cr(211) superlattice used as template for finite uniaxial antiferromagnet

• Comparison between MOKE and SQUID confirmed surface-initiated spin-flop transition

R.W. Wang *et al.* PRL **72** (1994) 920

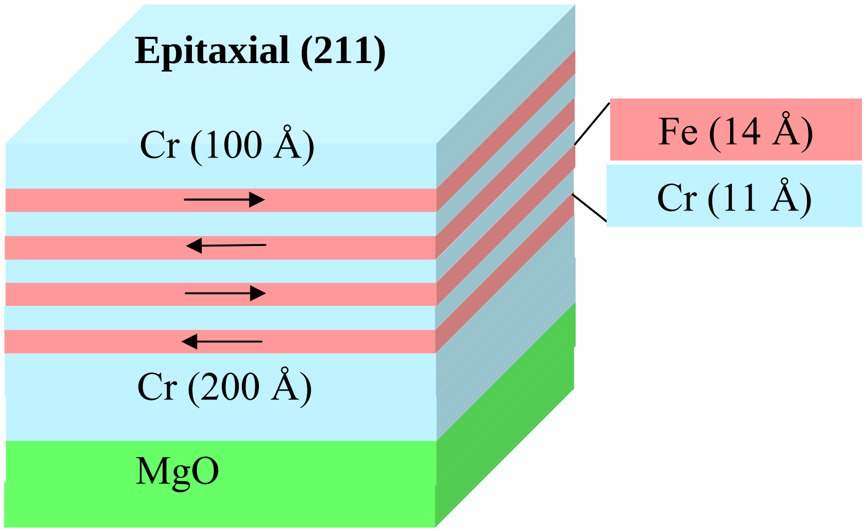

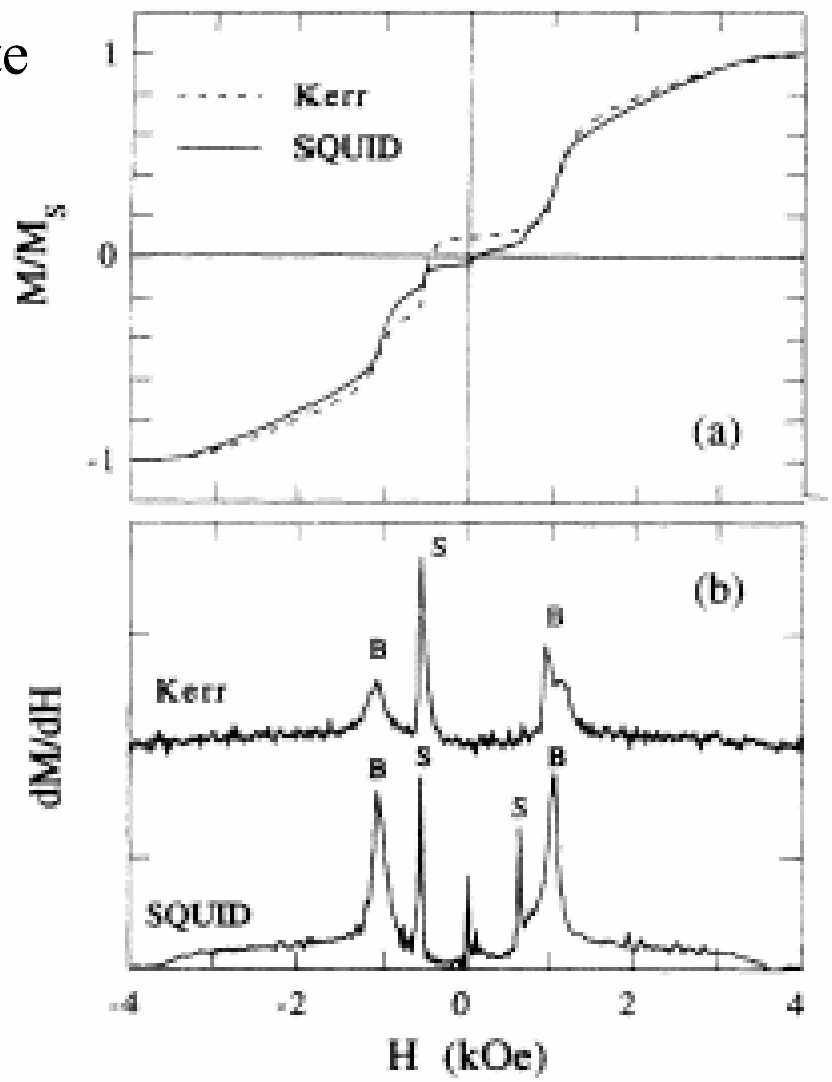

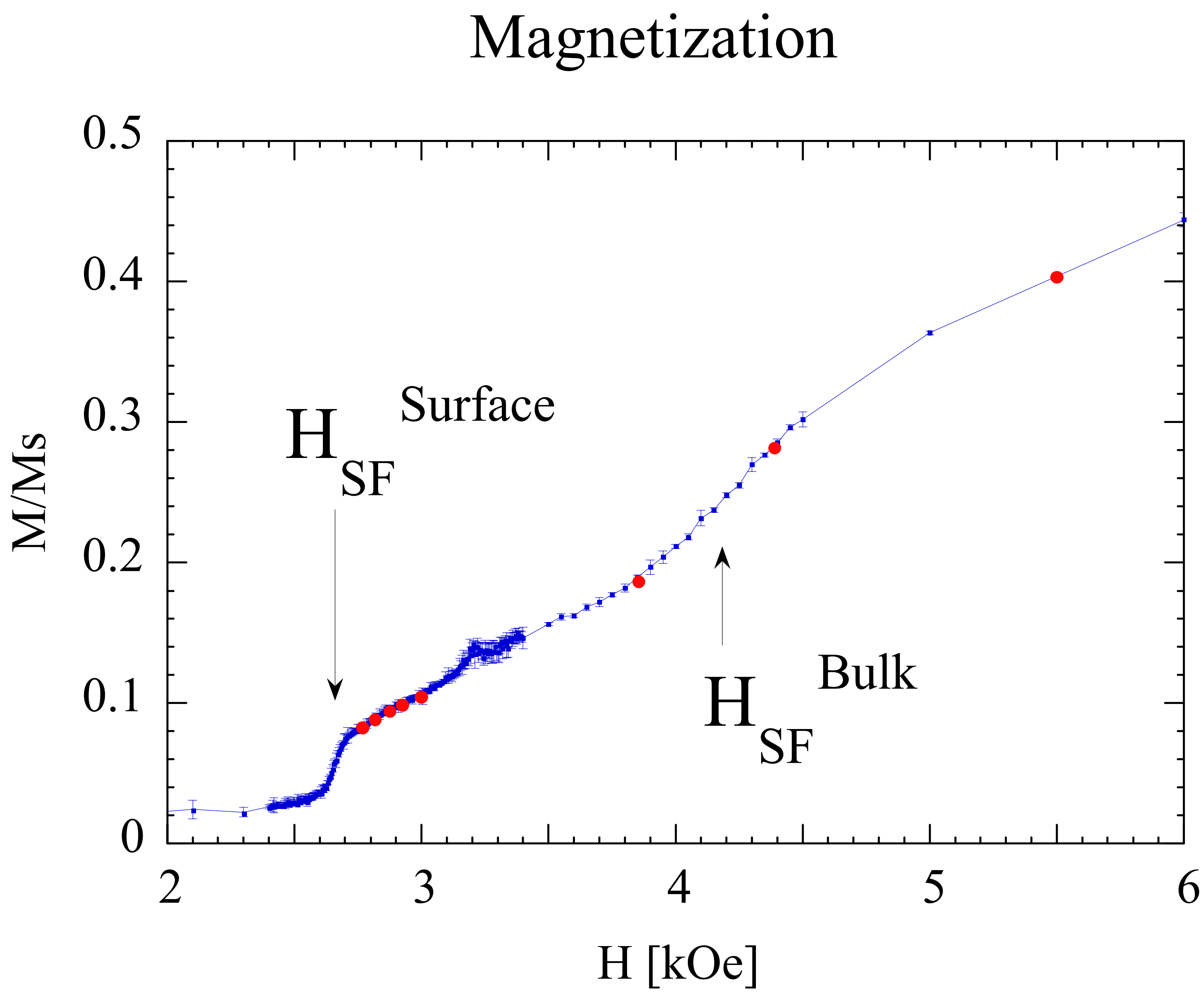

Magnetization
M/Ms
H [kOe]
0.5
0.4
0.3
0.2
0.1
0
2
3
4
5
6
H SF Surface
H SF Bulk

Polarized Neutron Reflectivity Experiment

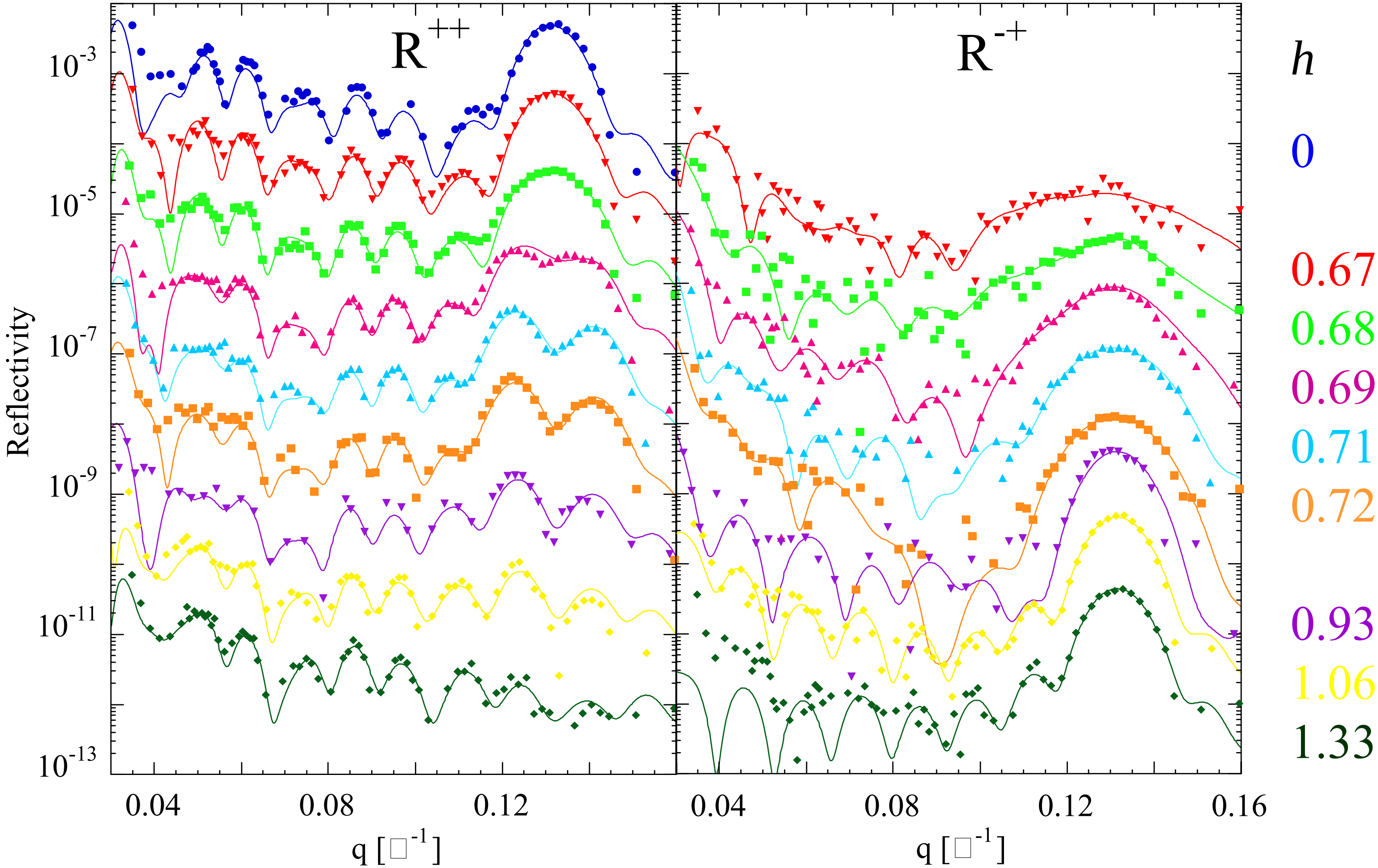

Bragg Peak Intensities

Simple AFM ordering

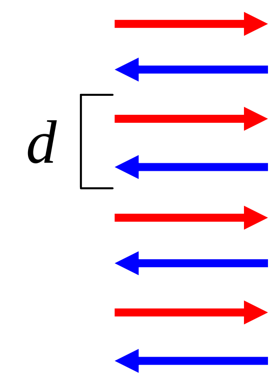

$$R \propto a^2 \left\{ \frac{\sin[qd\,2N/2]}{\sin[qd/2]} \right\}^2$$

Max. at: $q_B = 2\pi/d$

Min. at $(q - q_B) = \pm[1/(2N)]2\pi/d$

Anti-phase domain

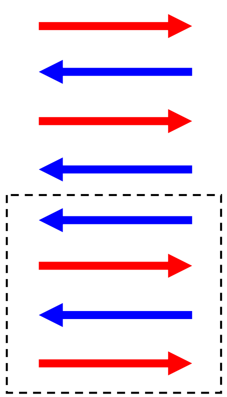

$$R \propto a^2 \left\{ \frac{\sin[qdN/2]}{\sin[qd/2]} \right\}^2 \times \cos^2[qd(N/2 + 1/4)]$$

Min. at: $q = q_B$

Max. at: $(q - q_B) \approx \pm[1/N]2\pi/d$

Polarized Neutron Reflectivity Experiment

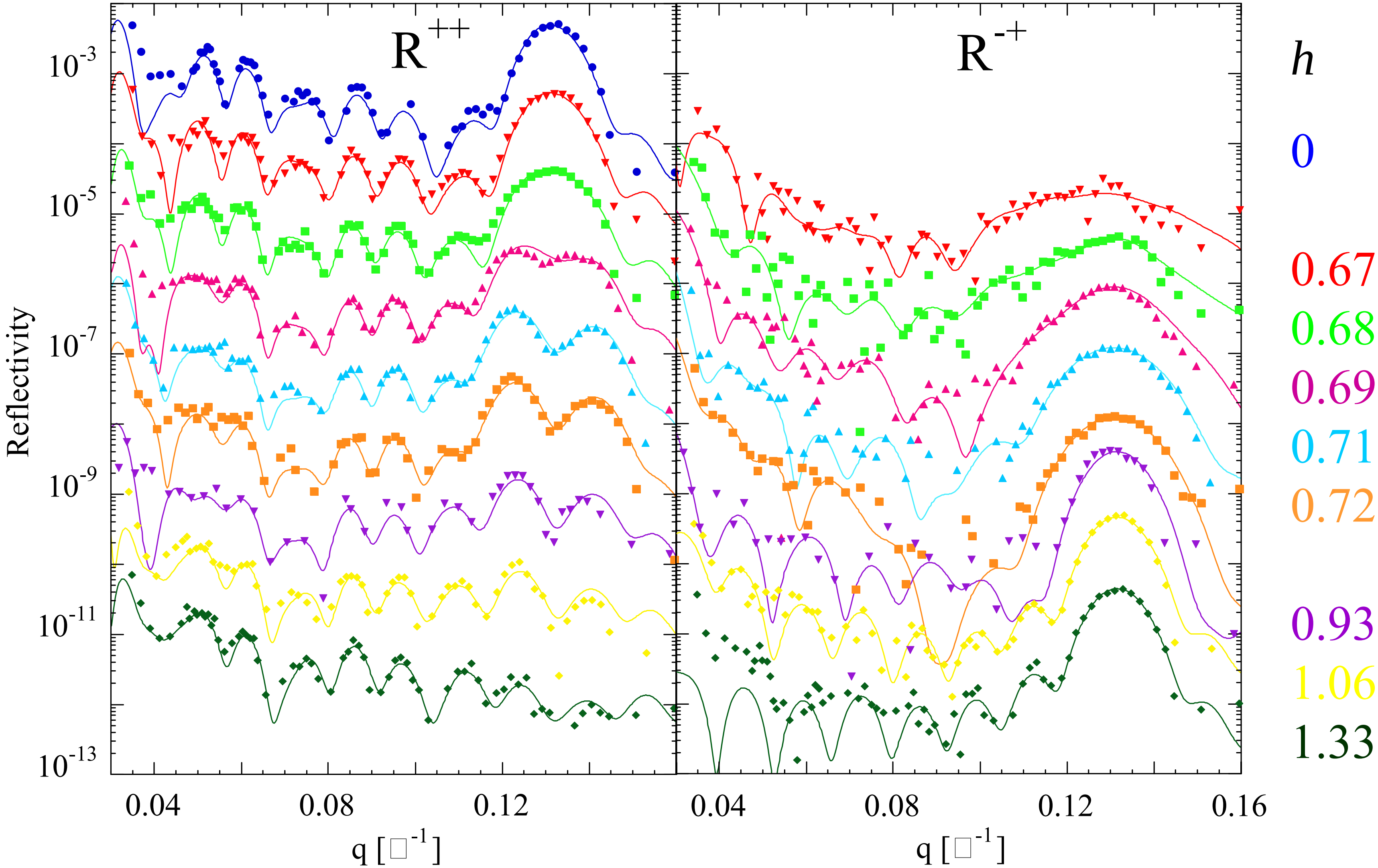

Analysis of Bragg Peak

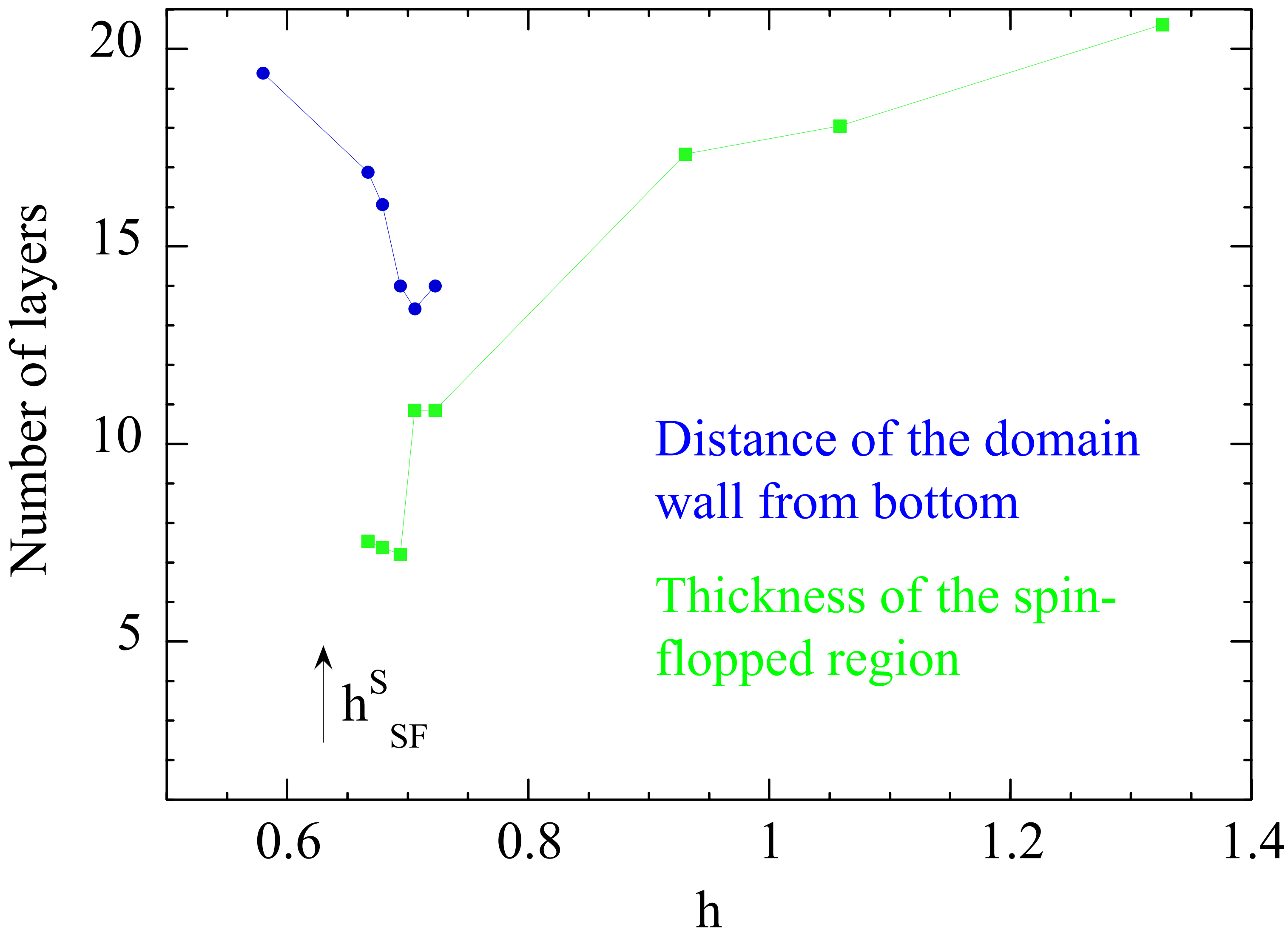

Evolution of Magnetization

SPRING MAGNETS

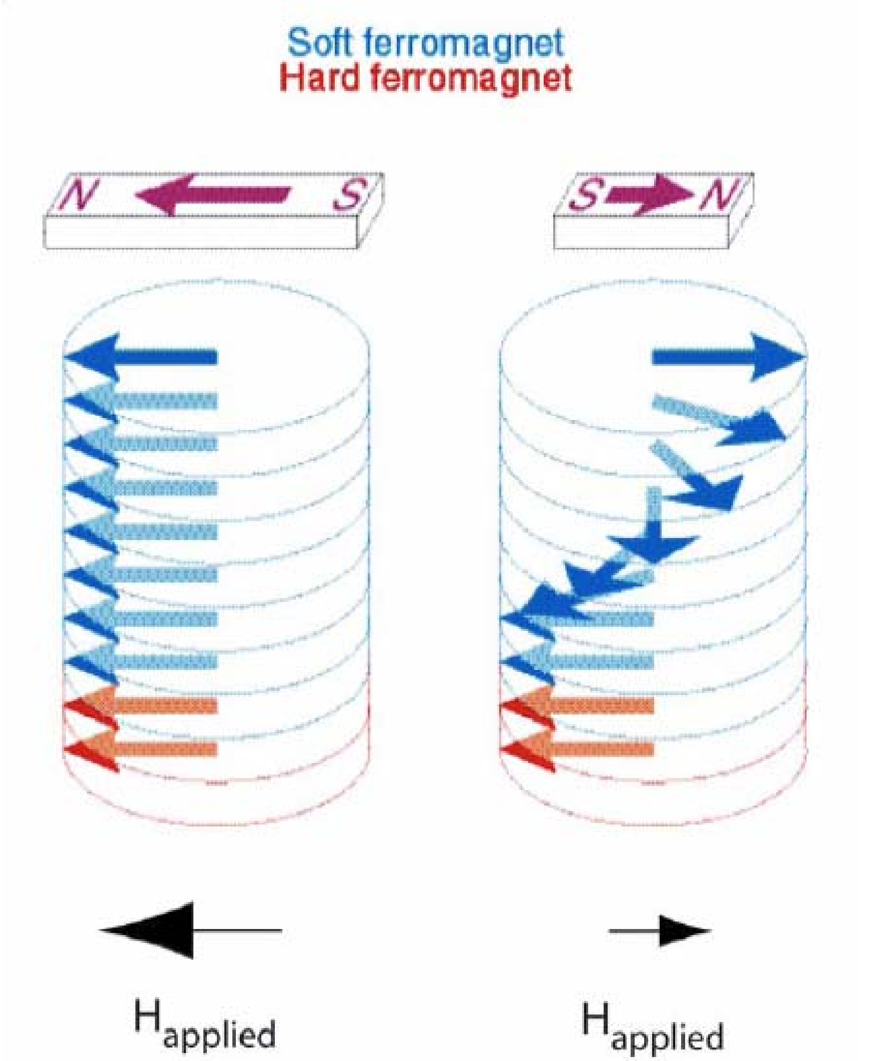

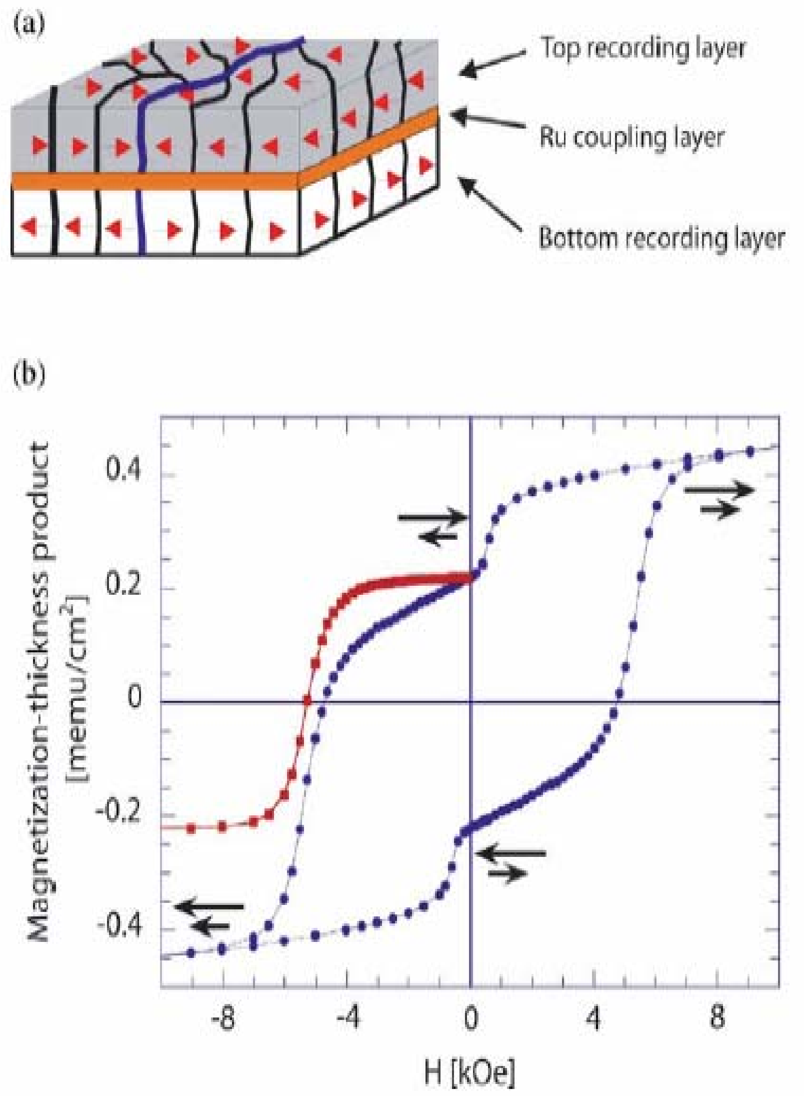

Micromagnetic model

$$E = -\sum_{i=1}^{N-1} \frac{A_{i,i+1}}{d^2} \cos(\theta_i - \theta_{i+1}) - \sum_{i=1}^{N} K_i \cos^2(\theta_i)$$

$$- \sum_{i=1}^{N} H M_i \cos(\theta_i - \theta_H). \qquad (4)$$

- 1-dimensional model
- Continuous twist of Fe
- Rotation of CoSm at high fields

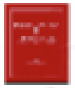
Current Issue

E. Fullerton et al.,
PRB 58, 12193 (1998)

12 198 FULLERTON, JIANG, GRIMSDITCH

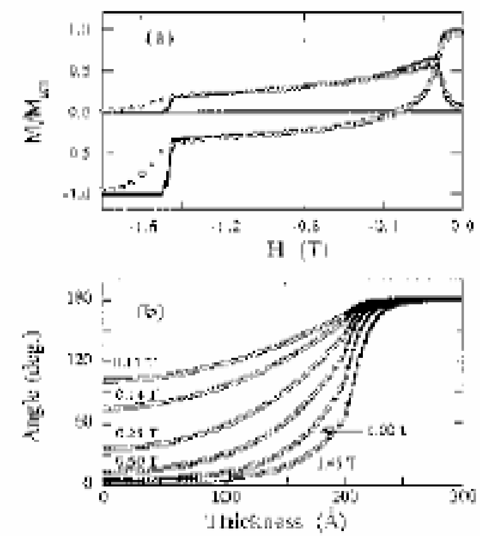

FIG. 7. (a) Low-temperature (25 K) demagnetization curves for the Sm-Co/Fe(200 Å) film shown in Fig. 6 compared to the model calculation (solid line) described in the text. The longitudinal and transverse components of the magnetization are given by the circles and triangles, respectively. (b) Representative spin configuration determined from the model calculation shown in (a). Open circles are Fe spins and filled circles are Sm-Co spins. The free Fe surface is located at zero and the Sm-Co/Fe interface is at 200 Å.

Simulation 4 and measurement

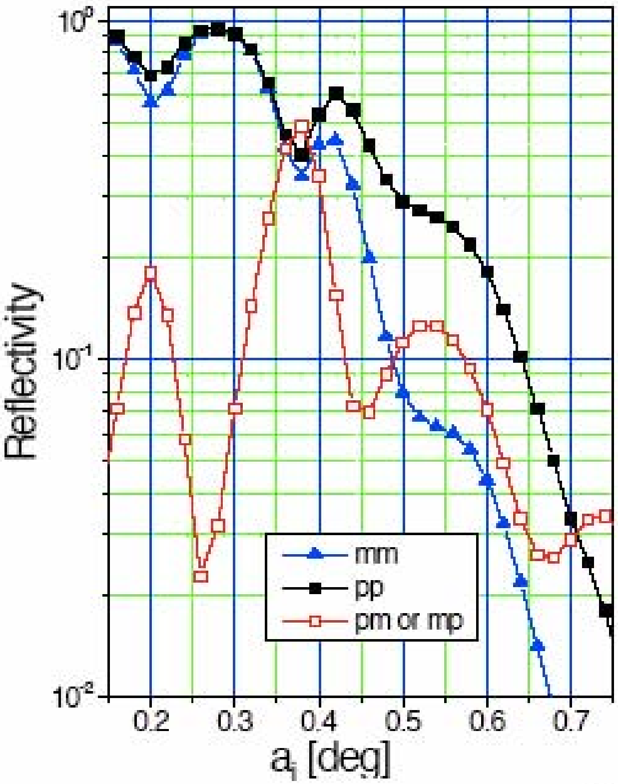

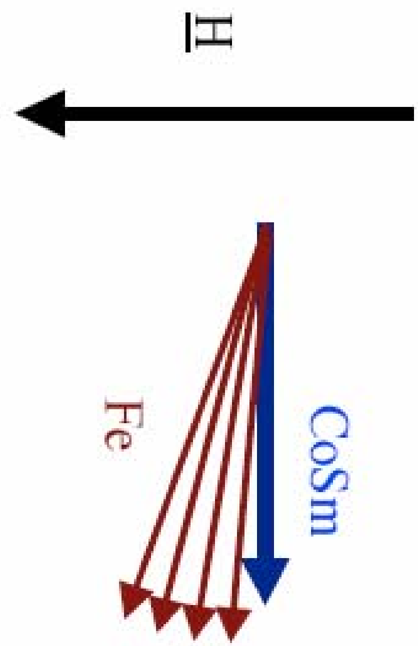

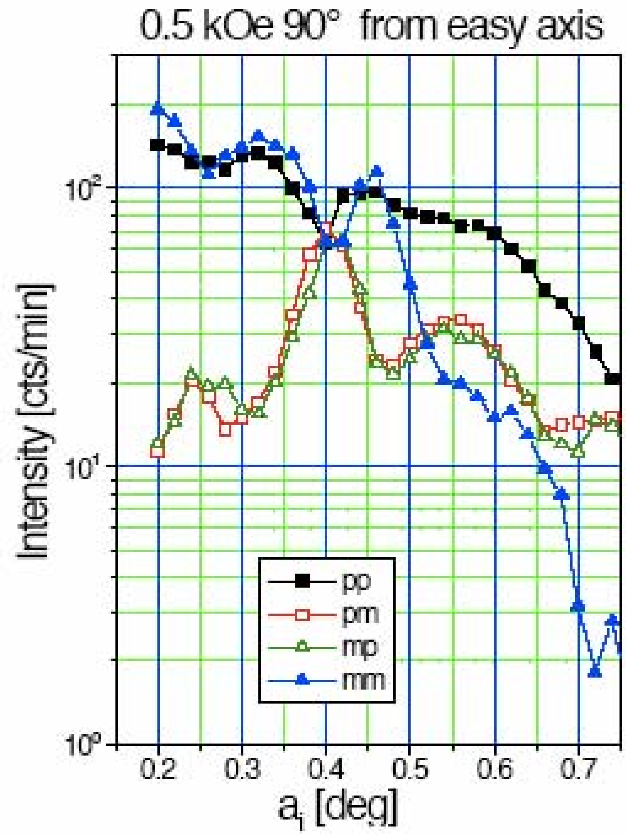

- All features reproduced: magnetic „spring“

CoFe on $CoFe_2O_4$
O'Donbovan
et al
PRL 88,
067201
(2002)

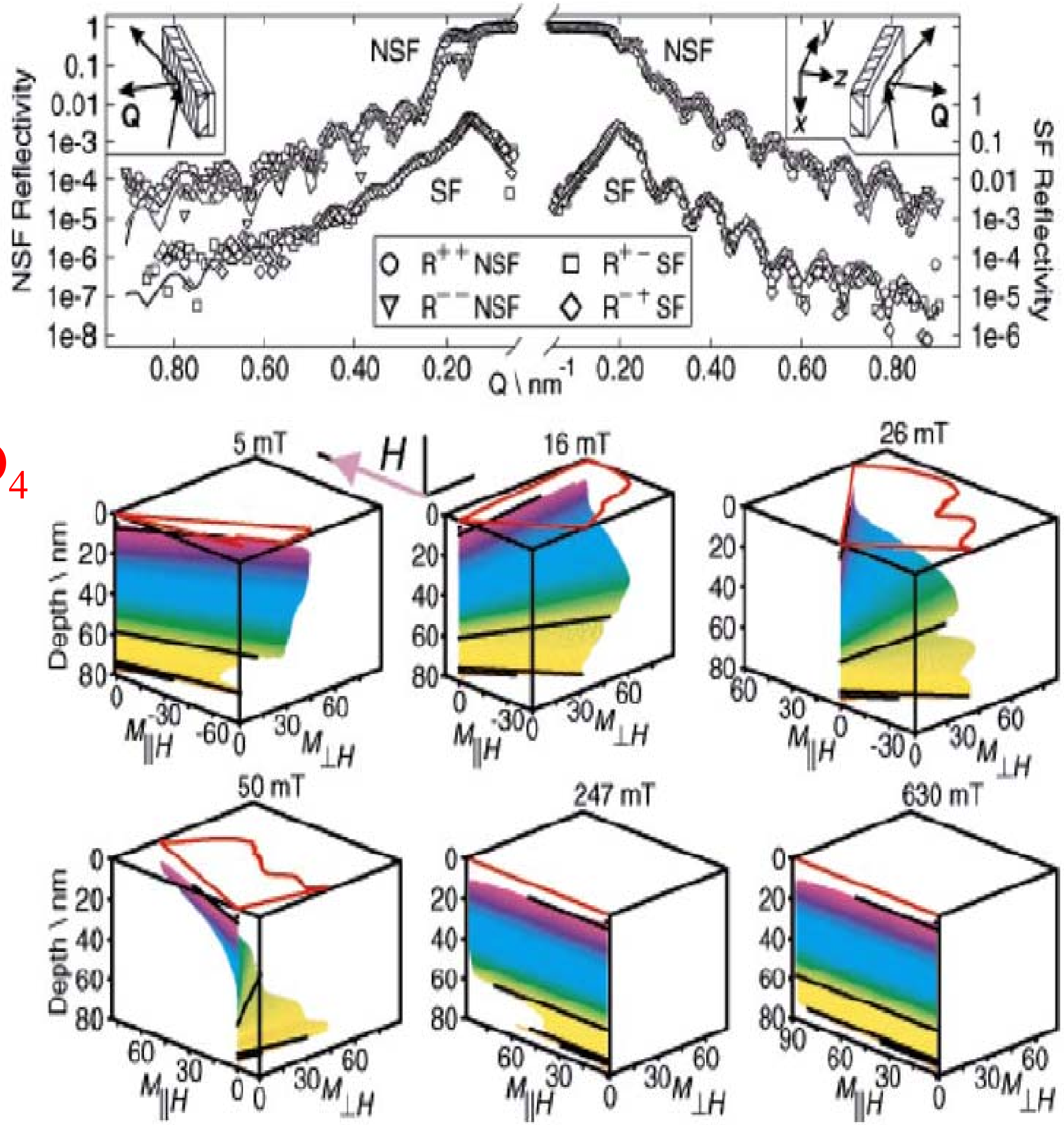

Fig. 16. (upper panel) Neutron reflectivity data taken from an exchange spring magnet. (lower panel) Schematic diagram showing the evolution of the magnetization in the soft layer at the coercive field, as deduced from neutron scattering data. Adapted from Ref. [273].

Sample

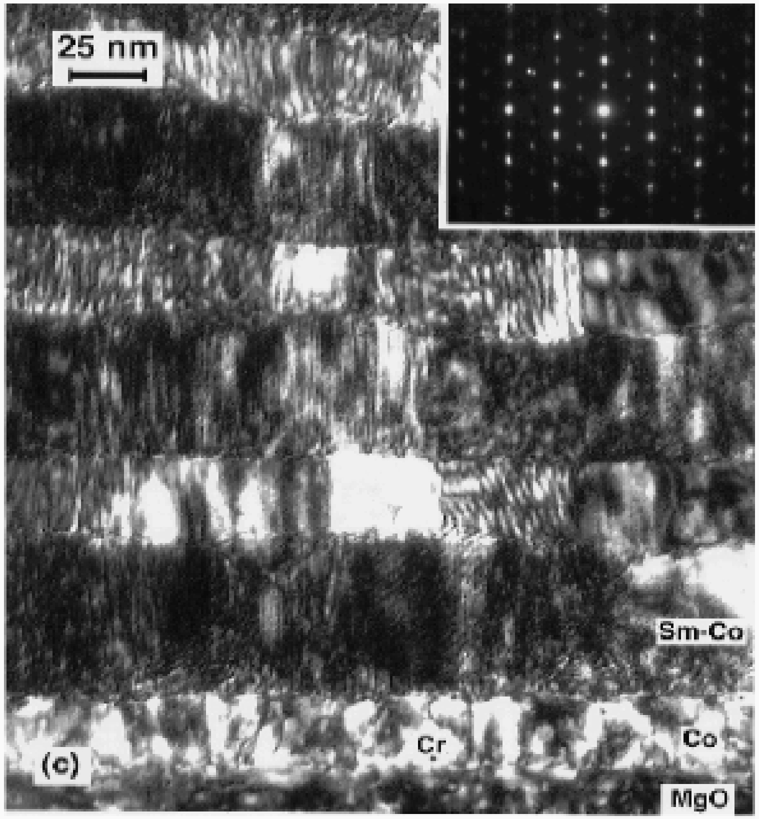

- 20nm Cr on MgO(110)
- 35nm Co_7Sm_2
- 20nm Fe
- 10nm Cr

E. Fullerton et al., APL 72, 380 (1998)

International School of Neutron Scattering
“Francesco Paolo Ricci”

September 25- October 6, 2006

Polarized Neutron Reflectometry

Gian Piero Felcher,
Argonne National Laboratory

Artwork prepared with the help of:

Chuck Majkrzak
Sunil Sinha
Suzanne te Velthuis
Frank Klose
Hartmut Zabel

Polarized neutron reflectometry
3. Toward 3D: domains and nanostructures

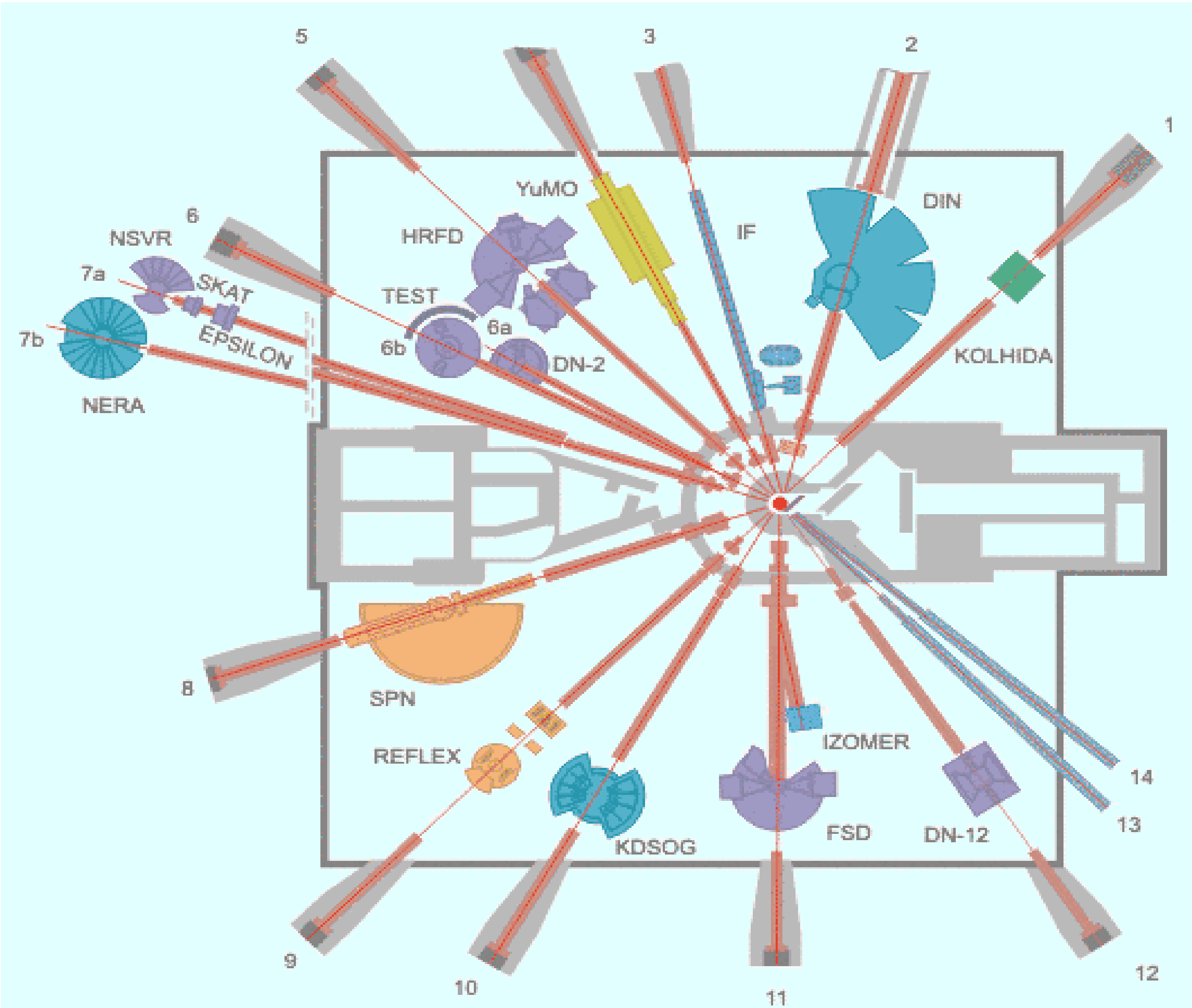

The pulsed reactor at The Joint Institute for Nuclear Research Dubna: instrument layout

New Magnetic Anisotropy

W. H. Meiklejohn and C. P. Bean
General Electric Research Laboratory, Schenectady, New York
(Received October 15, 1956)

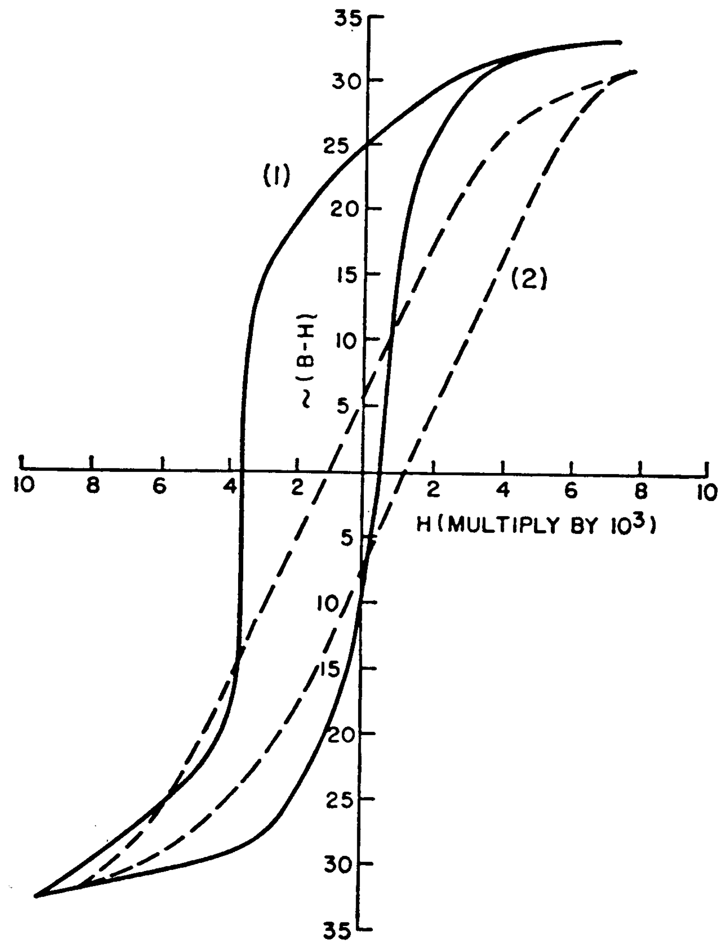

Fig. 1. Hysteresis loops at 77°K of oxide-coated cobalt particles Solid line curve results from cooling the material in a 10 00(oersted field. The dashed line curve shows the loop when cooled ir zero field

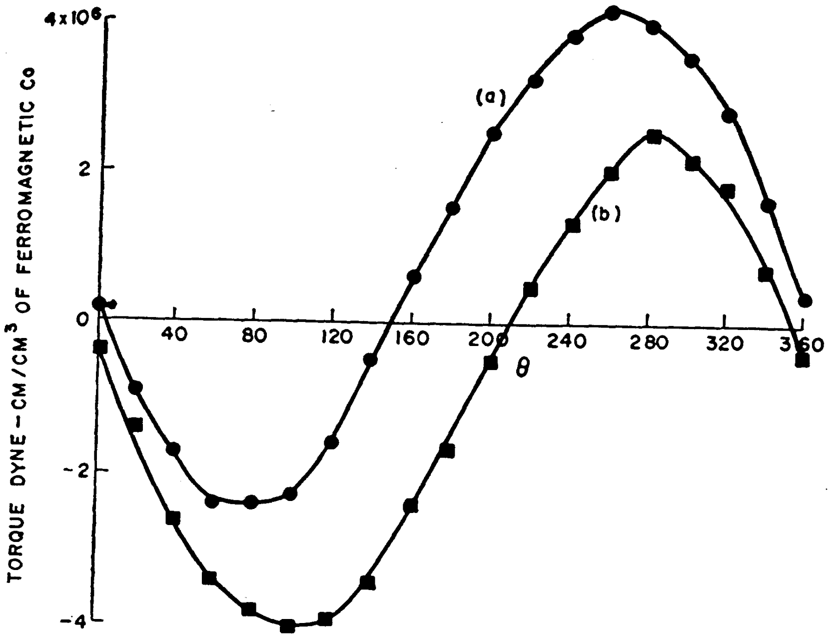

Torque curves on oxide-coated cobalt particles cooled in a field to 77°K, where θ is the angle between the cooling-field axis and the direction of the measuring field

$$TORQUE = K_1 \sin 2\theta + \Delta\sigma \cdot \frac{4\pi r^2}{\frac{4}{3}\pi r^3} \cdot \sin\theta$$

K_1 = uniaxial anisotropy

r = radius of cobalt particles

$\Delta\sigma$ = energy of unit interface area

but $$\Delta\sigma < \frac{1}{100} \cdot \frac{J}{a^2}$$

J = interface energy exchange

a = interlayer spacing

- Usually it is observed when a ferromagnet (FM) and an antiferromagnet (AF) are in contact

- Bias is assured by cooling the system (FM-AF) through the Néel temperature of the AF

It originates from magnetic interactions at the FM-AF interface

- Its strength is <1/100 of that predicted by the most simple model of exchange interaction

- It has been observed in systems coupling 3d metals with: FeMn, NiMn, NiO, CoO, FeF_2 etc.

QuickTime™ and a
TIFF (LZW) decompressor
are needed to see this picture.

Magnetic Thin Films

- Spin valve thin film structures are used as magnetic sensors
- Use Giant Magnetoresistance (GMR) effect
- Key components:
  - Interlayer exchange coupling
  - Exchange bias coupling between FM and AFM

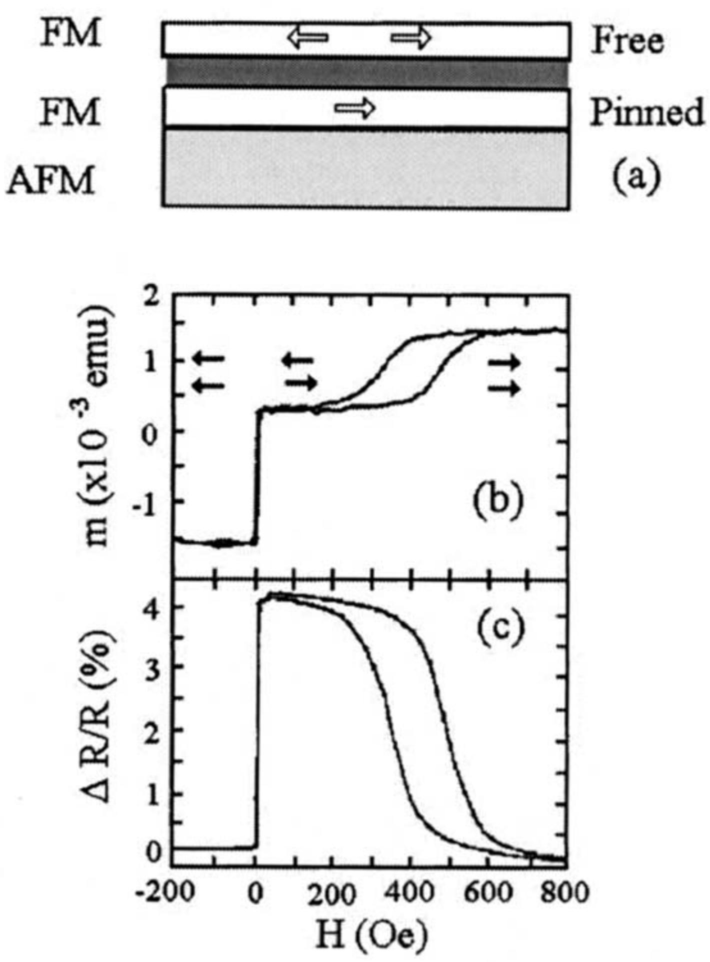

Dieny et al., PRB 43 (1991) 1297

QuickTime™ and a
TIFF (LZW) decompressor
are needed to see this picture.

J. MALOZEMOFF, PHYS. REV. B35, 3679 (1987)

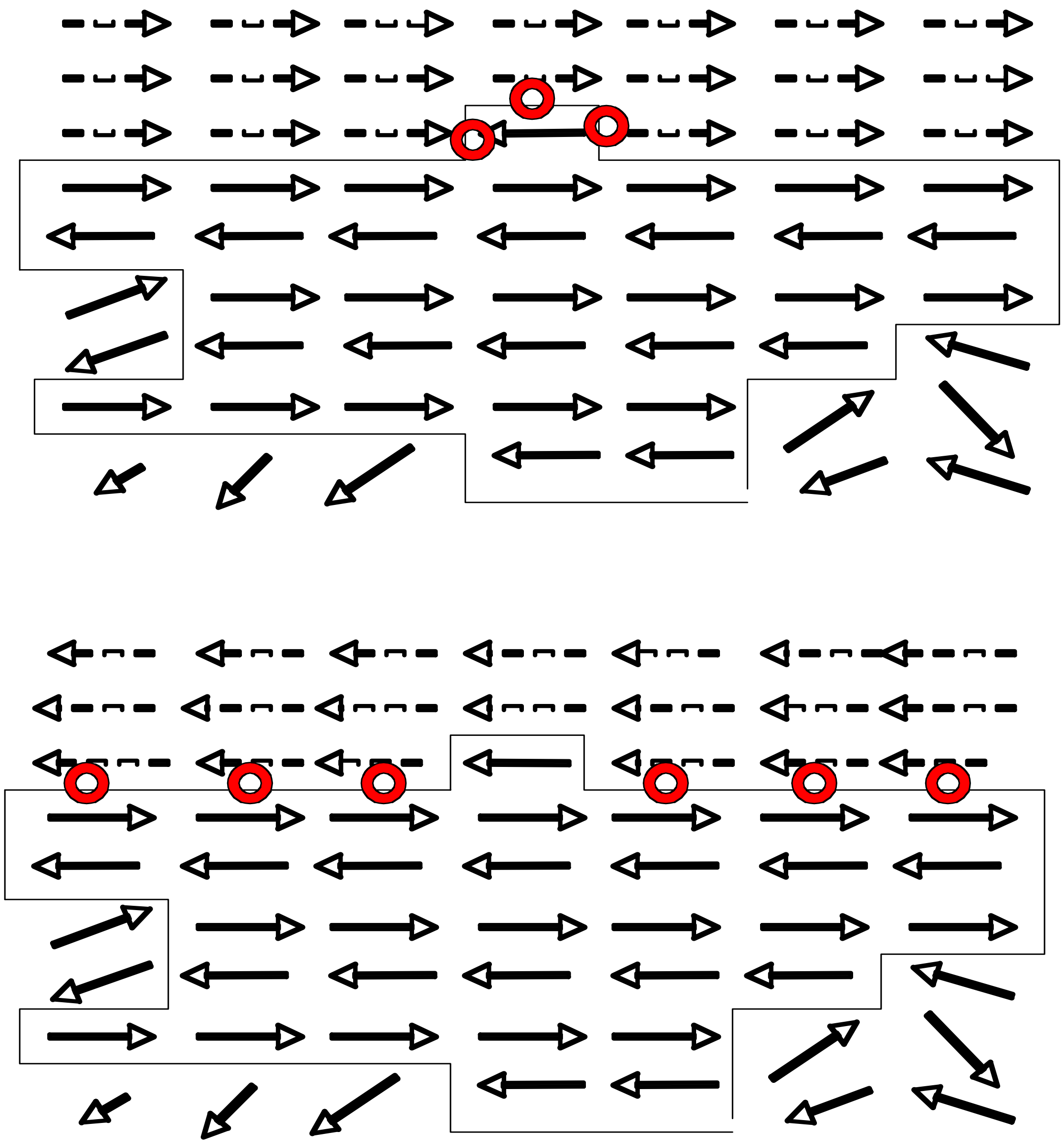

A.J. MALOZEMOFF, PHYS. REV. B35, 3679 (1987)

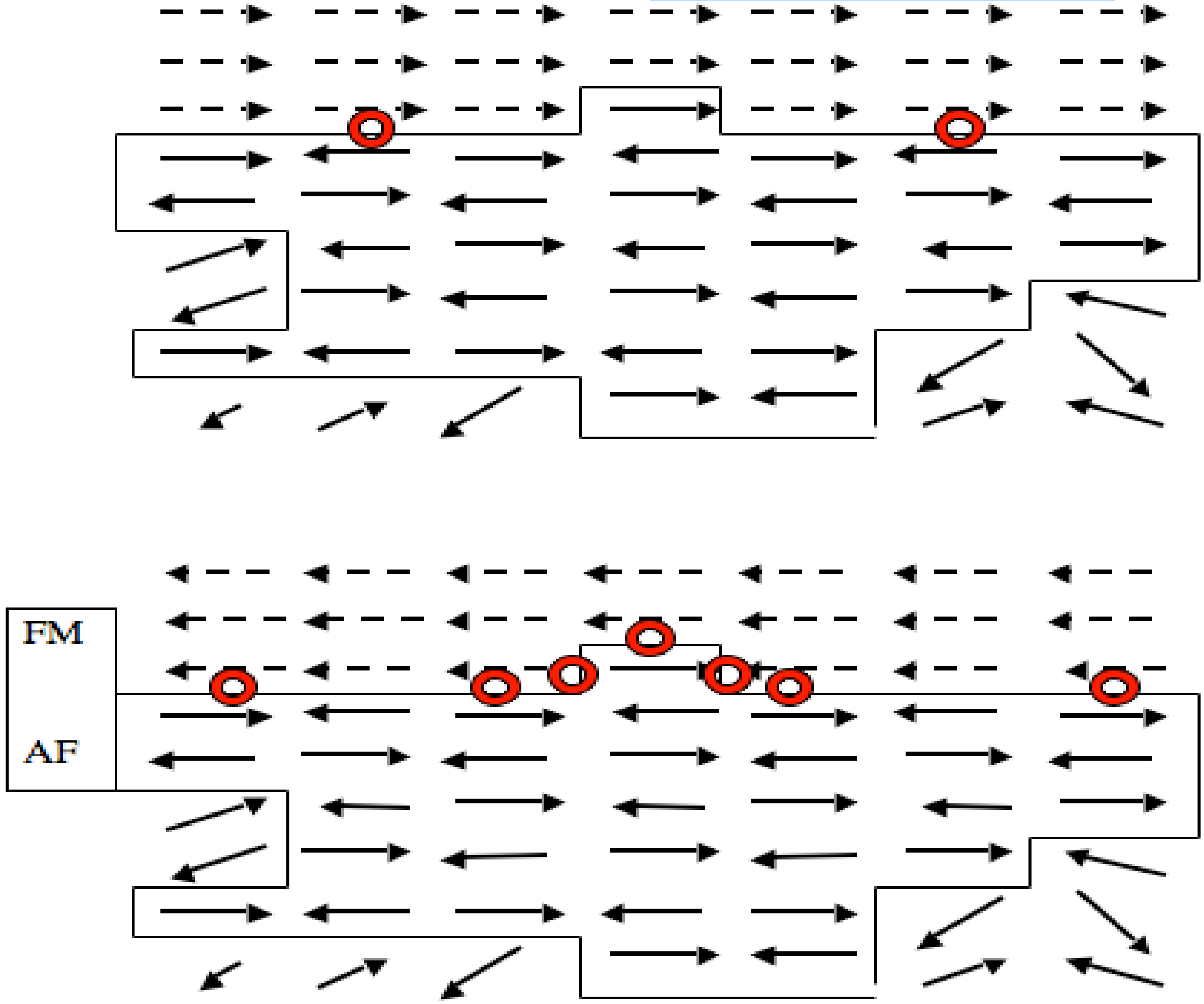

AF/F Double-Superlattice

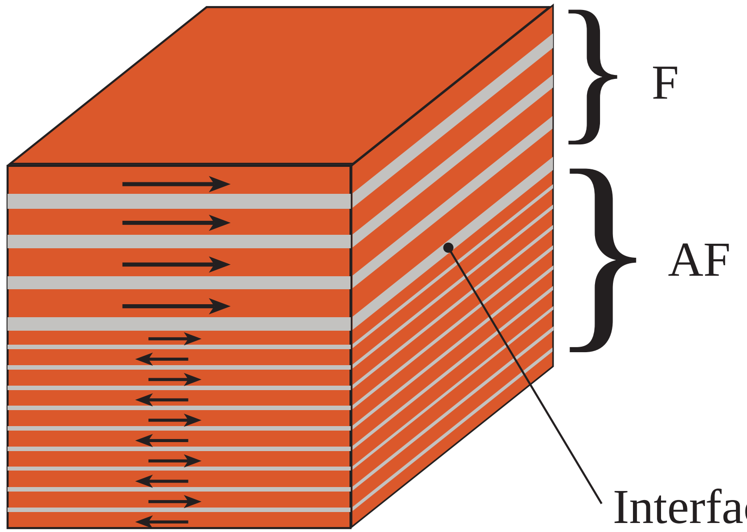

Model exchange bias system

- Configurable structure
- Tunable coupling
- Tunable anisotropy

Tuning of the physical properties

- Exchange

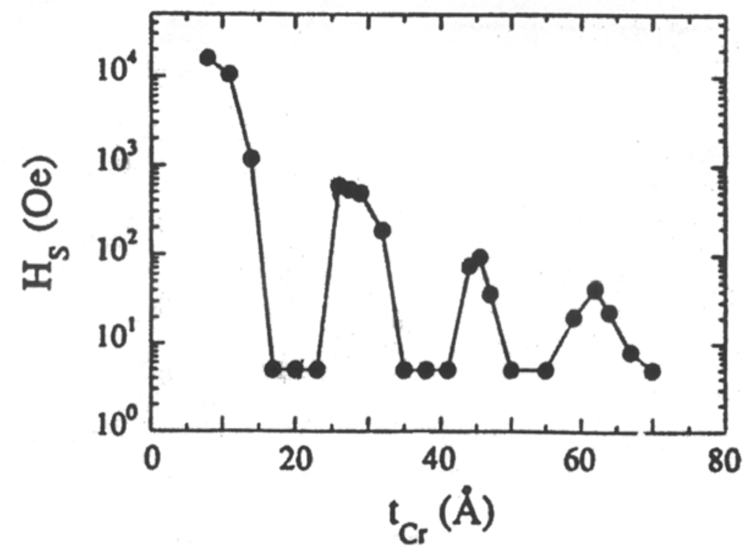

- Anisotropy

(211) Fe on (110) MgO

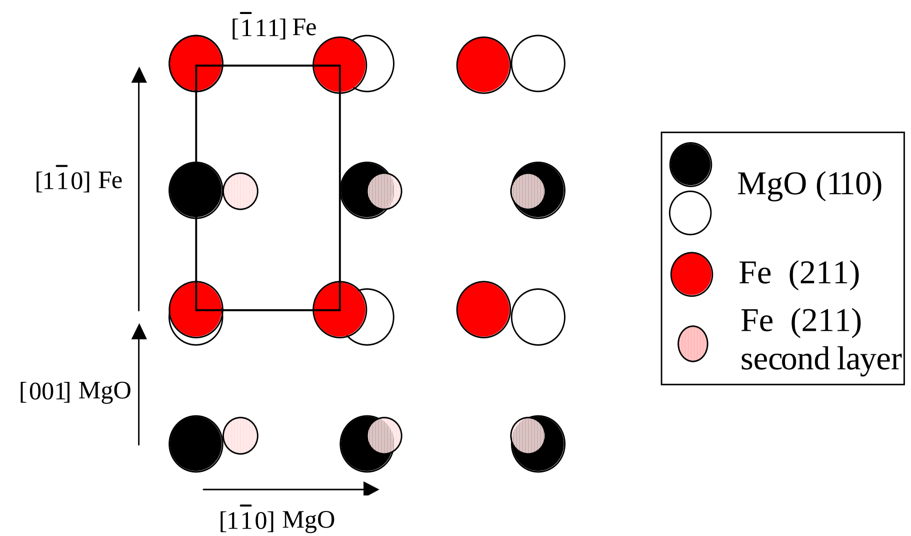

Magnetic properties

- Major Loop at room temperature

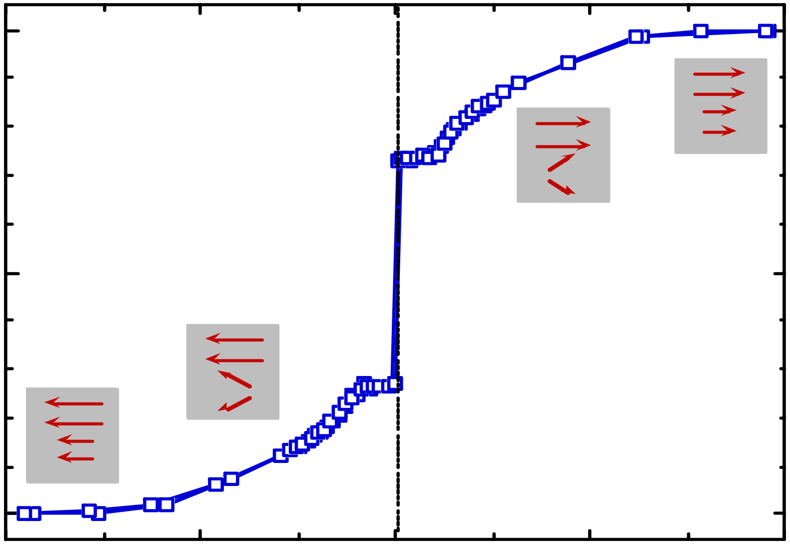

- Dependence of the Exchange bias field, $H_{E,}$ on the number of layers, n_F, in the F superlattice

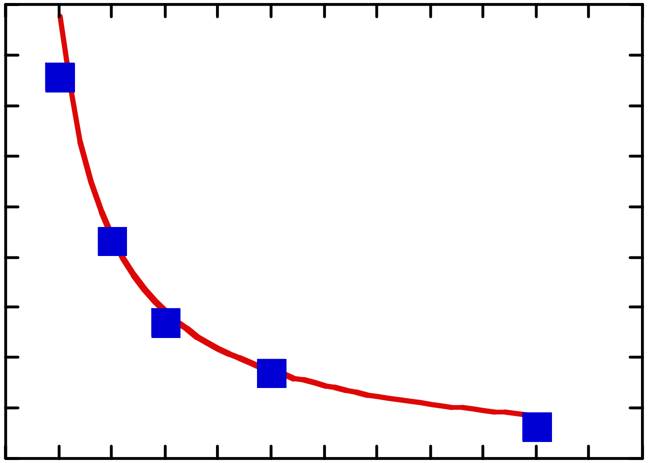

- Minor loop from +12 kOe at room temperature

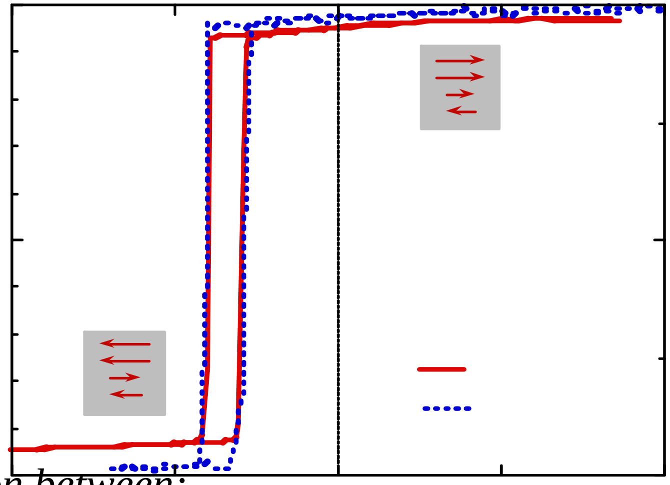

- $$H_E = \frac{J_{int}}{M_{Fe} d_{Fe} n_F}$$

Comparison between:

- J_{int} = 0.14 erg/cm^2 for 20

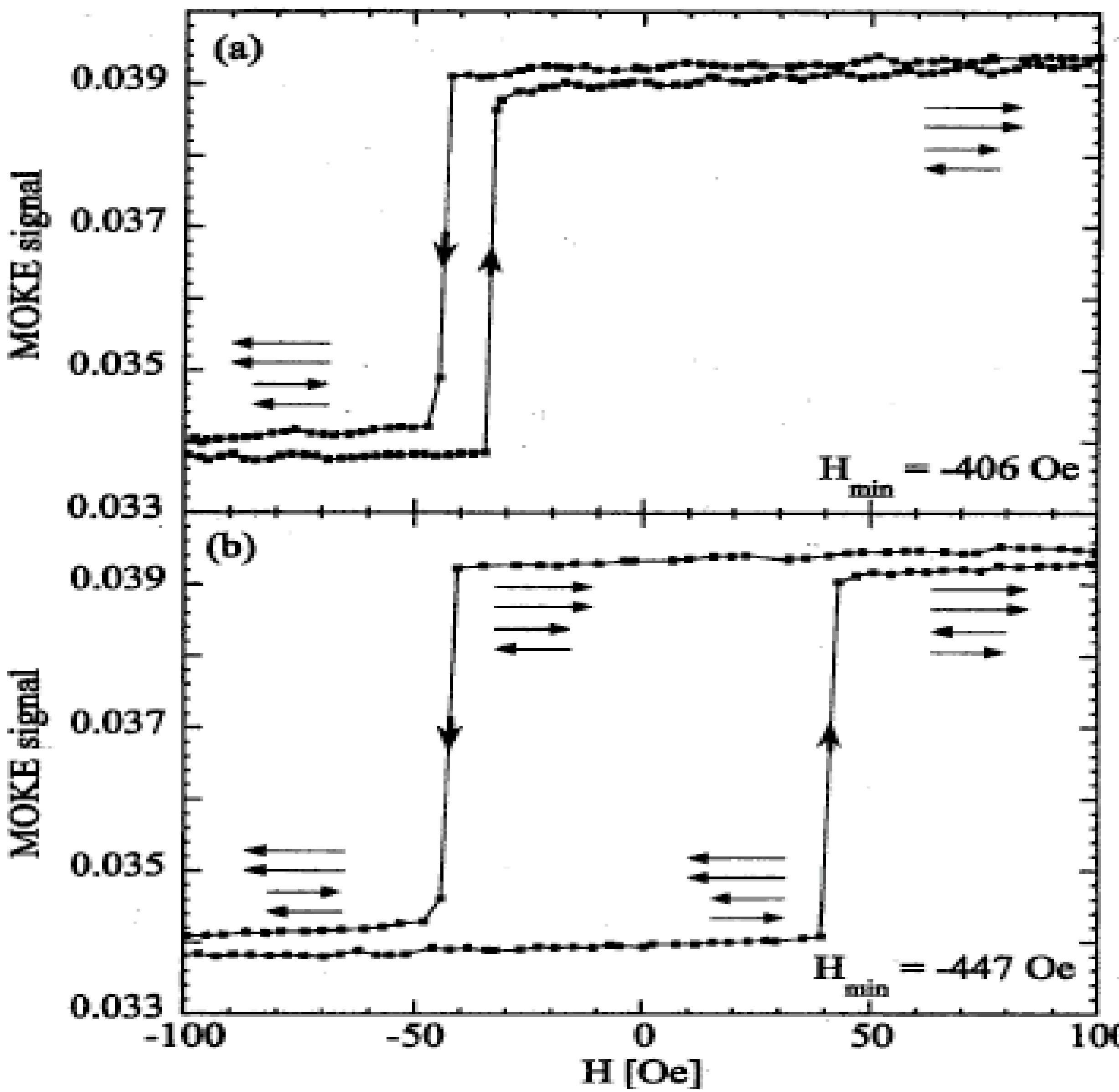

(a)
0.039
0.037
0.035
0.033
MOKE signal
H min = -406 Oe
(b)
0.039
0.037
0.035
0.033
MOKE signal
H min = -447 Oe
-100
-50
0
50
100
H [Oe]

Fe/Cr double superlattice

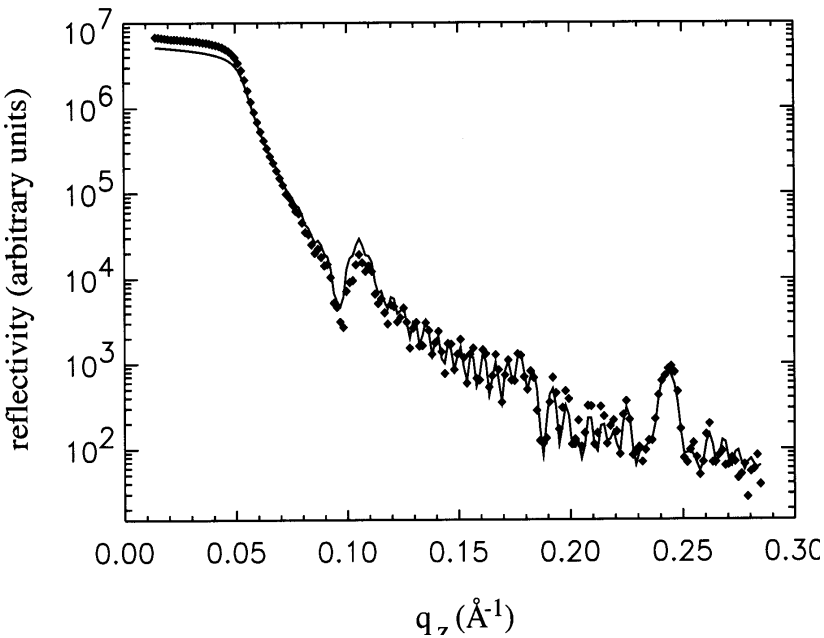

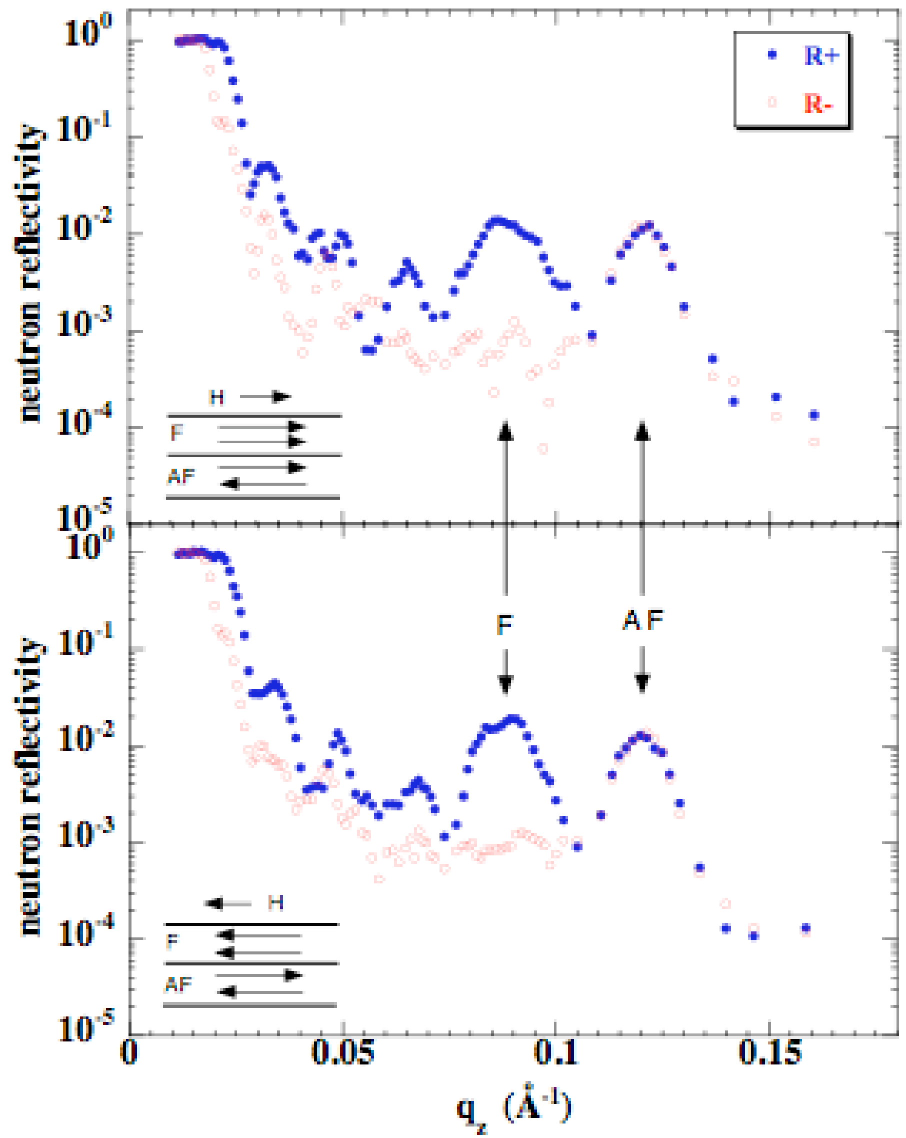

Layers		Thickness ( )	Scattering length density (10^{-6} $^{-2}$) X ray	Neutron
Cr	Cap	49	53.2 + 5.44i	2.97
Fe } × 5	F superlattice	54	58.3 + 7.53i	8.12 ± 4.4
Cr		17.8	53.2 + 5.44i	2.97
Fe } × 20	AF superlattice	14.3	58.3 + 7.53i	8.12 ± 4.4
Cr		12.1	53.2 + 5.44i	2.97
Cr	buffer	197	53.2 + 5.44i	2.97
MgO(110)	substrate		30.5 + 0.32i	5.97

Calculated reflectivity………compared with the experimental one

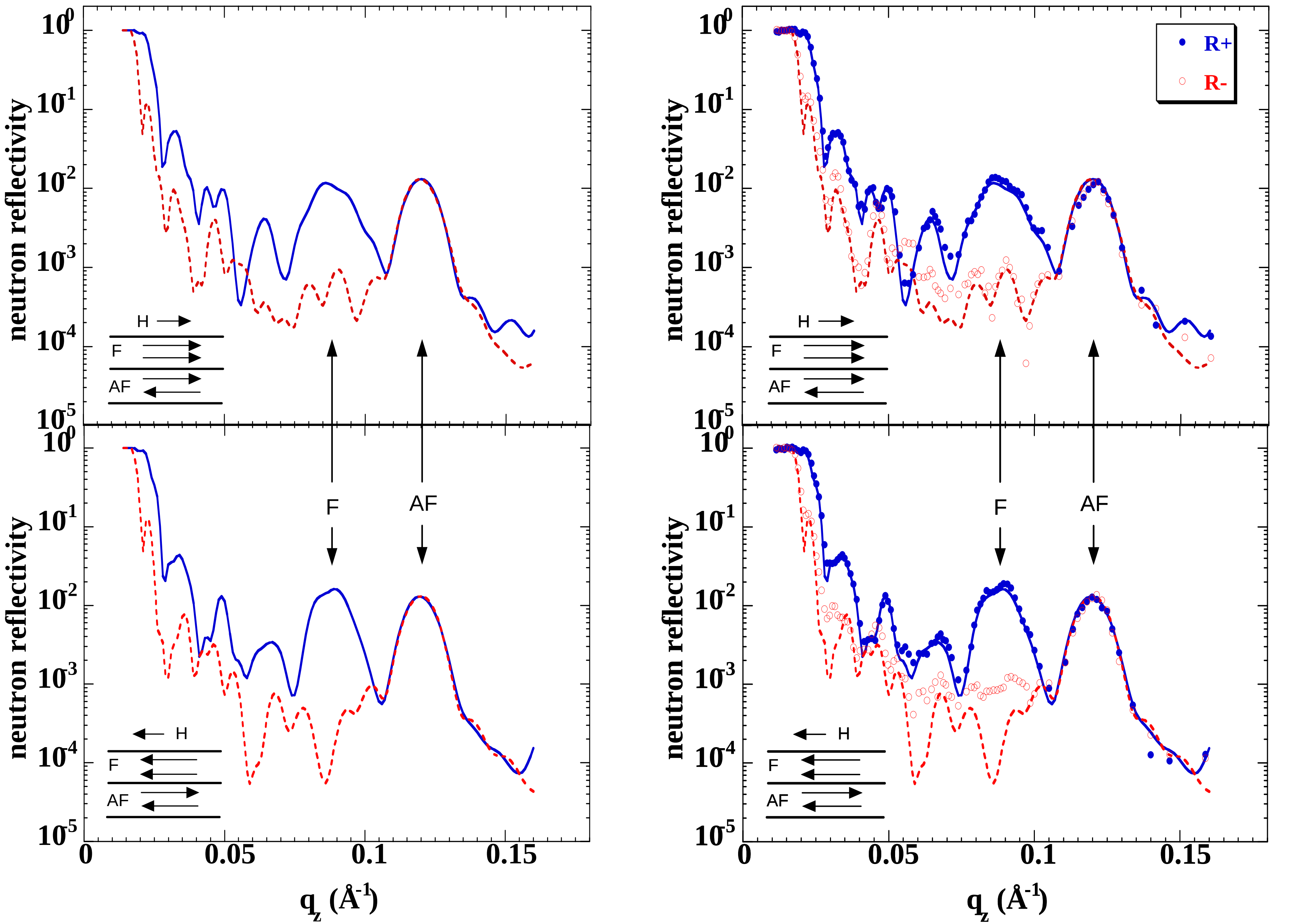

Exchange bias in thin Co/CoO bilayers

Exchange Bias

• After field cooling through T_N magnetization loop is shifted.

• Coercivity increases.

Co/CoO

• Additional training effect.

• Observation of spin dependent **off-specular** scattering.

Polycrystalline CoO(33 Å)/Co (139 Å)/Si

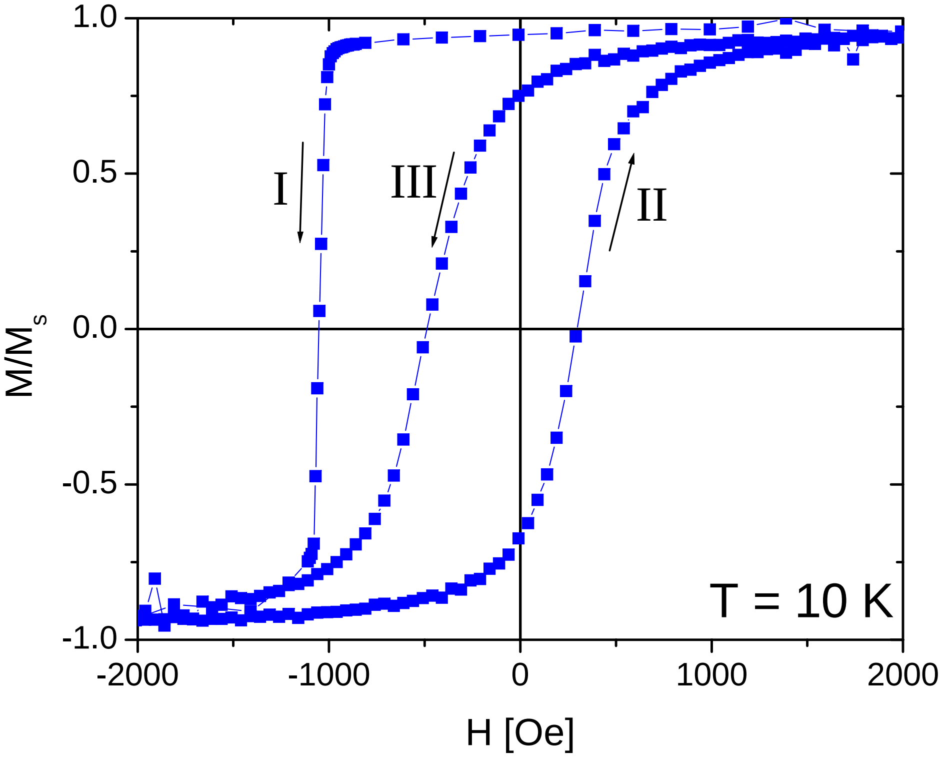

te Velthuis *et al* JAP 87 (2000), 5046

Reflectivity

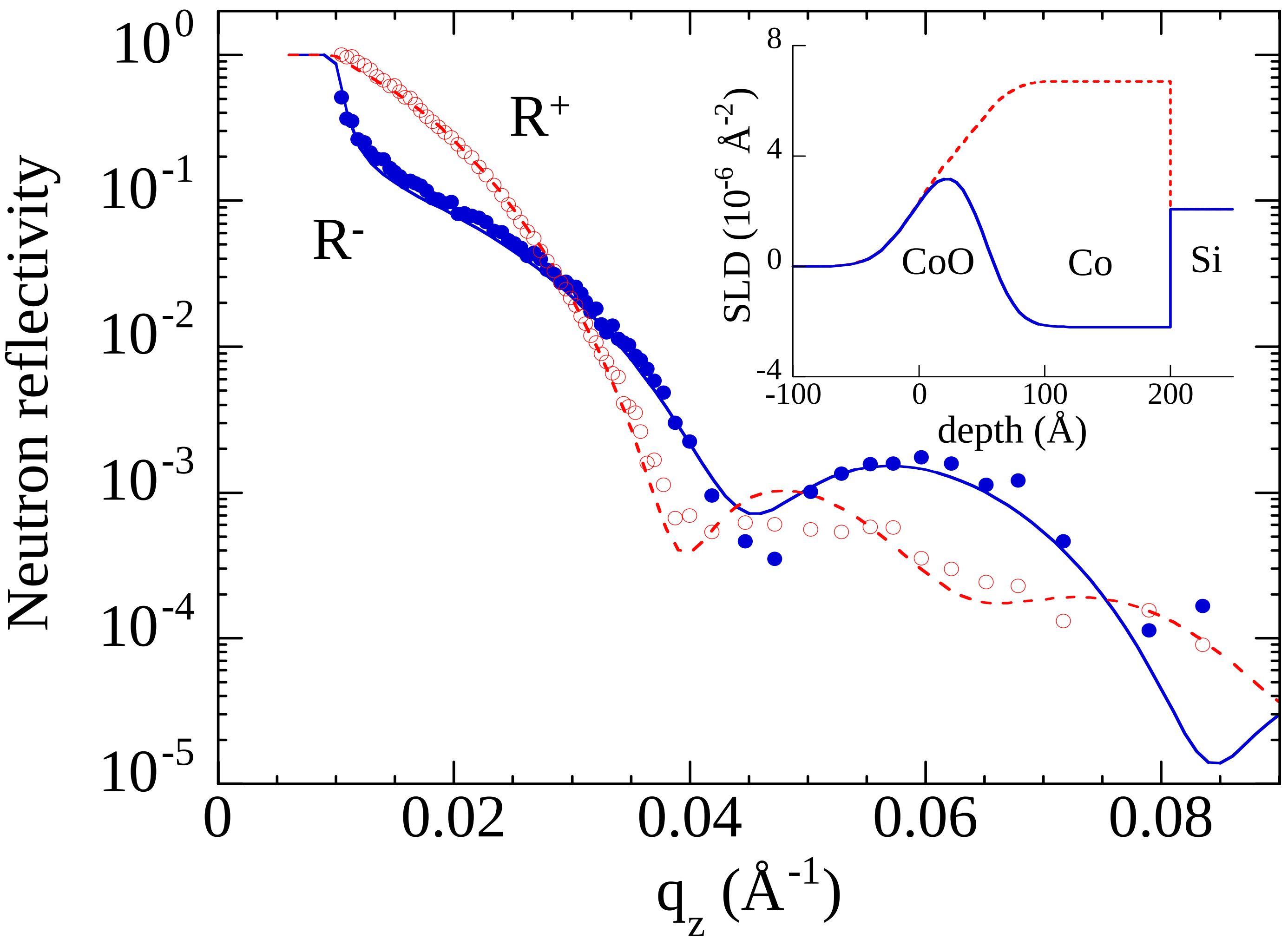

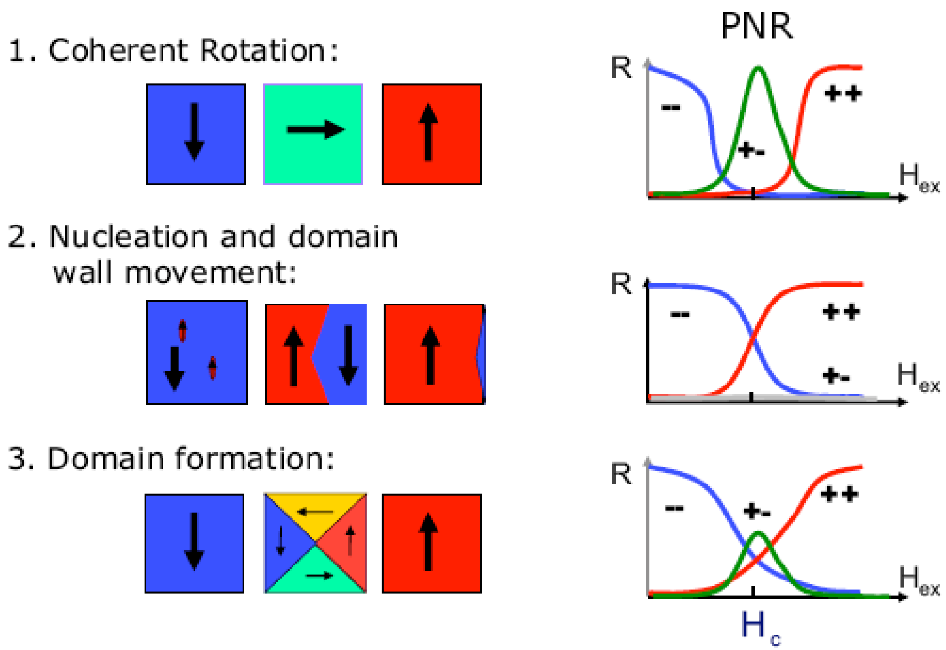

Figure 24: Sketch of three different possibilities for the magnetization reversal from negative saturation field to positive saturation field. This corresponds to only one branch of a magnetic hysteresis in an ascending field. Panel (a) shows schematically a reversal via a coherent rotation of the magnetization vector together with the respective specularly reflected intensity at a fixed scattering vector. In panel (b) domain nucleation and growth is assumed, and in panel (c) the reversal occurs via domain formation. For more details, see text.

Spin Flip Reflectivity

CoO(**33** Å)/Co (139 Å)/ Si

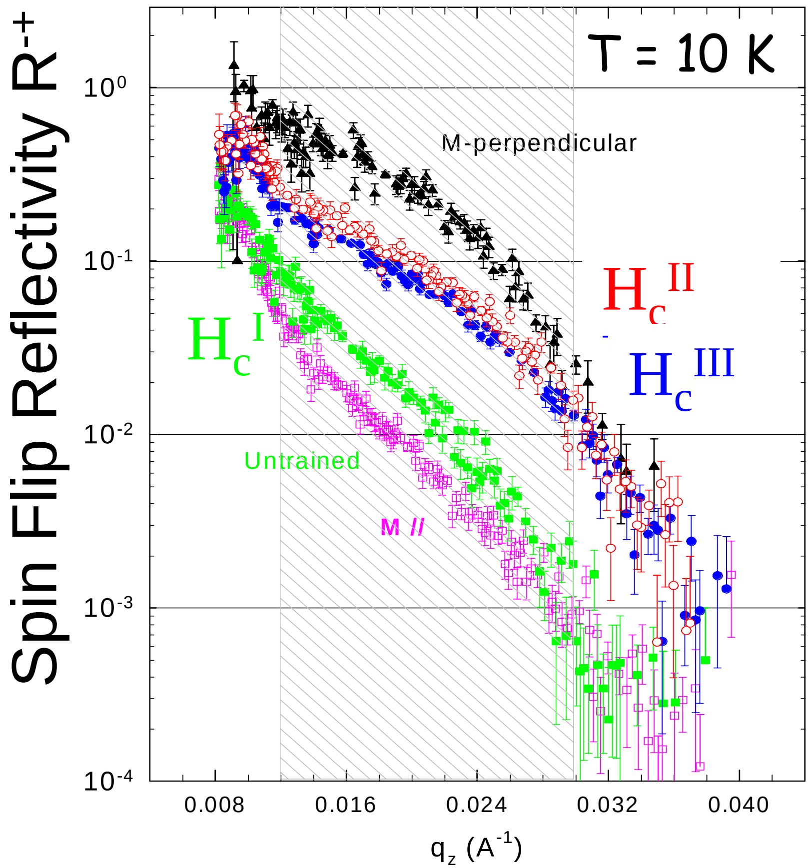

W.-T. Lee *et al.*, PRB 65, 224417 (2002)

[Co(164 Å)/CoO (**20** Å)/Au(34 Å)]$_{20}$/Al_2O_3

M. Gierlings *et al.*, PRB 65, 092407 (2002)

CoO(**30**Å)/Co(170Å)/
Ti(2000Å)/Cu(1000Å)/Al_2O_3

R. Radu *et al.*, JMMM 240, 251 (2002)

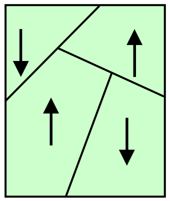

Uniaxial domain switching

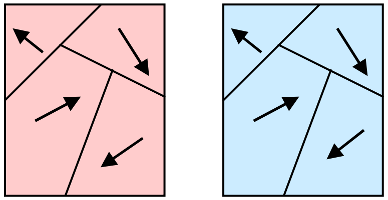

Rotation + domains

$$\frac{R^{++}(\varphi)-R^{--}(\varphi)}{R_s^{++}(0°)-R_s^{--}(0°)}=\frac{R^{+}(\varphi)-R^{-}(\varphi)}{R_s^{+}(0°)-R_s^{-}(0°)}=\cos\varphi, \quad (1)$$

$$\frac{R^{-+}(\varphi)}{R_s^{-+}(90°)}=\sin^2\varphi. \quad (2)$$

$$x^2=\langle\cos^2\varphi\rangle-\langle\cos\varphi\rangle^2$$
$$=\left\{1-\frac{R^{-+}(\varphi)}{R_s^{-+}(90°)}\right\}-\left\{\frac{R^{++}(\varphi)-R^{--}(\varphi)}{R_s^{++}(0°)-R_s^{--}(0°)}\right\}^2. \quad (3)$$

W.T. Lee et al, Phys.Rev. B 65, 224417 (2002)

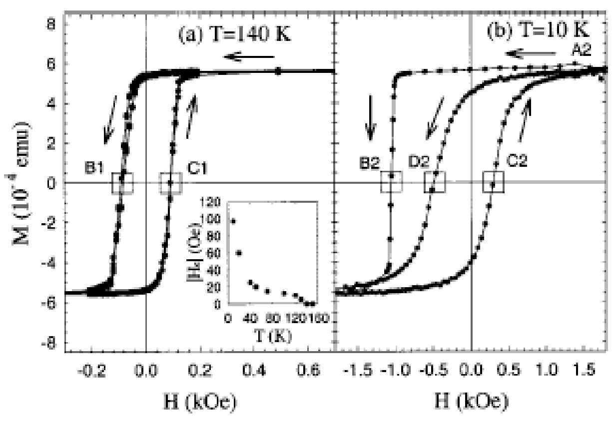

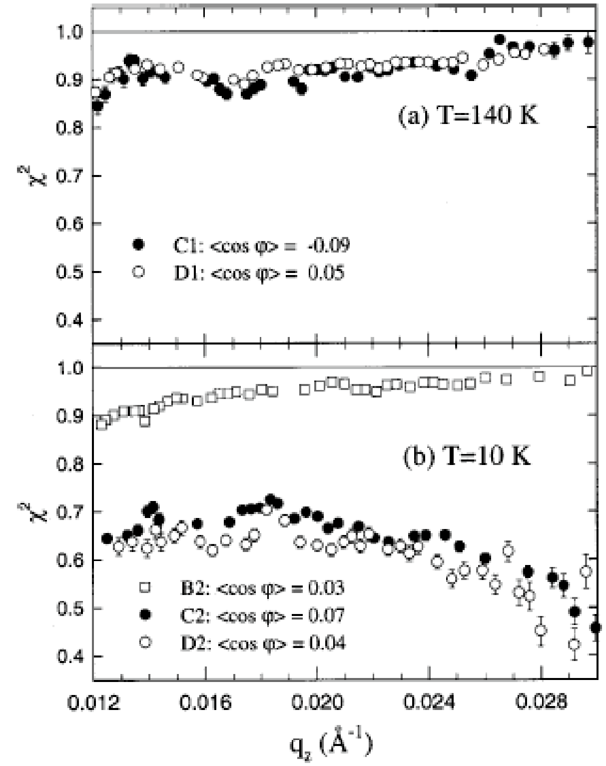

Figure 28: Left panel: Magnetic hysteresis of a CoO/Co bilayer taken at a temperature above the blocking temperature T_b; Right panel: χ^2 - values evaluated from PNR measurements taken at the designated remanent points and indicated in the left panel. For temperatures above the blocking temperature, χ^2 is essentially one. After field cooling to 10 K the χ^2 value remains one for the untrained magnetization reversal, but assumes values smaller than one in the trained state, indicative for the development of a angular distribution of domains. From Lee et al. [97]

Lateral domain distribution

Statistical Measure of Lateral Magnetic Moment Distribution

$$\chi^2 = \langle M_{//}^2 \rangle - \langle M_{//} \rangle^2 = 1 - \langle M_{\perp}^2 \rangle - \langle M_{//} \rangle^2$$

Case: Single Domain

$\langle M_{//} \rangle = M_{//}$
$\langle M_{\perp}^2 \rangle = M_{\perp}^2$
$\chi^2 = 0$

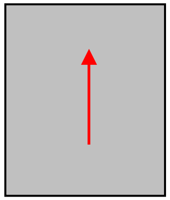

Case: Aligned domains

$\langle M_{//} \rangle \sim 0$
$\langle M_{\perp}^2 \rangle \sim 0$
$\chi^2 \sim 1$

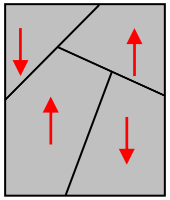

Case: Non-aligned domains

$\langle M_{//} \rangle \sim 0$
$\langle M_{\perp}^2 \rangle \neq 0$
$0 < \chi^2 < 1$

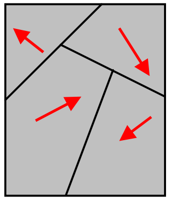

Magneto-Optical Imaging

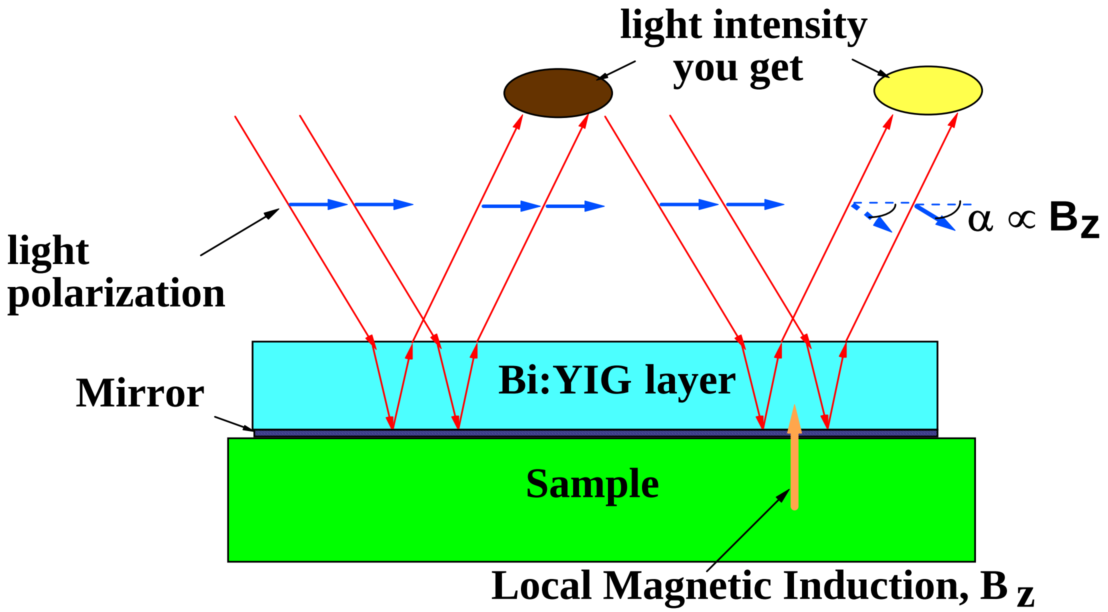

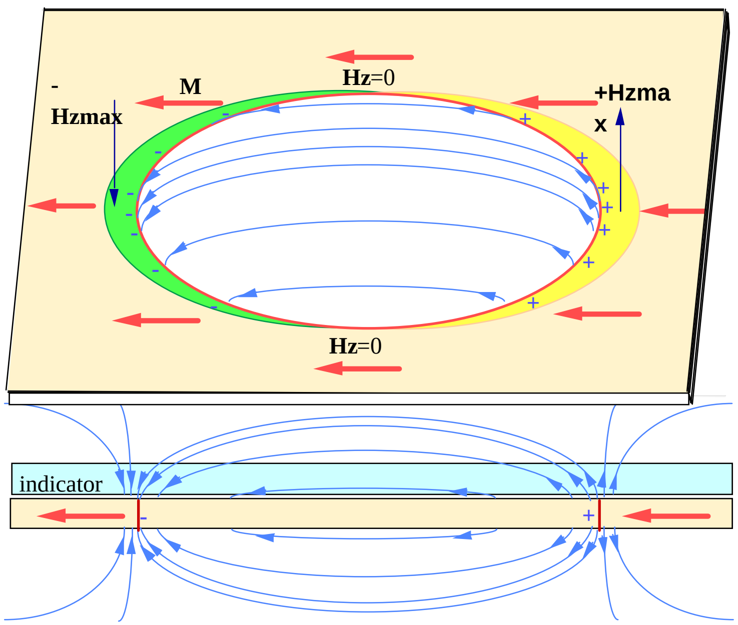

Ulrich Welp, Materials Science Division, ANL

Physica C 203 (1992) 149, PRL 86 (2001) 4386

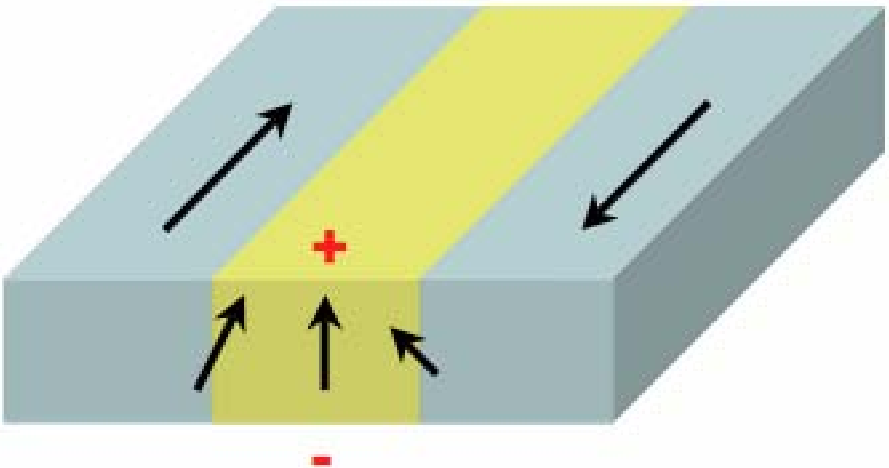

Bloch

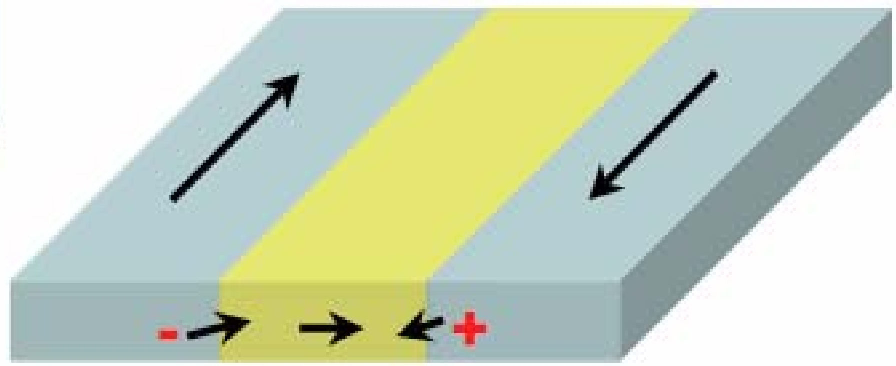

Néel

Exchange biased Co/CoO thin films

Sample: CoO(33 Å)/Co (139 Å)/Si, polycrystalline

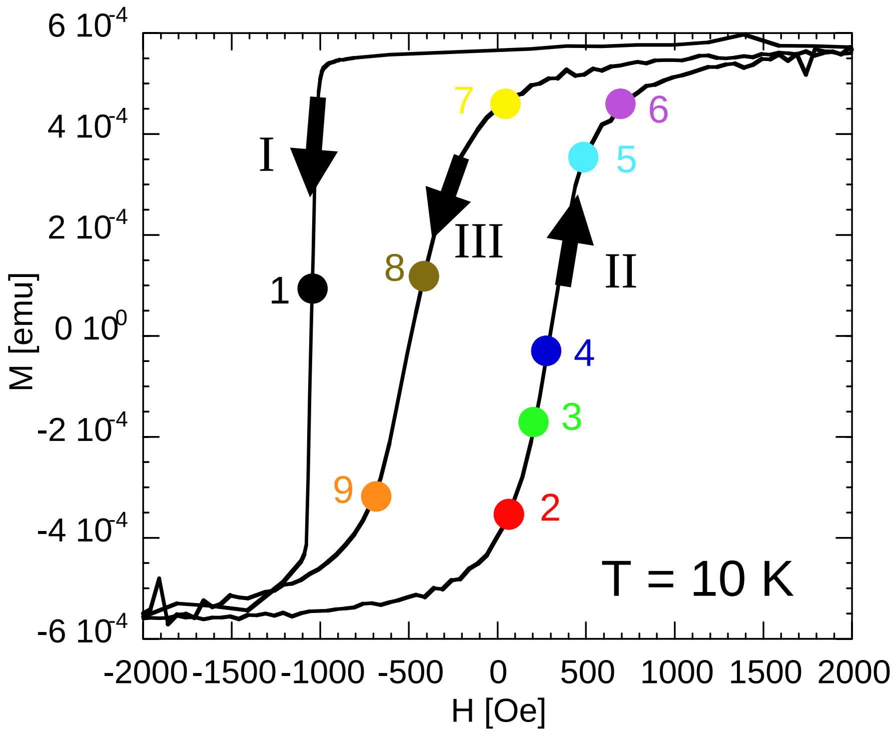

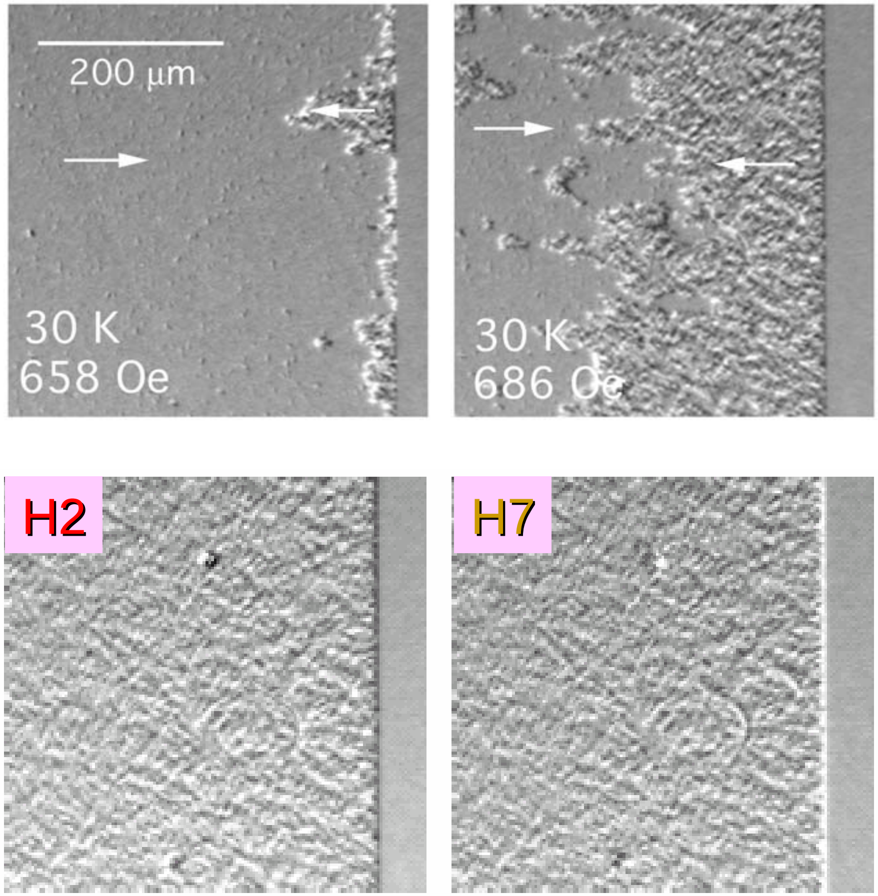

S.G.E. te Velthuis et al., JAP 87 (2000) 5046; W.-T Lee *et al*, PRB 65 (2002) 224417; Ulrich Welp *et al*, JAP**93** (2003) 7726;
Invited talks: PNCMI'02, PNCMI'04

Along trained curves (H ≈ 0)

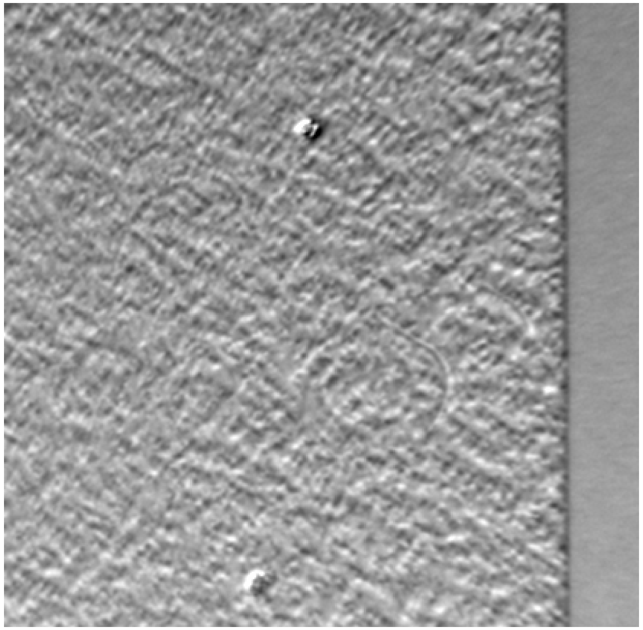

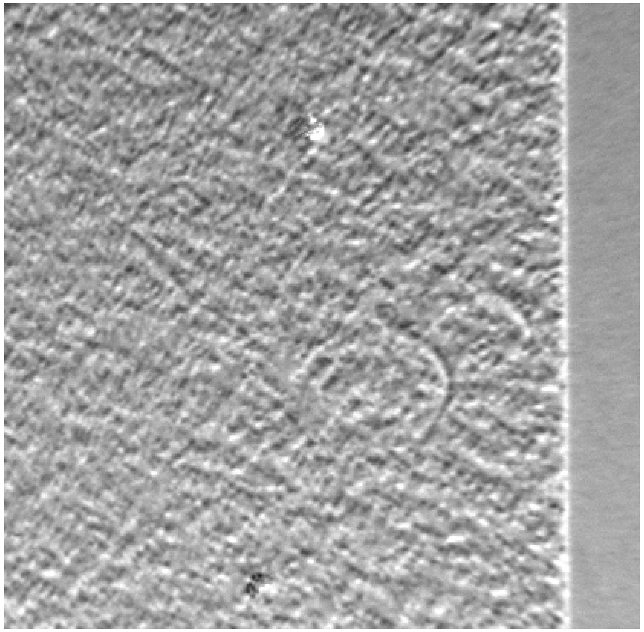

Room temperature

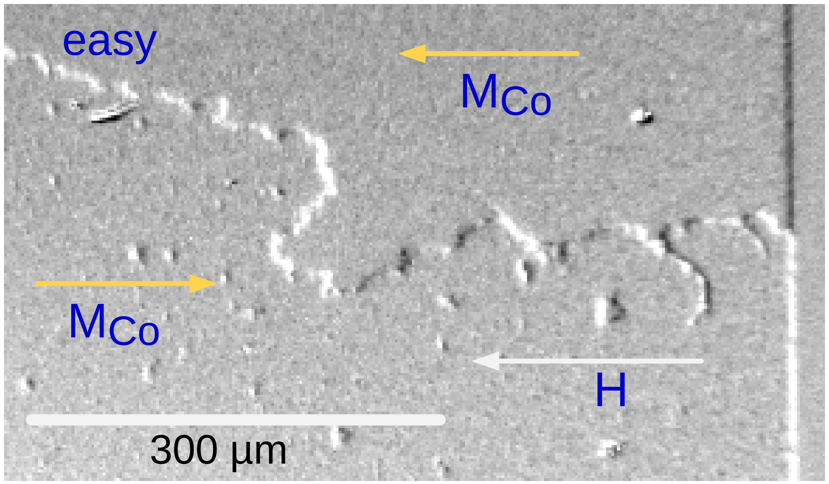

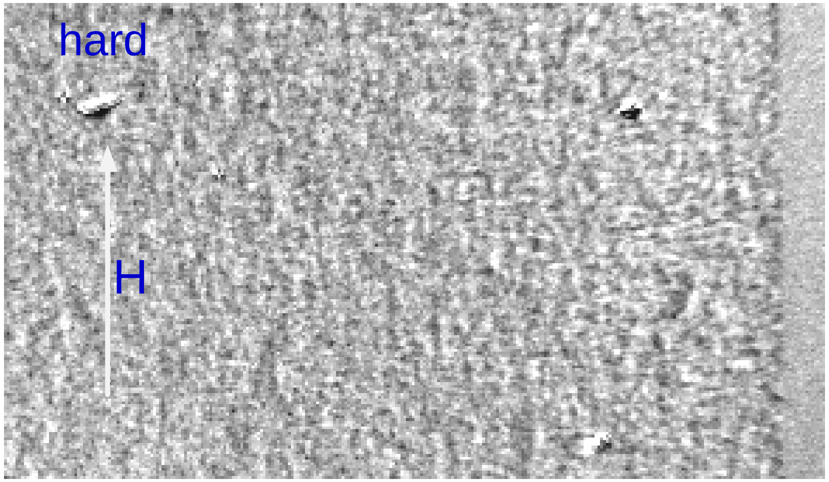

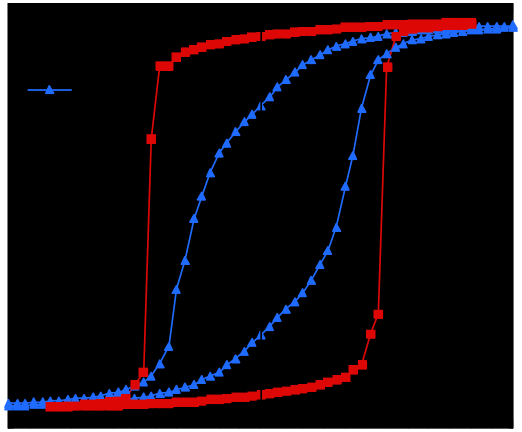

- Along easy axis reversal dominated by wall movement

- Along hard axis domains of similar size. But here the domain pattern **does change** with field.

Comparing images with opposite M_r

Sum

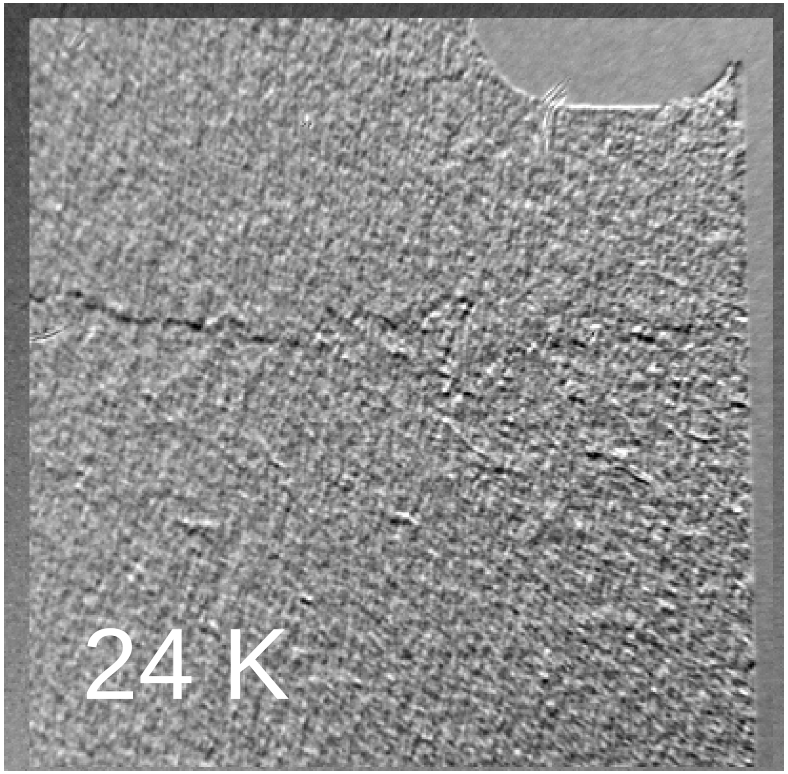

Difference

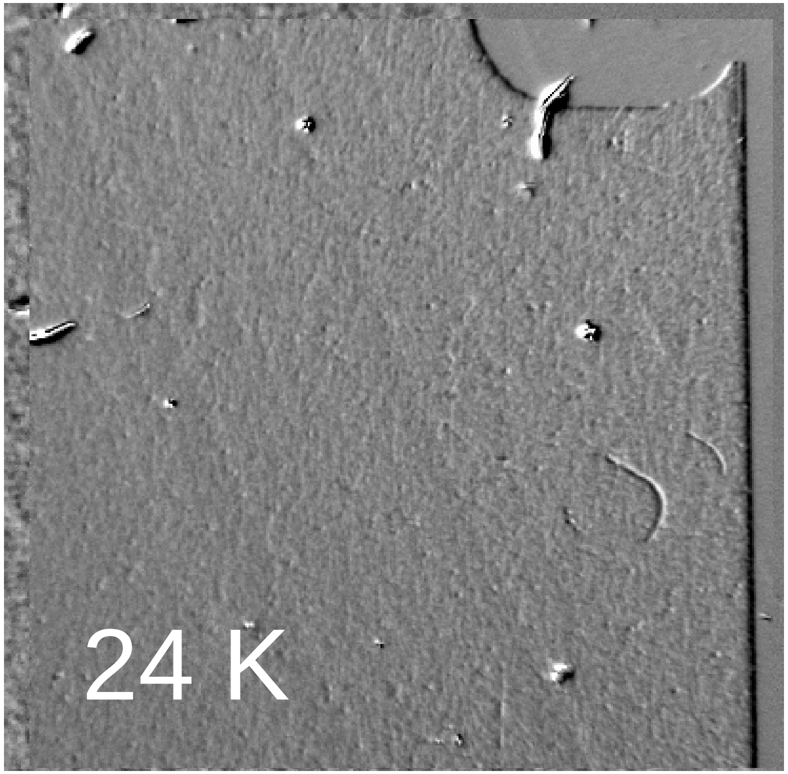

The magnetization rotation within Co domains in the biased state (24K) is different than along hard axis at RT.

• MO Image is dominated by contrast between components of M ⊥ H.

• Contrast from M ⊥ H does not change sign when cycling through hysteresis cycle, provided each domain always rotates towards same direction.

• Images of opposite remnant states show that in biased state (24 K), Co domain magnetizations are directed in the same orientation.

• Only unidirectional anisotropy (imposed by coupling with CoO) oriented at an angle with respect to H can cause this rotational behavior in FM domains.

Summary

Co/CoO

- **Magnetic hysteresis loops can be understood with the observation of the formation of domains.**

- **Once the domains are formed, the magnetization reversal behavior becomes one of uncorrelated rotation of domains magnetizations.**

  - **Rotation direction always the same in each domain.**
  - **Distribution of unidirectional anisotropies imposed by coupling with CoO.**

Puzzle:

Given that:

- **Domains** larger **than coherence length contribute to** specular intensity
- **Domains** smaller **than coherence length contribute to** scattering
- **MO imaging shows domains are 5-10 μm**
- **Lateral coherence length ~50 μm**

Does the Co/CoO film exhibit off-specular scattering?

International School of Neutron Scattering
“Francesco Paolo Ricci”

September 25- October 6, 2006

Polarized Neutron Reflectometry

Gian Piero Felcher,
Argonne National Laboratory

Artwork prepared with the help of:

Chuck Majkrzak
Sunil Sinha
Suzanne te Velthuis
Frank Klose
Hartmut Zabel

POLARIZED NEUTRON REFLECTOMETRY
4. The issues and the challenges

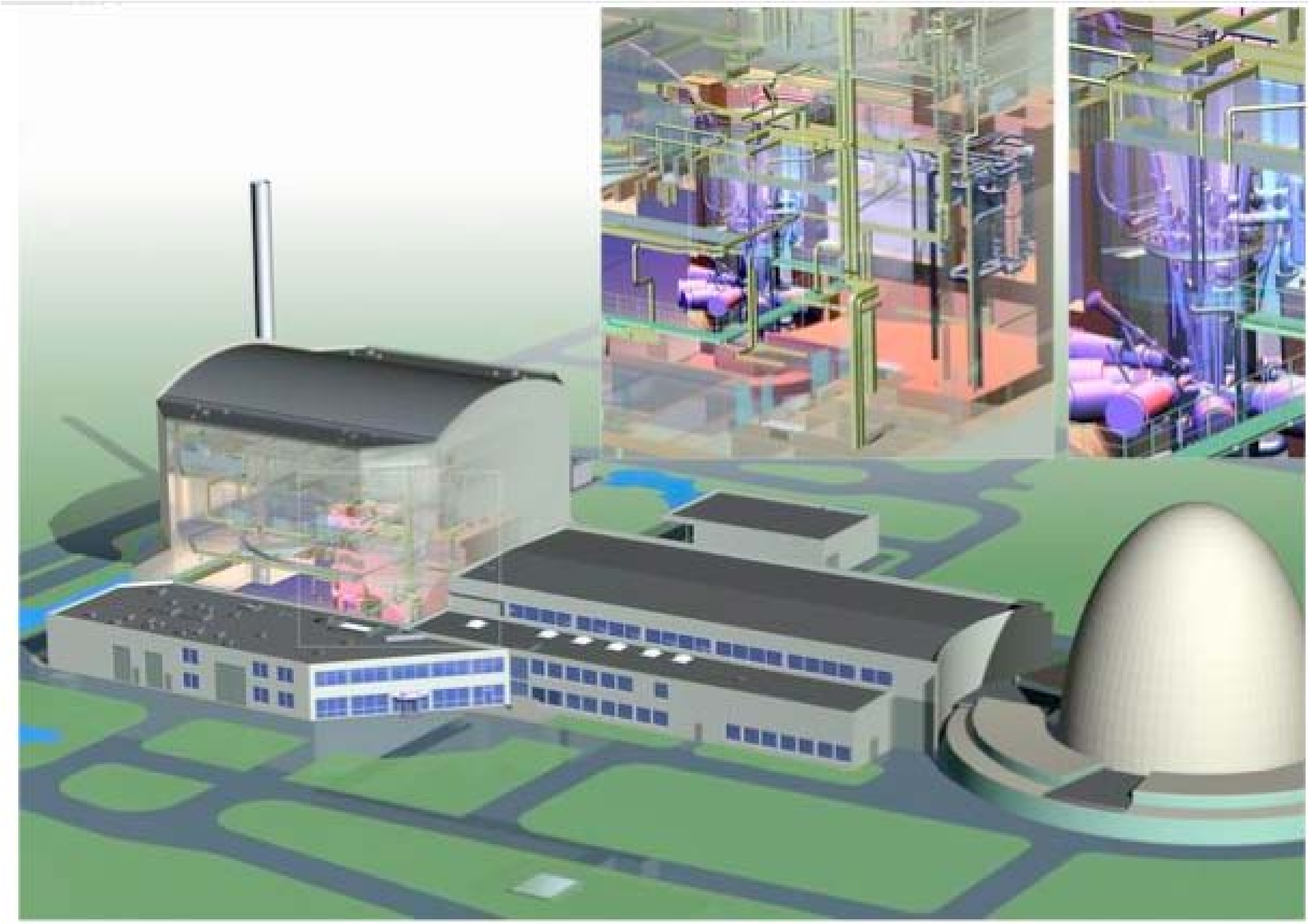

The FRM2 reactor "ATOMEI" in Munich

Exchange biased Co/CoO thin films

Sample: CoO(33 Å)/Co (139 Å)/Si, polycrystalline

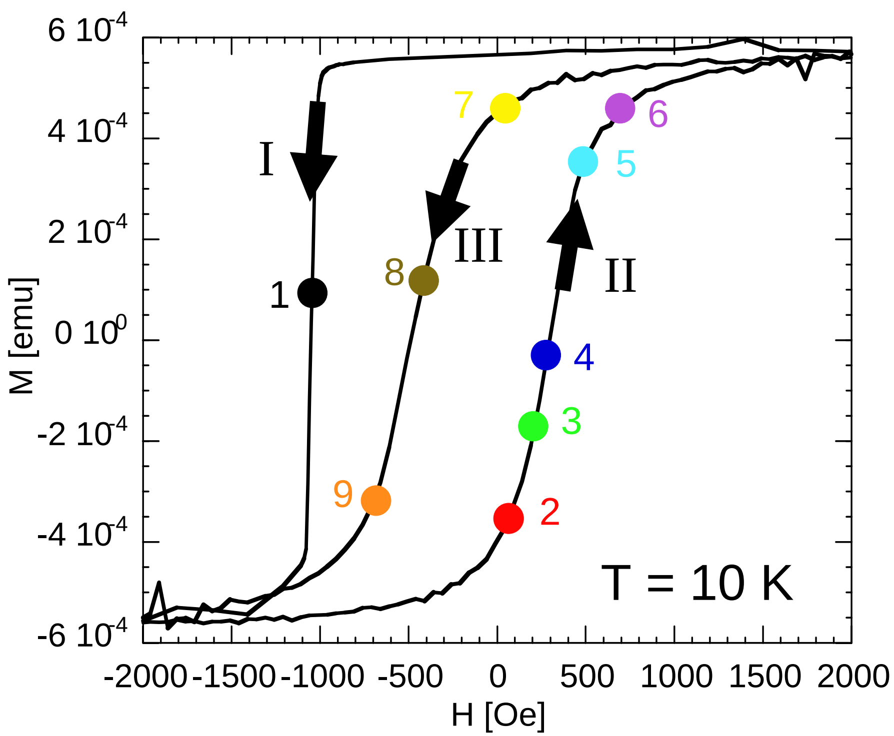

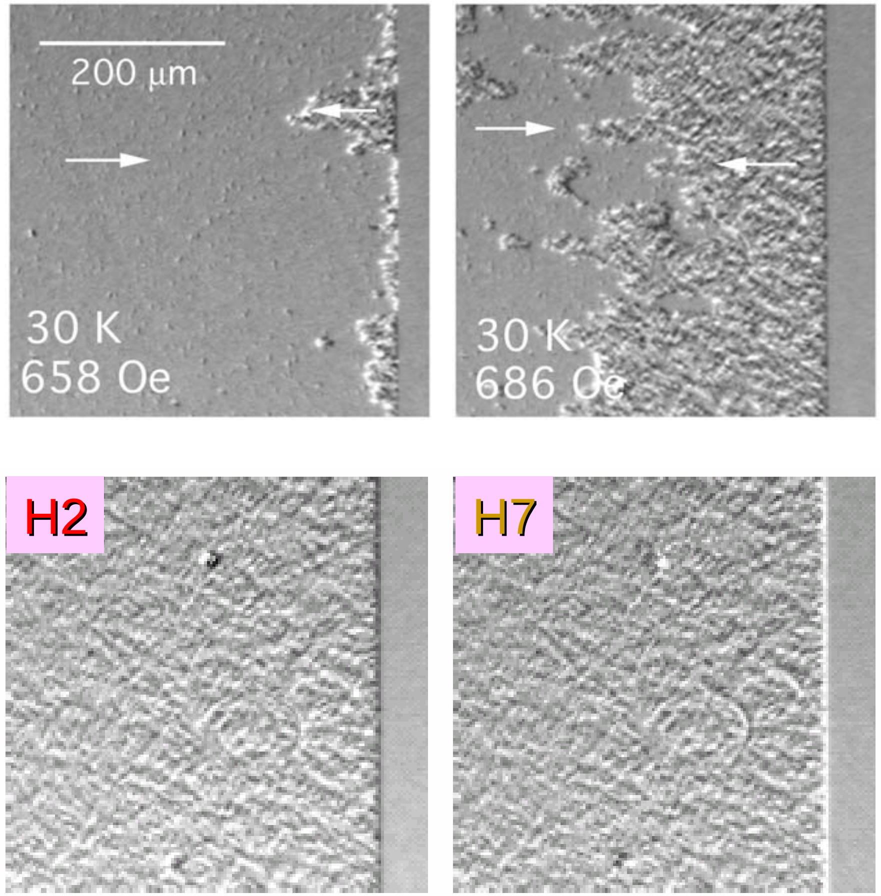

S.G.E. te Velthuis et al., JAP 87 (2000) 5046; W.-T Lee *et al*, PRB 65 (2002) 224417; Ulrich Welp *et al*, JAP**93** (2003) 7726;
Invited talks: PNCMI'02, PNCMI'04

Components of the scattering vector in grazing incidence geometry

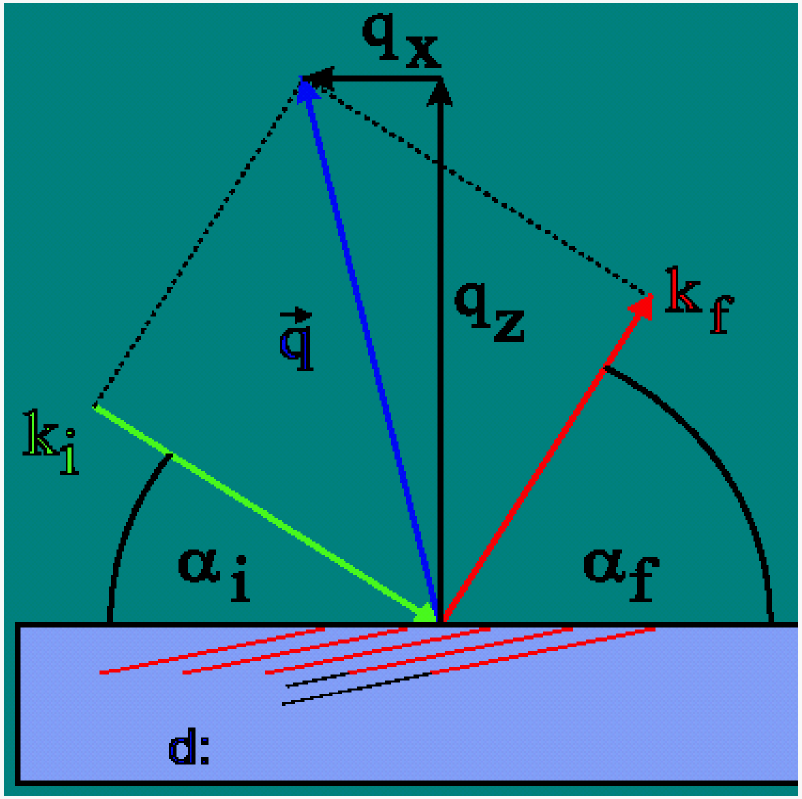

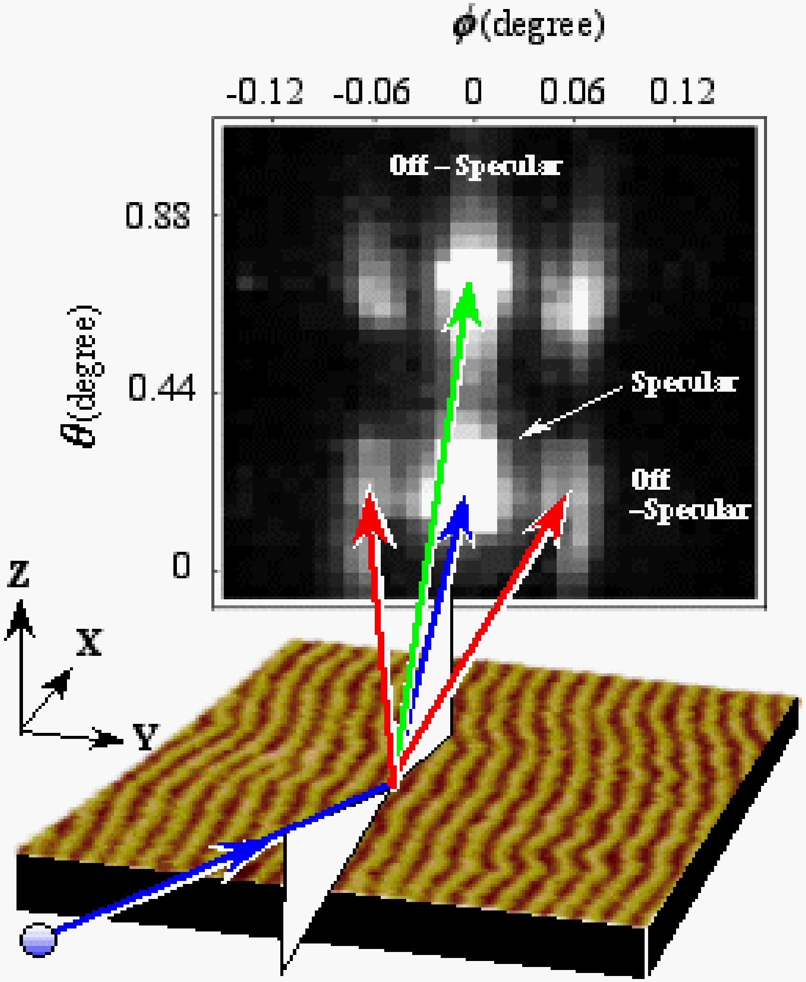

Geometry at grazing incidence

α_f Resolve with PSD

φ Resolve with Spin Echo

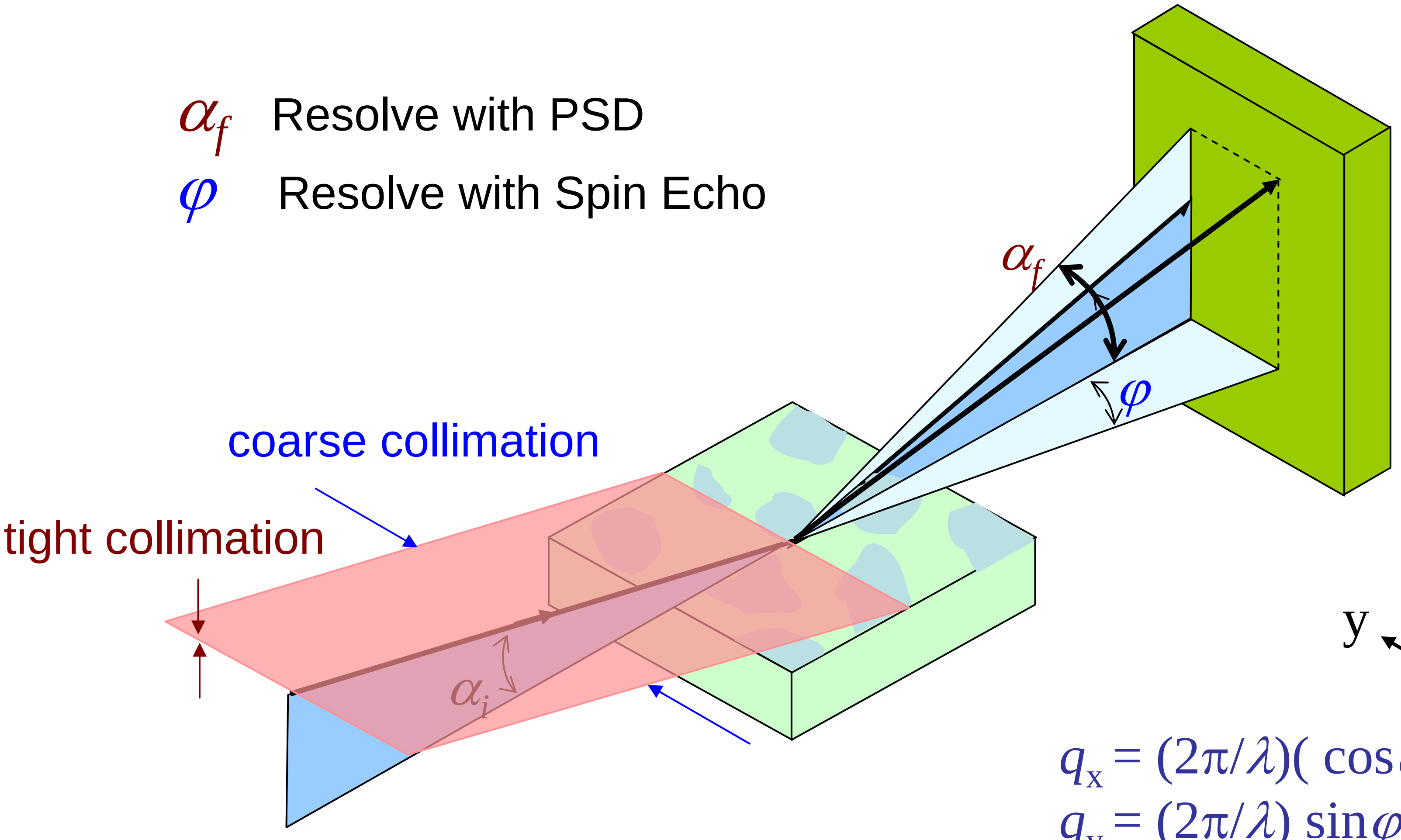

$q_x = (2\pi/\lambda)(\cos\alpha_f - \cos\alpha_i)$

$q_y = (2\pi/\lambda)\sin\varphi$

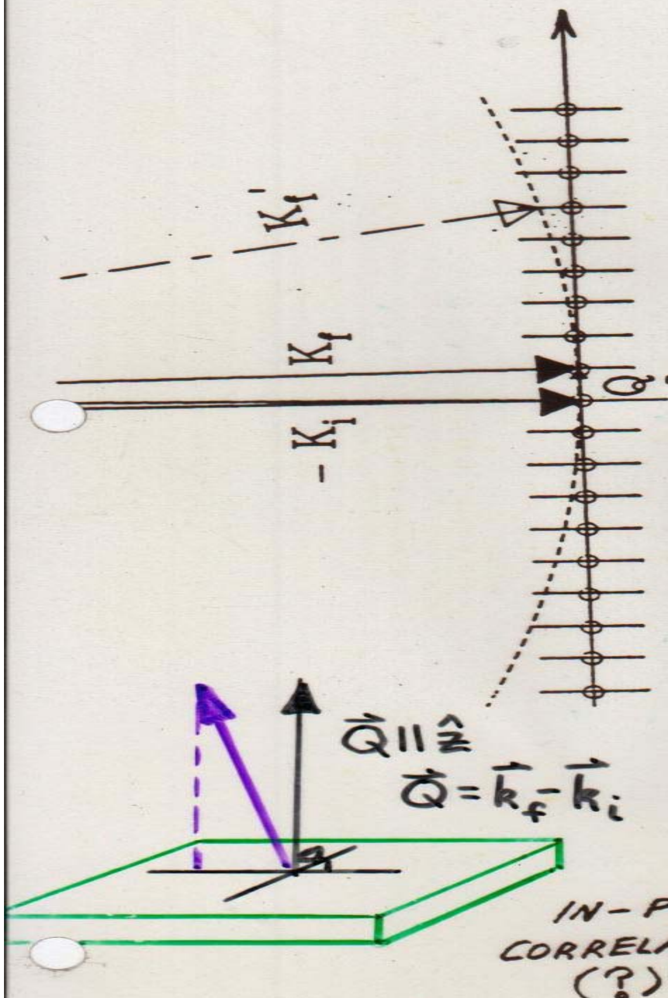

K_f'
K_f
- K_i
Q ~0.1 Å^-1
Q ∥ ẑ
Q = k_f - k_i

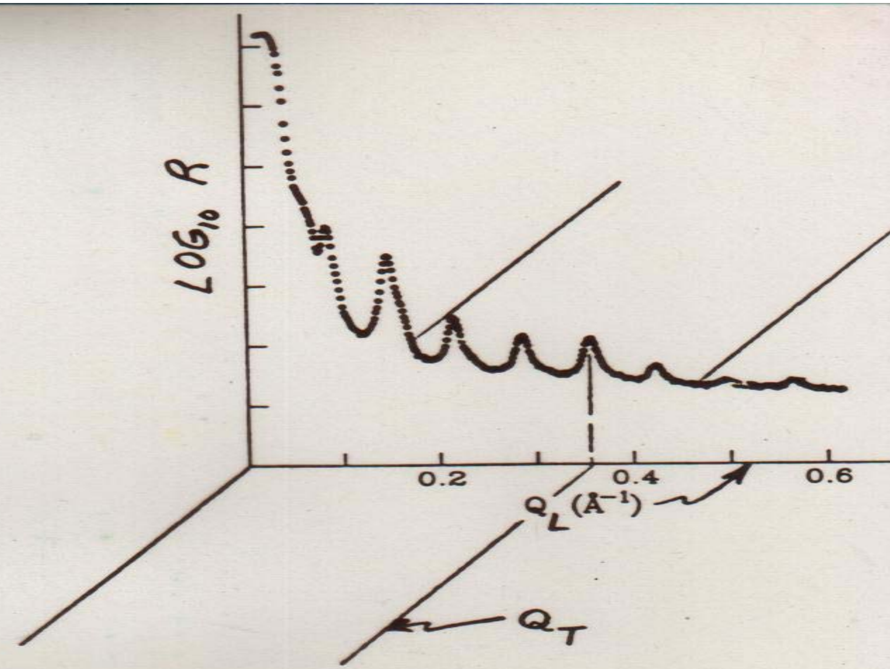

LOG10 R
0.2
0.4
0.6
Q_L (Å^-1)
Q_T

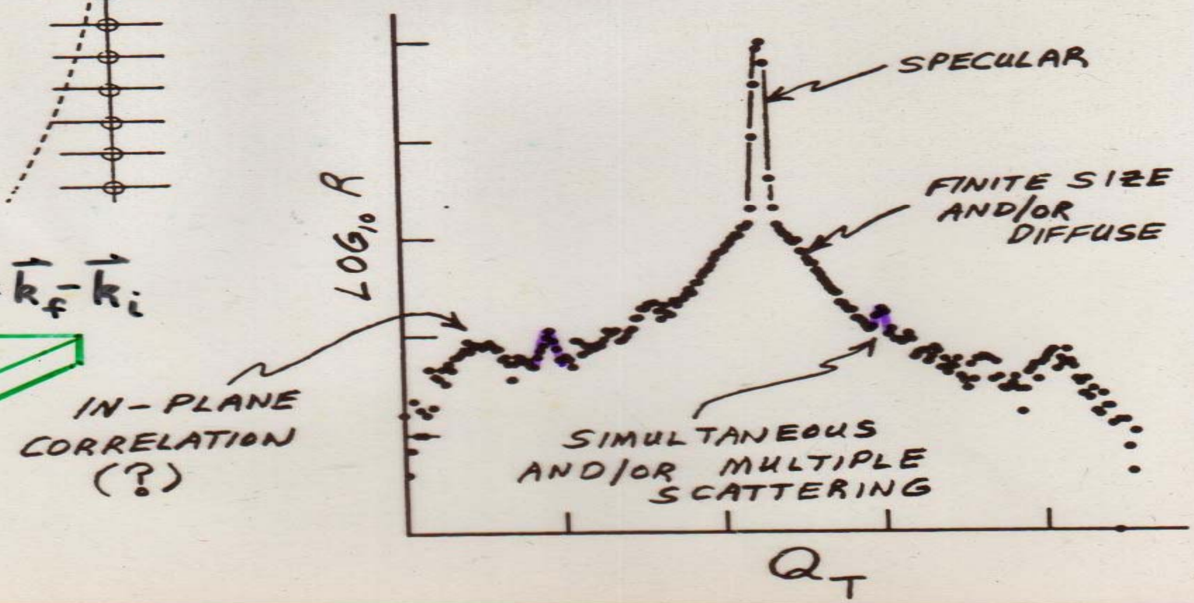

SPECULAR
FINITE SIZE
AND/OR
DIFFUSE
LOG10 R
IN-PLANE
CORRELATION
(?)
SIMULTANEOUS
AND/OR MULTIPLE
SCATTERING
Q_T

Alternative ways of presenting the off-specular scattering

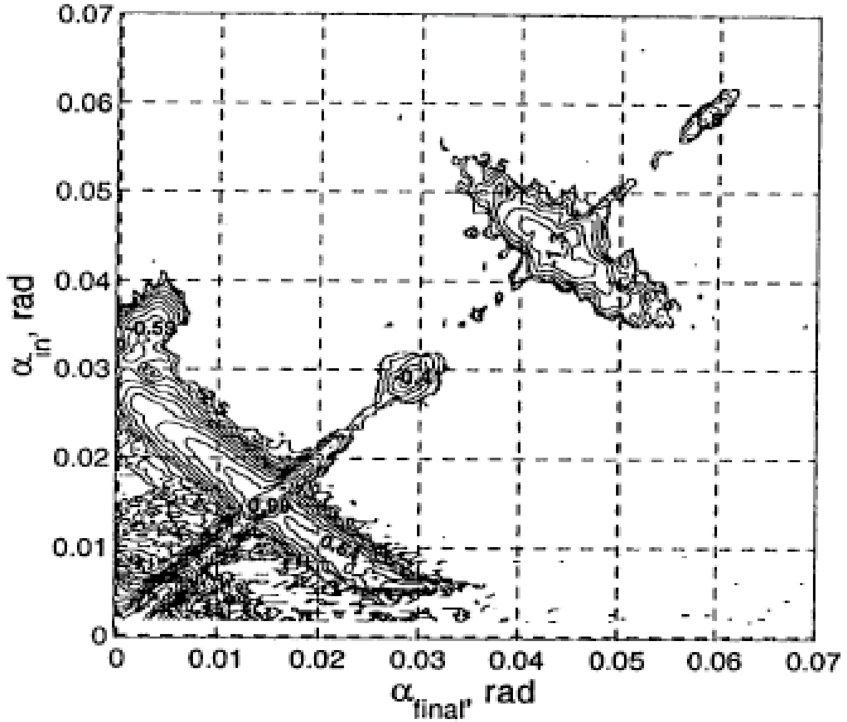

Fig. 4. Contour plot of an AF Fe/Cr multilayer, as a function of the angles of incidence α_{in} $(=\theta_{\text{i}})$ and scattering α_{final} $(=\theta_{\text{f}})$. The large peaks on the diagonal are AF [4].

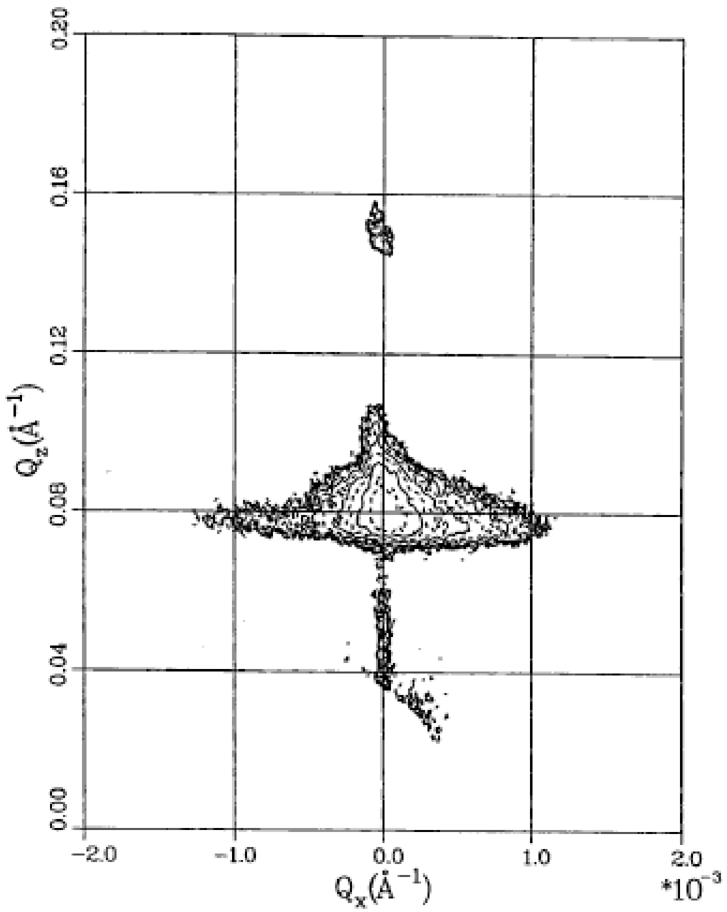

Fig. 5. Contour plot of an AF Fe/Cr multilayer, as a function of q_x, q_z. The strong innermost peak along the line $q_x = 0$ is AF; the outer weak one is structural [5].

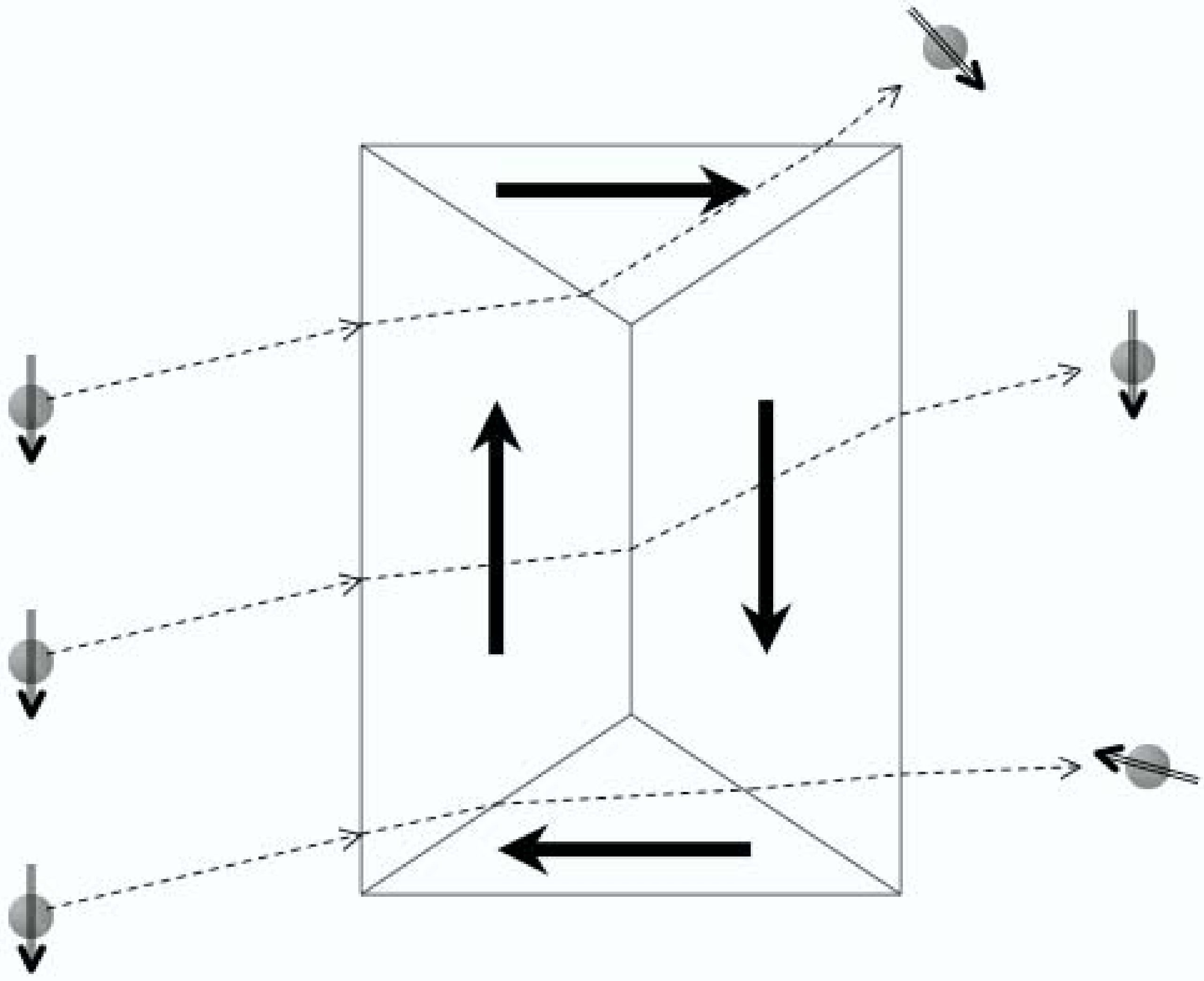

Magnetic off-specular scattering

4 terms can be counted: I^{++}, I^{+-}, I^{-+} , I^{--}

First magnetization reversal

- EVA reflectometer at ILL with polarized ^{3}He cell for polarization analysis

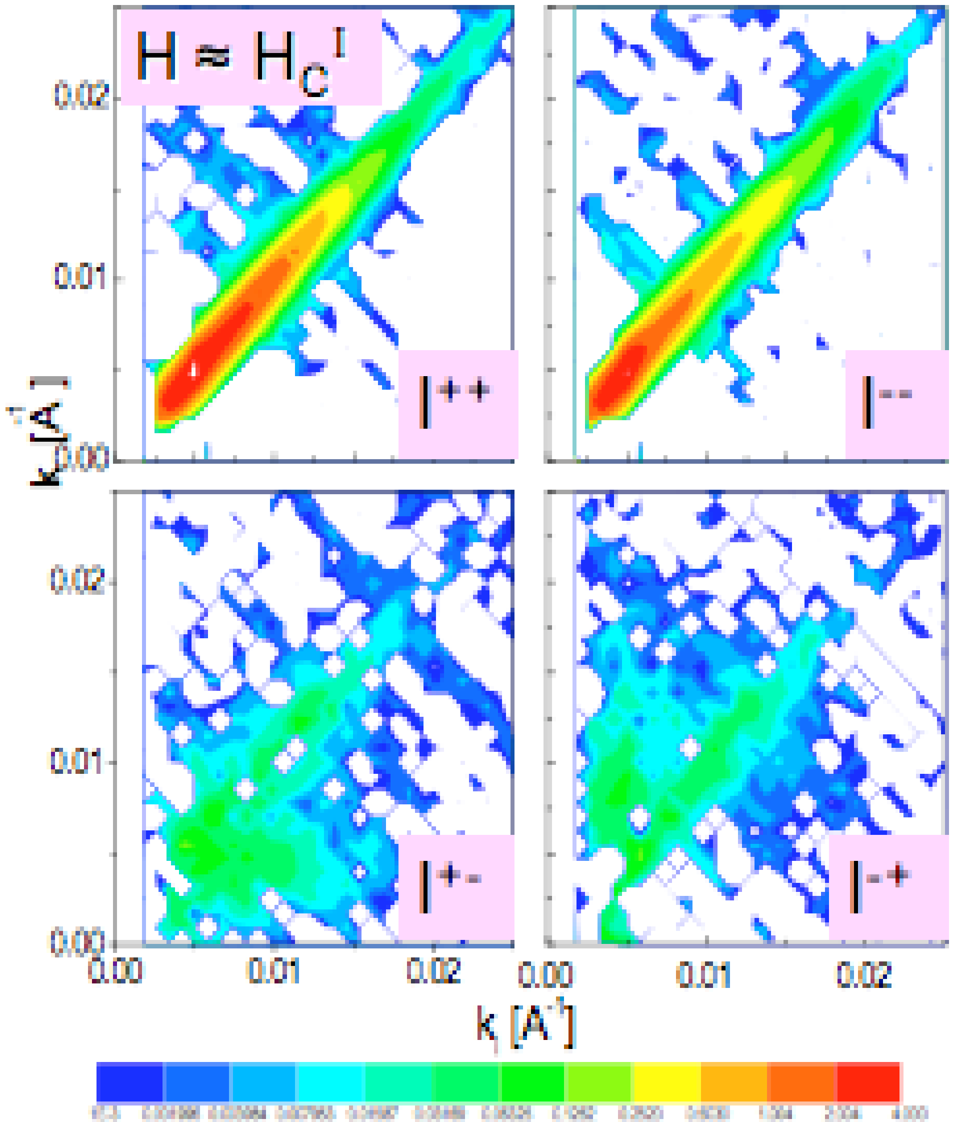

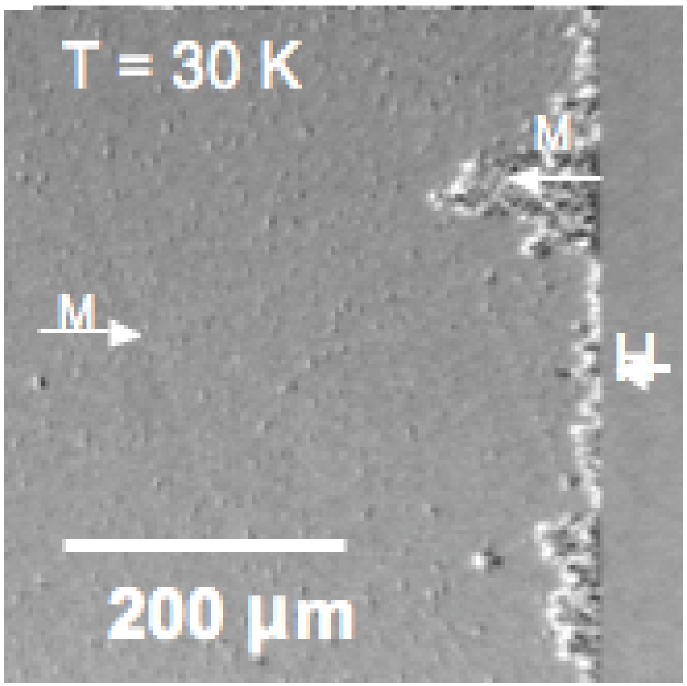

- Predominately non-spin flip reflectivity
- Weak spin flip off-specular scattering

- Domain wall rapidly moves into film, leaving behind small domains

Along trained curves (H ≈ 0)

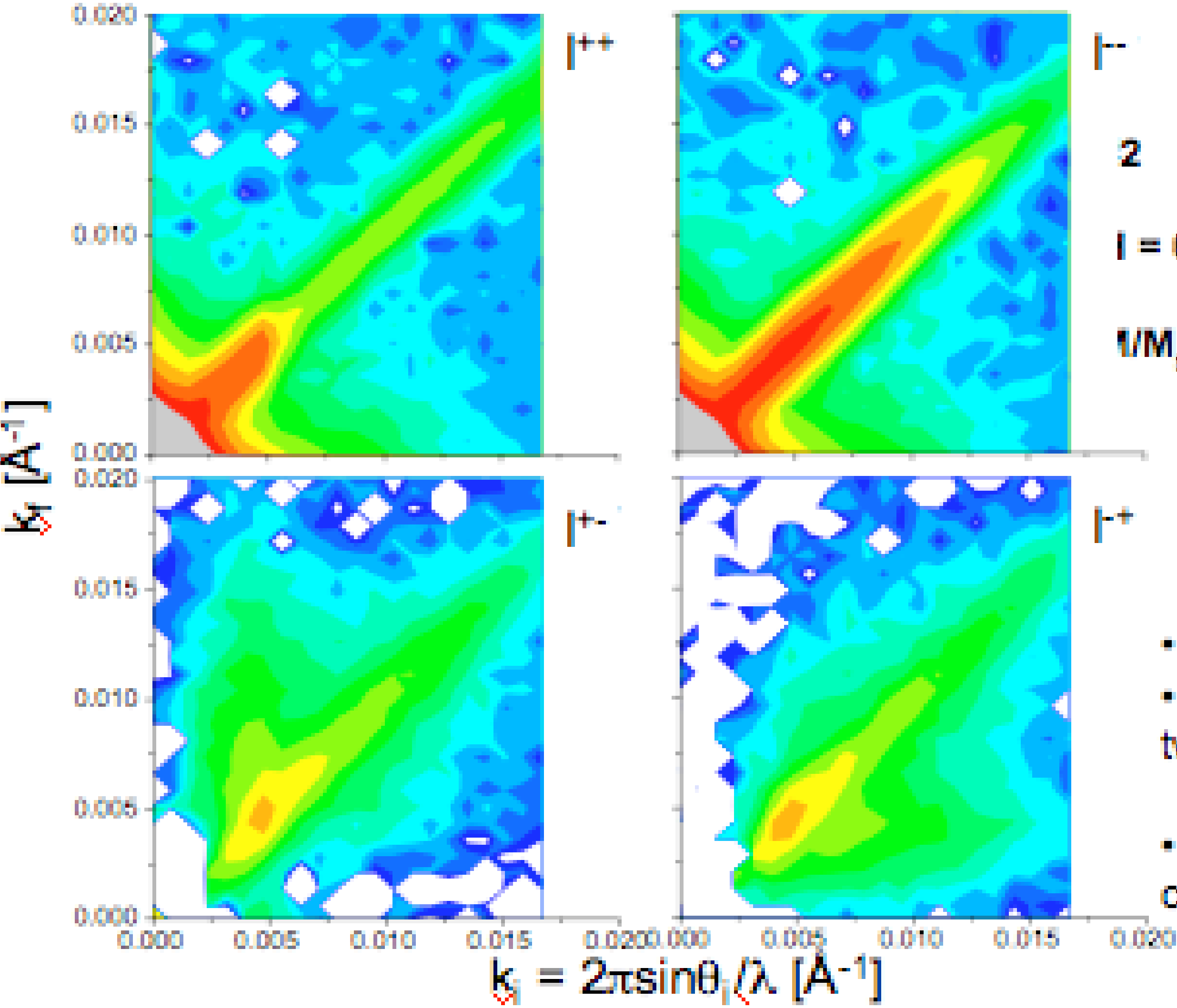

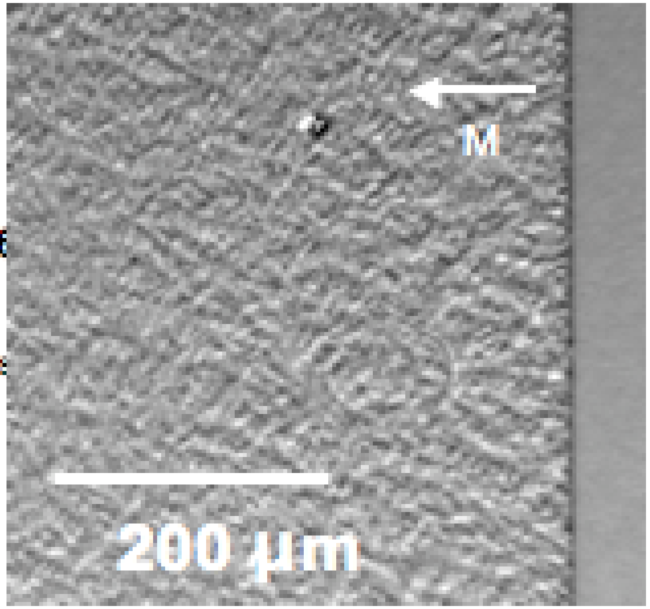

- Spin flip reflectivity + scattering
- Scattering is not symmetric for two spin flip cross-sections
- Domain pattern appears not to change

Subsequent magnetization reversals

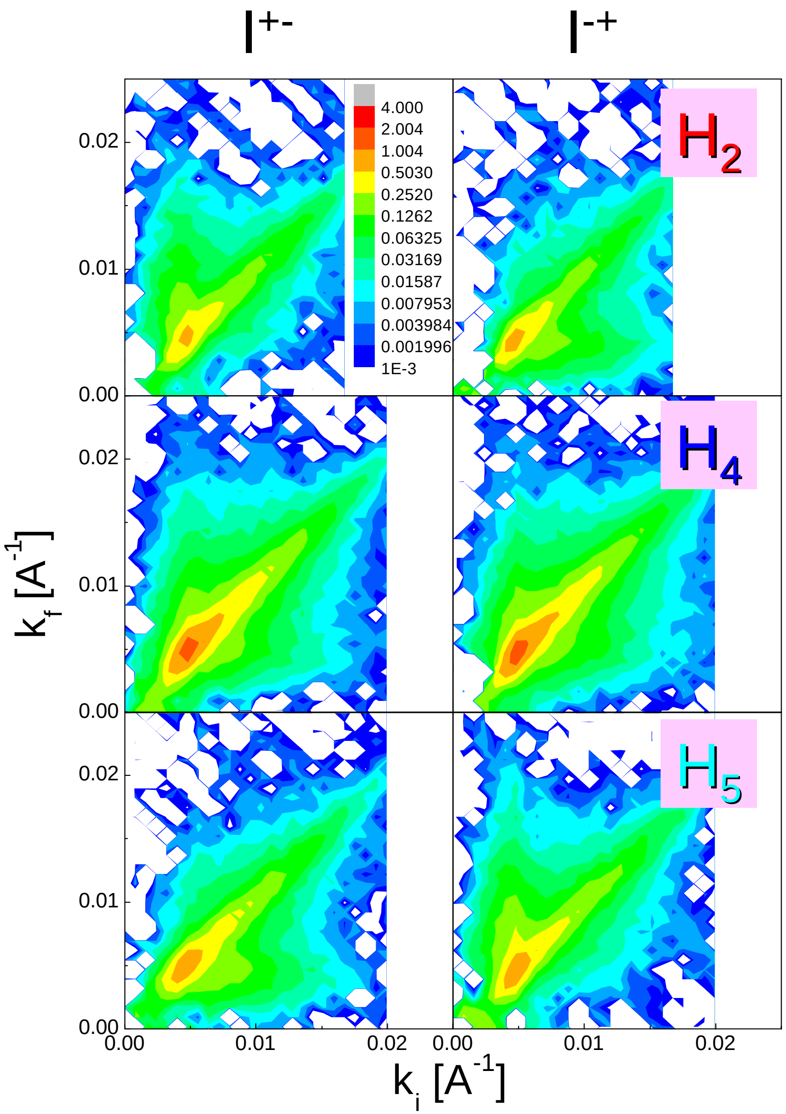

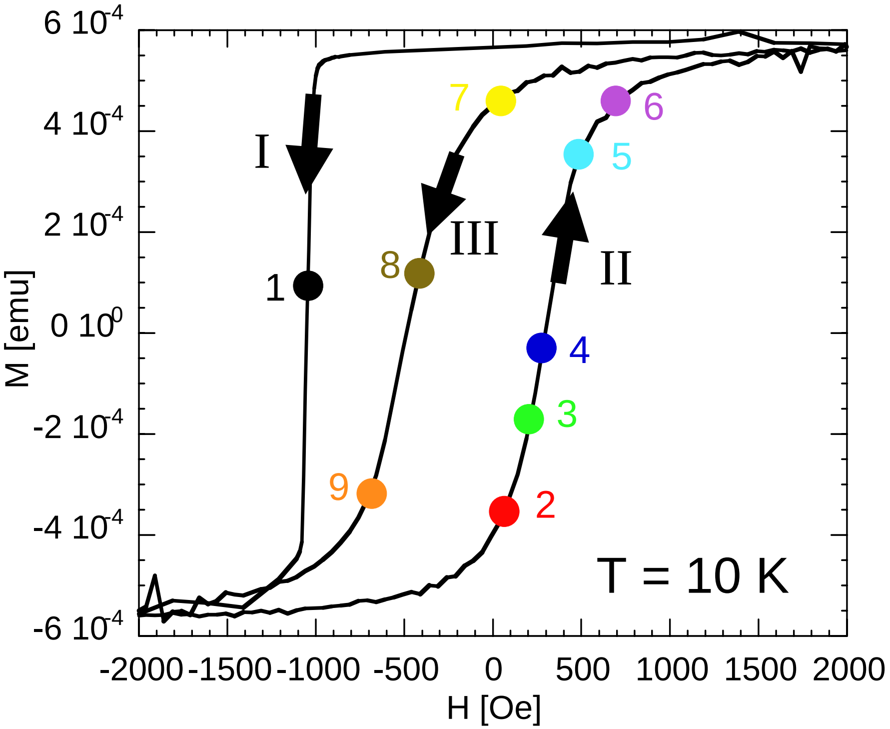

Exchange bias in thin Co/CoO films

EVA@ ILL
With ^{3}He analyzer
2001

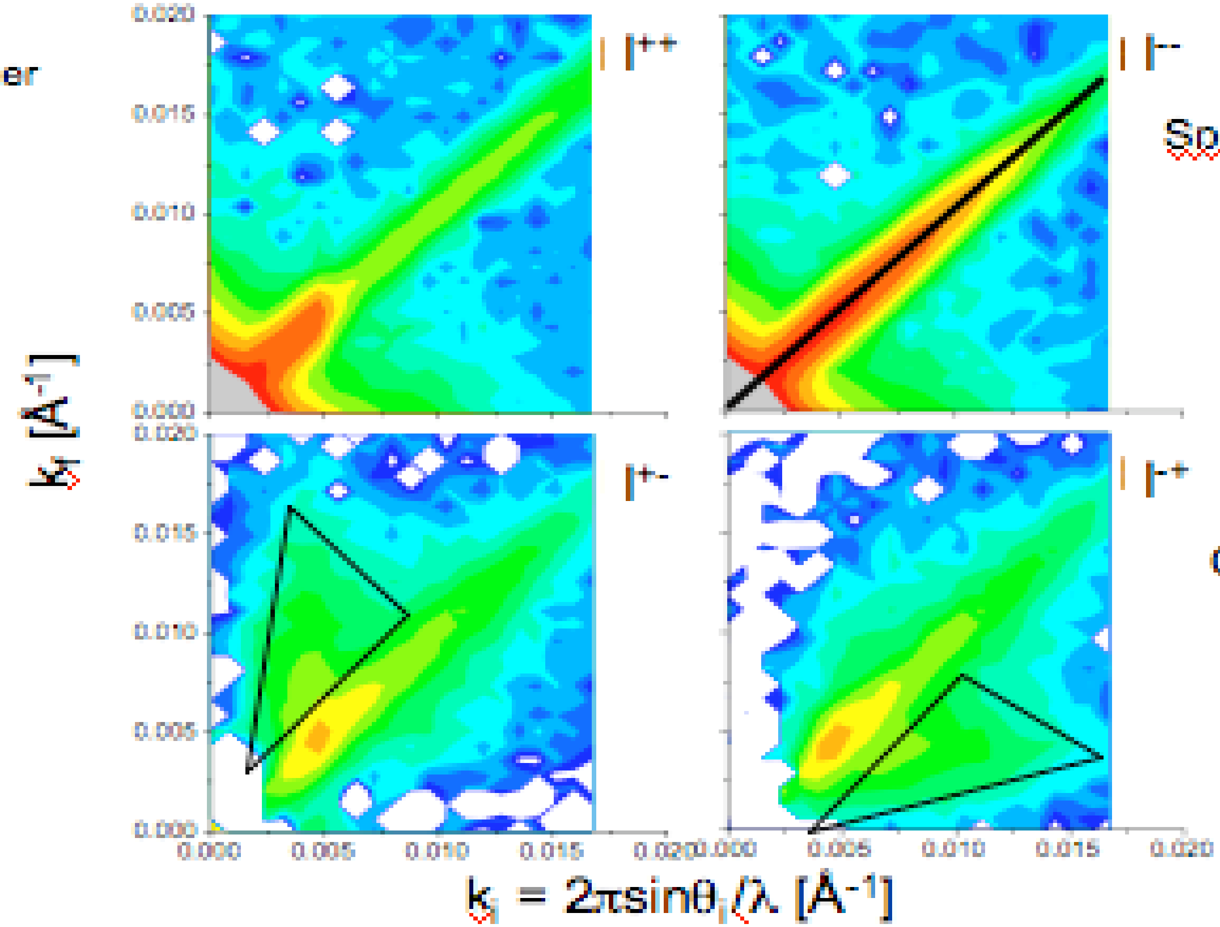

Specular reflection

Off- Specular
Scattering

S.G.E. te Velthuis et al., JAP 87 (2000) 5046; W.-T Lee *et al*, PRB 65 (2002) 224417; Ulrich Welp *et al*, JAP93 (2003) 7726;

Fe/Cr(001) superlattice

Top: experimental map (I^-)

Bottom: calculated map

Right:magnetic structure

V. Lauter Pasyuk et al,

PRL 89, 167203 (2002)

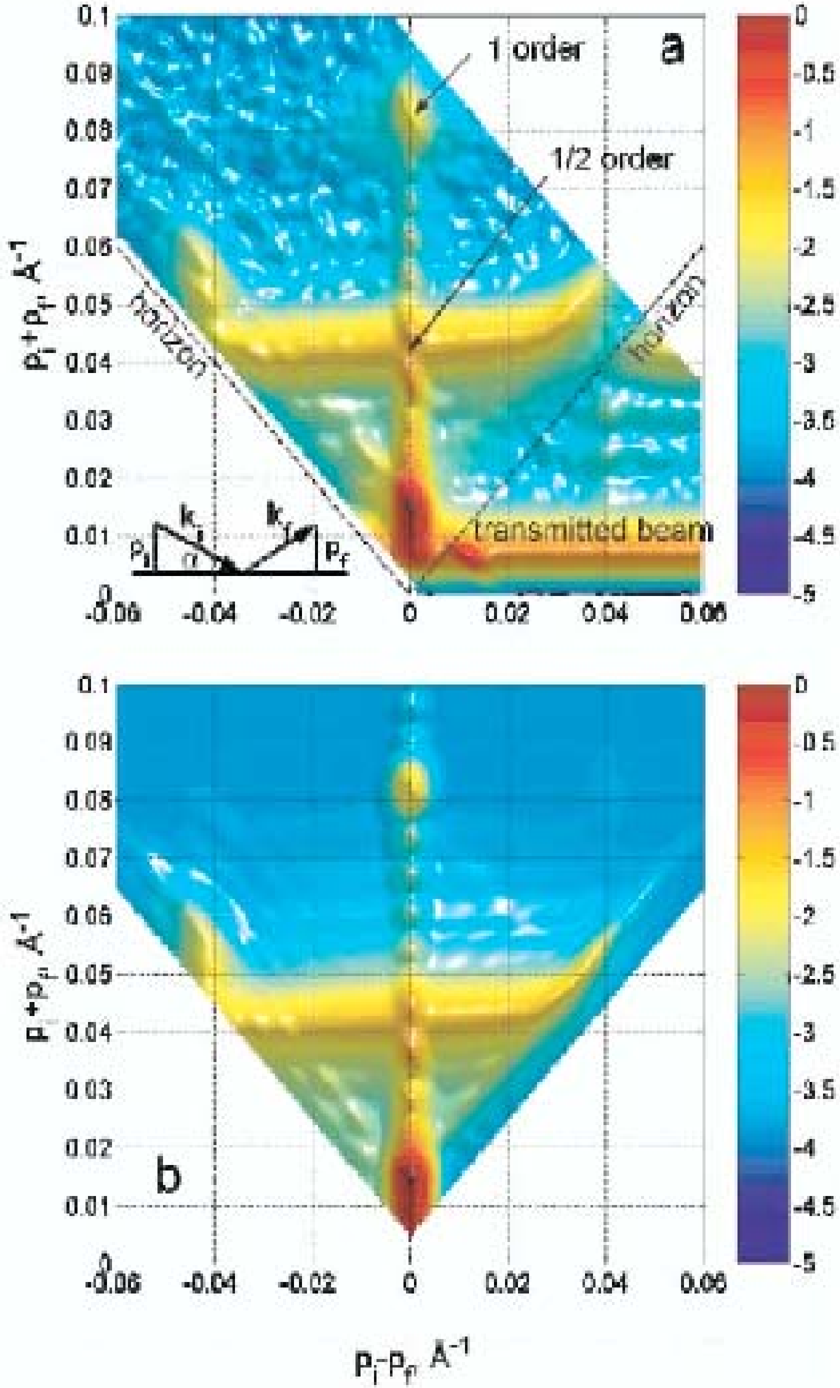

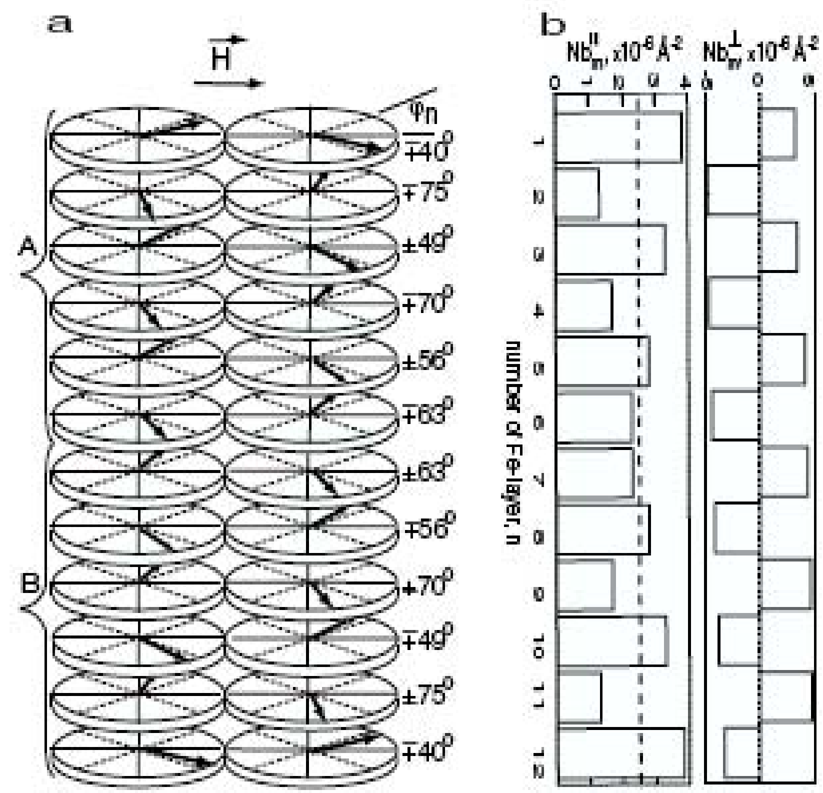

Distorted Wave Born Approximation (DWBA)

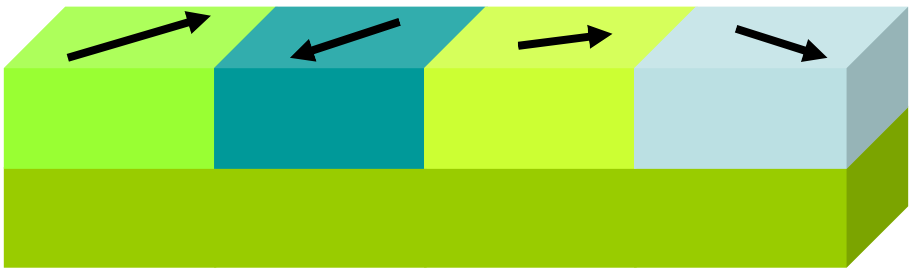

=

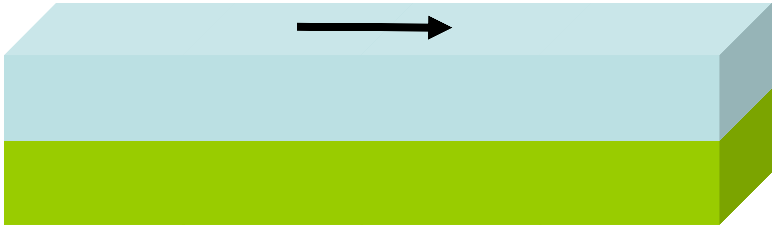

+

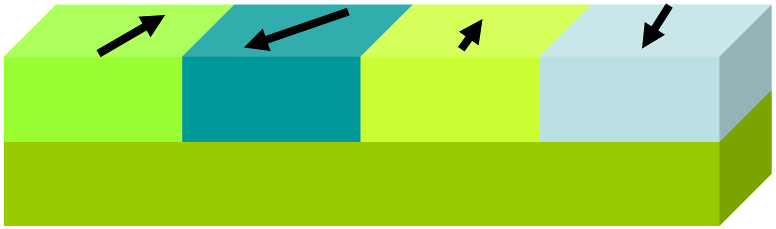

Reflectivity

Scattering

Correlated magnetic domains

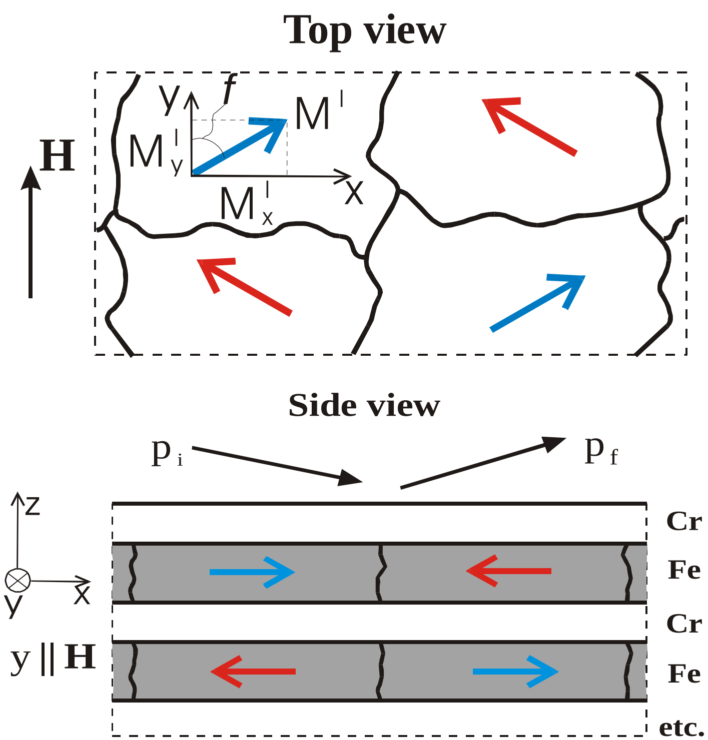

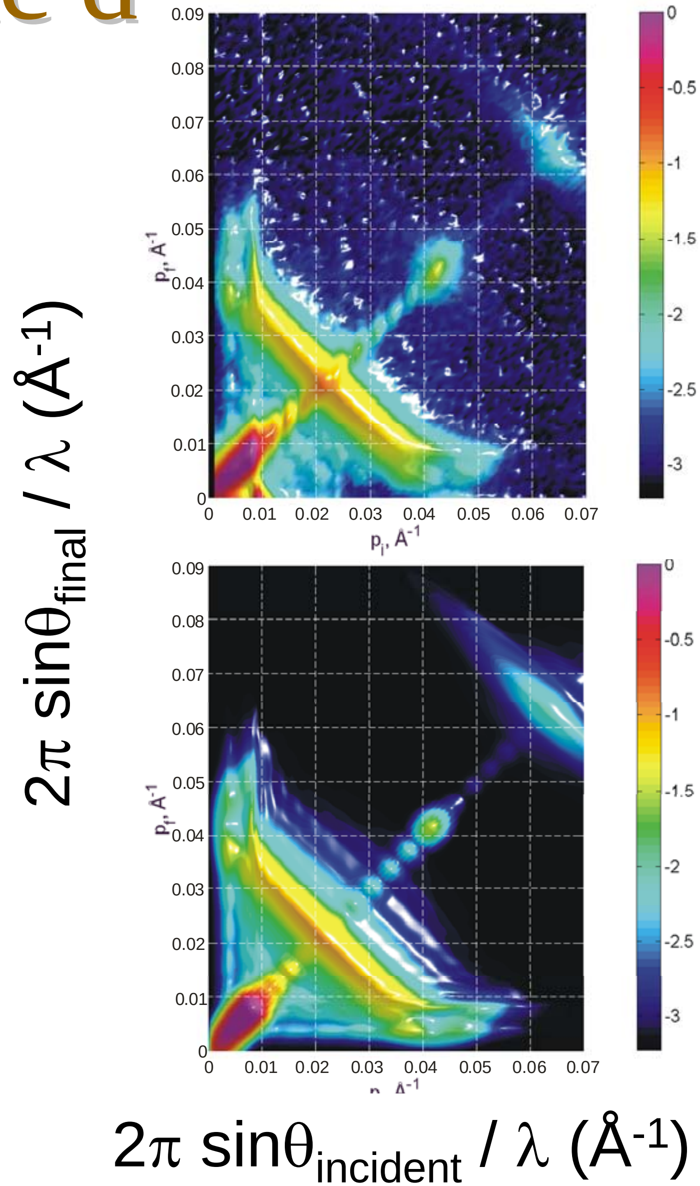

Magnetic domains in [Cr(9Å)/^{57}Fe(70Å)]x12 multilayers

O.Nikonov, V.Lauter-Pasyuk, B.Toperverg, H.J.Lauter, L.Romashev, E.Kravtsov, V.Ustinov

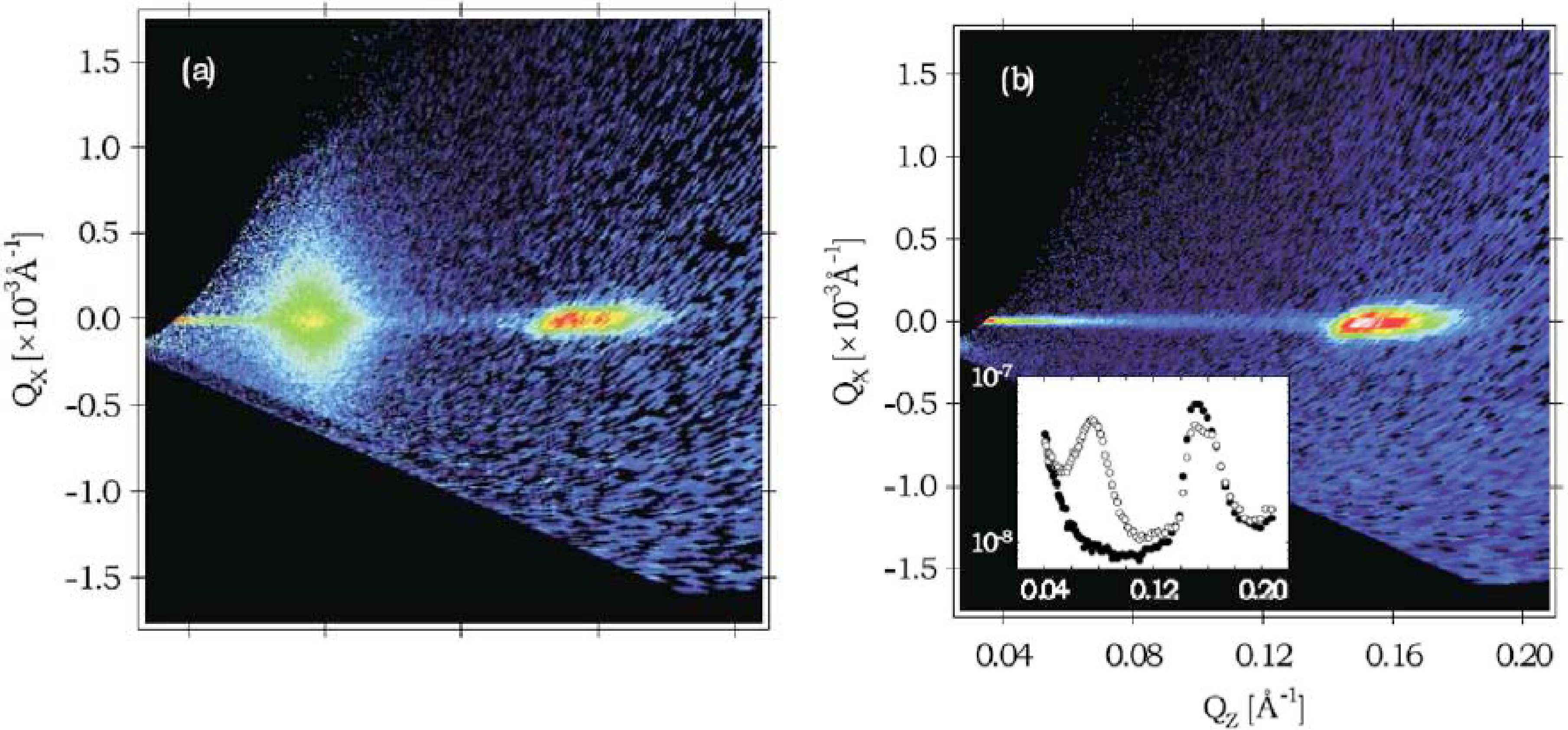

Figure 33: Partial reciprocal map from scattering of a Co(2 nm)/Cu(2nm) multilayer with 50 repeats. Here the reciprocal space is rotated by 90 compared to the schematic shown in Fig. ??. (a) Scattering pattern taken in remanence. The half order peak at $Q_z = 0.075$ Å^{-1} arising from antiferromagnetic coupling is clearly visible together with diffuse scattering surrounding this peak in the Q_x and Q_z direction. The first order peak at twice the wave vector is the first order multilayer structural Bragg peak. (b) The corresponding measurement in a saturation field of H = 700 Oe. The nuclear peak appears wider than the specular ridge because of instrumental resolution. The inset shows the specular reflectivity for the low (open symbol) and high (closed symbol) field data. (from Ref. [121])

S. Langridge et al, PRL 85, 4964 (2000)

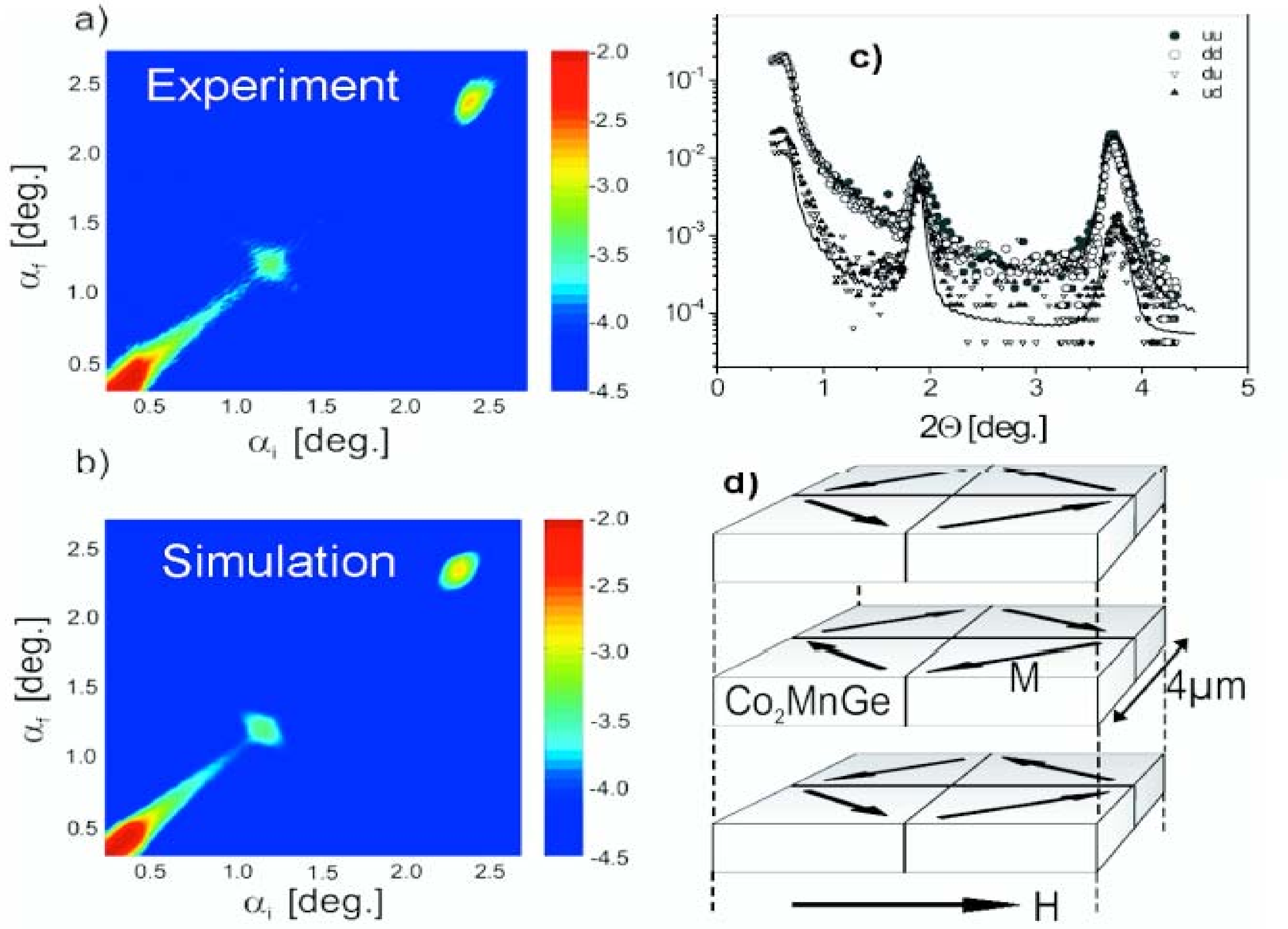

Co2MnGe(3nm/V(3nm) multilayer

A. Bergmann et al Phys.Rev.B 72, 214403 (2005)

simulation based on the Distorted Wave Born approximation

Fe implanted in yttrium stabilized zirconia
Fe crystals grown during annealing

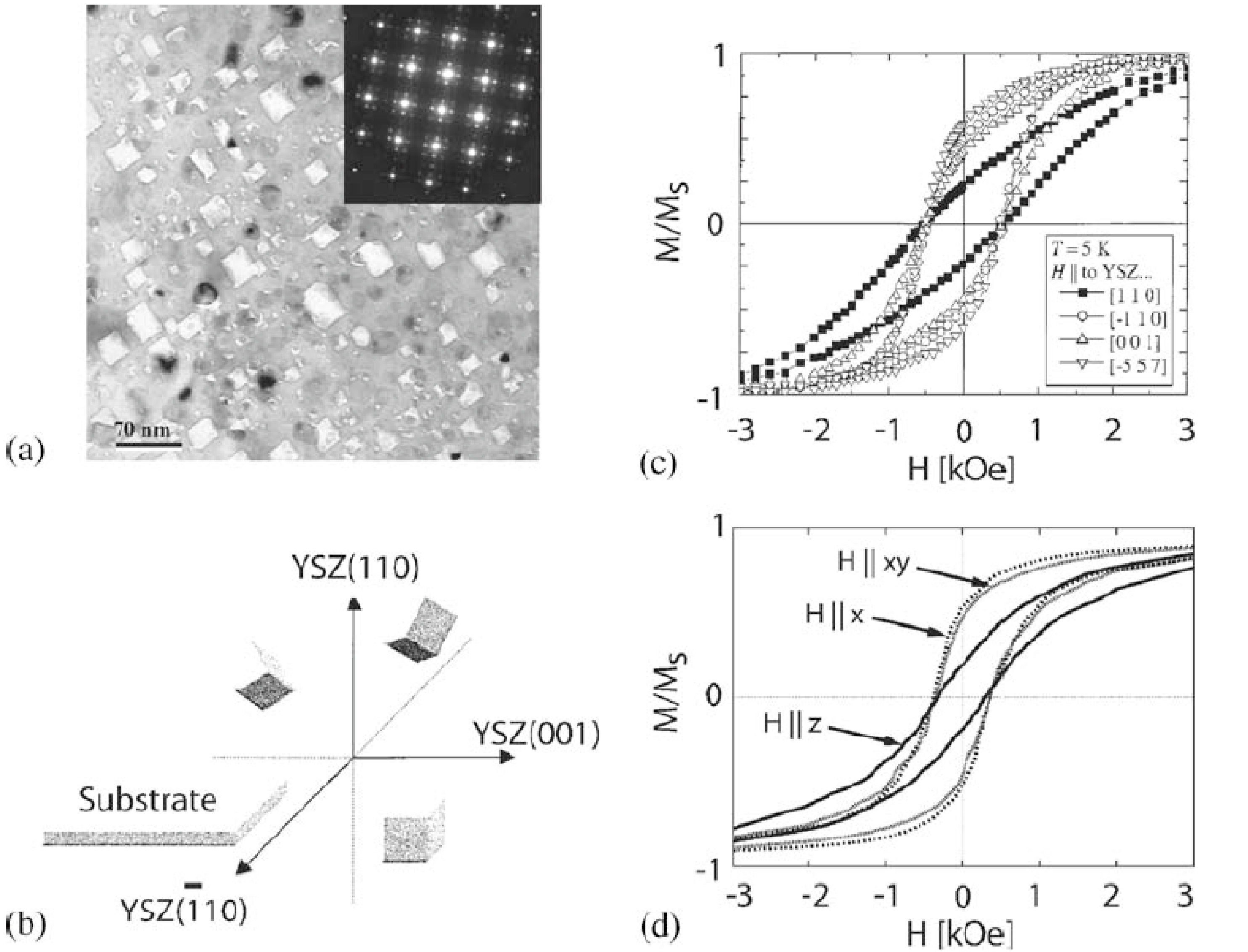

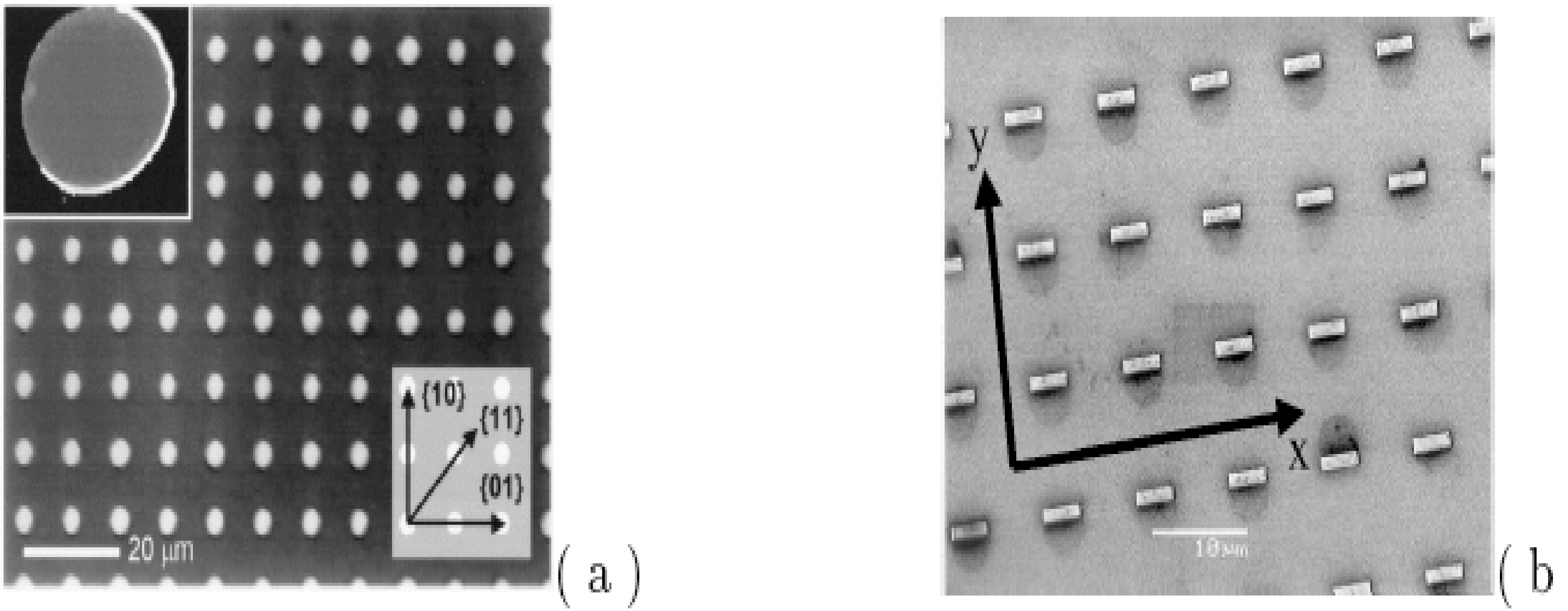

Figure 46: (a) Optical microscopy picture of an arrangement of Co disks in a square lattice with a 10 μm period [170]. The length of the white bar corresponds to 20 μm. The inset (upper left corner) shows an AFM image of a single disk. In the lower right corner the in-plane directions are defined. (b) SEM picture of an array of Co bars [171]. The white marker corresponds to 20 μm.

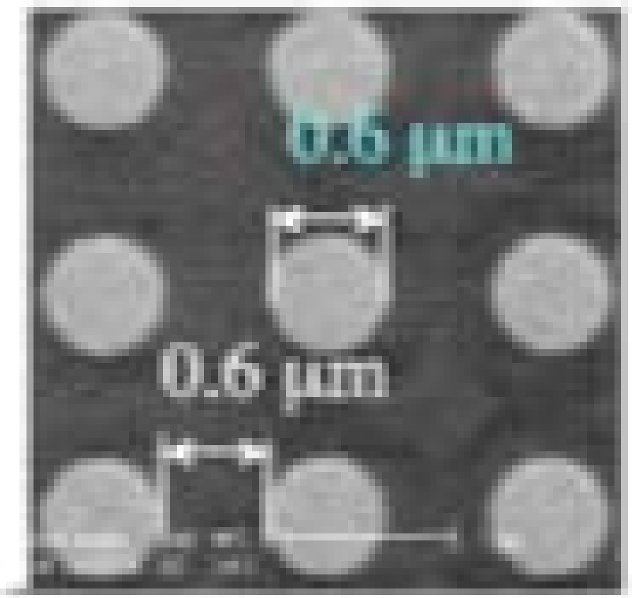

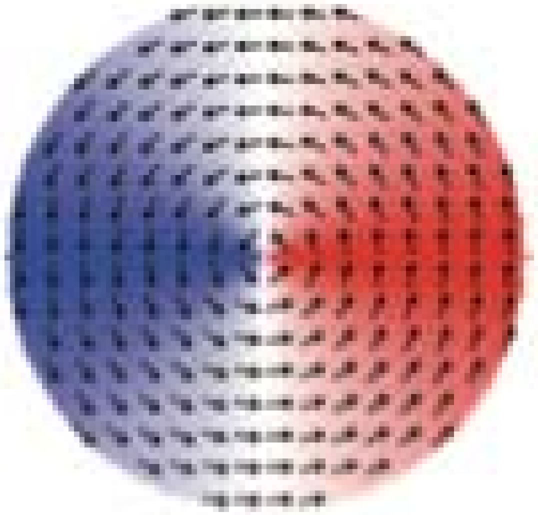

Array of permalloy disks, and their magnetization
S. Bader, Rev. Mod. Phys. **78**, 1 (2006)

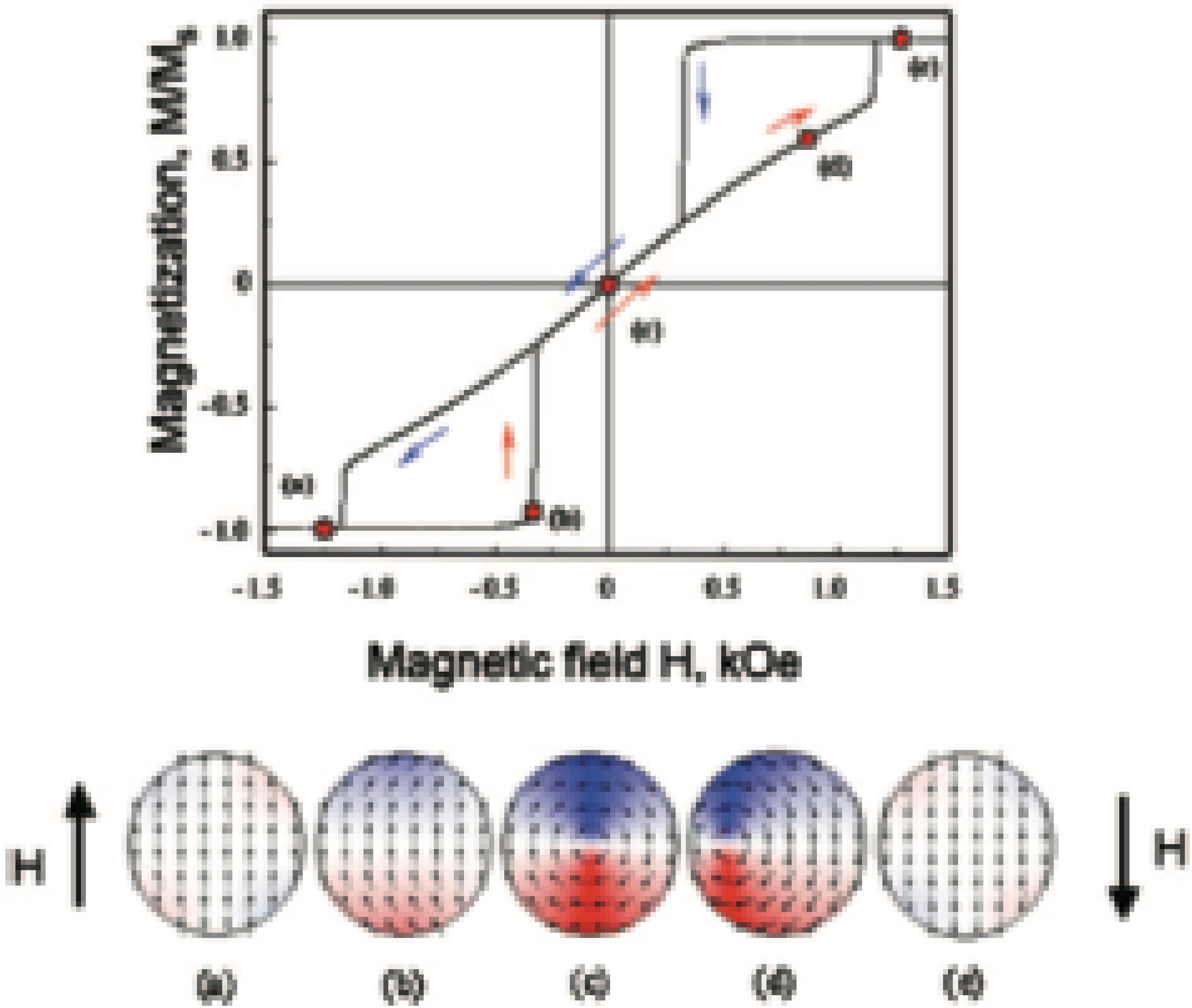
Magnetization, M/Ms
Magnetic field H, kOe
1.0
0.5
0
-0.5
-1.0
-1.5
-1.0
-0.5
0
0.5
1.0
1.5
(a)
(b)
(c)
(d)
(e)
H
H

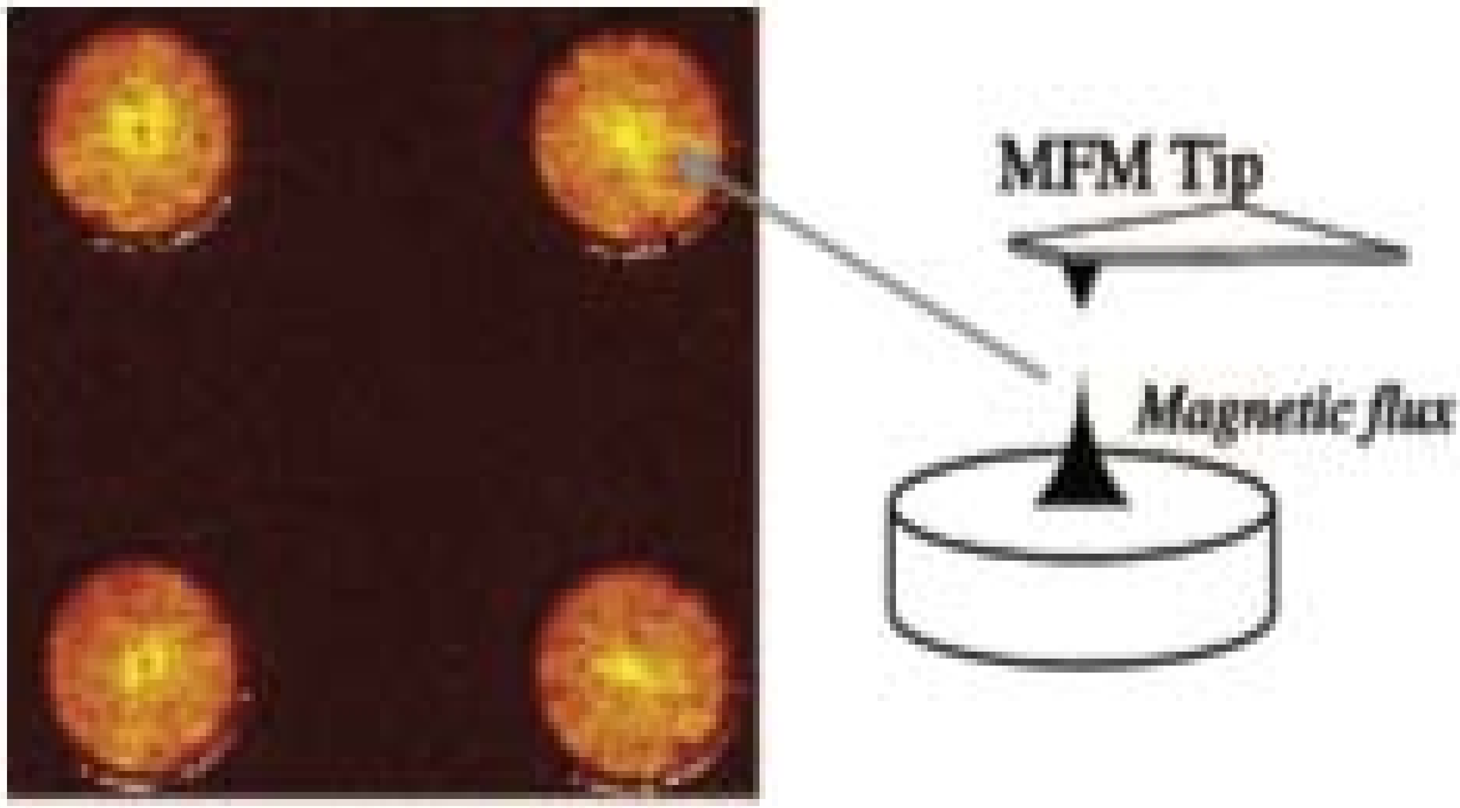

S.D. Bader Rev. Mod. Phys. 78, 1 (2006)

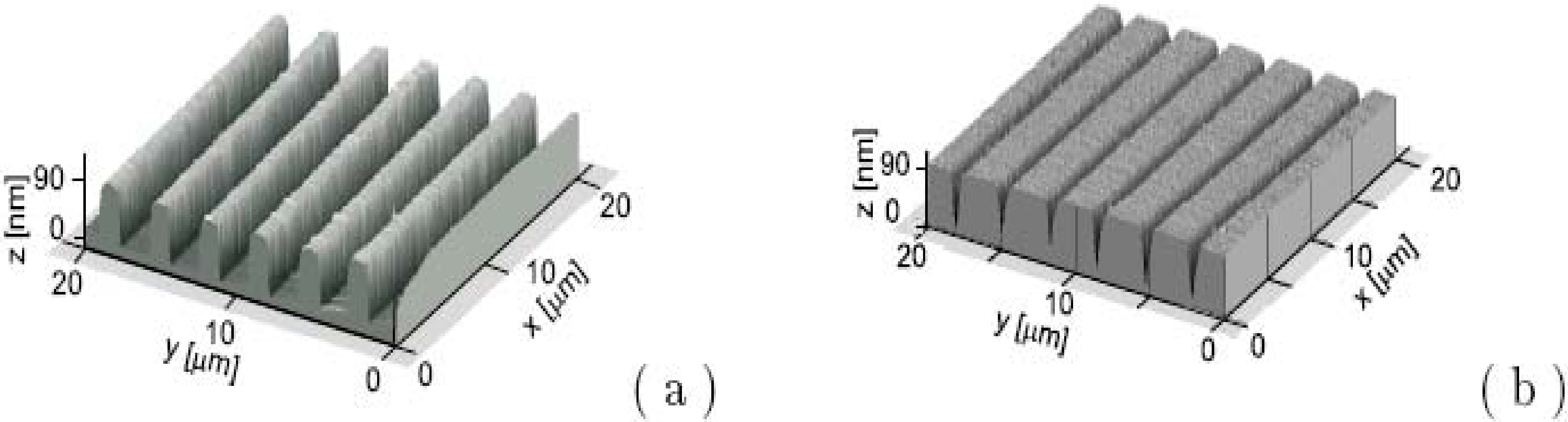

Figure 48: Surface topography of arrays of $Co_{0.7}Fe_{0.3}$ stripes obtained with an atomic force microscope shown in a 3-dimensional surface view. The displayed area is 20 x 20 μm^2. (a) Narrow stripes with a width of 1.2μm and (b) wide stripes with a width of 2.4μm.

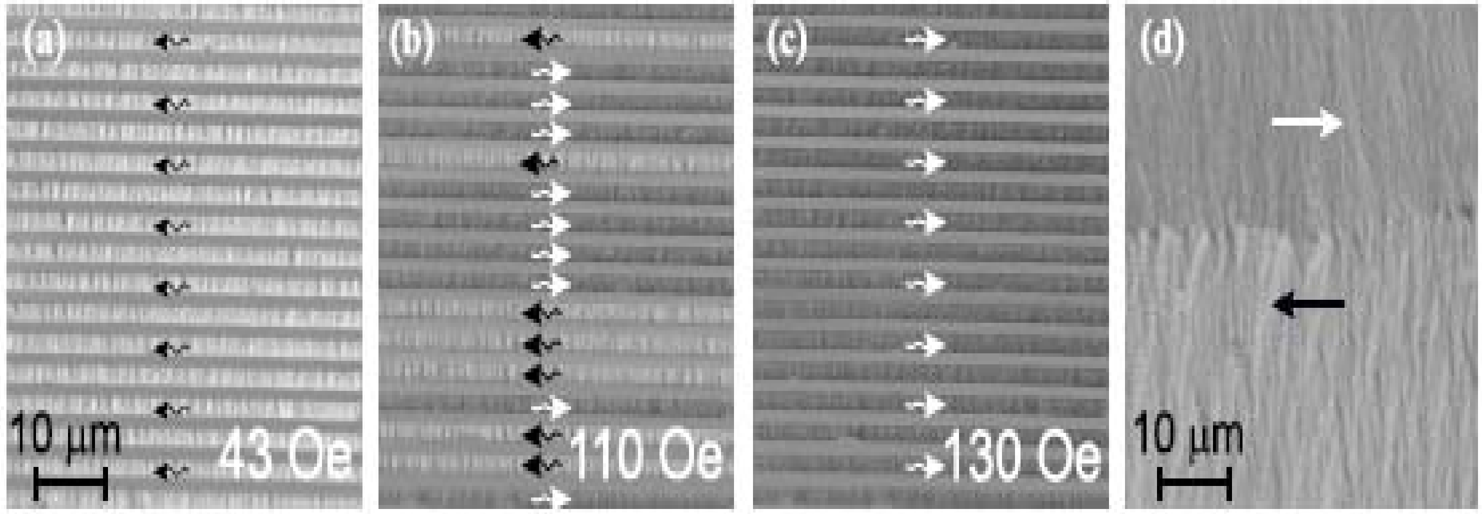

Figure 51: (Kerr microscopy images taken below H_c (a), at H_c (b), and above H_c (c) with the magnetic field aligned parallel to the stripes. The plane of incidence results in a top-down magnetooptical sensitivity axis perpendicular to the stripes. The curly arrows indicate the mean magnetization direction as well as the presence of ripple domains. (From Ref. [182]).

K. Theis-Bröhl et al, Phys. Rev. B71 (2005)

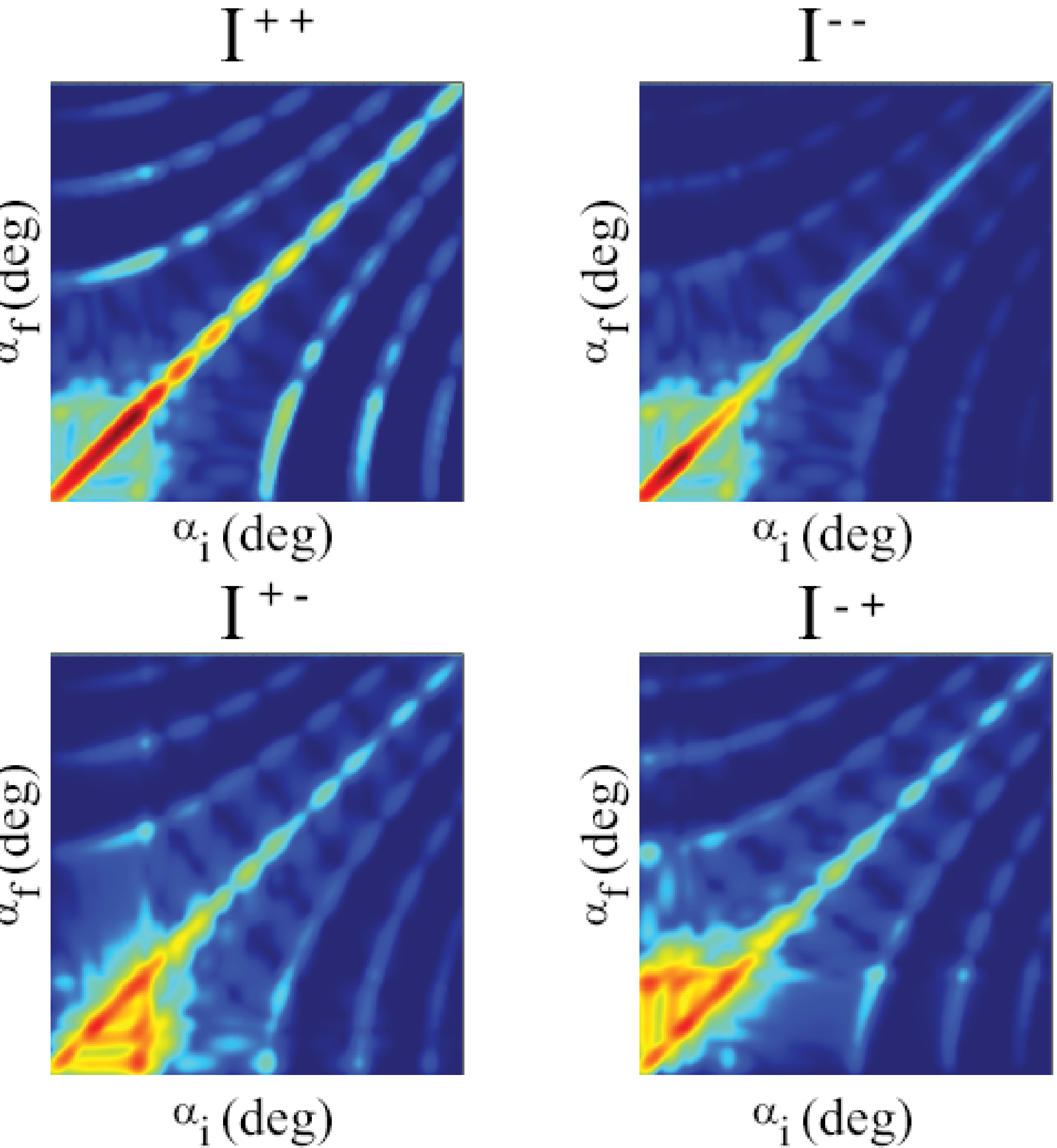

Neutron intensities
periodic stripe array
H=43 Oe

K. Theis-Bröhl et al,
Phys. Rev. B67, 184415 (2003)

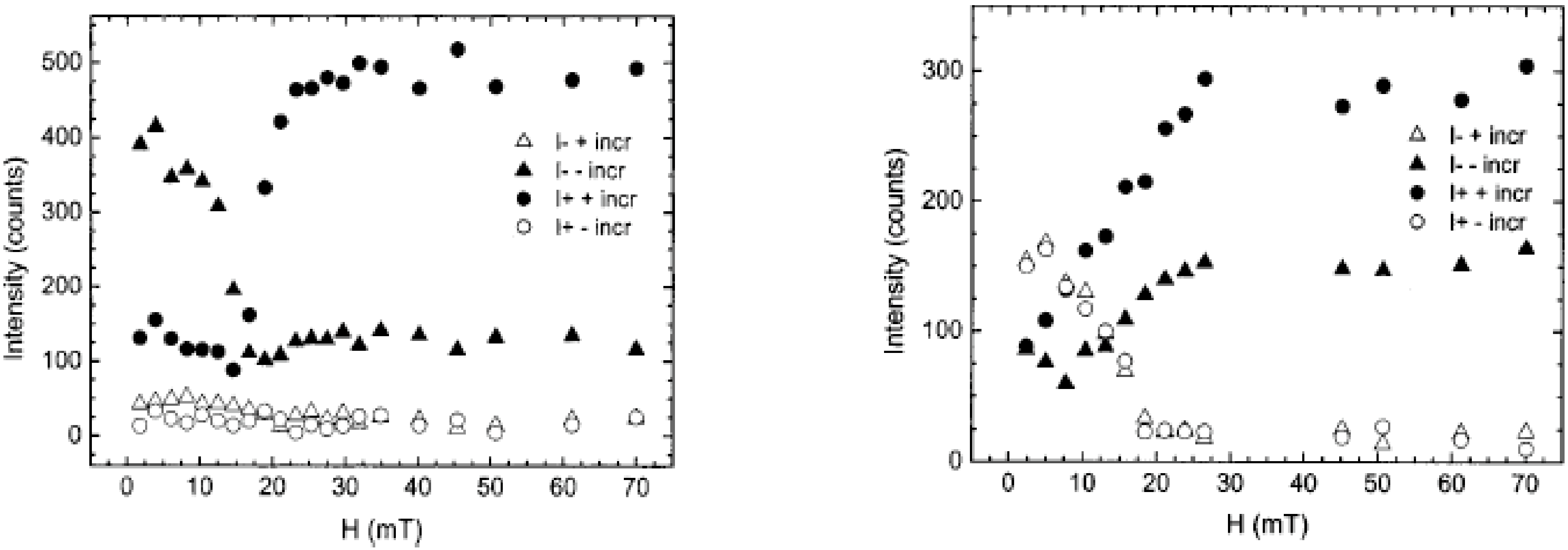

Figure 47: Intensity of the first-order off-specular satellite peak as a function of decreasing field H applied along the positive x direction of rectangular bars (left) and along the positive y direction of rectangular bars (right) [see Fig. 46(b)]. Prior to this experiment, the bars were saturated along the negative x direction. [171]

K. Temst et al, Superlattices and Microstructures 34, 87 (2003)

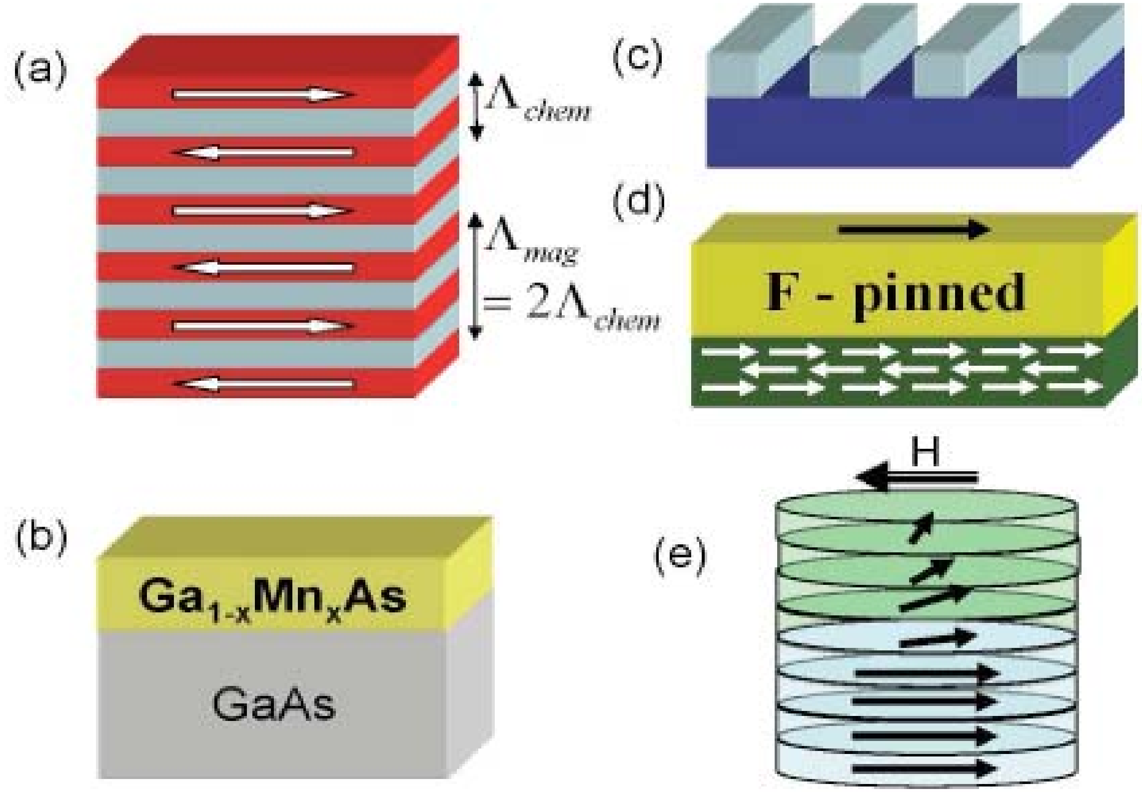

Figure 23: Selection of magnetic nanostructures investigated by polarized neutron reflectivity experiments. (a) Exchange coupled superlattice with antiferromagnetic order; (b) dilute magnetic semiconductor as spin-aligner in semiconductor heterostructures; (c) laterally patterned magnetic films; (d) bilayer of a ferromagnetic film on an antiferromagnetic substrate with exchange bias at the common interface; (e) spring magnetic consisting of a top soft magnetic layer on a hard magnetic layer, where twisting occurs only in the soft layer and in an opposing external magnetic field.

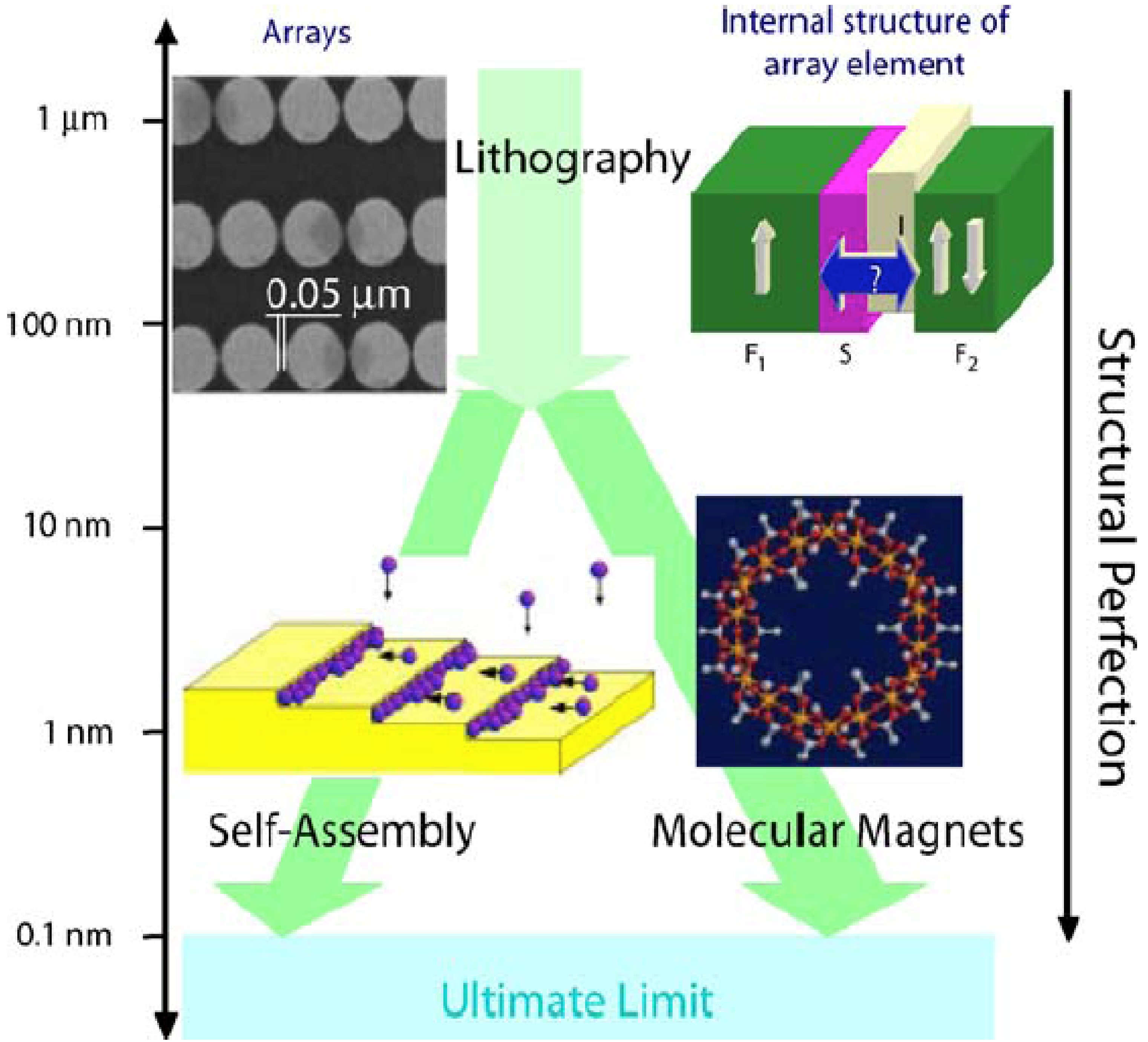

Arrays
Internal structure of array element
1 µm
100 nm
10 nm
1 nm
0.1 nm
0.05 µm
Lithography
I
?
F1
S
F2
Structural Perfection
Self-Assembly
Molecular Magnets
Ultimate Limit

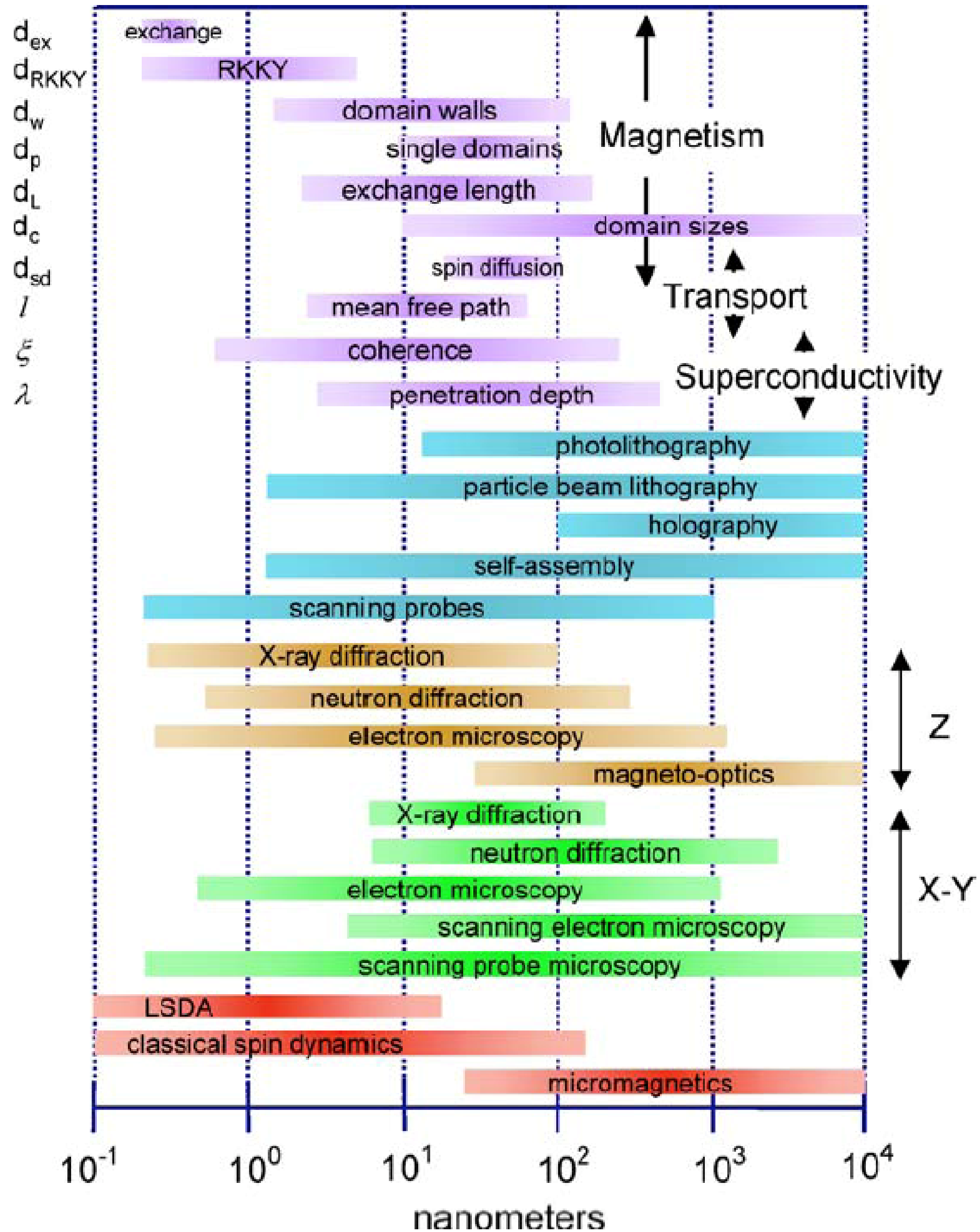

d_{ex}
d_{RKKY}
d_w
d_p
d_L
d_c
d_{sd}
l
ξ
λ
exchange
RKKY
domain walls
single domains
exchange length
domain sizes
spin diffusion
mean free path
coherence
penetration depth
Magnetism
Transport
Superconductivity
photolithography
particle beam lithography
holography
self-assembly
scanning probes
X-ray diffraction
neutron diffraction
electron microscopy
magneto-optics
Z
X-ray diffraction
neutron diffraction
electron microscopy
scanning electron microscopy
scanning probe microscopy
X-Y
LSDA
classical spin dynamics
micromagnetics
10^{-1}
10^{0}
10^{1}
10^{2}
10^{3}
10^{4}
nanometers

The SNS is being built at Oak Ridge, Tennessee by a partnership of 6 national laboratories. It will be a national user facility dedicated to neutron scattering research. In operation, the 1.4 MW accelerator system will provide 1 GeV protons that impact on a liquid mercury target to produce neutrons by the spallation process.

Four different moderators slow these neutrons to thermal or sub-thermal energies, and up to 24 different instruments utilize the resulting neutron beams for research.

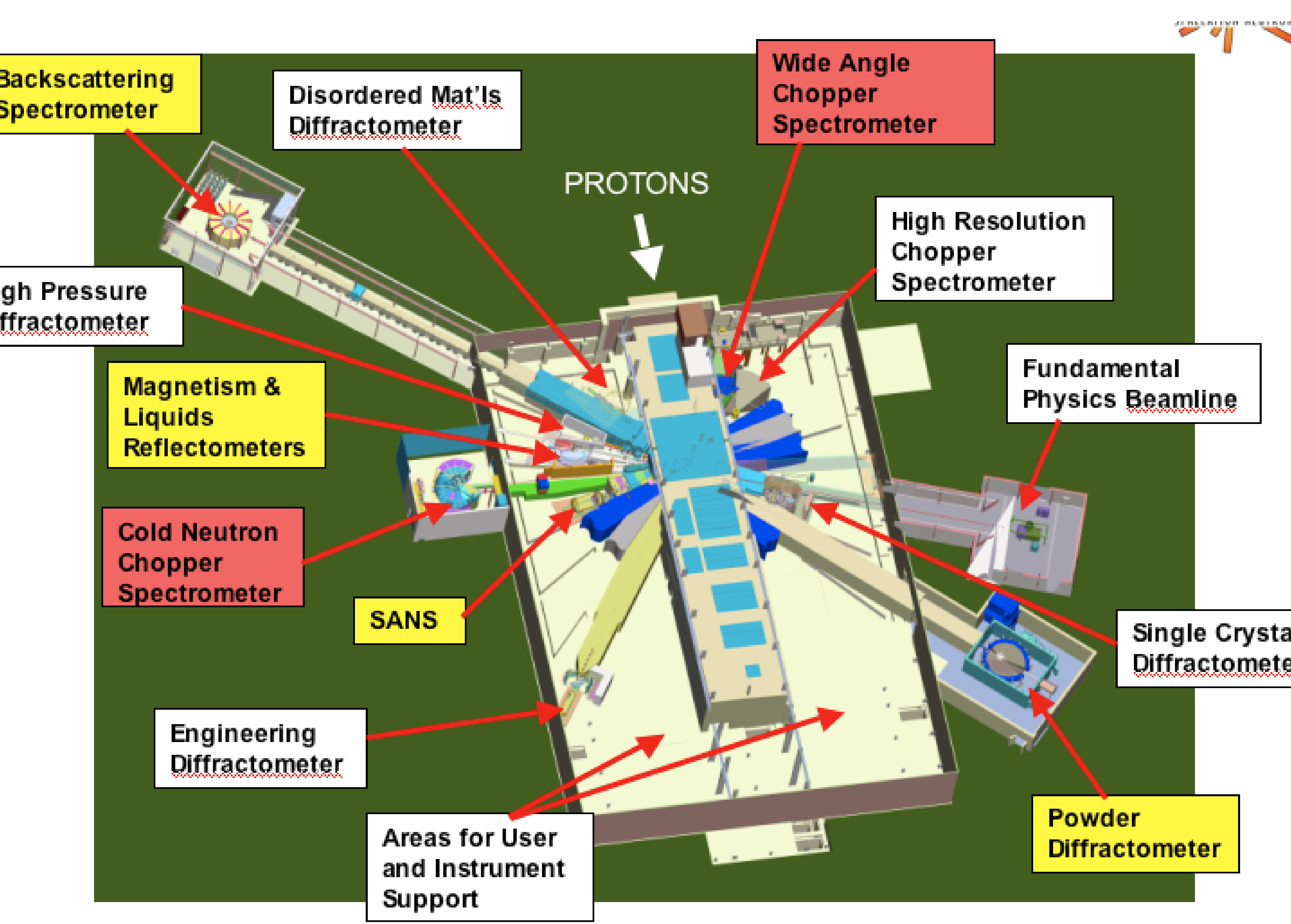

Backscattering Spectrometer
Disordered Mat'ls Diffractometer
Wide Angle Chopper Spectrometer
PROTONS
High Resolution Chopper Spectrometer
gh Pressure ffractometer
Fundamental Physics Beamline
Magnetism & Liquids Reflectometers
Cold Neutron Chopper Spectrometer
SANS
Single Crysta Diffractomete
Engineering Diffractometer
Areas for User and Instrument Support
Powder Diffractometer

Neutron Scattering and Nanostructures-References

Available online at www.sciencedirect.com

SCIENCE DIRECT®

ELSEVIER

Journal of Magnetism and Magnetic Materials 271 (2004) 103–146

journal of magnetism and magnetic materials

www.elsevier.com/locate/jmmm

Topical Review

Neutron scattering studies of nanomagnetism and artificially structured materials

M.R. Fitzsimmons[a,*], S.D. Bader[b], J.A. Borchers[c], G.P. Felcher[b], J.K. Furdyna[d], A. Hoffmann[b], J.B. Kortright[e], Ivan K. Schuller[f], T.C. Schulthess[g], S.K. Sinha[a,f], M.F. Toney[h], D. Weller[i], S. Wolf[j]

J Magn. Magn. Mater **271** (2004) 103-146

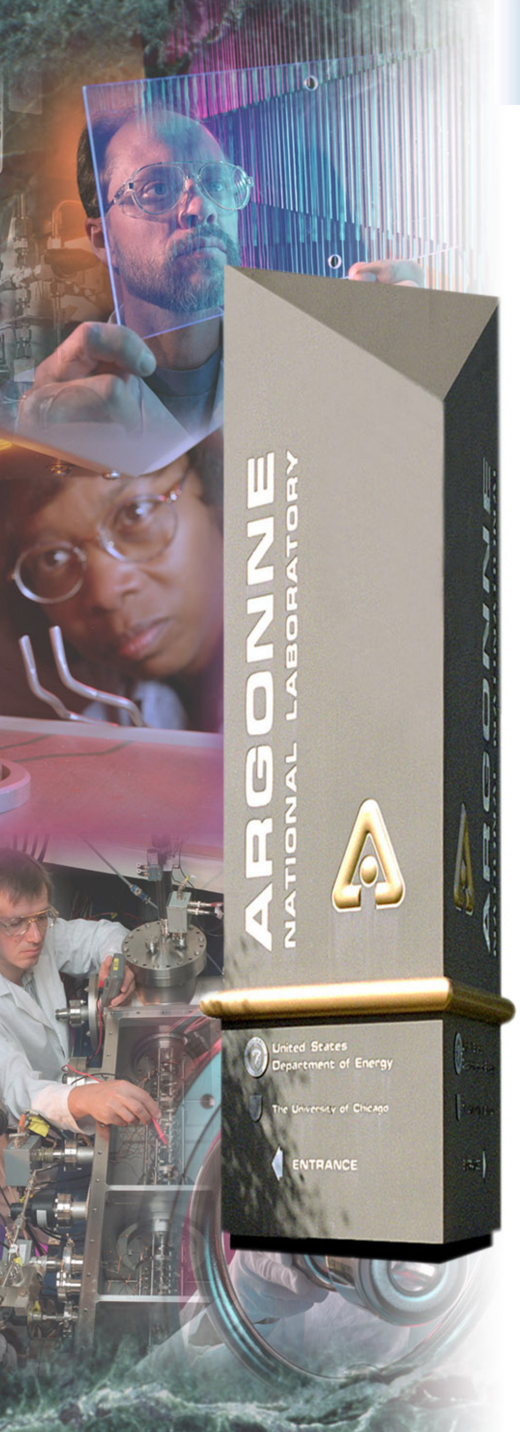

ARGONNE NATIONAL LABORATORY

Science enabled by spin-echo encoding of the neutron scattering vector

G. P. Felcher, P. Falus, S.G.E. te Velthuis

Argonne National Laboratory

A. Vorobiev, J. Major and H. Dosch

Max Planck Inst. für Metallforschung

R. Pynn

University of Indiana

Scuola F.P. Ricci, Pula, Sept. 29, 2006

THE UNIVERSITY OF CHICAGO

Office of Science
U.S. DEPARTMENT OF ENERGY

MAX-PLANCK-GESELLSCHAFT

Argonne National Laboratory is managed by
The University of Chicago for the U.S. Department of Energy

Spin-echo angular encoding

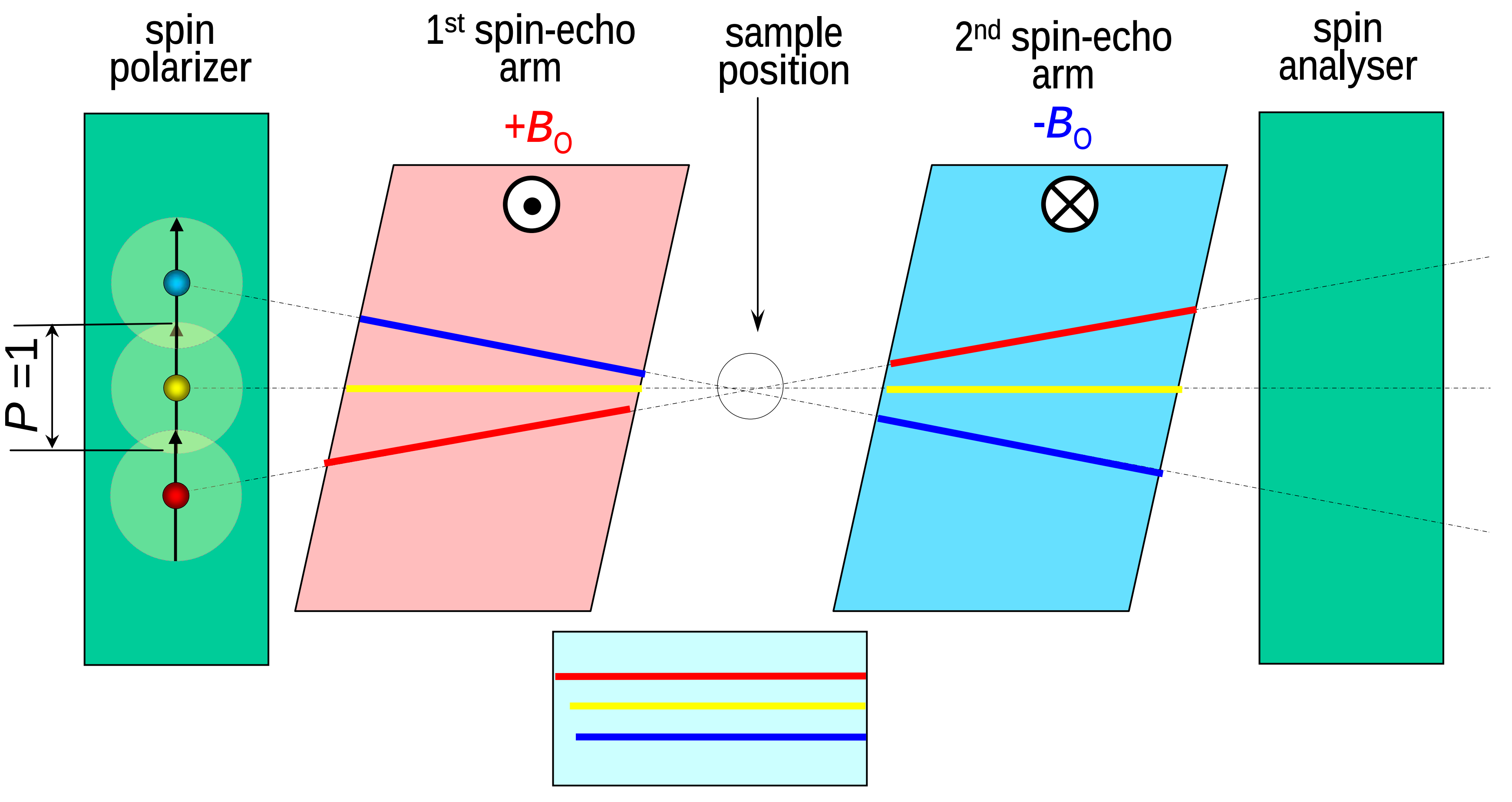

DIFFERENT PATH LENGTHS FOR THE DIFFERENT TRAJECTORIES !

Spin-echo angular encoding: no scattering case

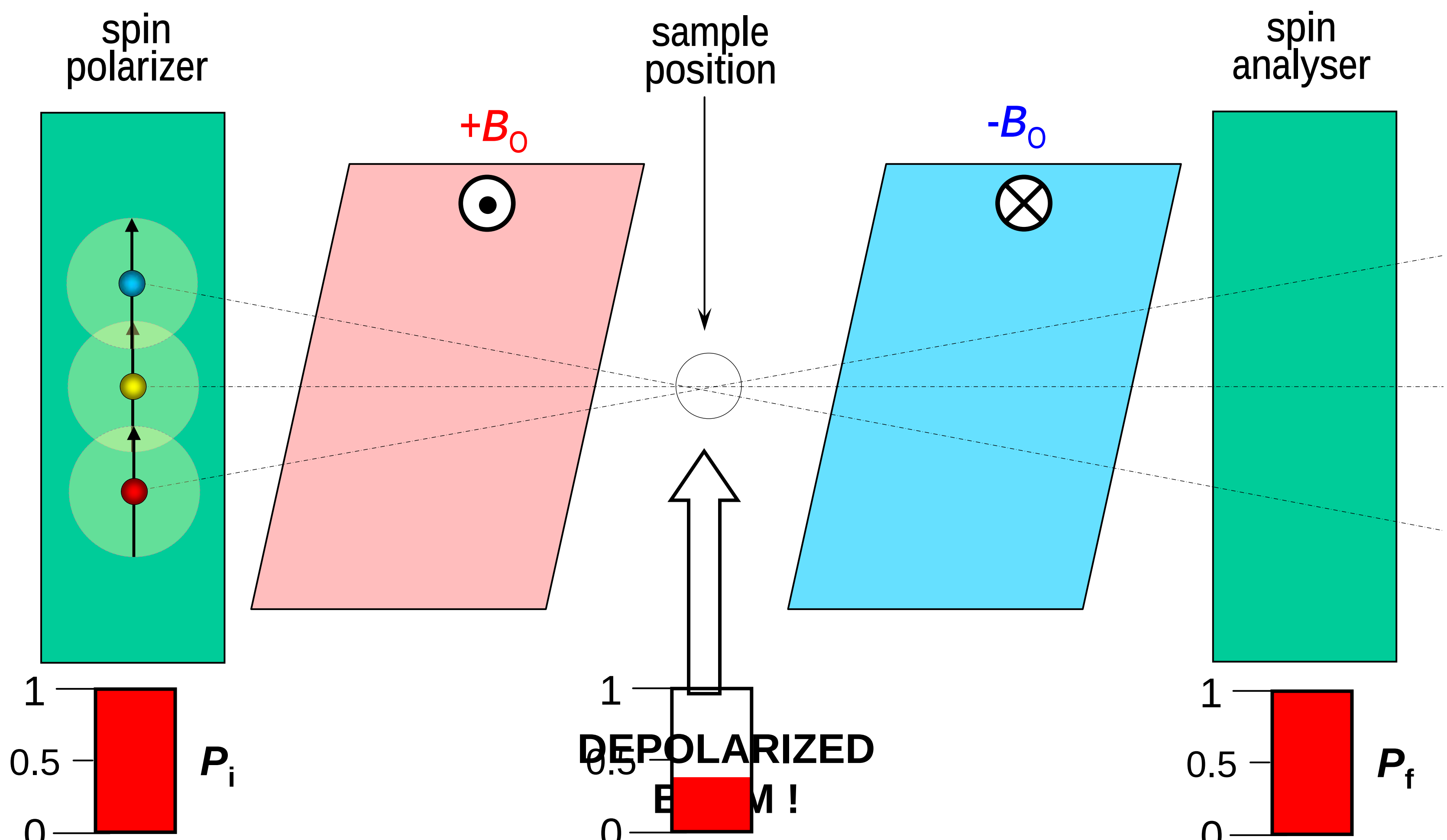

ALL SPINS
ARE PARALLEL:
FULL POLARIZATION

ALL SPINS
ARE PARALLEL AGAIN:
POLARIZATION
IS BACK

$$P_f = P_i$$

‘SPIN-ECHO’

Spin-echo angular encoding: scattering by the sample

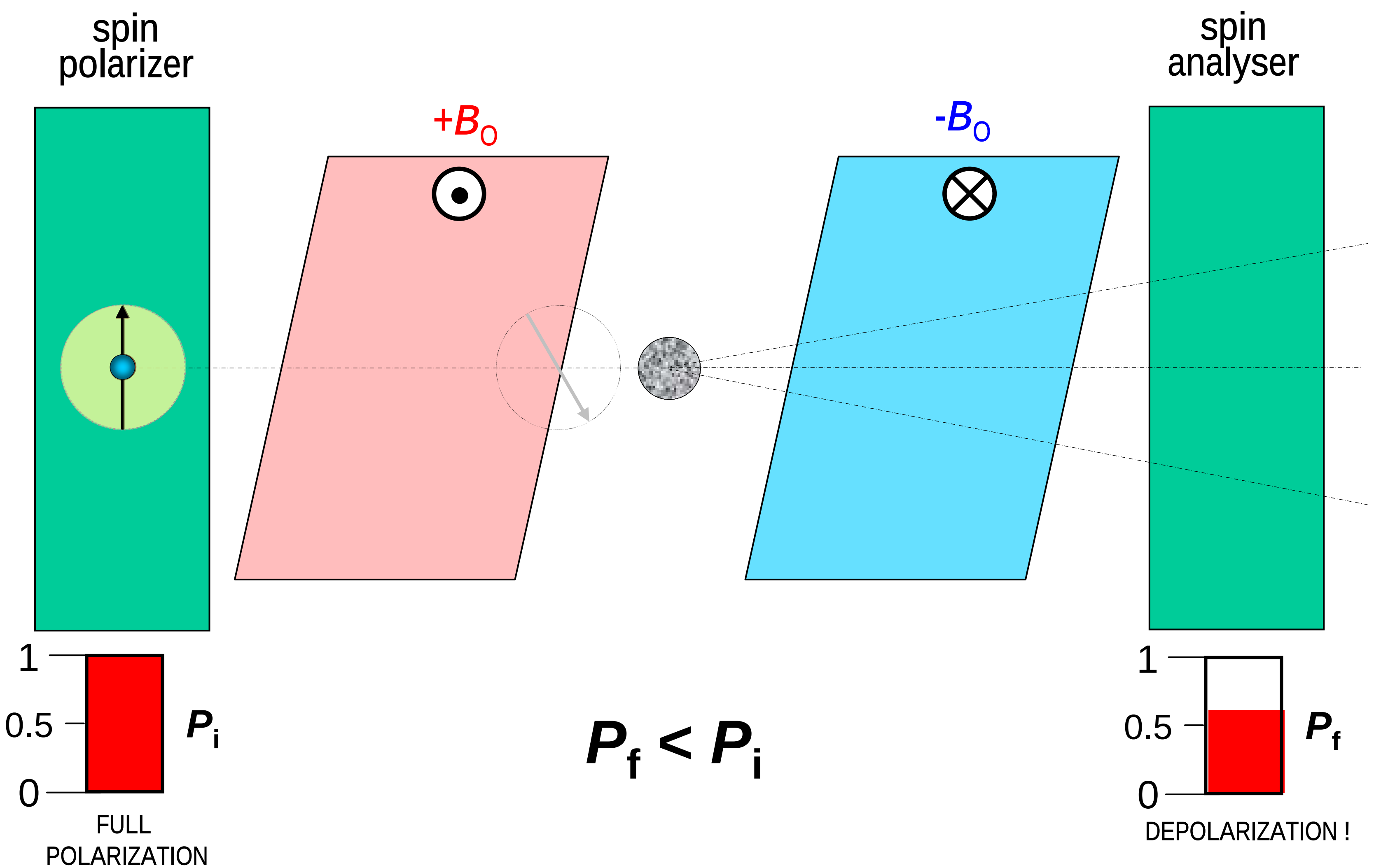

Spin-echo angular encoding: scattering by the sample

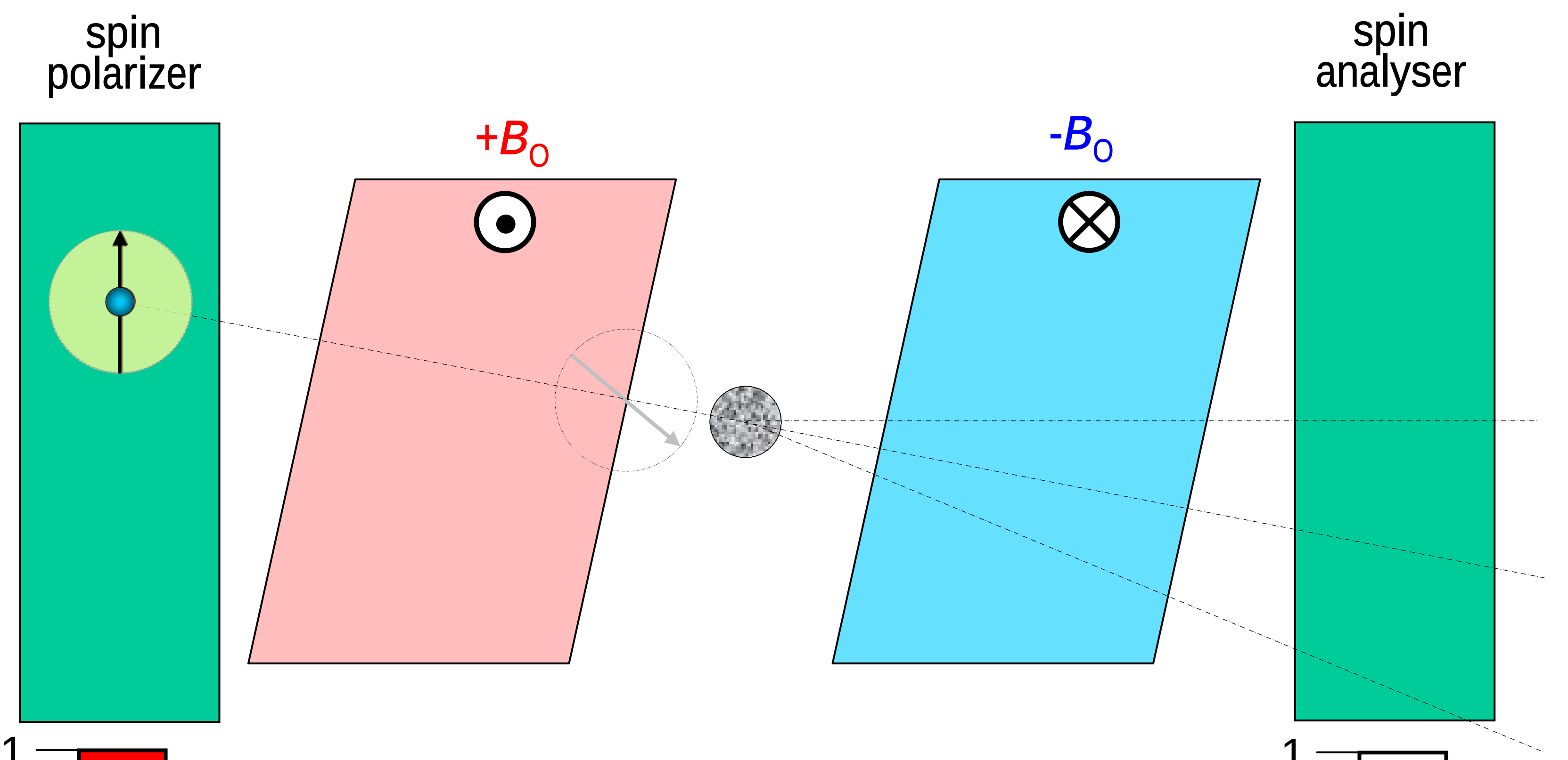

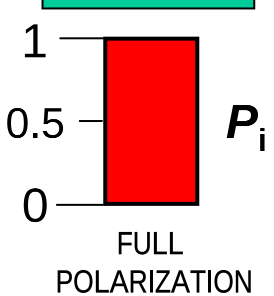

the same depolarization

$$P_f < P_i$$

independently of initial trajectory

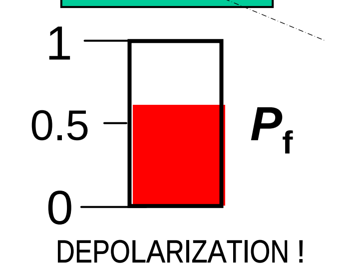

Spin-echo angular encoding: the equations

Neutron spin phase after both precession zones:

(one before, one after the sample)

$$\xi_1 - \xi_2 \approx \frac{2\pi\gamma_n Bd \cdot \cot\Theta \sin\varphi}{v}$$

$$= \left\{\frac{\gamma_n Bd\lambda \cdot \cot\Theta}{v}\right\}\left(\frac{2\pi\sin\varphi}{\lambda}\right)$$

$$\approx \delta \cdot q_y$$

The polarization is:

$$P(\delta) = \int S(q_x,q_y,q_z)\cos(\delta q_y)\mathrm{d}q_y / \int S(q_x,q_y,q_z)\mathrm{d}q_y \sim \boldsymbol{G(y)}$$

In our experiments:

SE length δ is tuned mechanically by changing Θ

Spin-echo angular encoding: the experiment

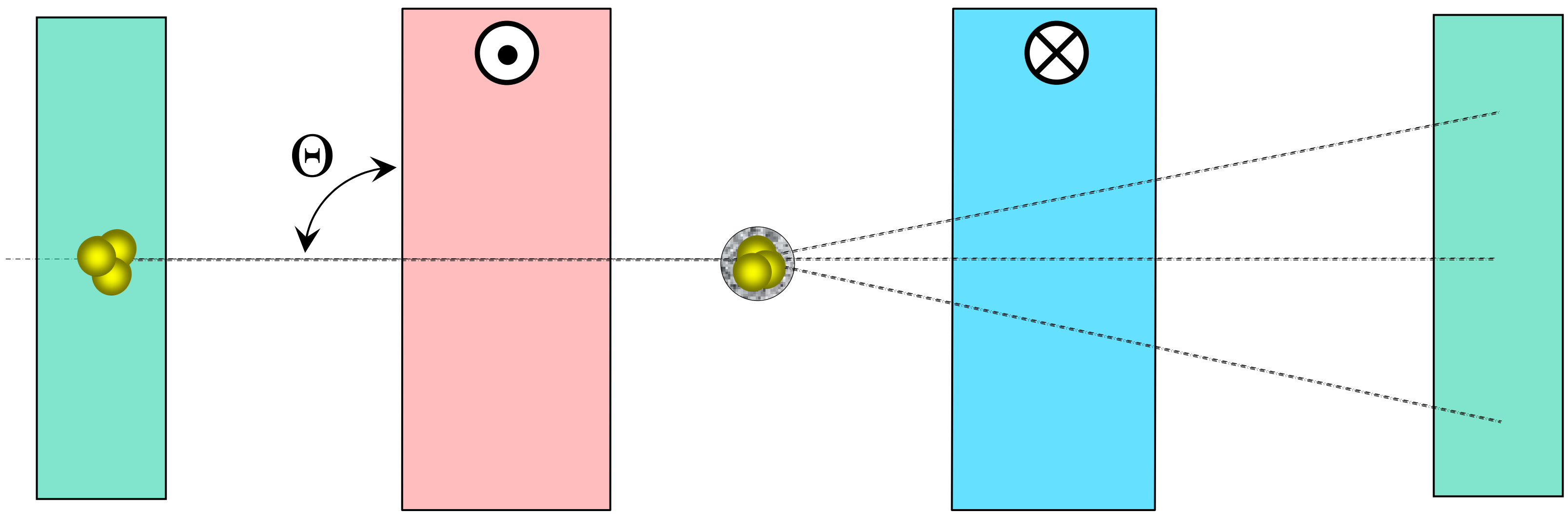

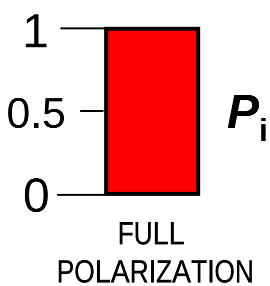

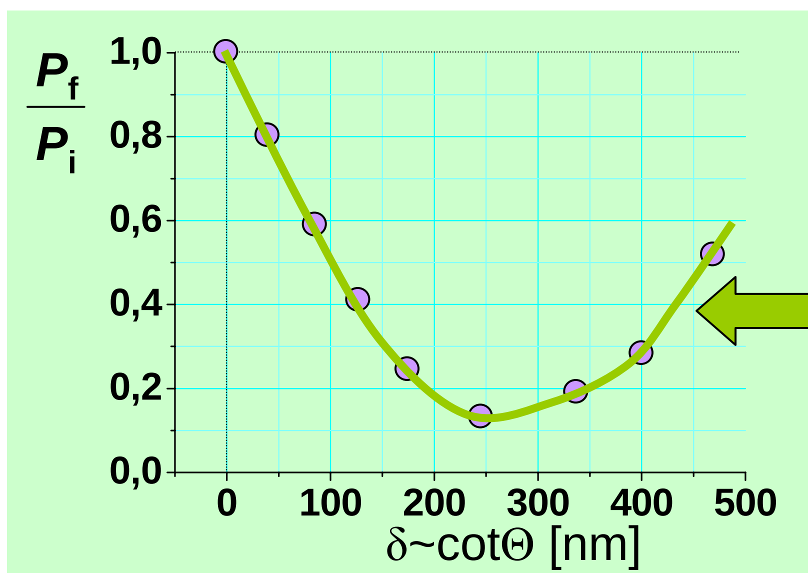

REAL-SPACE CORRELATION FUNCTION

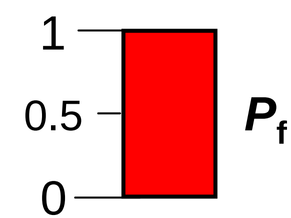

Geometry at grazing incidence

α_f Resolve with PSD

φ Resolve with Spin Echo

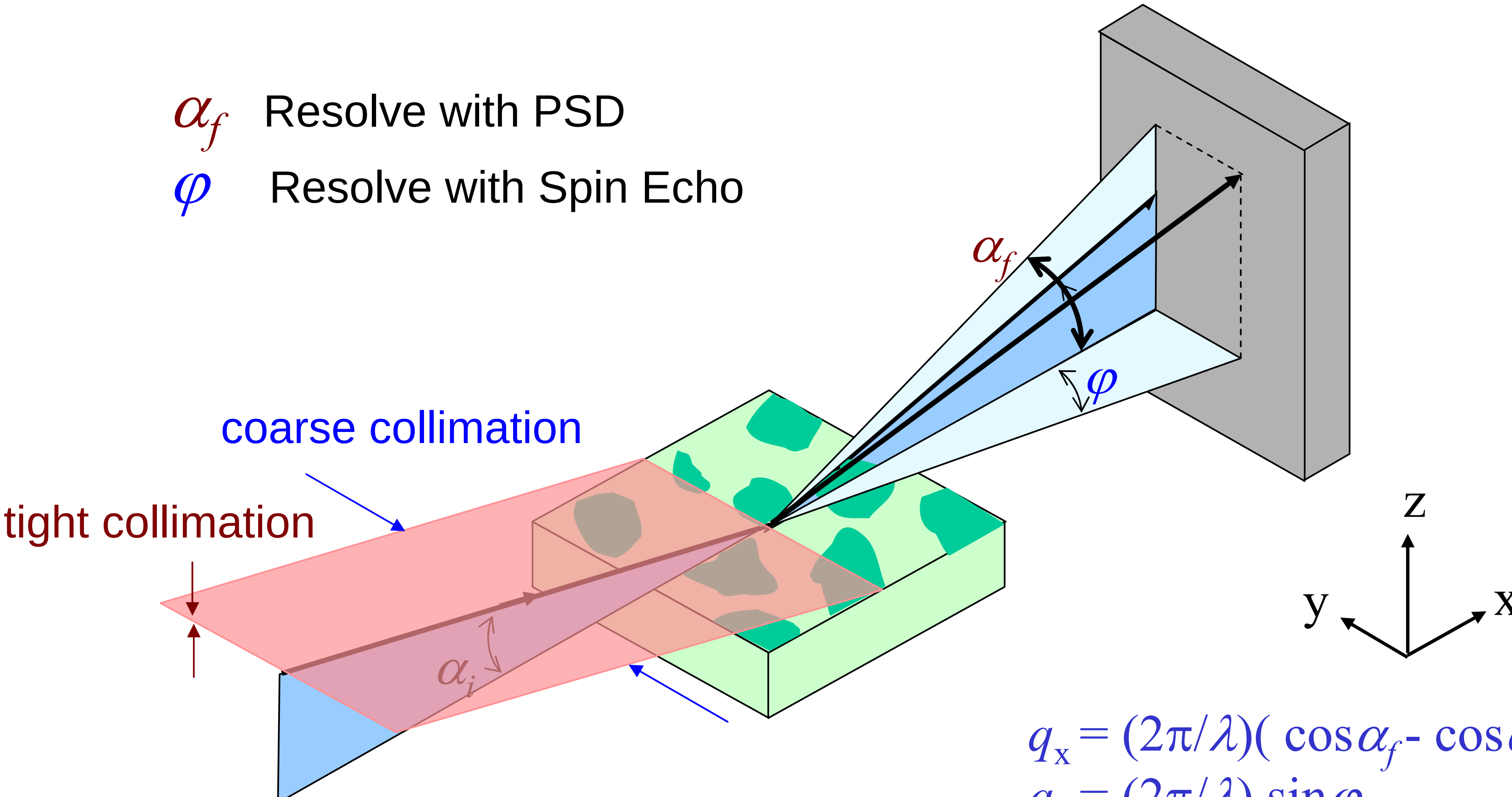

$$q_x = (2\pi/\lambda)(\cos\alpha_f - \cos\alpha_i)$$

$$q_y = (2\pi/\lambda)\sin\varphi$$

Grazing incident geometry

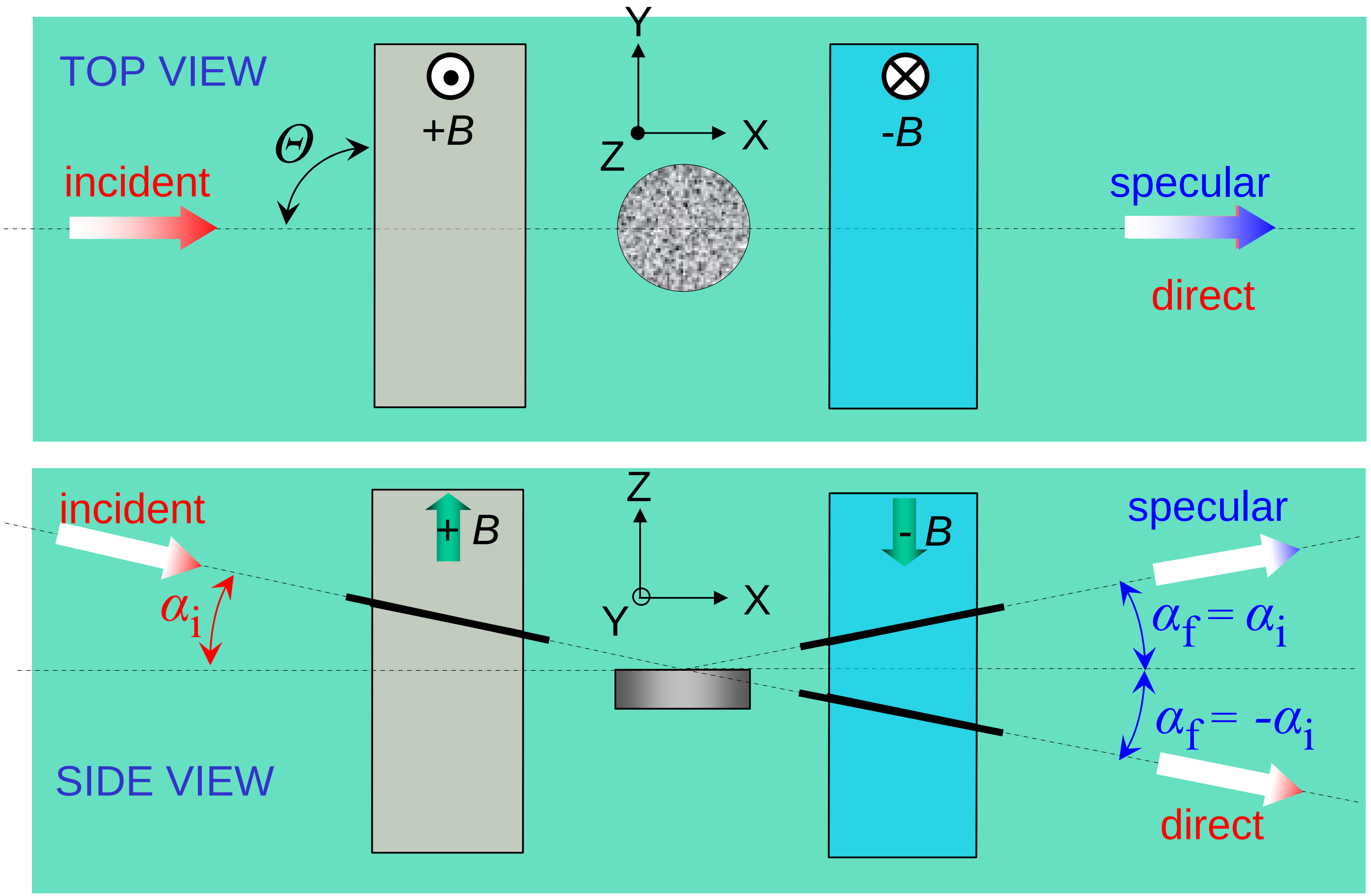

THE SAME POLARIZATION IN DIRECT AND SPECULAR BEAMS

EVA transformed into a SERGIS prototype instrument

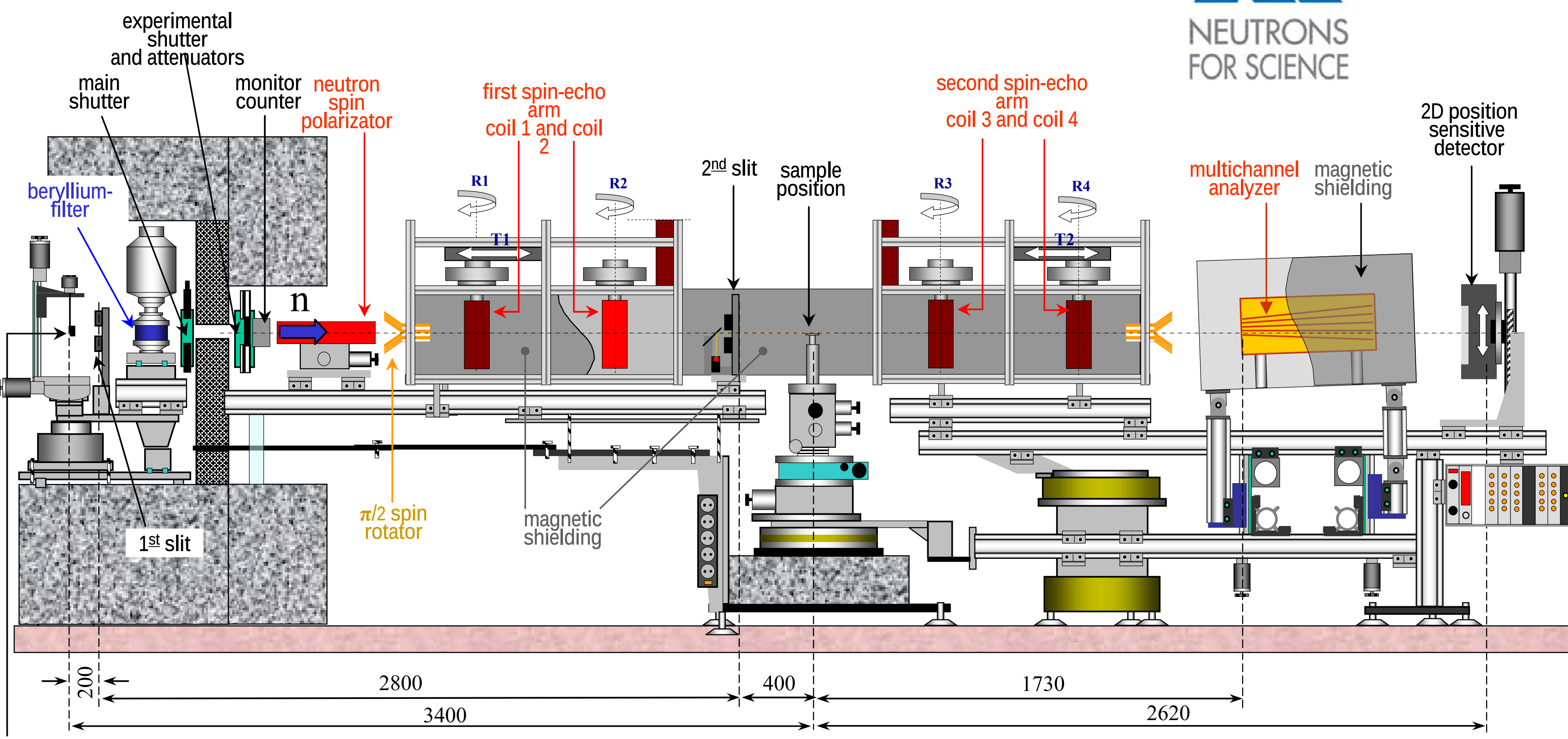

EVA during the transformation to SERGIS

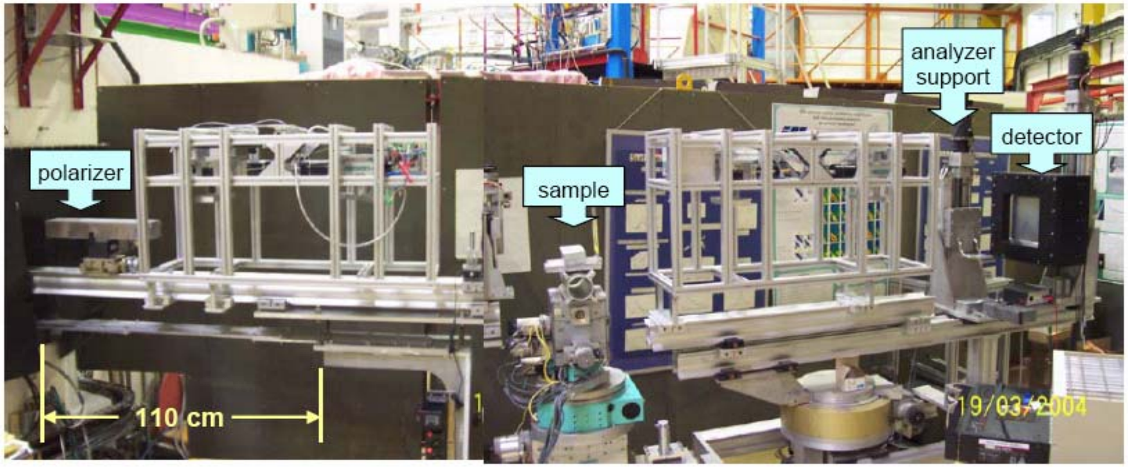

Beam size 50x5mm

Wave numbers covered:

$1 \cdot 10^{-3}$ - $4 \cdot 10^{-2}$ Å^{-1}

Max. SE time in classical

configuration (Θ=0) 0.07ns

Max. spin echo length 4500Å

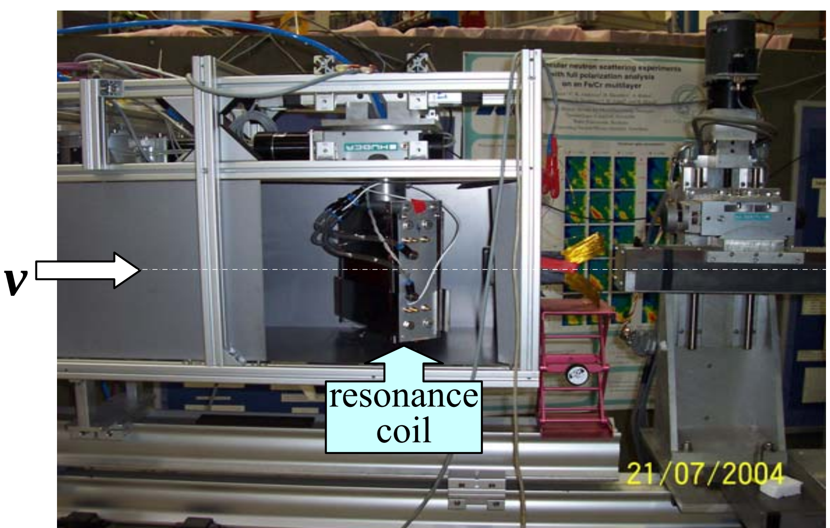

$$\delta = \left\{ \frac{\gamma_n B d \lambda \cdot \cot \Theta}{v} \right\}$$

λ (neutron wavelength) 5.5 Å

v (neutron velocity) 720 m/s

Θ (tilt of precession coil) 50º

B (magnetic field in leg) 78 G

d (length of precession leg) 50 cm

Beam geometry

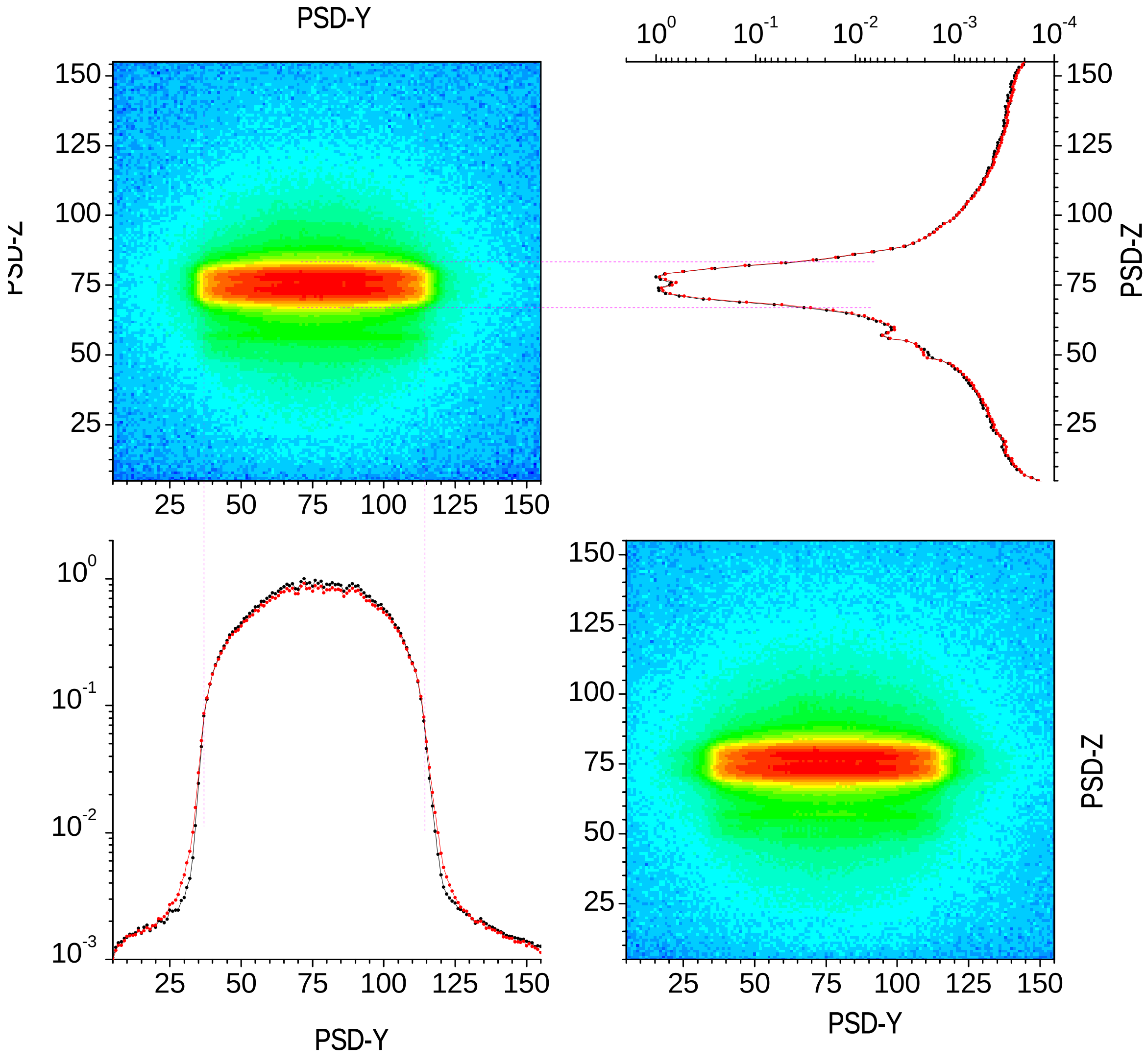

First SERGIS experiments at the dedicated set-up EVA

In transmission geometry (SESANS)

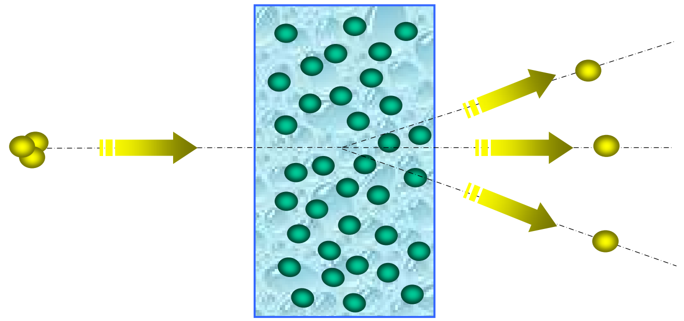

- colloids of polystyrene (PS) spheres
- structured Al_2O_3 film

In grazing incidence geometry (SERGIS)

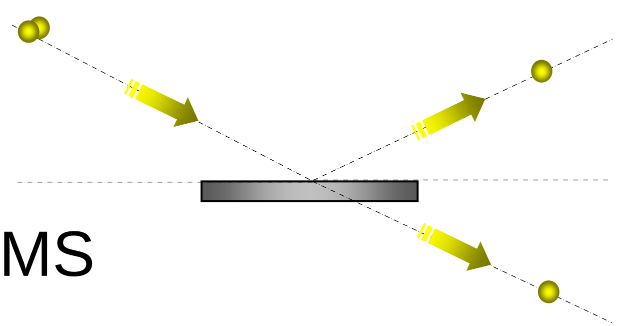

- Dewetted polymers on Si
  - ☒ homopolymer dPS
  - ☒ blend of homopolymers dPS and PpMS
  - ☒ diblock copolymer dPS-b-PpMS

SESANS results: Polystyrene spheres

2.5% polystyrene balls in 3:1 D_2O/H_2O

2mm thick cell

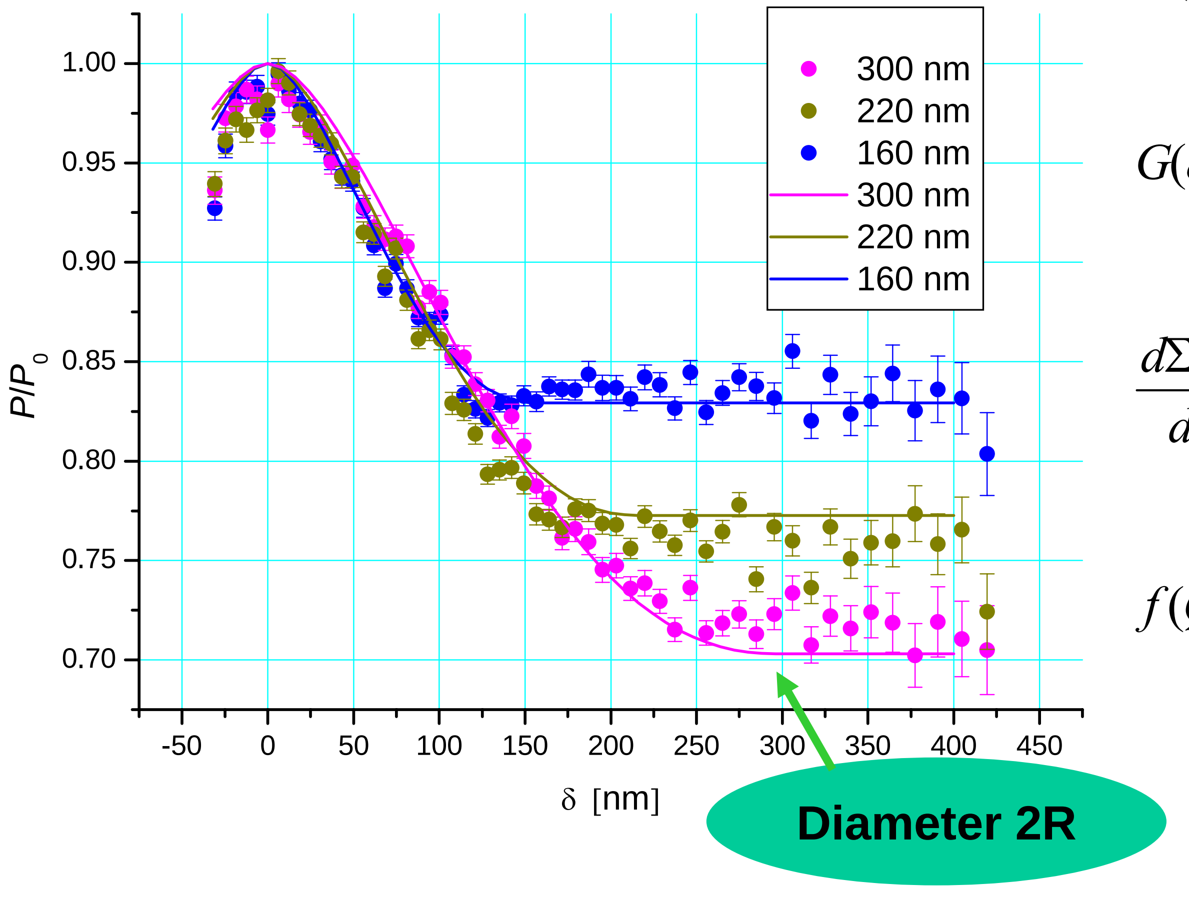

$$\frac{P(\delta)}{P(0)} = \exp\left[G(\delta) - G(0)\right]$$

$$G(\delta) = \frac{1}{k_0^2} \int_{-\infty}^{\infty} dQ_z \int_{-\infty}^{\infty} dQ_y \frac{d\Sigma(Q)}{d\Omega} \cos(Q_y \delta)$$

$$\frac{d\Sigma(Q)}{d\Omega} = V\phi_V t(\Delta\rho)^2 f^2(QR)$$

$$f(QR) = \frac{3\left[\sin(QR) - QR\cos(QR)\right]}{(QR)^3}$$

1D projection of the real space autocorrelation function

Comparison with D-22

Small angle

Scattering

at D-22

from a 2 mm cell

containing 2.5%

latex balls

300 nm diameter

into a solution

3:1 D_2O/H_2O

(P. Timmins, ILL)

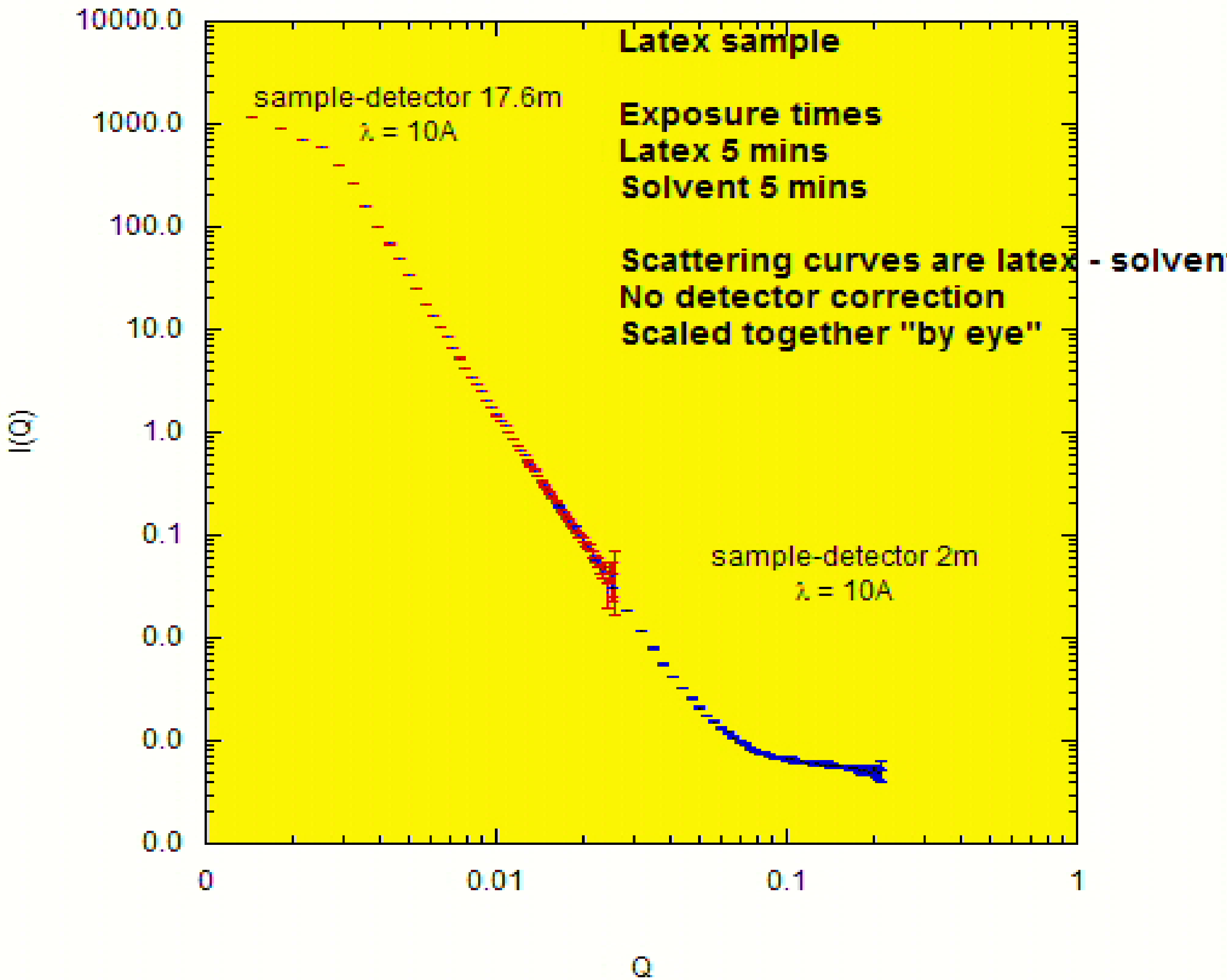

Anodized Aluminium Oxide (AAO)

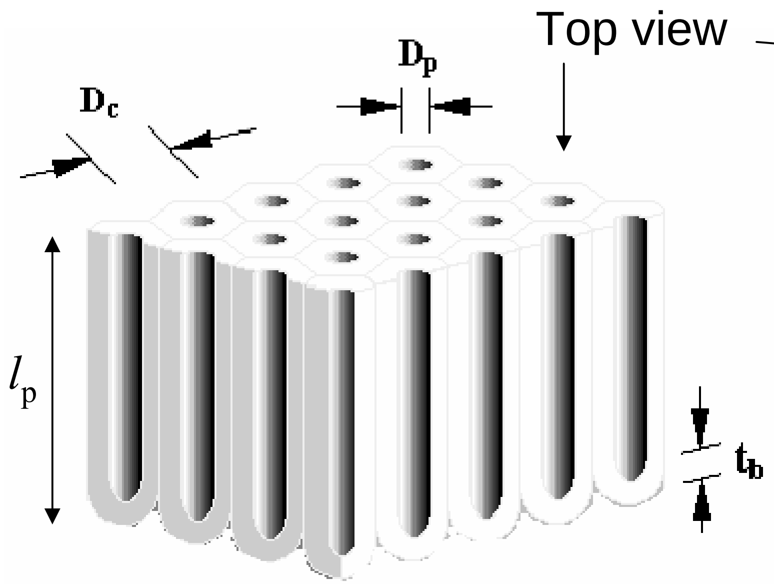

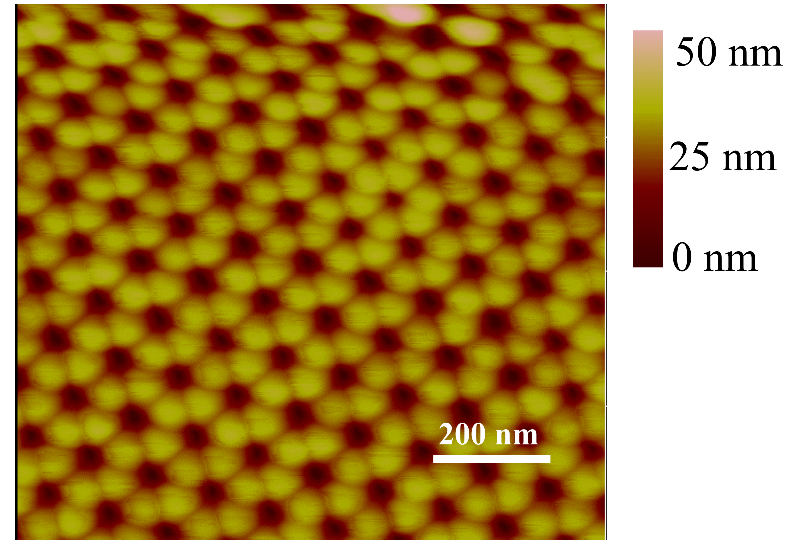

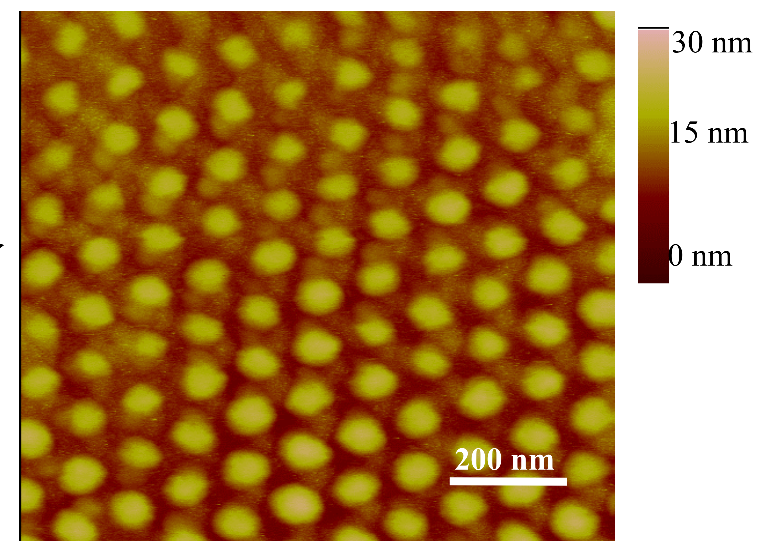

Sample: Al_2O_3 from Tao Xu (ANL)

D_c, pore-to-pore distance = ~120nm
D_p pore diameter =50-60 nm
t_b barrier layer thickness =~20nm
l_p length of pore ~ 30 microns

SANS results: Anodized Aluminium Oxide

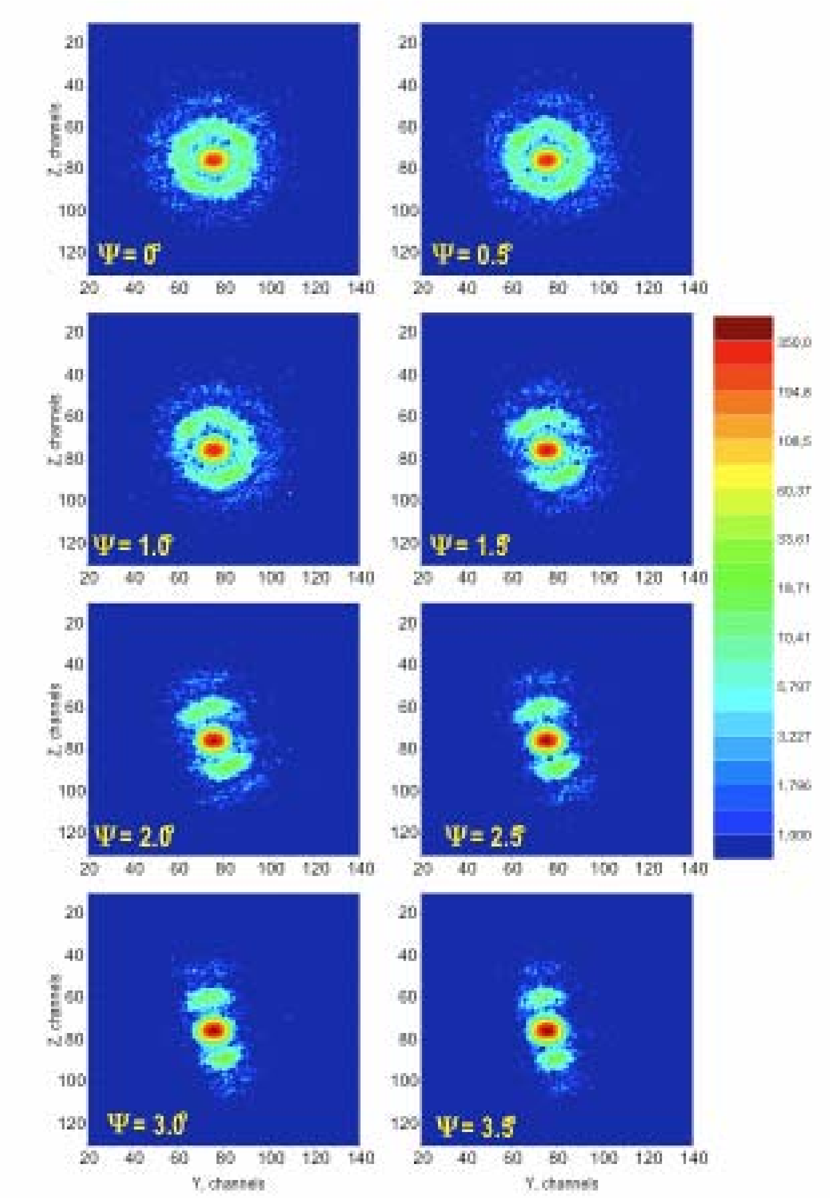

Small angle scattering from AAO as a function of the angle of the film's normal to the incident beam.

Size of the beam: 2 x 2 mm
Neutron wavelength: 5.5 Å
Sample/detector distance 2.75 meters

Geometry of scattering from one element of the AAO lattice.

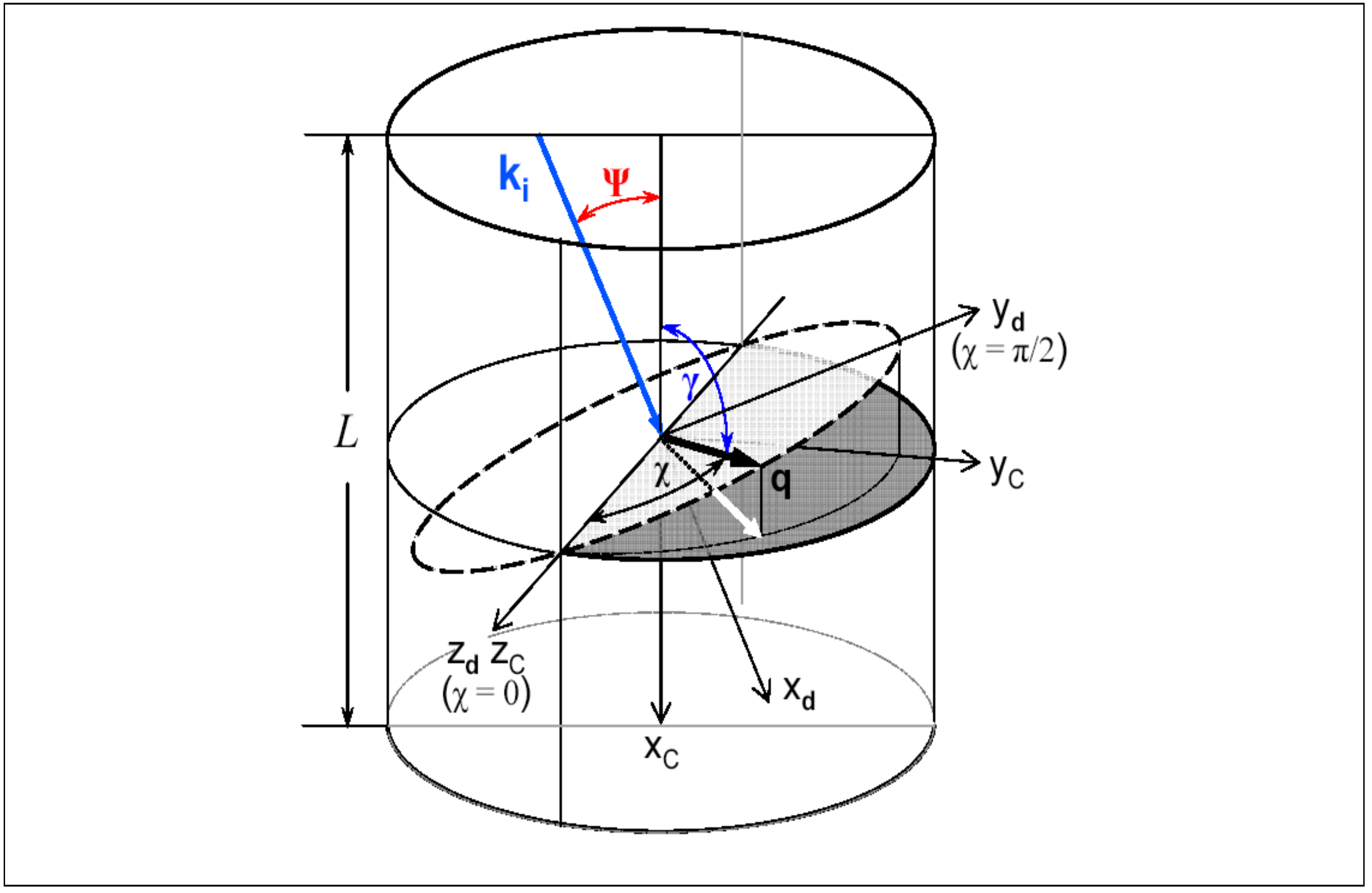

2-dimensional scattering pattern of AAO

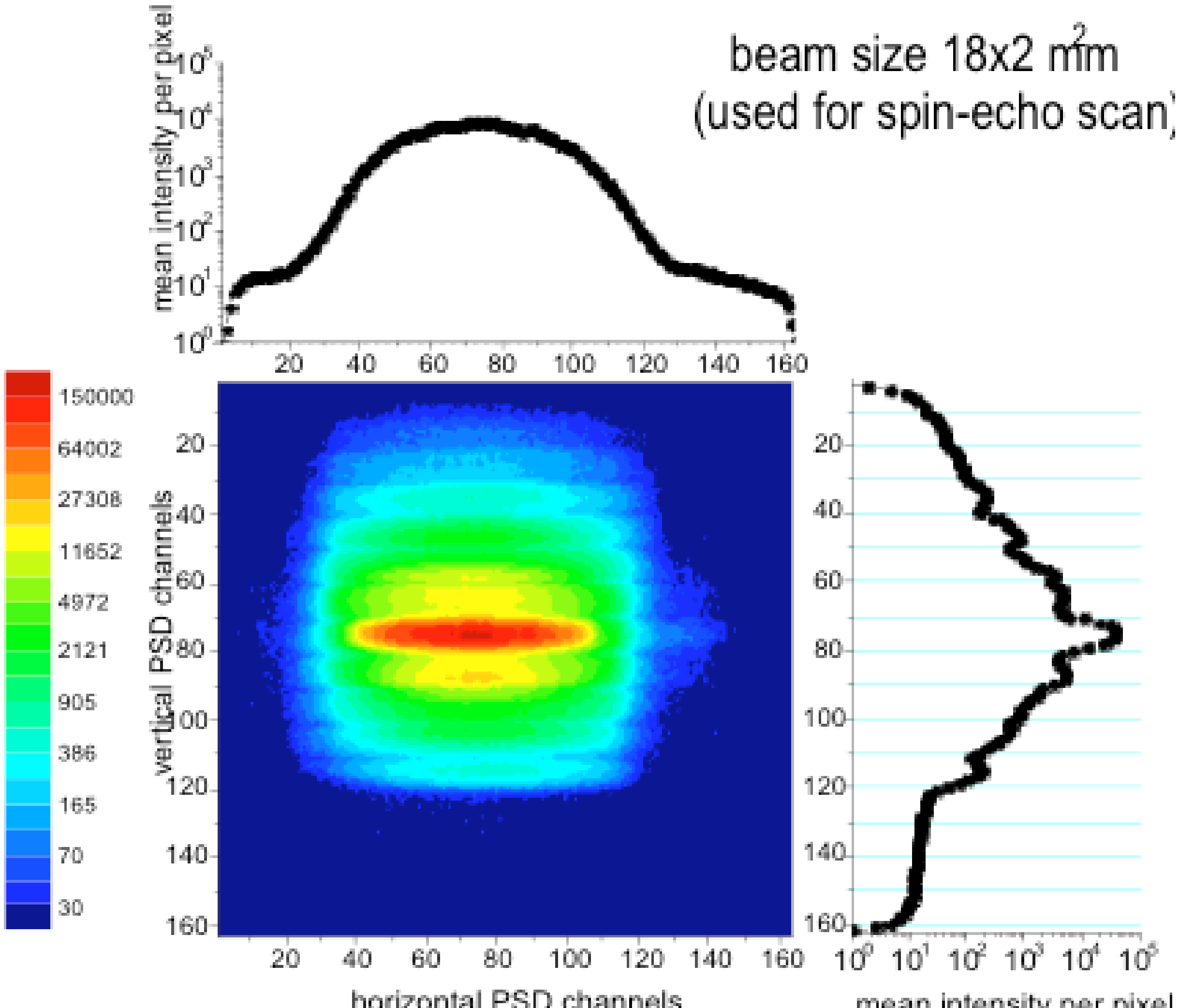

AAO. Correlation function in real space

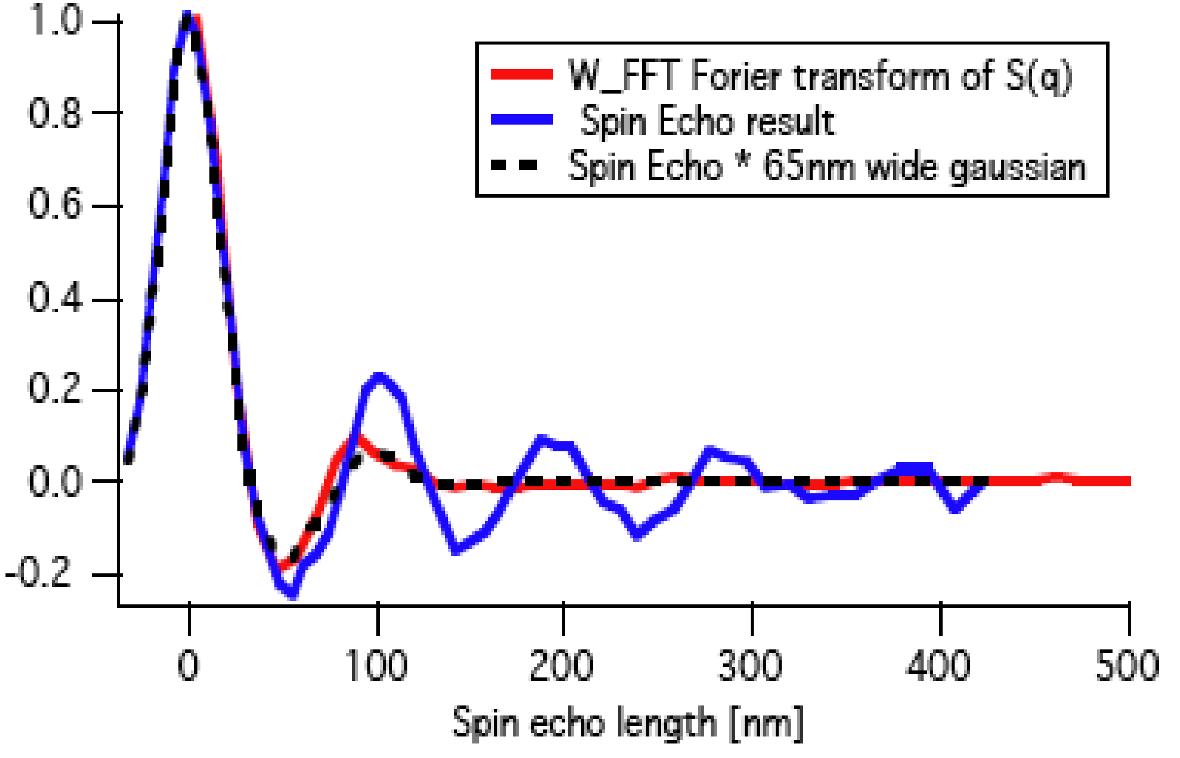

SESANS results: Anodized Aluminium Oxide

Reciprocal Space (SANS)

Intensity map ~ S(Q)

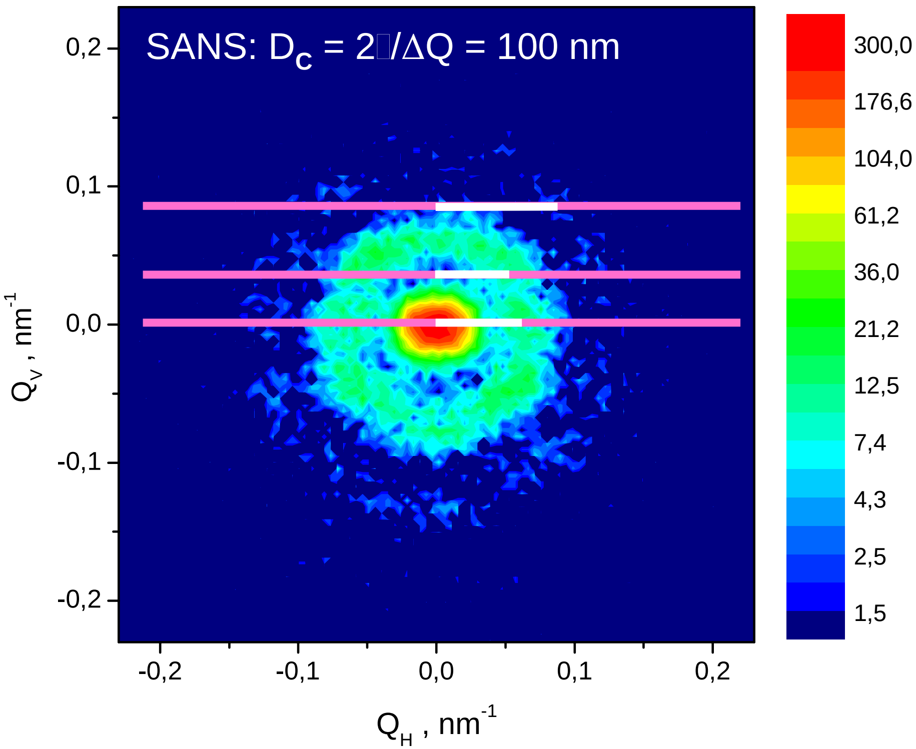

2×2 mm^2 beam

Reciprocal & Real Space (Spin Echo SANS)

Polarization map ~ G(y)

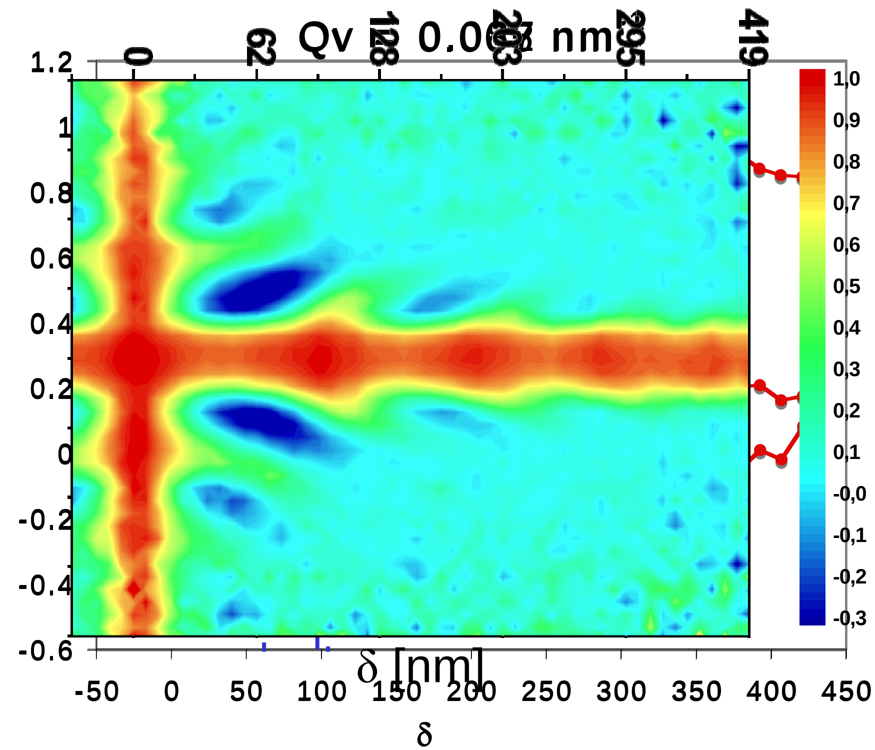

10×2 mm^2 beam

Spin-echo set-up for grazing incidence geometry

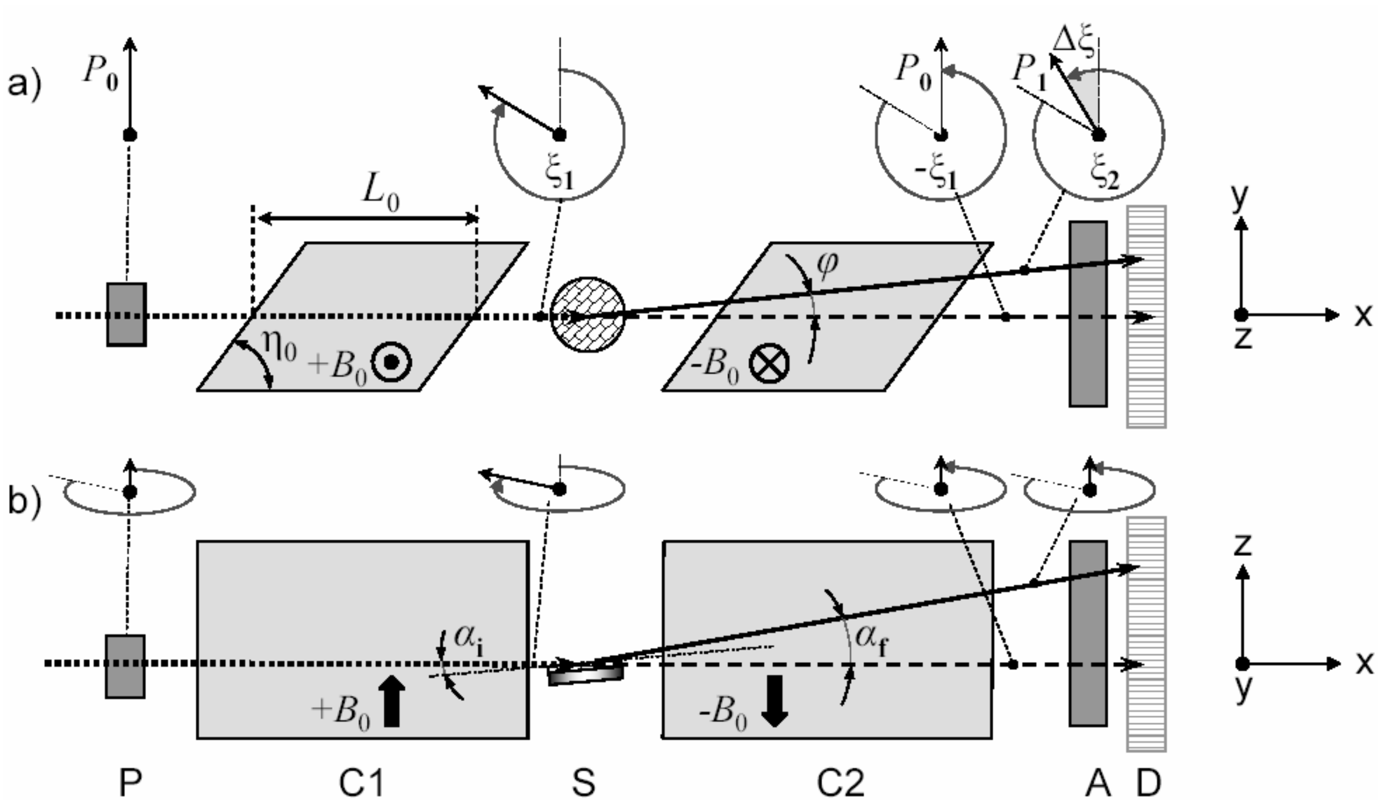

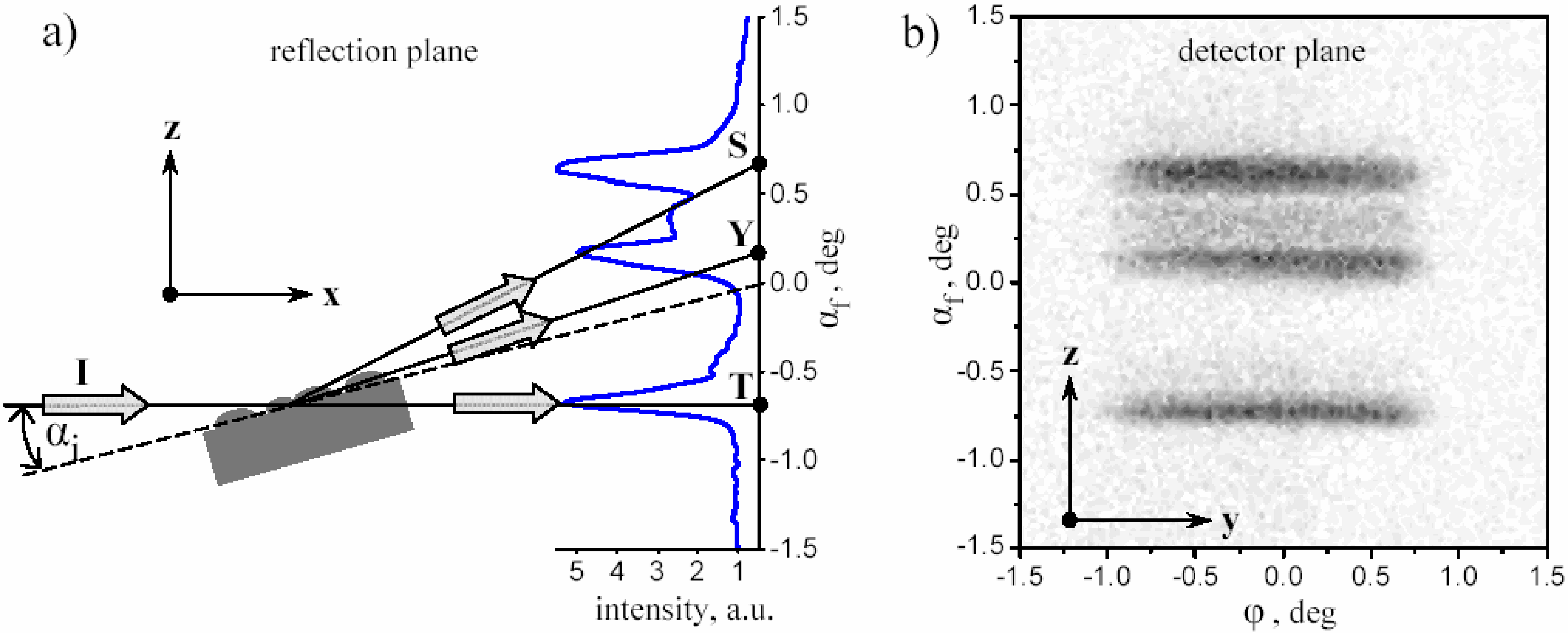

a) scattering geometry. The incident beam (I) impinges on the sample surface at a shallow angle α_i; transmitted (T), specular (S) and diffuse (Y) intensities are simultaneously recorded by PSD.

b) Image taken by 2-dimensional PSD during real experiment. The size of the incoming beam at the sample position was 302 mm².

Dewetting of polymer-blend films from Silicon

AFM picture of drops of d-polystyrene/ polyparamethylstyrene on silicon

Zoomed AFM picture

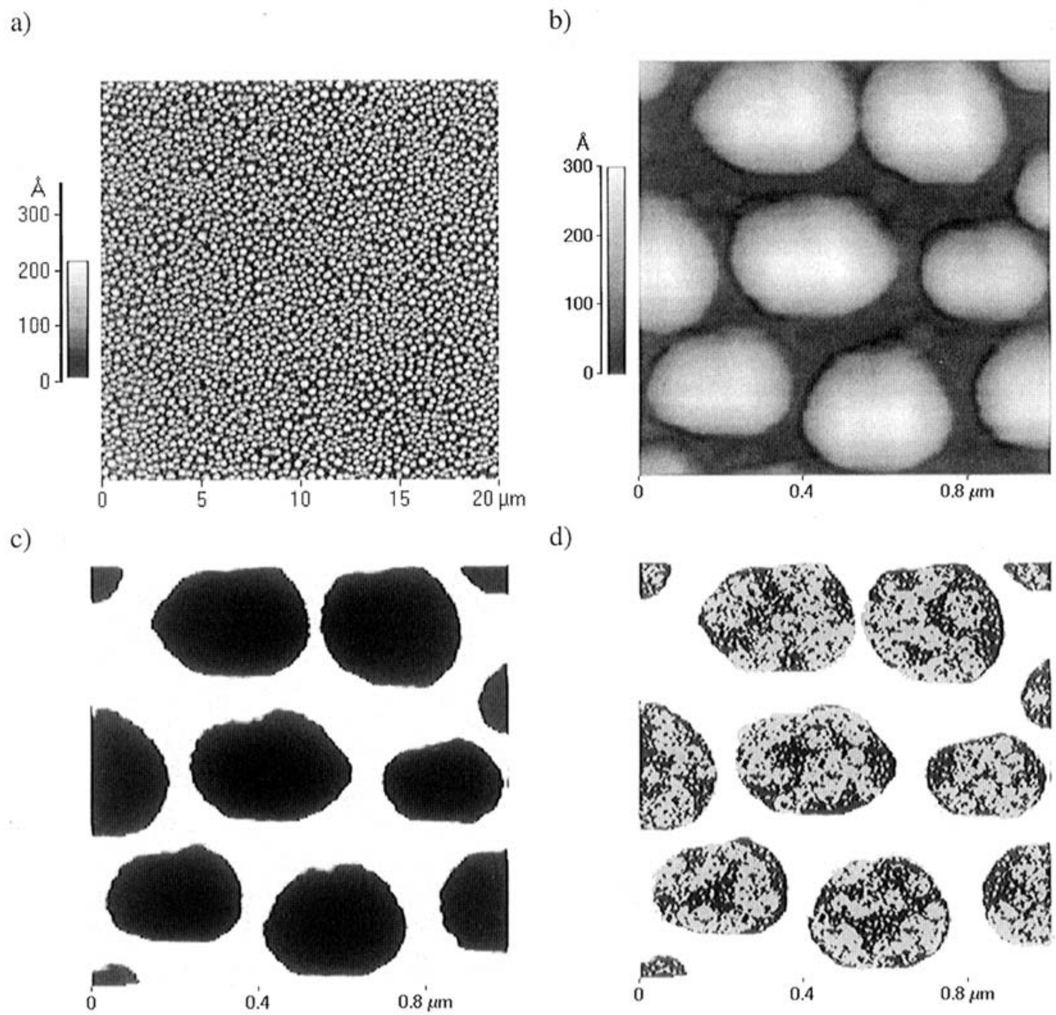

Model of scattering length densities as seen by X-rays(GISAXS)

Model of scattering length densities as seen by neutrons (GISANS)

A comparative study of P. Müller-Buschbaum et al., Physica B*283*,53 (2000)

Homopolymer dPS (deuterated polystyrene)

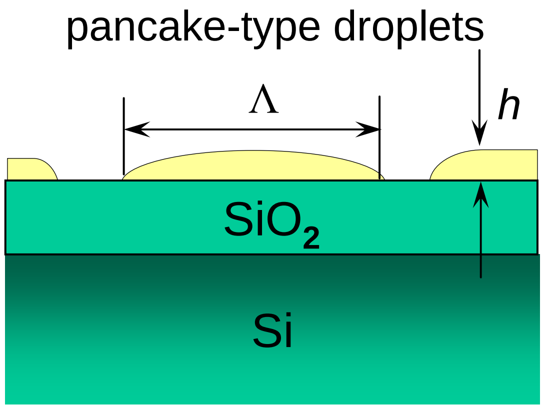

P. Müller-Buschbaum et al.
J. Phys.: Cond. Mat. 17 (2005) S363–S386

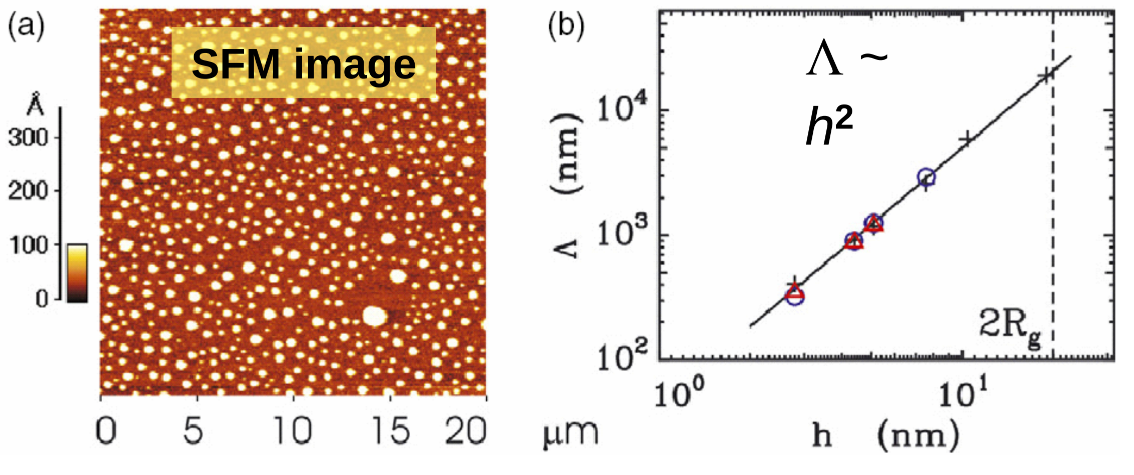

Diffraction figure in transmission and reflection geometry

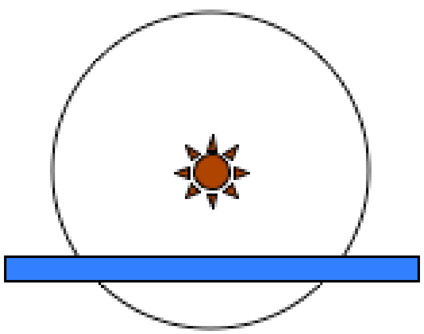

Fig. 6. Scattering in the transmission and in the reflection geometry.

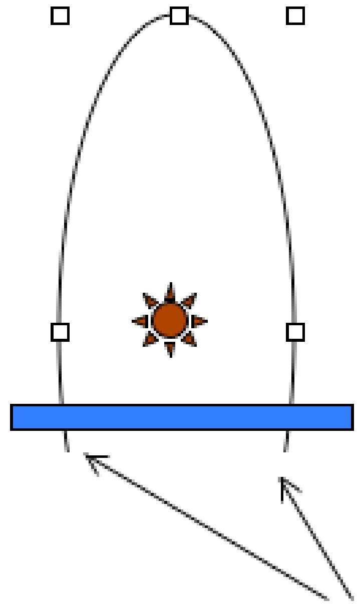

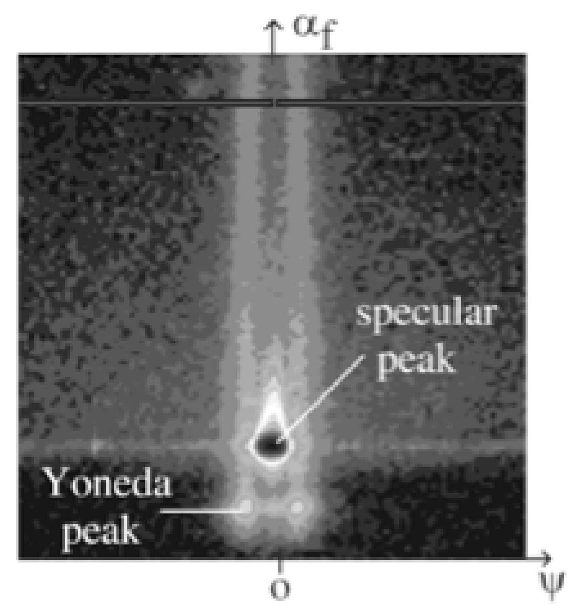

	Transmission	Reflection
q_x	$\cos\vartheta_f - \cos\vartheta_i$	$\cos\vartheta_f \cos\varphi - \cos\vartheta_i$
q_y	$\sin\vartheta_f \sin\varphi$	$\cos\vartheta_f \sin\varphi$
q_z	$\sin\vartheta_I + \sin\vartheta_f \cos\varphi$	$\sin\vartheta_f + \sin\vartheta_i$

GISANS from copolymer droplets D22(ILL), 8 hours

Reflectivity experiment

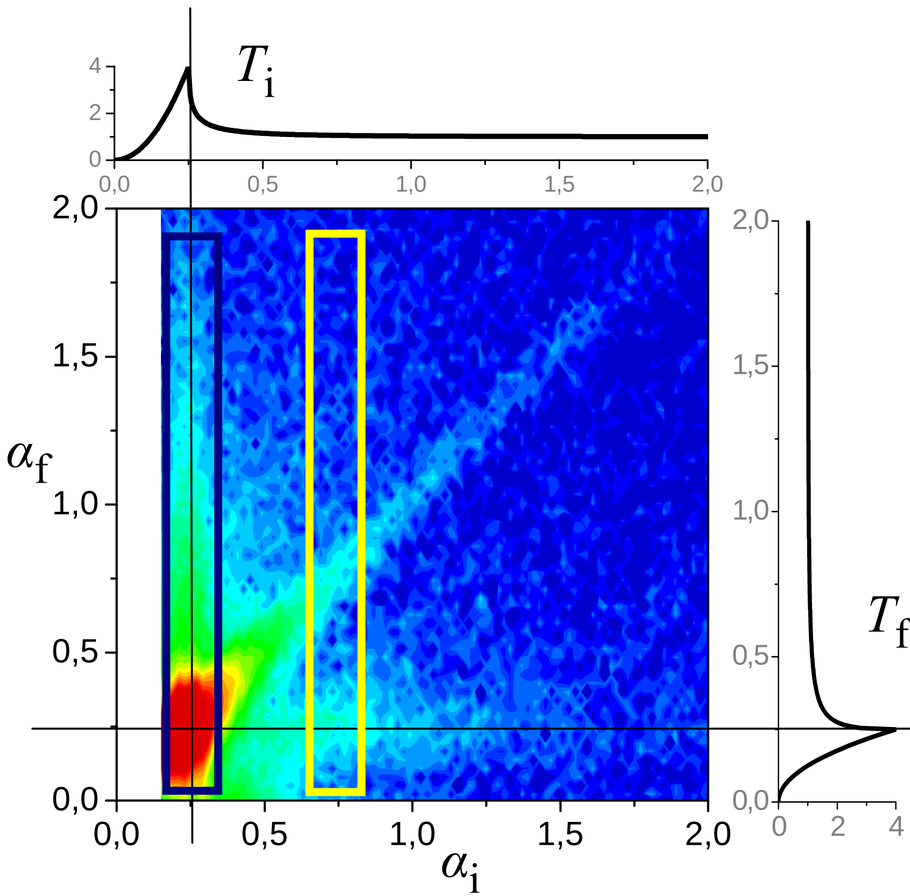

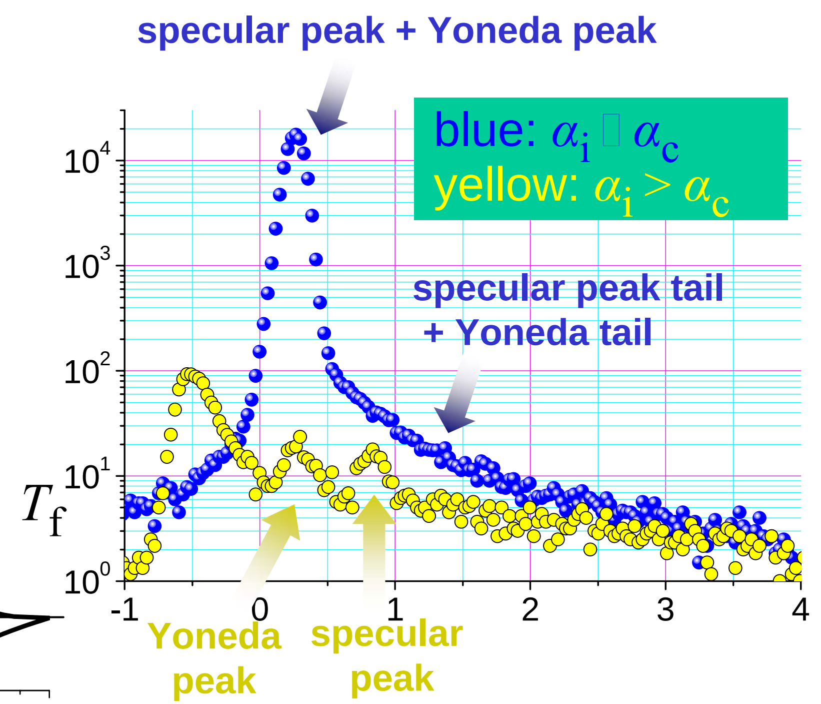

Yoneda anomalous scattering
(enhanced diffuse scattering)

Scattering is better separated from specular & direct beam than in transmission geometry

Contamination of the signal

P **– polarization**
I **– intensity**

$$P_{\mathrm{exp}} = \frac{I_R \cdot P_R + I_D \cdot P_D}{I_R + I_D}$$

indexes:
R **– refernce (specular or direct beams)**
D **– diffuse scattering**
exp – measured

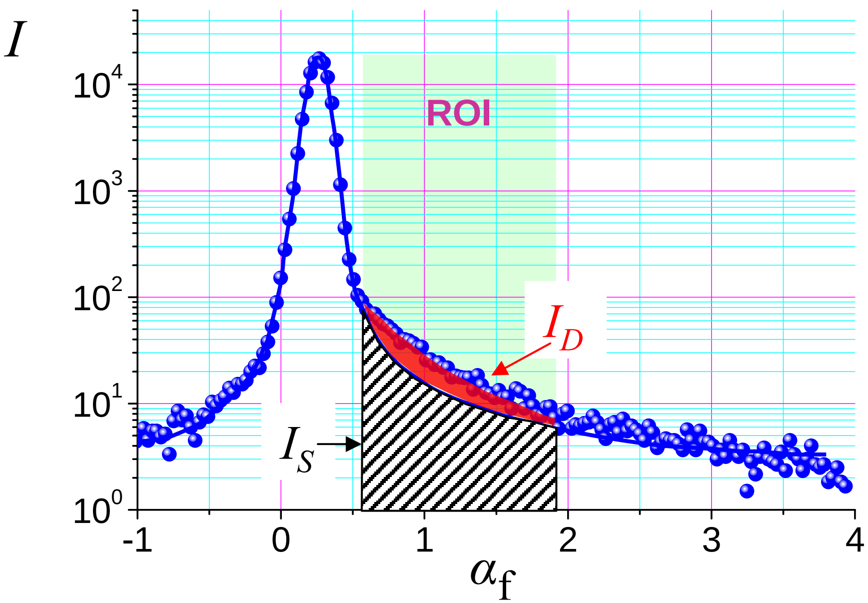

α_{i} □ α_{c}
"Yoneda wing"

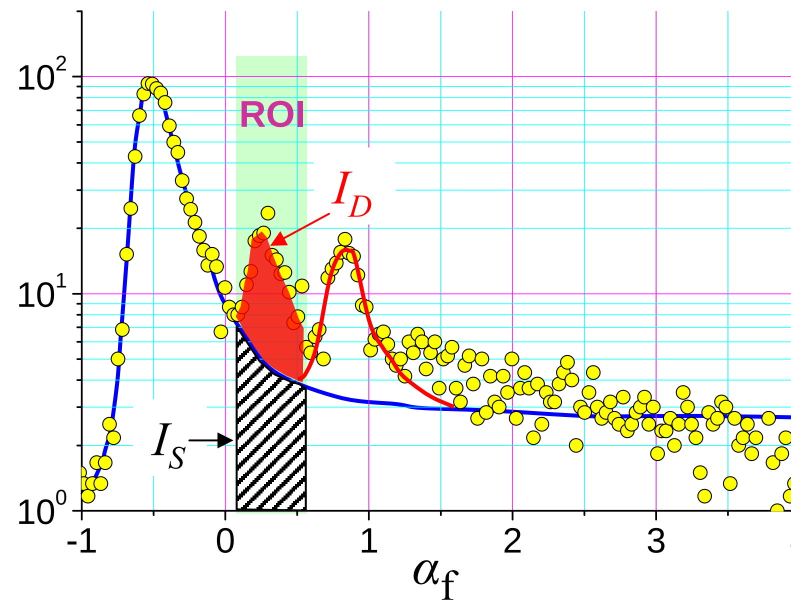

$\alpha_{\mathrm{i}} > \alpha_{\mathrm{c}}$
"Yoneda peak"

Calculated scattering at grazing incidence

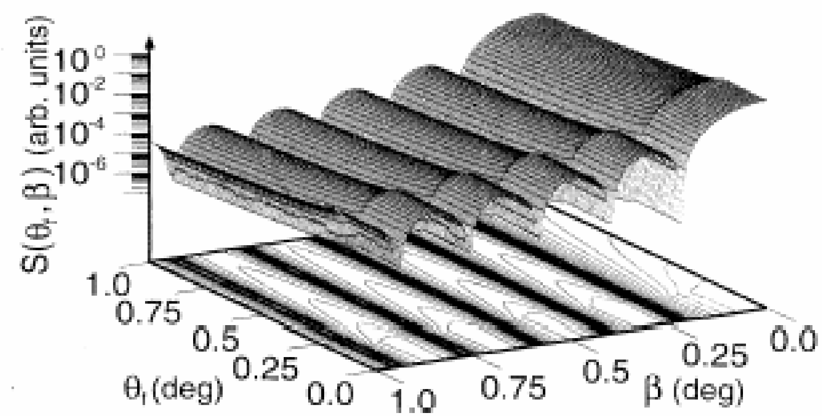

FIG. 5. The diffuse structure factor for columnar structures with the same correlation function as in Fig. 4 plotted as a function of β and θ_f. The radius is $R = 1000\lambda$, the angle of incidence $\theta_i = 0.5°$, and the index of refraction $n = 1 - 6.1 \times 10^{-6} + i \times 10^{-7}$.

Rauscher, Salditt and Spohn, PRB 52, 16855 (1995)

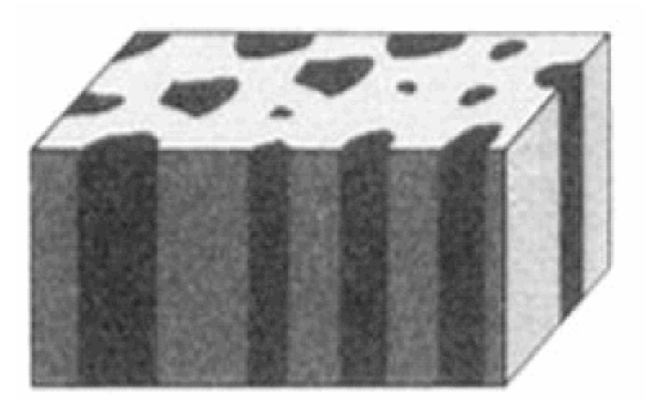

Columnar geometry of the density fluctuations

The scattering pattern is quite similar at all angles in the plane of specular reflection

SERGIS results: Homopolymer

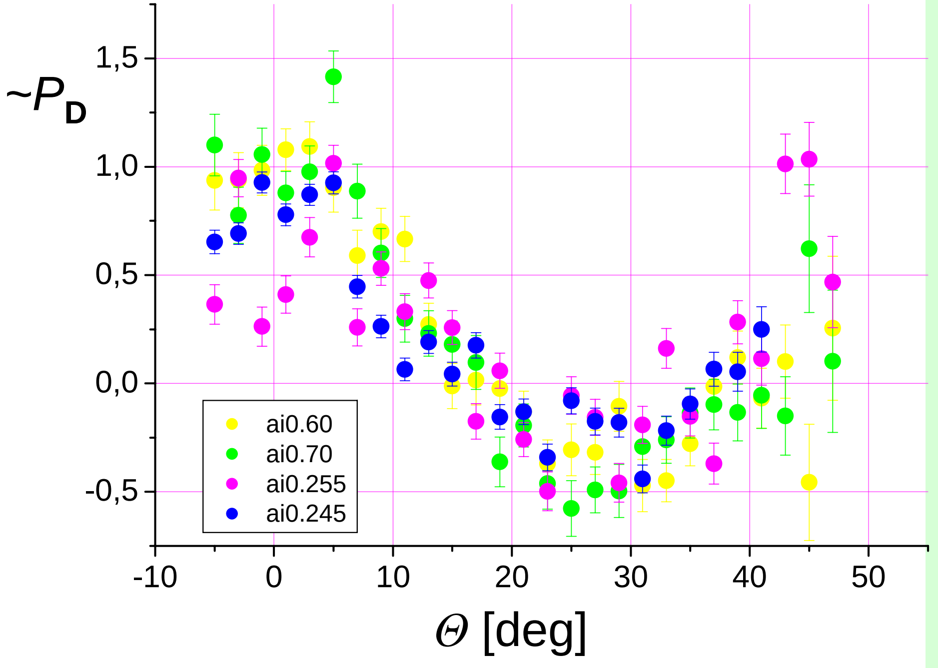

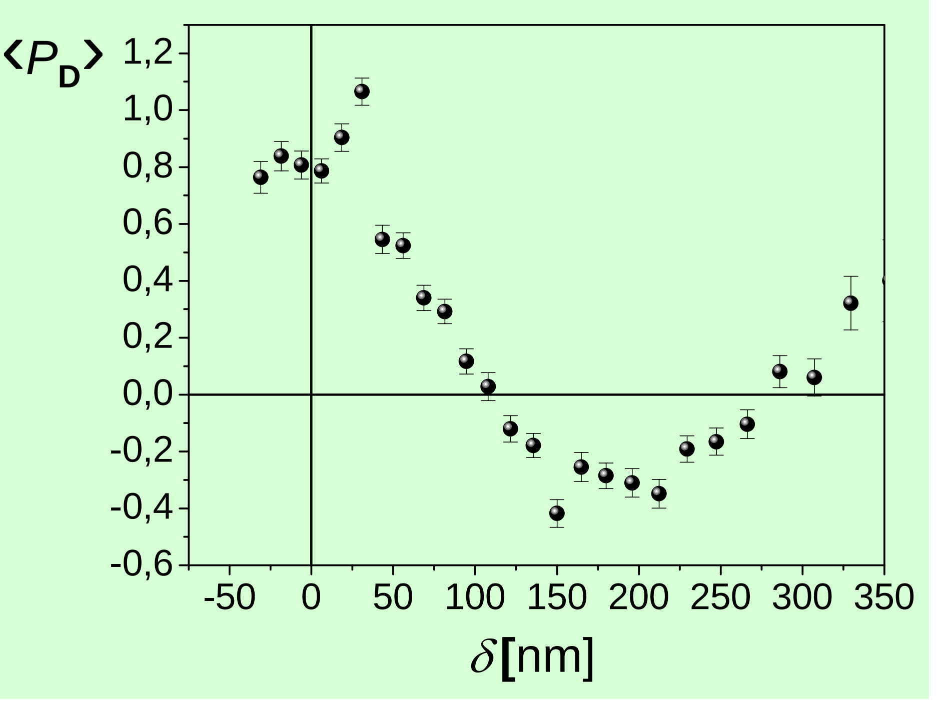

SERGIS results: PpMS (polyparamethylstryrene):dPS BLEND 3:2

P. Müller-Buschbaum et al.
J. Phys.: Cond. Mat. 17 (2005) S363–S386

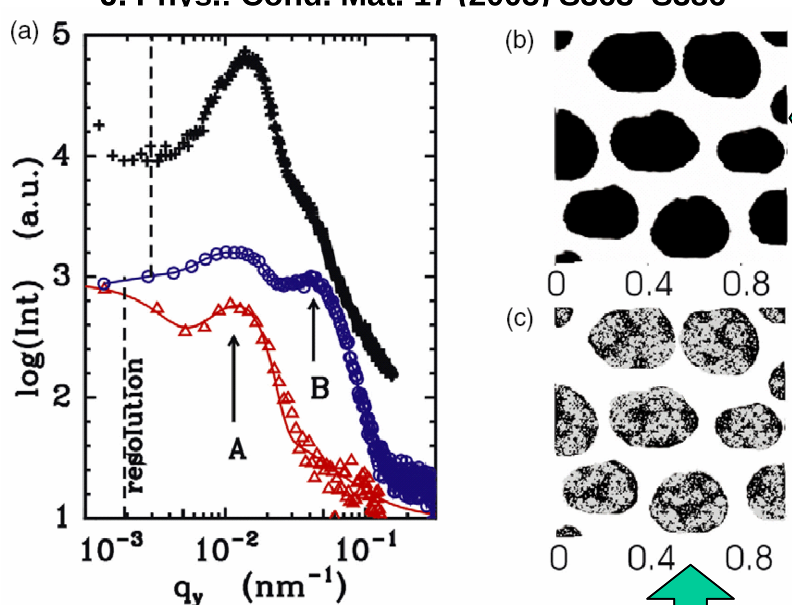

GISAXS

SFM:
$\Lambda \sim h^2$
pancake-type droplets

GISANS:
no internal regular phase separation

SERGIS

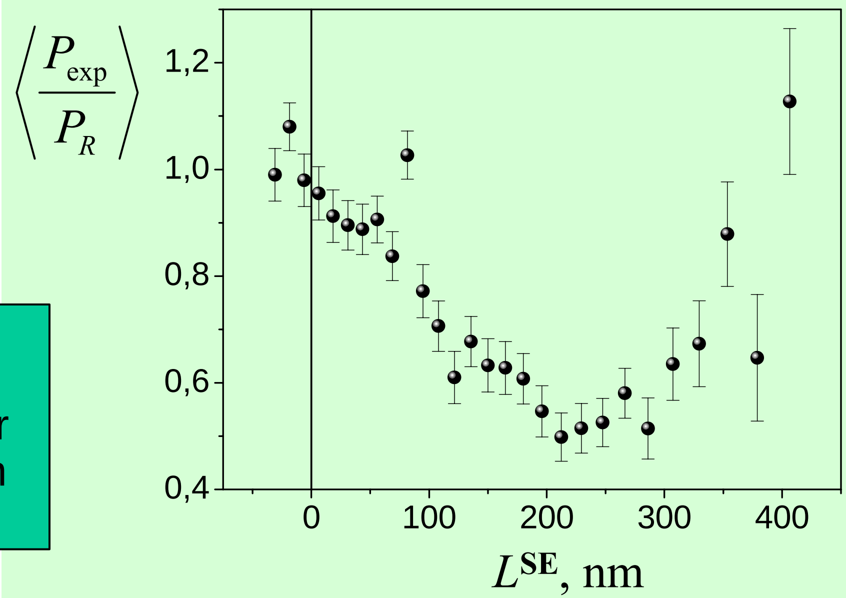

SERGIS results: Diblock Copolymer poly(styren-block-paramethylstryrene) P (S-b-pMS)

P. Müller-Buschbaum et al.
J. Phys.: Cond. Mat. 17 (2005) S363–S386

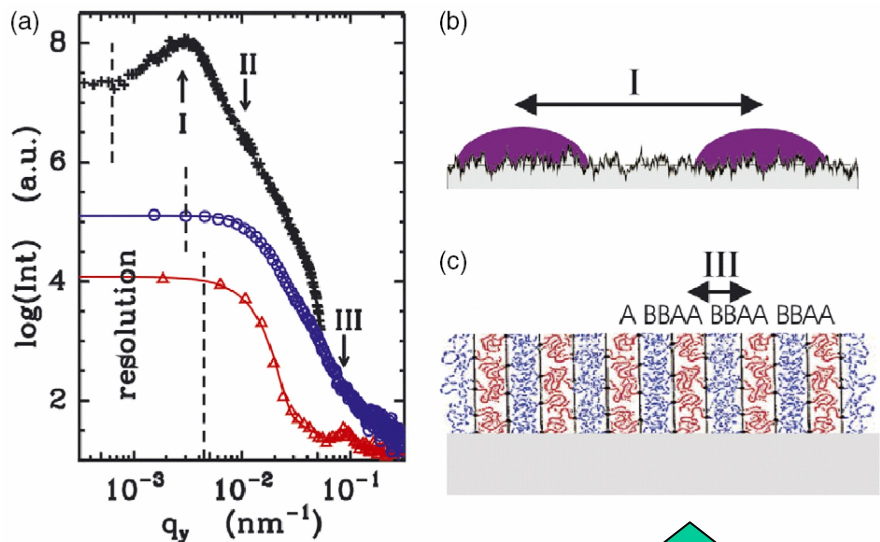

SFM:
$\Lambda \sim h^1$
'spherical' droplets

GISANS:
regular phase separation

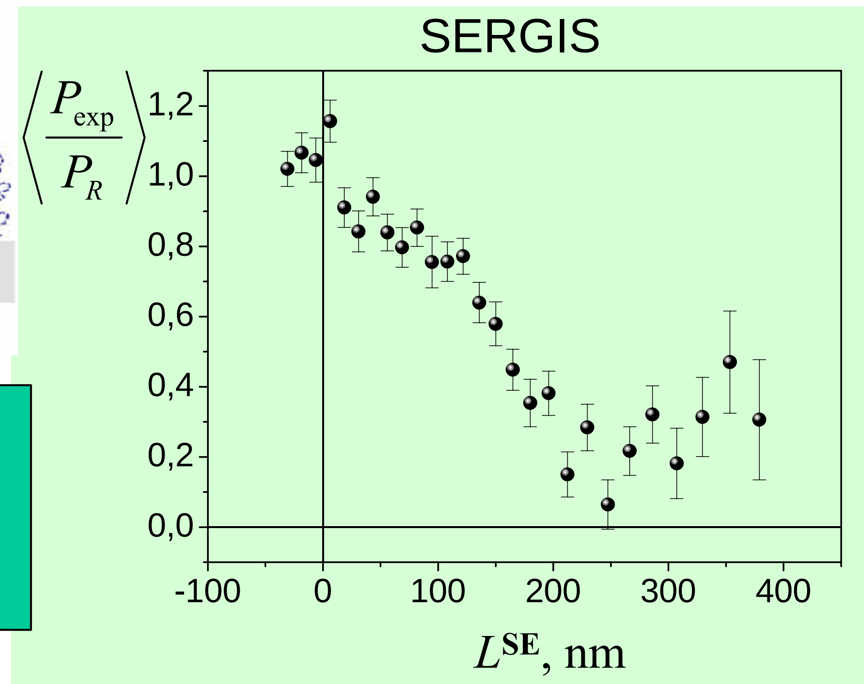

Comparison of samples

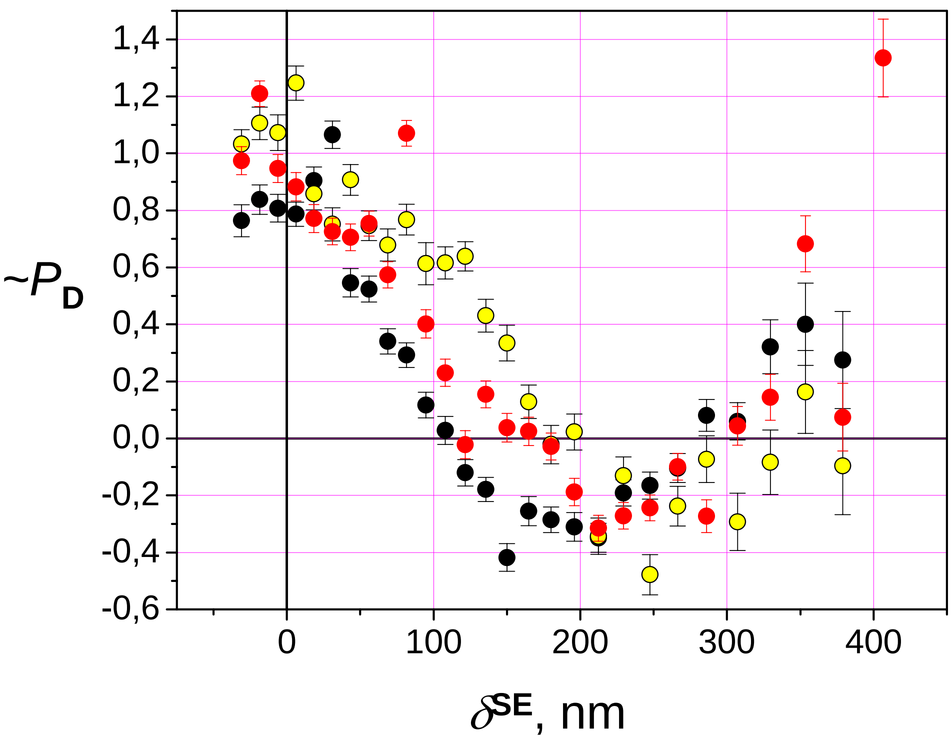

HOMOPOLYMER pancake-type droplets ($\Lambda \sim h^2$)

BLEND pancake-type droplets ($\Lambda \sim h^2$)

DIBLOCK 'spherical' droplets ($\Lambda \sim h^1$)

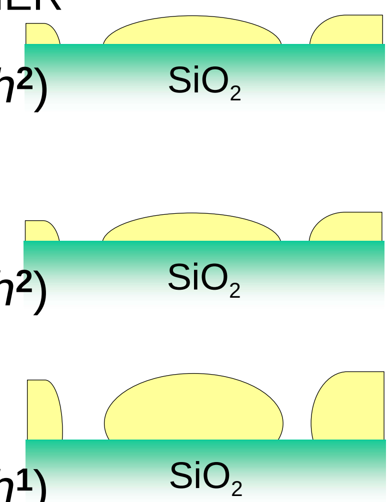

EXPERIMENTAL DATA AND CALCULATED CORRELATION FUNCTIONS

BLEND SAMPLE

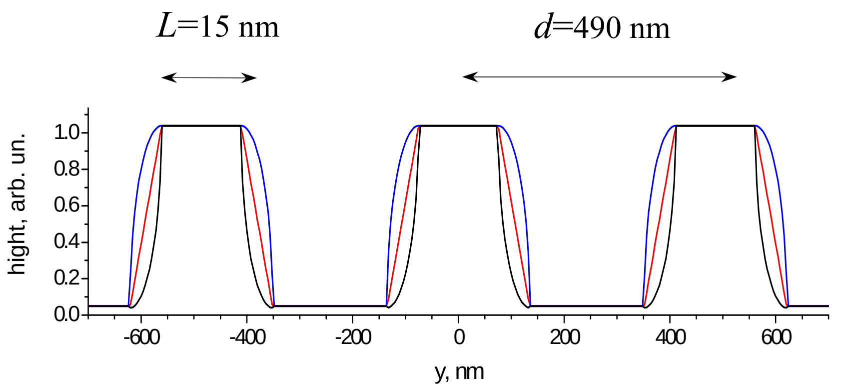

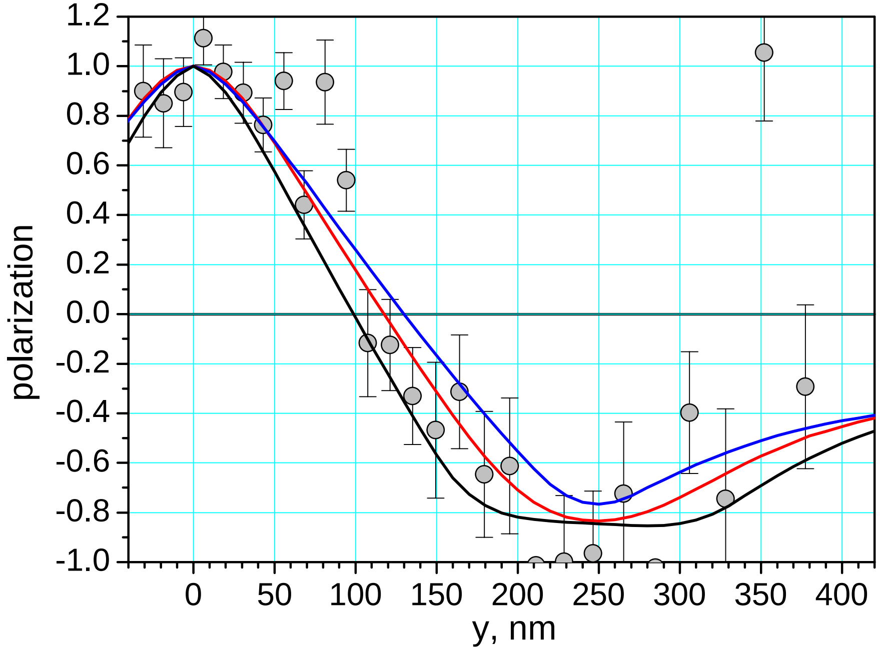

DIBLOCK COPOLYMER

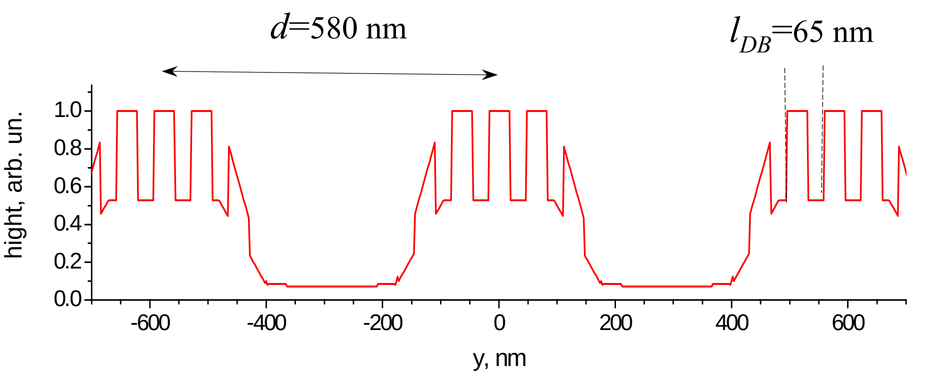

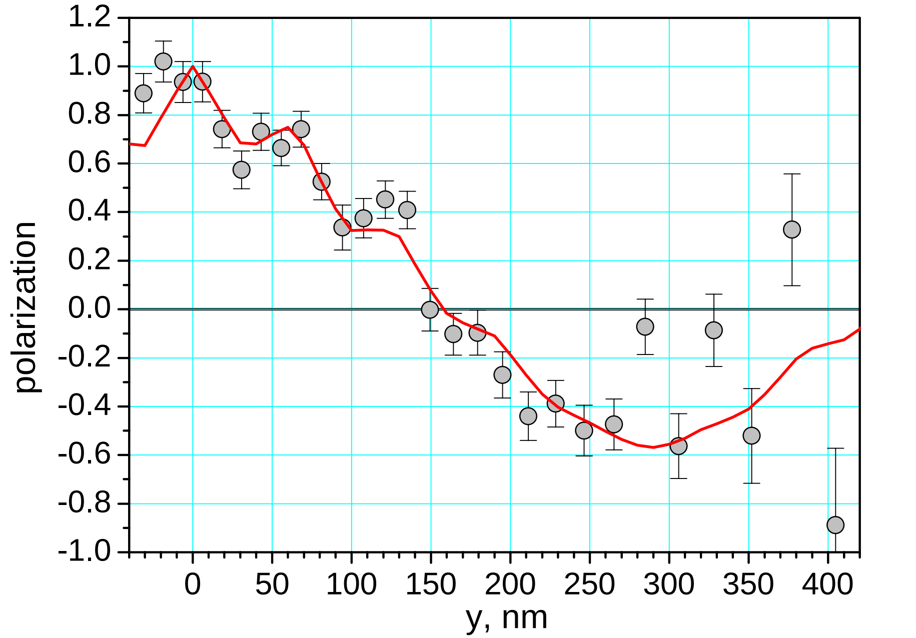

SERGIS findings on droplets of copolymer on silicon:

- SERGIS detects 2 periodicities at the surface
- The first is related to the droplet/droplet distance
- The second to a vertical layering of the copolymer

Does the copolymer layering propagate from droplet to droplet?

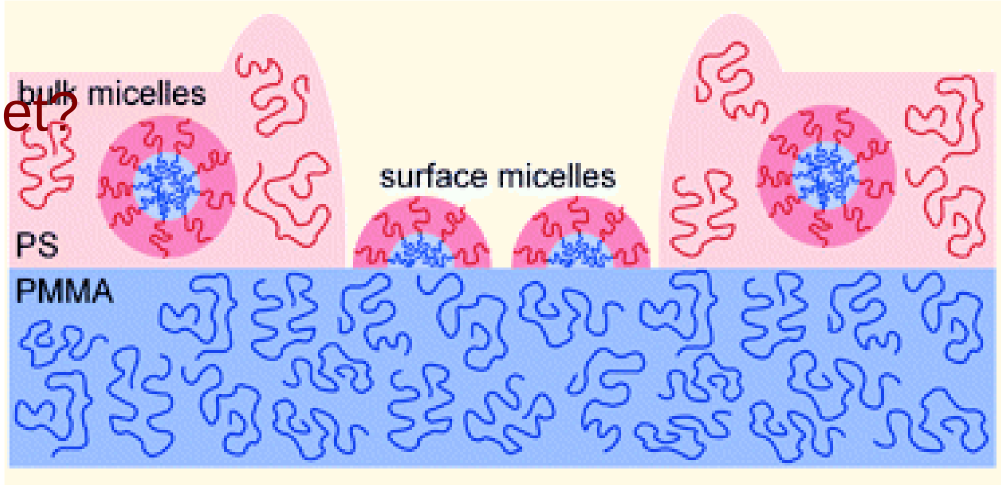

Image from:
"dewetting behavior of a block copolymer/homopolymer thin film on an immiscible homopolymer substrate"

B. Wei, J. Genzer and R.J. Sontak
Langmuir 20, 8659 (2004)

The mother of all experiments: Membrane Protein Structure/Function

SERGIS is an excellent probe
For near surface
2-dimensional correlations
Range: 5nm-1μm.

Several instruments
Active or planned
(IRI Delft, ISIS,FRM2,
J-Parc,NIST,SNS…)

At SNS it should have
~100 times the power of
EVA